CERN-2004-011
22 November 2004
Physics Department

ORGANISATION EUROPÉENNE POUR LA RECHERCHE NUCLÉAIRE
CERN EUROPEAN ORGANIZATION FOR NUCLEAR RESEARCH

WORKSHOP ON FUTURE PHYSICS @ COMPASS

CERN, Geneva, Switzerland
26–27 September 2002

PROCEEDINGS

Editors: F. Bradamante, G. Mallot
and S. Paul

GENEVA
2004

CERN Scientific Information Service–550–November 2004

Abstract

These Proceedings summarize the contributions to the Workshop Future Physics at COMPASS, dedicated to the NA58 experiment at CERN. The COMPASS Experiment (COmmon Muon and Proton Apparatus for Structure and Spectroscopy) comprises a deep inelastic scattering programme with muons and spectroscopy programme with hadron beams. The workshop focused on the latter programme, which has not yet started. The status of the experiment is outlined and future options for the muon programme are discussed at the end.

Future Physics @ COMPASS

CERN, September 26-27 2002

Nucleon Spin Structure

Transversity

DVCS

χPT Tests

Exotics and Glueballs

Double Charmed Baryons

Scientific Advisory Committee

G. Altarelli (CERN)
F. Bradamante (Trieste)
C. Detraz (CERN)
M. Faessler (München)
J. Feltesse (CERN)
S. Forte (Roma)
M. Garcon (Saclay)
W. Kühn (Giessen)
E. Leader (London)
E. Klempt (Bonn)
A. Magnon (Saclay)
G. Mallot (CERN)
V. Metag (Giessen)
V. Obraztsov (Protvino)
A. Olchevski (Dubna)
A. Palano (Bari)
S. Paul (München)

Local Organizing Committee

F. Bradamante (Trieste)
C. Detraz (CERN)
F. Kunne (Saclay)
M. Lamanna (CERN)
G. Mallot (CERN)
S. Paul (München)

http://compass-cw2002.web.cern.ch/compass-cw2002/

http://compass-cw2002.web.cern.ch

Preface

Five years after approval the COMPASS experiment started to take first data in 2001. The main objectives of the first years of data taking (until the shutdown in 2005) are the study of nucleon spin structure using deep-inelastic scattering of muons. The **gluon spin structure** will be investigated using open charm production on a polarized target as well as the production of hadrons produced at large transverse momenta. The flavour-decomposed **quark spin structure** on the other hand is studied by the analysis of the leading hadron flavour in such processes. In addition to the longitudinal spin structure COMPASS also investigates **transverse quark spin** structures using a transversely polarized target. These studies will give significant and important results in the first running periods for the COMPASS experiment, which are being pursued with a reduced setup compared to that of the original proposal. Owing to the significantly shorter running times than originally envisaged, these measurements will not, however, allow the precision originally proposed to be achieved and thus will be continued in later years.

In addition to the above-mentioned measurements, the approved COMPASS physics programme contains detailed studies of light hadronic states (glueballs, exotic mesons) in different production processes, the study of chiral perturbation theory by soft scattering processes, as well as charmed hadrons. For this purpose the COMPASS detector should be completed.

In the recent medium-term planning the CERN management expressed its strong interest towards a continuation of the COMPASS physics programme well beyond the shutdown in 2005, namely covering the period 2006–2010. The basis of the continuation is a very convincing physics programme based on the original COMPASS proposal. As this document dates back eight years, the CERN management (represented by the director of research C. Detraz) proposed to hold a workshop on Future Physics @ COMPASS and offered to host such a workshop at CERN. The purpose of this workshop was to review the physics programme outlined in the proposal and to possibly complement it by new ideas. It is in this spirit that the COMPASS group organized this discussion, which took place at CERN in September 2002.

The workshop was divided into several sections first outlining the present status of the experiment (both on hardware and analysis issues) and then the experiment framework for future measurements. These measurements focus on the study of hadronic systems using various hadron beams and which may only be addressed very briefly in the present running period. **New input** came from the consideration of photoproduction of exotics, thereby complementing efforts undertaken at JLAB for doubly charmed baryon studies thanks to recent measurements by the SELEX experiment at FNAL. In addition the field of deep-inelastic scattering has more recently been widely opened by theory by the developments of so-called generalized parton distributions allowing nucleon structure to be completely mapped, a project maybe as ambitious as the human genome project.

The organizers of this workshop are much indebted to their colleagues from COMPASS and to CERN in particular, which gave much help in the organization of this workshop. Last but not least we thank the members of the Scientific Advisory Committee and the Local Organizing Committee who prepared a very friendly and fruitful atmosphere.

Franco Bradamante Stephan Paul

Scientific Advisory Committee

G. Altarelli (CERN)
F. Bradamante (Trieste)
C. Détraz (CERN)
M. Faessler (München)
J. Feltesse (CERN)
S. Forte (Rome)
M. Garçon (Saclay)
W. Kühn (Giessen)
E. Leader (London)
E. Klempt (Bonn)
A. Magnon (Saclay)
G. Mallot (CERN)
V. Metag (Giessen)
V. Obraztsov (Protvino)
A. Olchevski (Dubna)
A. Palano (Bari)
S. Paul (München)

Local Organizing Committee

F. Bradamante (Trieste)
C. Détraz (CERN)
F. Kunne (Saclay)
M. Lamanna (CERN)
G. Mallot (CERN)
S. Paul (München)

Contents

THE COMPASS SPECTROMETER: STATUS AND PERFORMANCE

S. Dalla Torre
INFN, Sezione di Trieste, Italy

Abstract
The status and performances of the COMPASS spectrometer at the end of the first year of data taking, namely September 2002, is reviewed in detail. Particular attention is paid to the innovative aspects of the apparatus, which are essential to fulfil the whole COMPASS physics programme in the COMPASS critical environment (high beam fluxes, high trigger rates and quite crowded events); these aspects have also the merit of opening the way to future experimental studies in similar extreme conditions.

1. INTRODUCTION

The COMPASS Collaboration, consisting of more than 200 physicists from 26 Institutions from all over Europe, Russia, Japan, Israel and India is performing the experiment NA58, an experiment devoted to hadron physics at the CERN SPS [1]; this scientific goal is pursued with a rich, twofold research programme (as already indicated in the Collaboration acronym: Common Muon and Proton Apparatus for Structure and Spectroscopy):

- Nucleon spin structure, with particular emphasis on:
  - Gluon polarization ΔG(x)/G(x)
  - Flavour-separated polarized distribution functions Δq(x)
  - Transverse-spin distribution functions Δ_Tq(x)
  - Spin-dependent fragmentation ΔD_q^{Λ}
- Spectroscopy items, and more precisely:
  - Primakoff reactions
  - Polarizability of π and K
  - Glueballs and hybrids
  - Semileptonic decays of charmed mesons and baryons
  - Double-charmed baryons.

Nucleon spin structure measurements are performed using the SPS polarized muon beam scattered off polarized nucleon targets; the spectroscopy programme foresees the use of secondary hadron beams and a variety of targets, including some cryogenic ones. While beam and targets are different for the various measurements, the large majority of the spectrometer detectors are common to both physics programmes. The present status of the experimental apparatus and its actual performances are discussed in the following sections. Up to now, the experiment has collected data with muon beam for polarized deep-inelastic scattering (DIS) measurements: in discussing the status, some reference to items specific to this part of the research programme (like the polarized target) and to performances with muon beam are given.

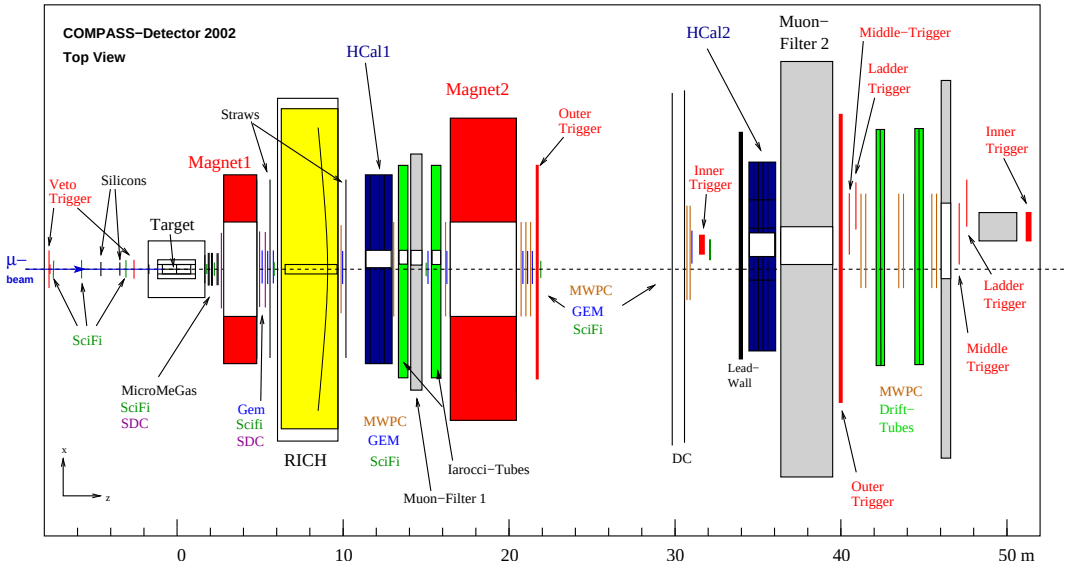

Fig. 1: The COMPASS spectrometer, top view.

2. THE SPECTROMETER LAY-OUT

The COMPASS experimental apparatus (Fig. 1) is a two-stage spectrometer, namely a Large Angle Spectrometer (LAS), placed immediately downstream of the target to allow for wide angular acceptance (± 180 mrad) and the Small Angle Spectrometer (SAS), downstream of the first one. In the original design, both spectrometers were equipped with analysing magnets (SM1, bending power: 1 Tm; SM2, bending power: 4 Tm), trackers telescopes, electromagnetic and hadronic calorimeters, muon filters and a RICH for hadron identification. Presently, for the first phase of the experiment, the spectrometer on floor includes most of this set-up, while part of the large-area trackers of the second spectrometer, the read-out electronics of the electromagnetic calorimeters and RICH-2, foreseen for hadron PID in SAS, are missing. The COMPASS Collaboration is now considering the completion of the spectrometer.

The spectrometer extends over a total length of $\sim$60 m and several detectors have quite considerable transversal dimensions. These dimensions have imposed the construction of several relevant mechanical structures, as, for instance, the ones shown in Figs. 2, 3 and 4.

3. THE POLARIZED TARGET

The COMPASS polarized target [2] is formed of two cells, each 60 cm long, housing the target material, with opposite polarization. The heart of the system is formed by the ^{3}He–^{4}He dilution refrigerator that allows the target material to be kept at a temperature well below 1 K (typically: 50 mK) and the superconducting solenoid, designed to provide 2.5 T field with homogeneity at 10^{-4} level. The COMPASS solenoid, a new superconducting magnet with wide aperture to ensure $\pm$180 mrad acceptance for the first spectrometer is not yet available: its construction by industry has, so far, not been successful; present perspectives for the successful construction of the COMPASS solenoid are quite favourable. Presently, the COMPASS polarized target makes use of the excellent solenoid built for the polarized target (Fig. 5) of the SMC experiment, with field homogeneity within 2×10^{-5}: the acceptance is reduced to $\pm$70 mrad. Both the SMC magnet and the future COMPASS one can also provide a transverse magnetic field (up to 0.5 T) to make possible target transverse polarization, for key measurements included in the COMPASS physics programme.

The target material used so far is irradiated ^{6}LiD, a material characterised by an extremely favourable dilution factor ($\sim$50%) and which allows for very high values of nucleon polarization. The COM-

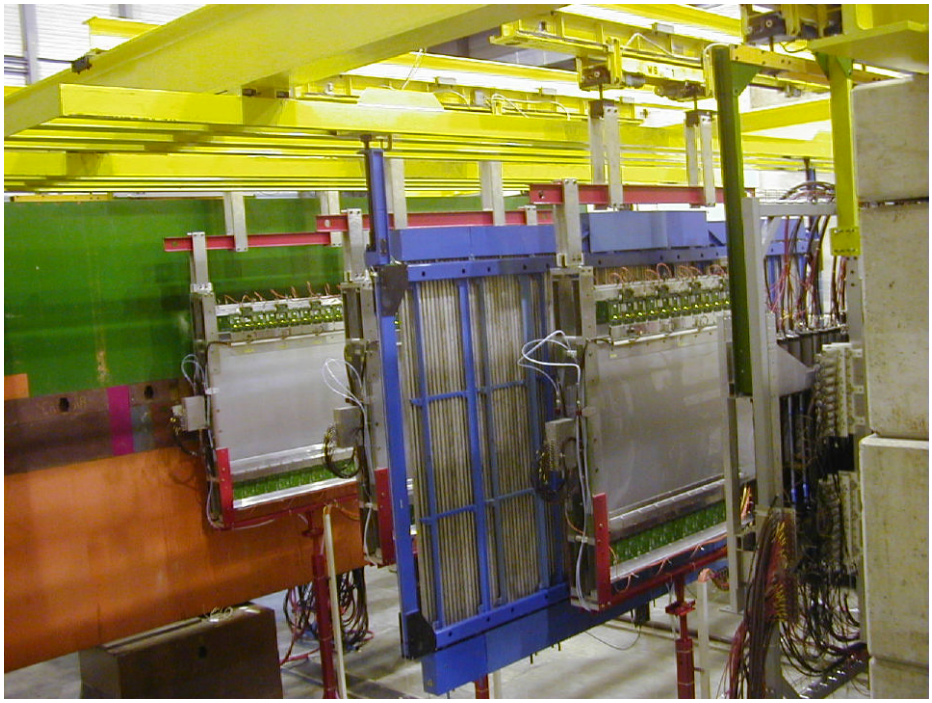

Fig. 2: The support of some tracking detectors in the region of Muon Wall 2; two stations of MWPCs and one of steel drift tubes are visible.

Fig. 3: The large frame of the electromagnetic calorimeter ECAL1.

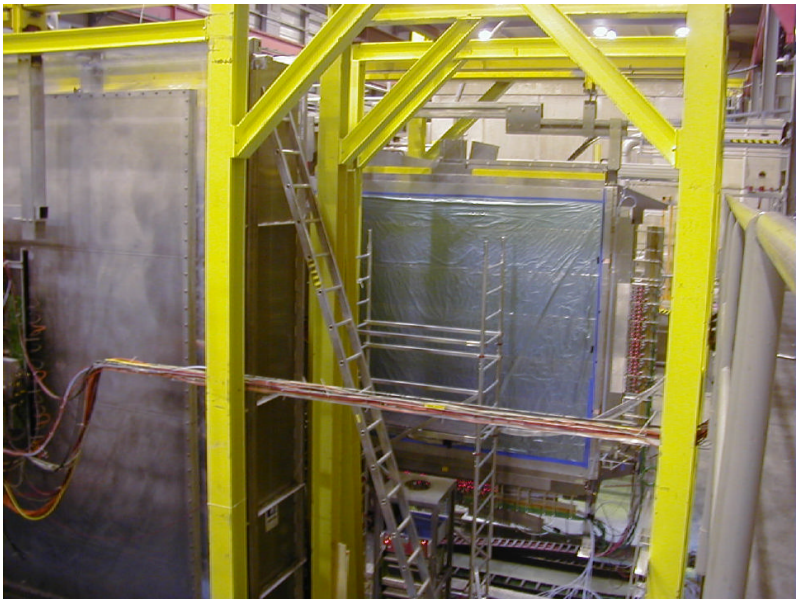

Fig. 4: The support structure of the large area trackers in the RICH-1 region allowing trackers to be rolled in the on-beam position and out for maintenance interventions; the RICH vessel is also partially visible.

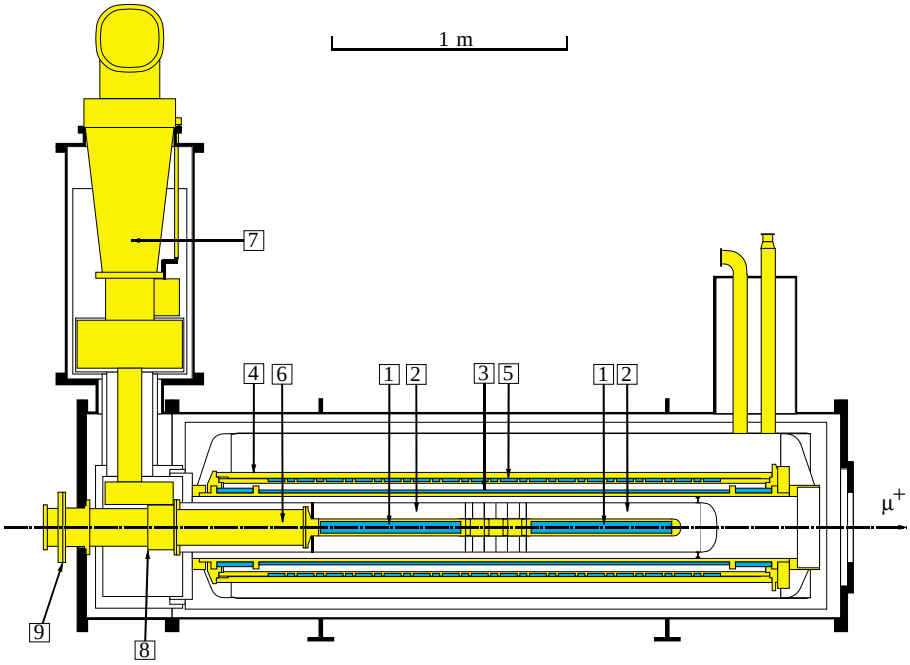

Fig. 5: The SMC target cryostat with the target holder as used in 1993 (from Ref. [3]). (1) target cells, (2) microwave cavity, (3) solenoid coil, (4) dipole coil, (5) correction coils, (6) dilution refrigerators, (7) precooler of ^{3}He, (8) indium seal, and (9) external seal.

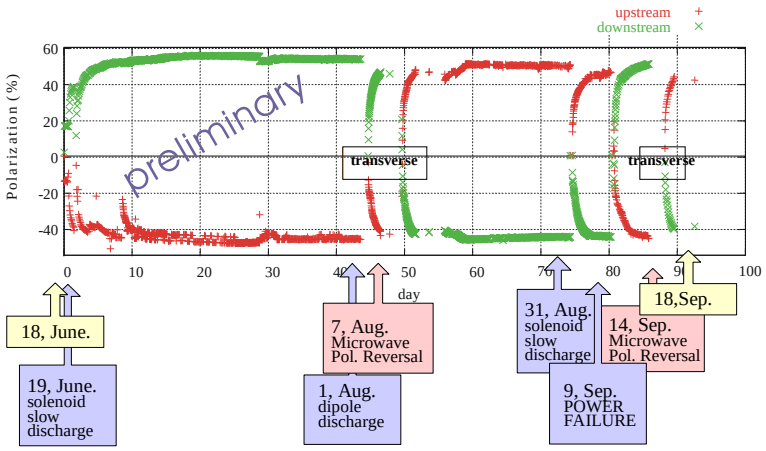

Fig. 6: The measured polarization (preliminary) in the upstream (+) and downstream (x) target cell respectively during the 2002 run; the polarization cannot be measured during transverse spin orientation.

PASS polarized target is the first large-scale one in which this material is used. A world polarization record at 2.5 T was obtained in 2001: -47% in one cell and +54% in the other one. In 2002, the quite satisfactory performance of the polarized target during the whole run (Fig. 6) confirms that the instrument is not only adequate for making records, but it is a reliable tool for good physics measurements.

The spin relaxation time in longitudinal mode (2.5 T) is too long to be measured, in transverse spin mode (0.4 T), it is longer than 1000 h. When target polarization is transversally aligned, the frozen spin mode is the only possible operational mode, a mode in which the target polarization cannot be monitored continuously: this long relaxation time is a prerequisite for the data taking with transverse target polarization. About 24% of the 2002 data-taking period was dedicated to collecting data with transverse orientation of the target polarization.

4. THE TRACKERS OF THE COMPASS SPECTROMETER

The requirements for the performance of the trackers are quite different at different distances from the beam axis: three families of trackers are present in the spectrometer: the Very Small Area Trackers (VSAT), the Small Area Trackers (SAT) and the Large Area Trackers (LAT), illustrated in the following sections.

4.1 The very small area trackers

In the very central region, only technologies capable of standing extremely intense beams can be employed; moreover good time-resolution capabilities are needed to disentangle the information from the event of interest from that of the preceding and following ones.

The **Beam Momentum Station (BMS)** makes possible the measurement of the incoming particle momentum on an event-by-event base. It consists of an analysing magnet which separates the particles, according to their momenta, in the vertical plane, and four hodoscopes of scintillator counters, with horizontal elements and granularity of 5 mm. The hodoscopes are from previous experiments at the SPS muon beam line, will the high-voltage power supply and the TDC read-out is a new COMPASS installation. The achieved time resolution is $\sim$300 ps, the BMS overall efficiency is $\sim$90% and the momentum resolution is better than 0.7% at 160 GeV/c.

A system of 9 stations of **scintillating fibre hodoscopes** [4] (Figs. 7 and 8) allows the measurement of 21 coordinates along the beam line, upstream and downstream of the target. These detectors have an enormous rate capability: up to 5 MHz per fibre. The total system includes 2668 fibre channels and

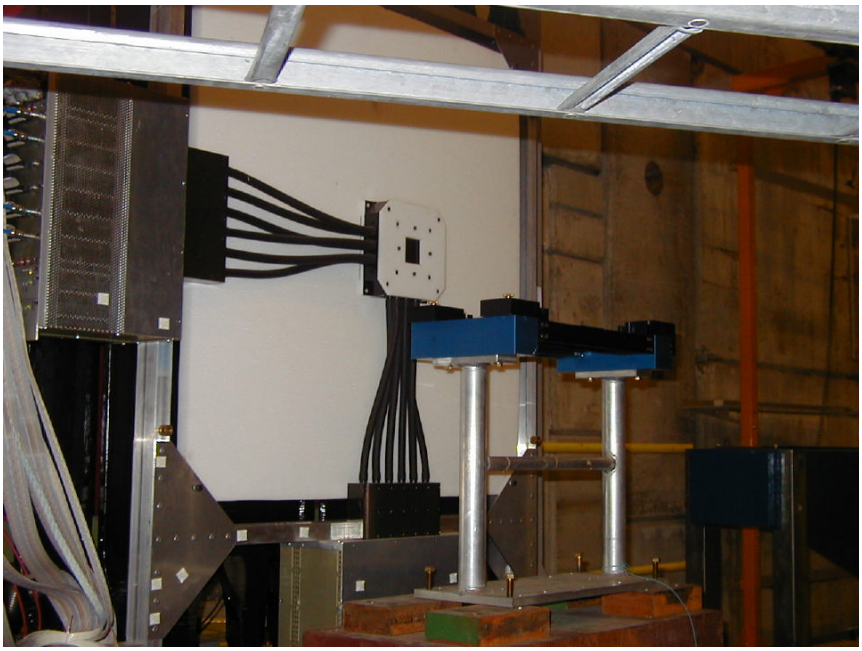

Fig. 7: One of the scintillating fibre stations installed in the COMPASS spectrometer; clear fibres connect the active region and the multianode PMTs, located far from the beam line.

4008 discriminator channels. Fibre diameters range from 0.5 to 1 mm. Fibre material is SCSF-78MJ by Kuraray Corporation. Fibres are read by multianode photomultiplier tubes H6568 from Hamamatsu. Particles to be detected cross typically 3–3.5 mm of scintillating material, thanks to the multiple layer arrangement of the fibres. The typical efficiency is $\sim$99%, while time resolution ranges between 350 and 550 ps (Fig. 9). Space resolution is also quite good: 130 μm or 250 μm, according to the different fibre diameters.

Two stations of **silicon strip detectors** (Figs. 10 and 11), four views each, having 50 $\times$ 70 mm^2 surface, with 50 μm pitch, complement the tracking of the incoming beam trajectories. They exhibit high efficiency ($\sim$99%) and 3 ns time resolution (Fig. 12) (see Ref. [5] for more details).

4.2 The small area trackers

These tracking detectors cover a region of $\sim$20 cm from the beam axis, with the exclusion of the central region, where the particle rate is very high ($\sim$3 cm with respect to the beam axis). Two different types of novel gaseous detectors are used in COMPASS for the small area tracker set-up: they are micromegas [6] (micromesh gaseous detectors) and GEM detectors [7] (see Fig. 13 for a schematic description of the basic detector principle and Fig. 14 for a picture of a typical GEM foil). For both types, we have, in the COMPASS spectrometer, the first installation of large surface units.

Micromega detectors form, in the COMPASS spectrometer, a telescope of 3 stations (Figs. 15 and 16), for a total number of 12 measured coordinates; the active surface is 40$\times$40 cm^2 with a central dead zone of 5 cm in diameter. They form a telescope placed between the target and the first analysing magnet SM1. They have a typical space resolution of 70 μm, time resolution better than 10 ns and efficiencies larger than 97%.

The **GEM** system consists of 10 stations, each equipped with two detectors for the measurement of 4 coordinates (each detector has two-dimensional read-out elements); the detector surface is 30$\times$30 cm^2, with a central circular dead zone with 4 cm diameter. Space resolution is $\sim$50 μm, time resolution $\sim$12 ns and typical efficiency in the range 96–97% [8].

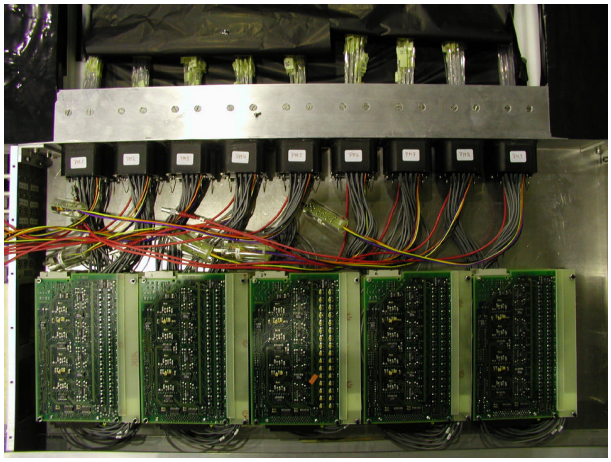

Fig. 8: Terminal edge of the clear fibres, multianode PMTs and the front-end electronics of one of the scintillating fibre stations installed in the COMPASS spectrometer.

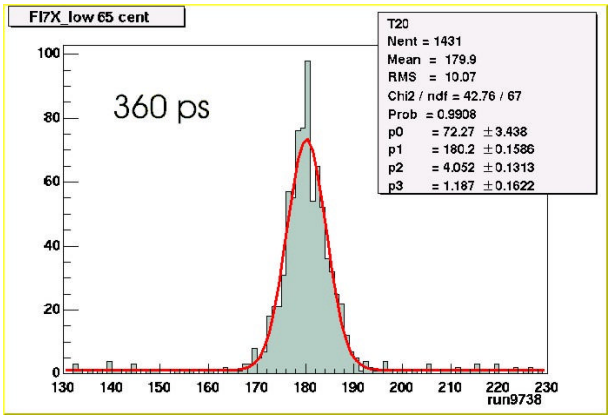

Fig. 9: Time resolution of one of the COMPASS scintillating fibre hodoscopes: 360 ps has been obtained for this unit.

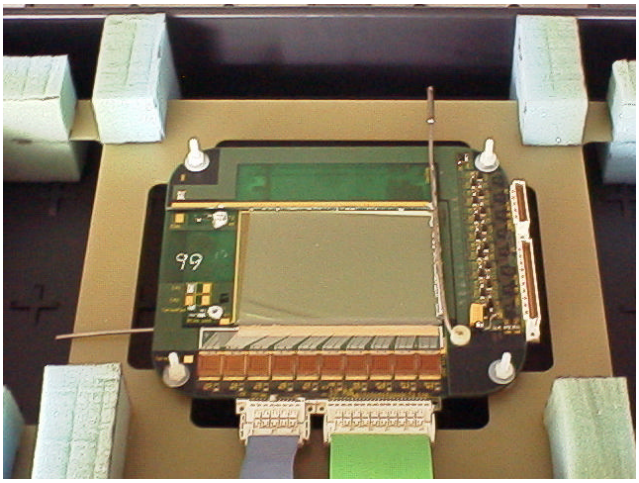

Fig. 10: One of the silicon strip detectors used for beam particle tracking in the COMPASS spectrometer.

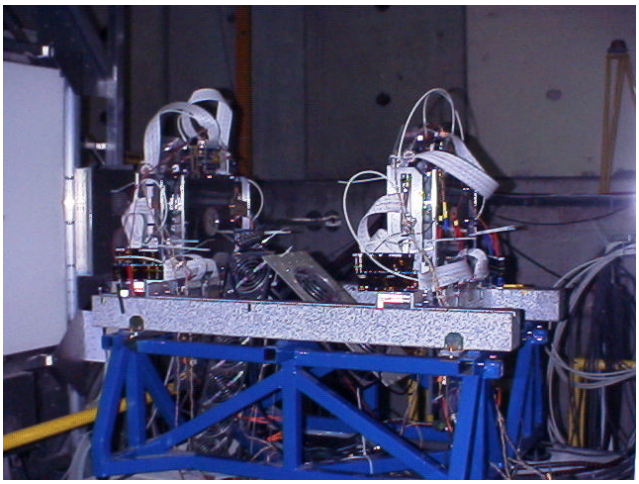

Fig. 11: The two stations of silicon strip detectors measuring incoming beam trajectories in the COMPASS spectrometer.

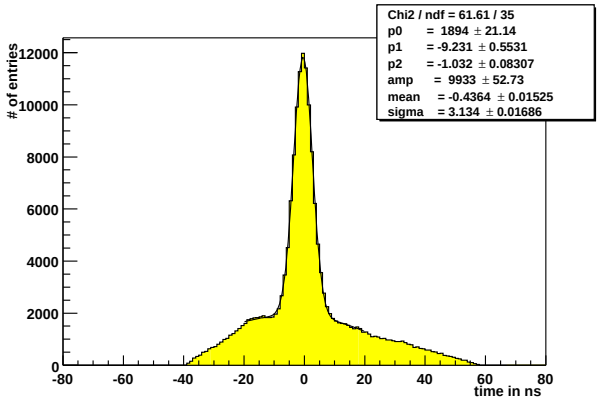

Fig. 12: Time resolution of the COMPASS silicon strip detectors.

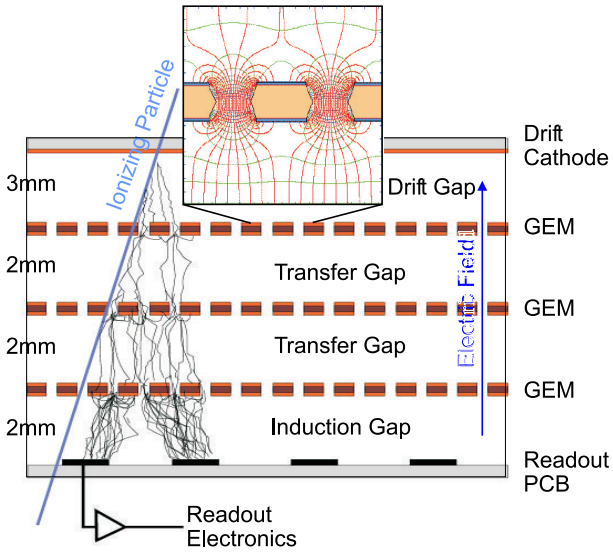

Fig. 13: Working principle of GEM detectors. At each GEM foil, charge multiplication is obtained applying a potential difference between the two faces of the foil itself (see the frame showing a zoom of the GEM foil); the total detector gain is obtained with a set of three foils.

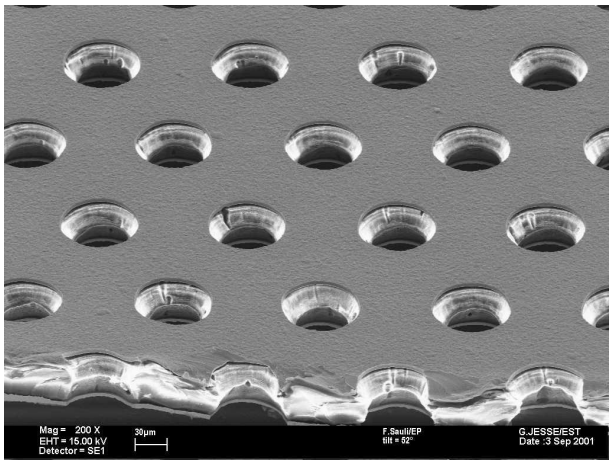

Fig. 14: Picture of a GEM foil.

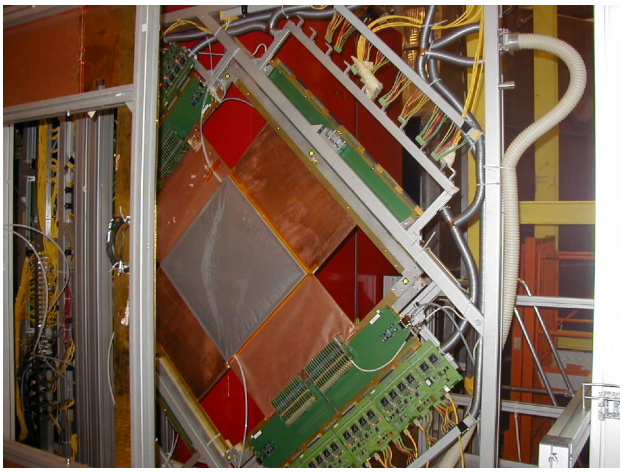

Fig. 15: One of 40×40 cm^2 micromegas built for the COMPASS spectrometer.

Fig. 16: The micromega telescope installed in the COMPASS spectrometer.

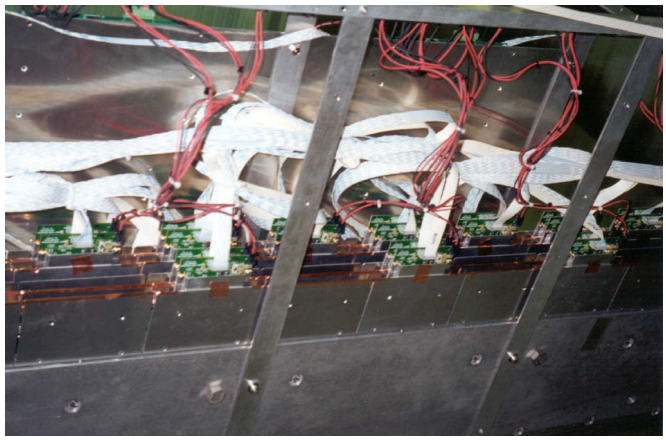

Fig. 17: The front-end cards of the drift chambers W4-5.

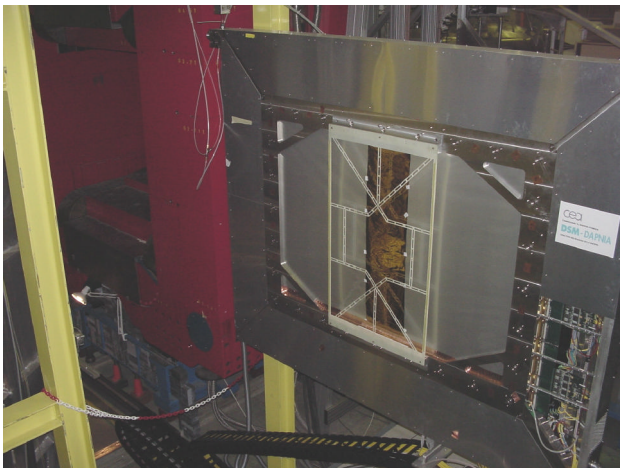

Fig. 18: One of the three SDC drift chamber detectors installed in the COMPASS spectrometer; the support of one of the GEM stations is also visible.

4.3 The large-area trackers

Telescopes of large-area trackers (all with surfaces of several m^2) are formed by detectors with four different designs, some of them are new detectors, namely drift chambers SDC and straw tube planes, others come from previous experiments and have been refurbished: MWPCs from the OMEGA spectrometer and the large drift chambers W4-5, from the SMC experiment. The read-out systems of the refurbished detectors are completely new, designed to match the basic requirements of the COMPASS data acquisition system (see Fig. 17 and Section 8).

The **SDC system** includes three drift chamber stations (Fig. 18), each measuring 8 coordinates with 7 mm drift cells; the space resolution is $\sim$170 μm (Fig. 19) and the efficiency ranges between 95% and 99.8%.

The **COMPASS straw tube** telescope includes 15 Double Layer (DL) planes (2.3×1.6 m^2) of tubes, 6 mm diameter and 10 mm diameter at the plane external edges [9] (Fig. 20). Nine DL planes were operational in 2002, while now all 15 DL are installed in the spectrometer. The straw tube planes have a space resolution $\sim$270 μm and efficiencies ranging between 85% and 98%.

The largest tracking set in SAS is formed by 11 **MWPC stations**, for a total amount of 34 planes

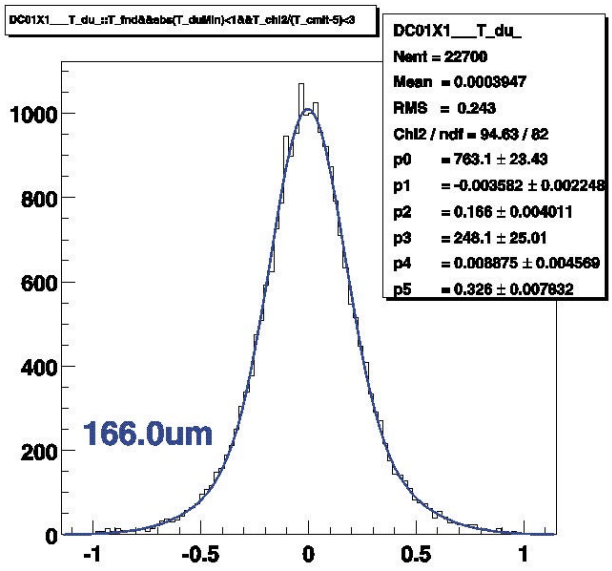

Fig. 19: Typical space resolution (166 μm in this example) of the SDC planes.

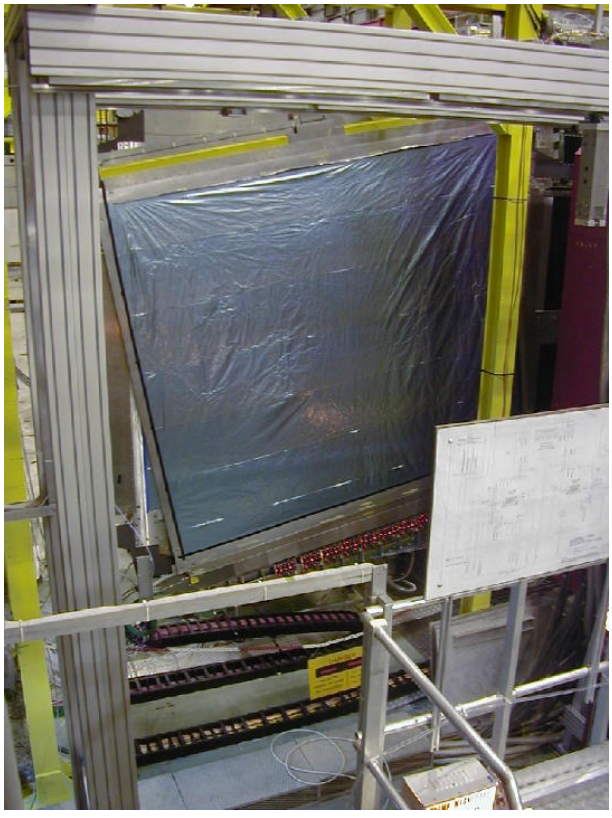

Fig. 20: A straw detector double layer mounted in the COMPASS set-up; the aluminium-coated Mylar protective foil, which separates the dry atmosphere surrounding the tube and the external atmosphere, and the front-end read-out electronics are visible.

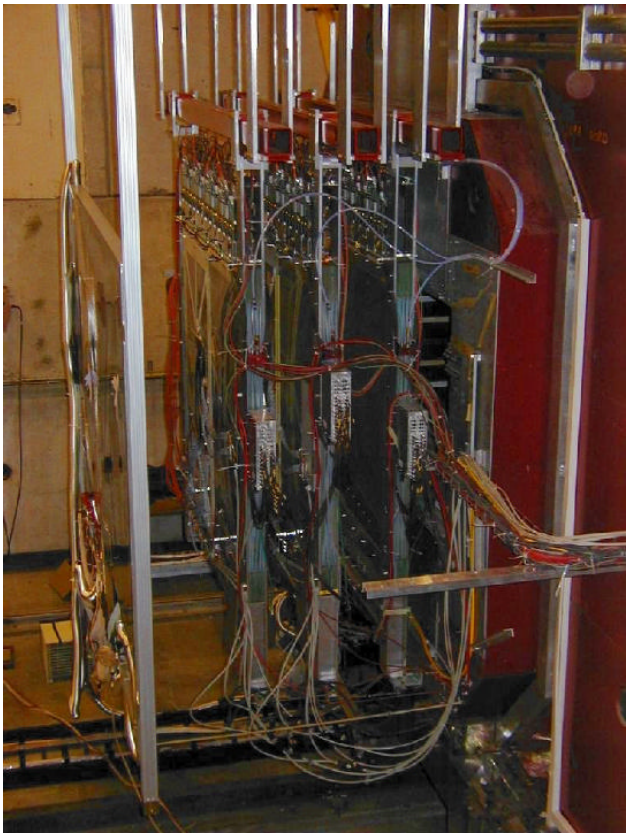

Fig. 21: Three of the 11 MWPC stations included in the COMPASS spectrometer.

of 2 mm pitch anode wires. These detectors, fully operational in 2001, exhibit a mean efficiency of 99.3%. MWPC trackers, previously used in the OMEGA spectrometer at CERN SPS, have been fully refurbished introducing a central dead zone to make them compatible with COMPASS high beam rates. Three stations are visible in Fig. 21.

Two large size drift chambers, named **W4-5**, were added to the COMPASS set-up in 2002 (Fig. 22). These detectors open the possibility of measurements at large Q^2 and made possible the first data taking with a transversely polarized target during the 2002 run. More W4-5 stations will be available for the 2003 run and the access to the large Q^2 domain will be completed by other large-area trackers under discussion in the context of the completion of the COMPASS spectrometer.

5. COMPASS CALORIMETRY

Both COMPASS spectrometers are equipped with electromagnetic and hadron calorimeters: ECAL1 and HCAL1 in the LAS, ECAL2 and HCAL2 in the SAS.

Both, HCAL1 and HCAL2, are sandwich type calorimeters made up of iron converters and scintillator plates. The light collection is performed with wave-length-shifting fibres. These two calorimeters are fully mounted and instrumented. Their measured resolution is

- HCAL1 (Fig. 23)
  $\sigma/E = 59.4\%/\sqrt{E} \oplus 7.6\%$ for π
  $\sigma/E = 24.3\%/\sqrt{E} \oplus 0.6\%$ for e^-
- HCAL2:
  $\sigma/E = 65\%/\sqrt{E} \oplus 4\%$ for π.

The electromagnetic calorimeters are not yet operative. ECAL1 is made up of lead glass blocks from previous GAMS and OLGA calorimeters; all blocks are available, the calorimeter support is in

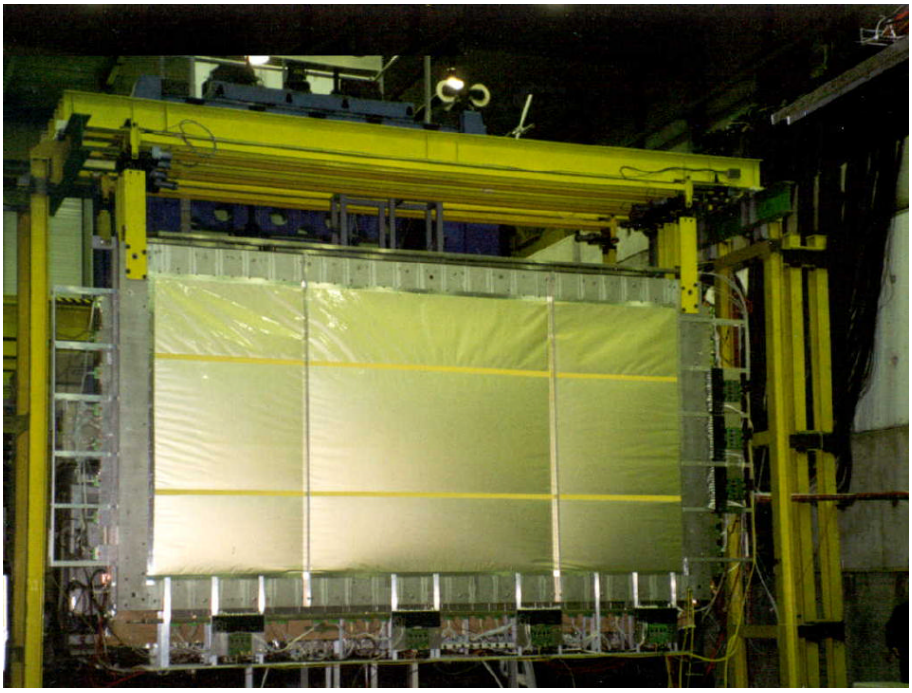

Fig. 22: Front of one of the drift chambers W4-5.

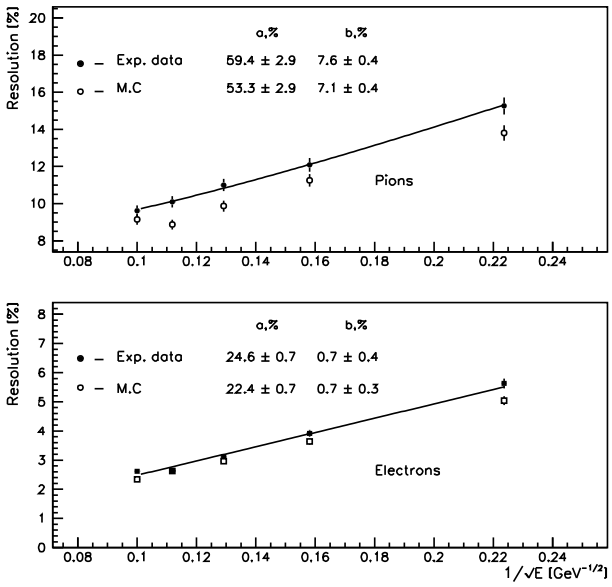

Fig. 23: The measured HCAL1 resolution for pions (upper plot) and for electrons (lower plot).

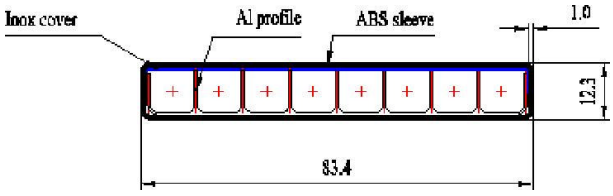

Fig. 24: The basic geometry of the Muon Wall 1 trackers: they are aluminium 'Iarocchi tube' detectors.

production. The known resolution of the OLGA calorimeter is $\sigma/E = 5.8\%/\sqrt{E} \oplus 2.3\%$. ECAL2 is made up of blocks from GAMS to be complemented by sandwich type elements (of either the pappardelle or Shashlik type); the LG blocks are presently mounted and partially instrumented.

6. PARTICLE IDENTIFICATION IN COMPASS

Muon identification is performed with muon filters, while hadron identification is pursued with RICH detectors. RICH-1, equipping LAS, is already operative while RICH-2, the high momentum partner, which will complete SAS, is one of the major projects foreseen for the completion of the spectrometer.

6.1 The muon walls

Muon filters are implemented in both spectrometers: Muon Wall 1 (LAS) and Muon Wall 2 (SAS). The detectors of Muon Wall 1 are planes (4×2 m^2) of aluminium 'Iarocchi tubes' (the basic geometry is presented in Fig. 24, while a picture of the detectors is given in Fig. 25). They sandwich a 60 cm thick iron absorber. The detectors employed in Muon Wall 2 are planes of 3 cm diameter steel drift tubes; the absorber, 2.4 m thick, is formed of concrete blocks.

6.2 COMPASS RICH-1

RICH-1 [10] has been designed to separate π's and K's with momenta up to $\sim$ 60 GeV/c in a high-intensity environment and to cover the full acceptance of the large-angle spectrometer. The material has been minimised to preserve the tracking resolution of the small-angle spectrometer and the energy resolution of the downstream electromagnetic and hadronic calorimeters. The main parameters achieved are:

- RADIATOR: A 3 m long C_4F_{10} radiator at atmospheric pressure, with a contamination of oxygen and moisture kept below 5 ppm, to have a transmittance higher than 80% for 165 nm photons, for a typical path length of 4.5 m.
- VESSEL: For the vessel ($\sim$ 80 m^3) non polluting materials were used, mainly aluminium. The incoming leakage rate is $\sim$ 3 Pa$\times$l/s.
- MIRRORS: The mirror system consists of spherical mirrors, radius of curvature 6.6 m, segmented in 116 hexagonal and pentagonal pieces covering a total area $>$ 20 m^2 (Fig. 26). Two spherical surfaces focus the Cherenkov photons onto two sets of photon detectors placed above and below the acceptance region. These mirrors have a local deviation of the shape from the spherical $\sigma_\theta < 0.2$ mrad, a maximum deviation from the nominal radius of curvature $\delta_R/R = 0.5\%$ and a reflectance $> 80\%$ down to 165 nm.
- PHOTON DETECTOR: Taking into account the large area to be instrumented (5.3 m^2) and the need for a pixel size of $\sim$1 cm, MWPCs with segmented CsI photo-cathodes were chosen. These UV photon detectors were developed in the context of RD26 [11] and, later, for the ALICE HMPID project [12], and adopted for several other projects [13]. RICH-1 is equipped with 8 identical

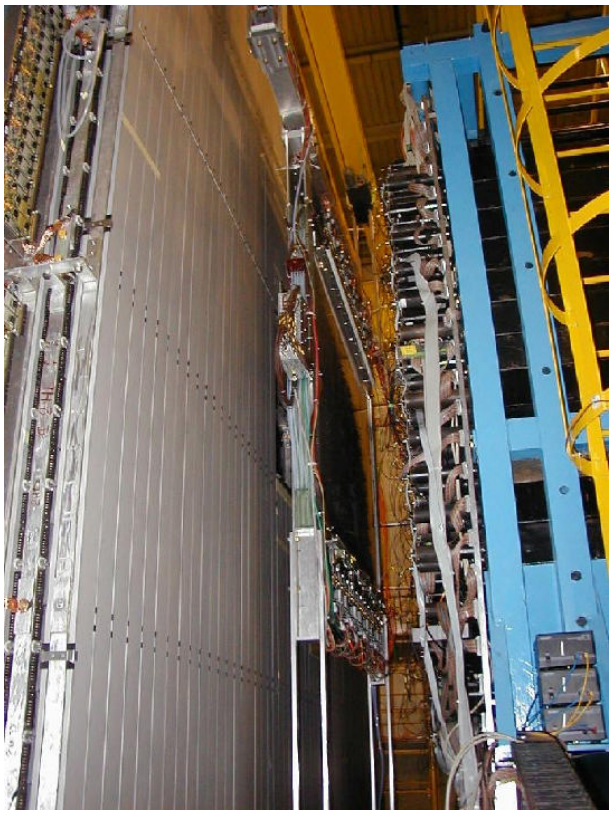

Fig. 25: Muon Wall 1: the muon filter of the Large Angle Spectrometer.

chambers, each one having an active surface of 576×1152 mm^2 (Fig. 27). Two 576×576 mm^2 double-layer PCBs, each segmented in 5184 8×8 mm^2 pads, coated with CsI form the photocathode planes (for more details about the coating technique see Ref. [14]). Silica quartz windows (600×600×5 mm^3) separate the radiator from the photon detectors.

– FRONT END ELECTRONICS The 82 944 channels, equipped with analog readout electronics, correspond to $\sim 40\%$ of the total number of channels of the experiment.

– MATERIAL BUDGET: The total radiation length is 22.5% of X_0. The major contributions to the material budget in the acceptance is given by the radiator (10.5% of X_0); the other contributions are quite reduced: the mirror substrates (5.5% of X_0), the mirror mechanical supports (2.5% of X_0) and the front and rear vessel windows (2% of X_0 each). In the beam region, where a He-filled pipe is used, particles have to cross only 1.6% of X_0.

Figure 28 shows an event from the RICH on-line event display. The preliminary resolution of the measured Cherenkov angle resolution for ultrarelativistic particles is 0.4 mrad (Fig. 29); a flavour of the RICH performances is presented in Fig. 30.

7. THE COMPASS TRIGGER FOR THE DEEP INELASTIC SCATTERING PROGRAMME

The set-up forming the COMPASS trigger for the DIS programme (Fig. 31) consists of almost 500 dedicated scintillator counter channels, viewed by PMs, read via dedicated, custom discriminator boards. Mean-timer circuits are used for those scintillator strips, which, because of their length, are equipped with PMs at both ends. Custom mean-timer boards allow to form correlations between different hodoscopes in an extremely short time. The COMPASS trigger for the DIS programme is based on the correlation of the information from different hodoscopes in order to select scattered-particle trajectories originating from the target. To increase the trigger purity, in particular in the small Q^2 domain, the information from

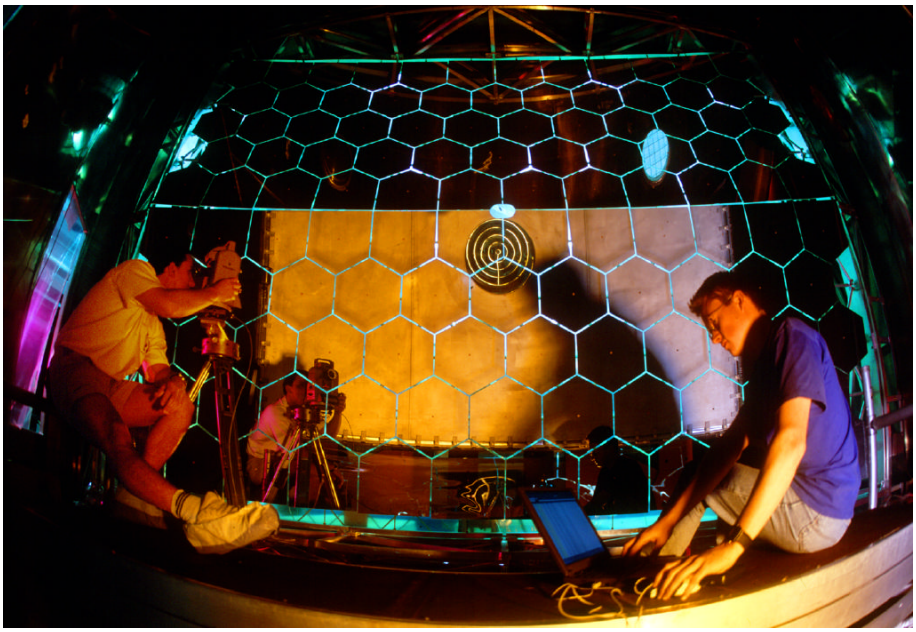

Fig. 26: The mirror wall during the alignment of the mirrors.

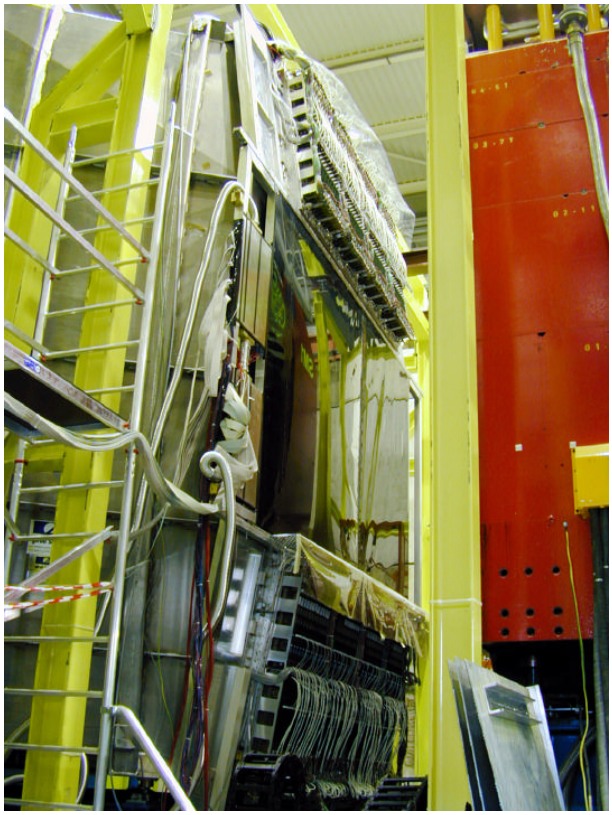

Fig. 27: RICH-1 upstream side: the photon detectors, top and bottom sets, fully equipped with read-out electronics are visible.

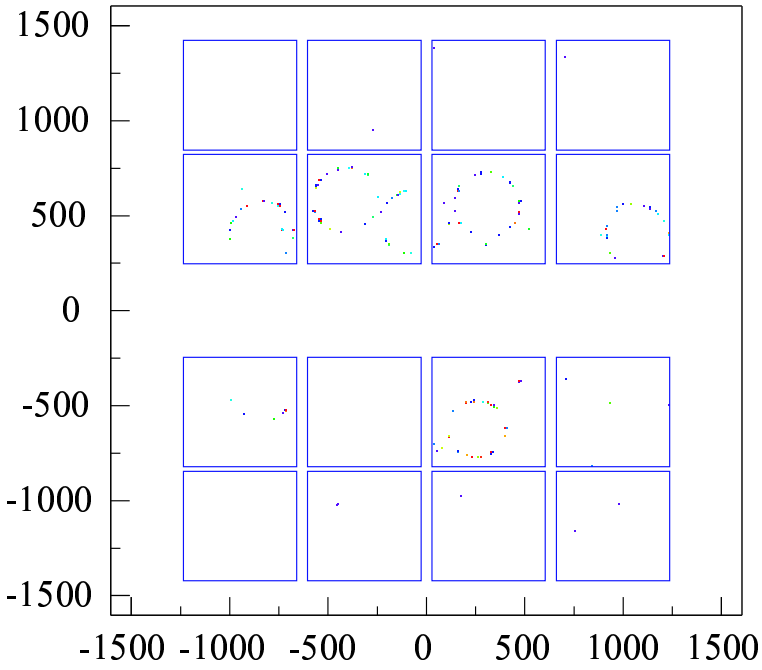

Fig. 28: An event from the RICH on-line event display.

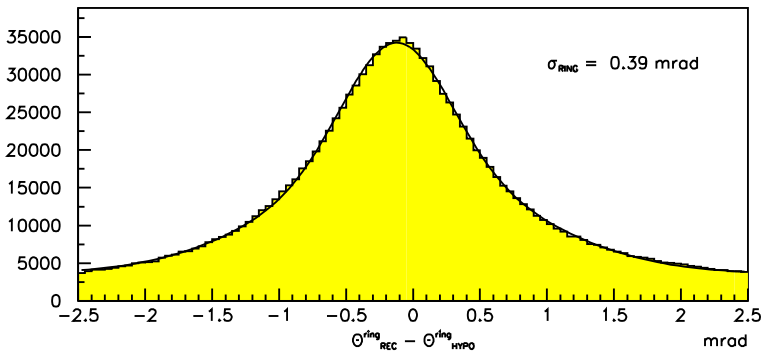

Fig. 29: Preliminary resolution of the measured Cherenkov angle for ultrarelativistic particles.

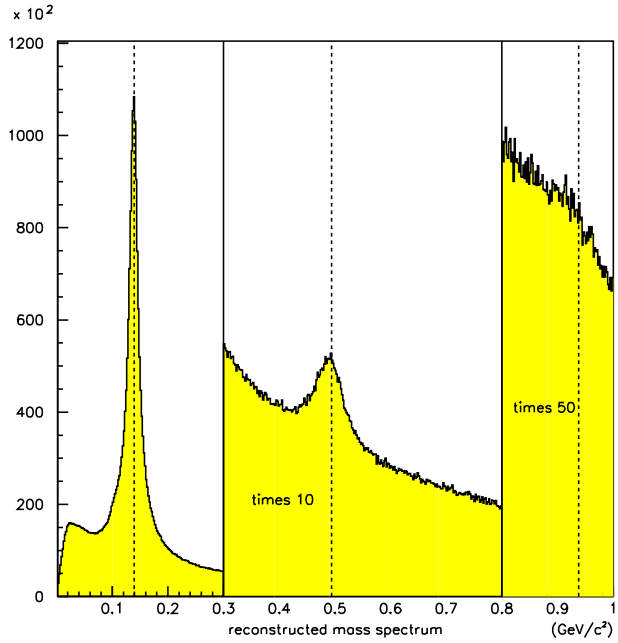

Fig. 30: Preliminary mass spectrum obtained with COMPASS RICH-1; π and K peaks are clearly visible; there is also an indication of a proton signal.

the hodoscopes is complemented with that of the hadron calorimeters (Fig. 32). Different combinations of hodoscope information allow the various kinematical regions to be spanned (Fig. 33).

8. FRONT-END ELECTRONICS AND DATA ACQUISITION

The 191 000 electronic channels of the COMPASS spectrometer are read by a read-out system characterised by its pipelined architecture and by a design which makes it fully extendible [15]. An overall scheme of the COMPASS read-out and data acquisition system is presented in Fig. 34.

Different front-end chips are used (such as a SFE16 preamplifier-discriminator for the micromegas, APV25 for GEMs and silicon detectors, MAD4 and ADS8 for large area trackers, COMPASS-GASSIPLEX for RICH-1 read-out). The front-end and digitising boards (based, for the conversion to digital information, on chips like F1-TDC [16] for several trackers, FIADC for calorimetry and AD 9201ARS for RICH-1) transfer the information to custom VME boards (CATCHes [16] for most of the detectors, GeSiCA for GEMs and silicon trackers). In particular, RICH front-end BORA boards [17] perform a first sparsification and data reduction stage thanks to the use of distributed intelligence: each front-end board is equipped with a powerful DSP and an FPGA. From VME boards, data are transferred via optical S-links to large memory buffers, spill buffers, hosted in PCs, where the data of a whole burst are stored. The SPS duty cycle is $\sim 25\%$: the use of large-memory spill buffers allows the whole SPS cycle to be used to increase the effective bandwidth downstream of the buffers themselves. All the electronics read-out components from front-end to spill buffers are custom designed.

The Data Acquisition System (DAQ) (Fig. 35), downstream of the large memory buffer, is based on commercial devices: its heart is the Gigabit Ethernet Switch, which allows the information to be distributed from the spill buffers to a net of 12 event-builder PCs. The DAQ software is based on ALICE DATE.

The present performances of the overall read-out and DAQ system can be summarised by the following figures: at ~ 5 kHz trigger rate over the spill duration (~ 5 s), the read-out and DAQ dead time is 7%, while the typical event size is ~ 40 kB, corresponding to data rates of 220 MB/s during spill,

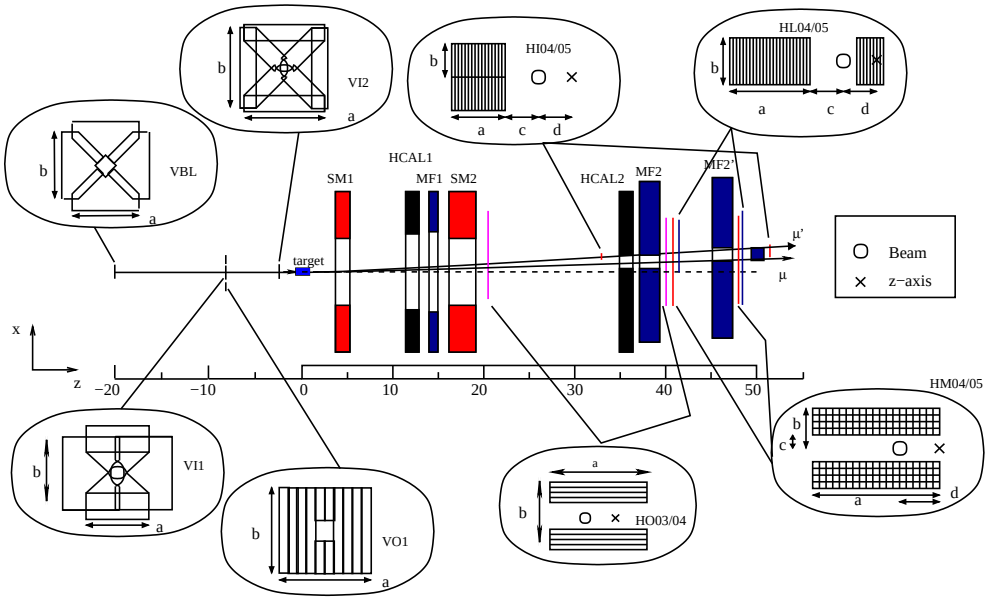

Fig. 31: COMPASS DIS trigger: the various hodoscopes forming the set-up.

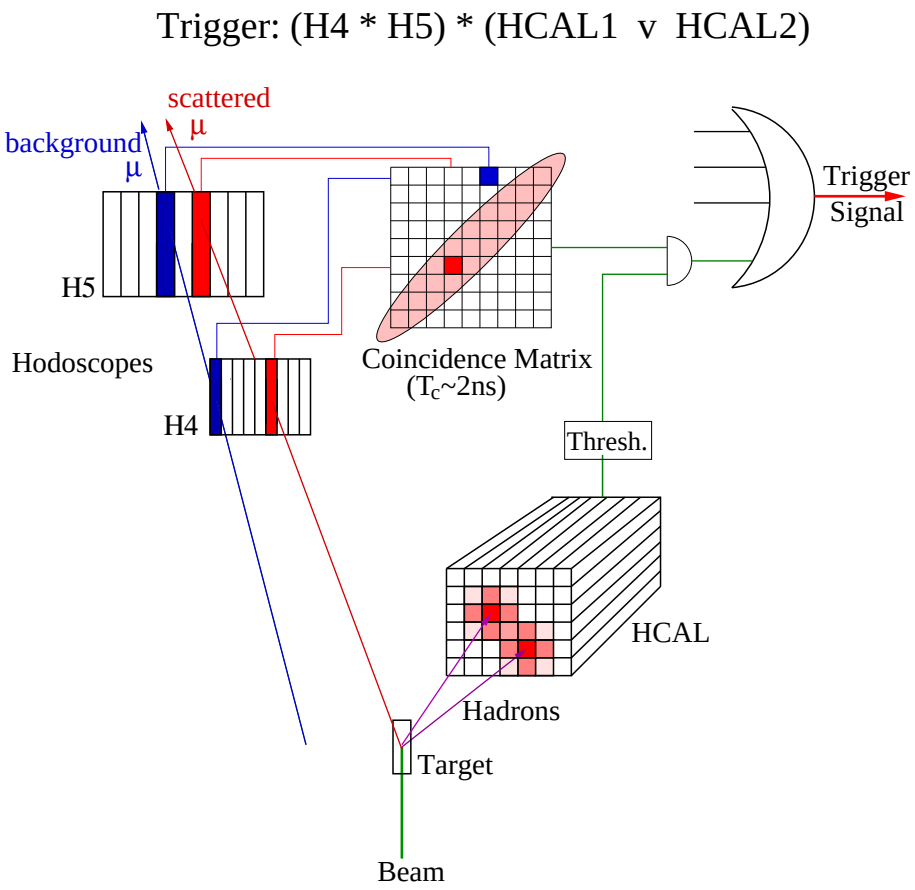

Fig. 32: Scheme demonstrating the working principle of the COMPASS DIS trigger.

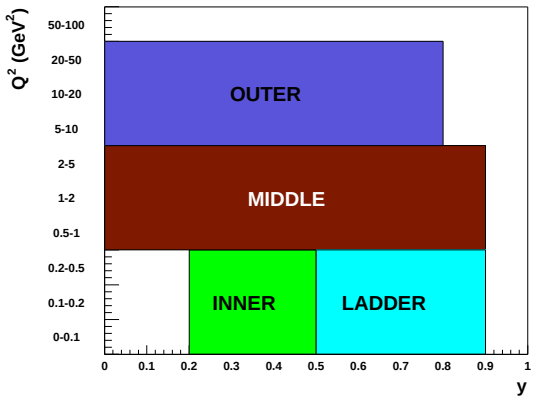

Fig. 33: COMPASS DIS trigger: kinematic regions, in the (y, Q^2) plane, covered by the different combinations of the trigger hodoscopes.

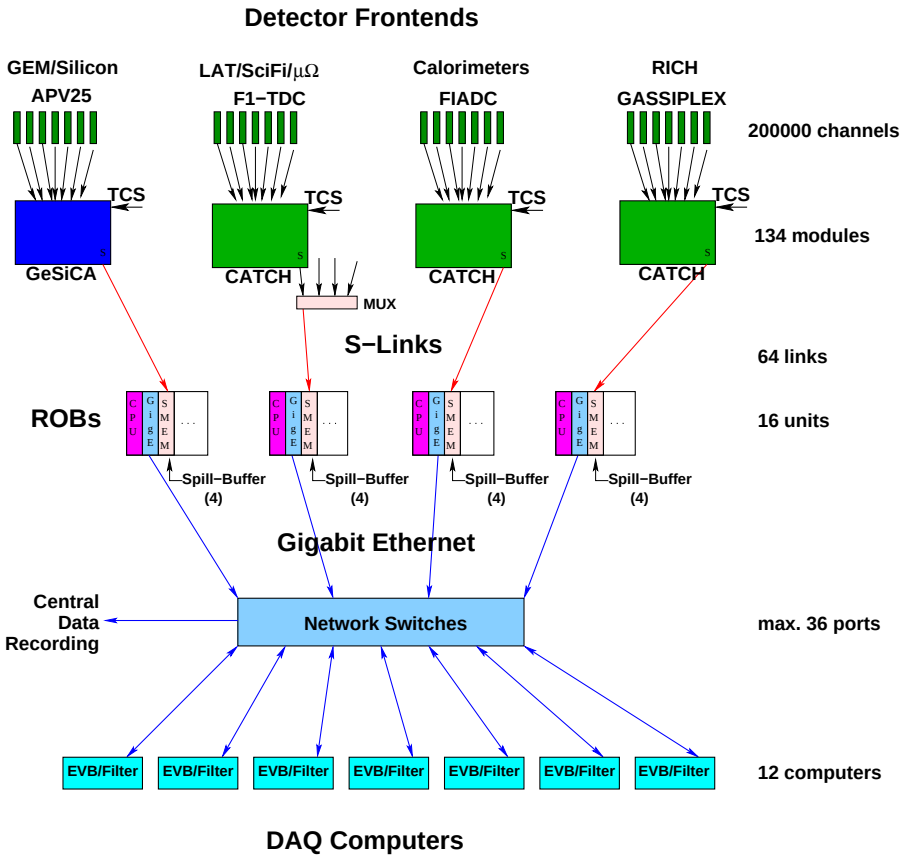

Fig. 34: Overall scheme of the COMPASS read-out and data acquisition system.

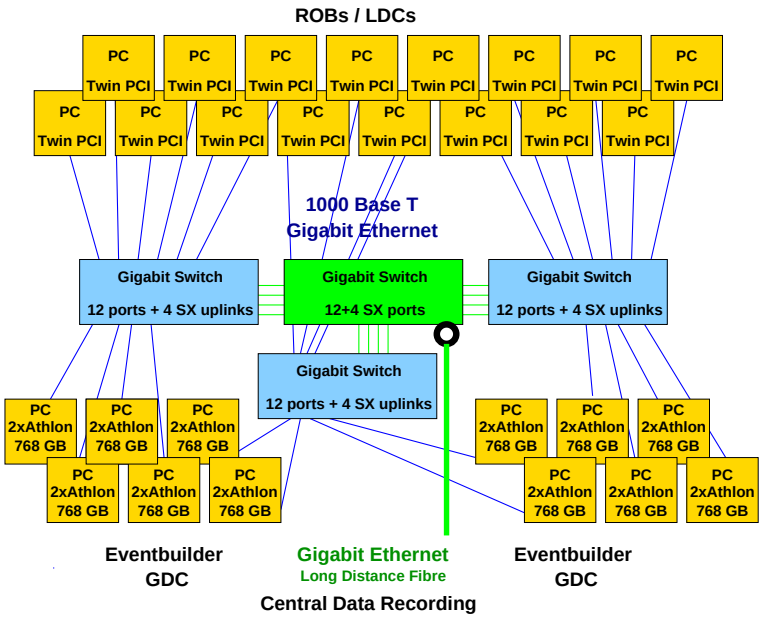

Fig. 35: Scheme of the PC net which forms the heart of the COMPASS data acquisition system.

from front-end and to the spill buffers and 60 MB/s DC downstream of the spill buffers. This figure is comparable with data rates expected for LHC experiments, being only two or three times smaller. Work is in progress to reduce the DAQ dead-time in 2003.

The read-out and DAQ system reached, after the first weeks of the 2002 run period, active time rates of $\sim 85\%$. It was thus possible to collect, during the 2002 run, 260 TB of data, corresponding to 5 billion events. The foreseen figure for the data flow from the COMPASS experiment to the central data recording facility of 3 TB/d was exceeded during the last period of 2002 data taking.

9. COMPLEMENTS OF THE SPECTROMETER

The efficient operation of a modern experiment requires some necessary complementary tools for the slow control of the experimental apparatus and the on-line check of data consistency and quality.

The increasing complexity of experiments and apparatuses and the corresponding enlargement of the collaborations impose efficient, up-to-date solutions for the circulation of information and its availability in real time: the COMPASS electronic log-book is one of the Collaboration instruments answering this challenge.

9.1 The Detector Control System

The aims of the COMPASS Detector Control System (DCS) include

- operator control of hardware systems like the HV and LV ones
- monitoring and data archiving over long-term periods of hardware parameters (such as HV and LV systems, crates, gas systems, pressure and temperature sensors, data taking, cooling systems and data from the SPS accelerator)
- alarm handling and
- information visualisation.

For COMPASS DCS, the Framework package, based on PVSS and designed at CERN for LHC experiments, has been adopted. Data from PC work-stations running Linux and NT systems, from VME CPUs and from fieldbuses (like VME, CANbus, Profibus, serial RS232 lines) are precessed.

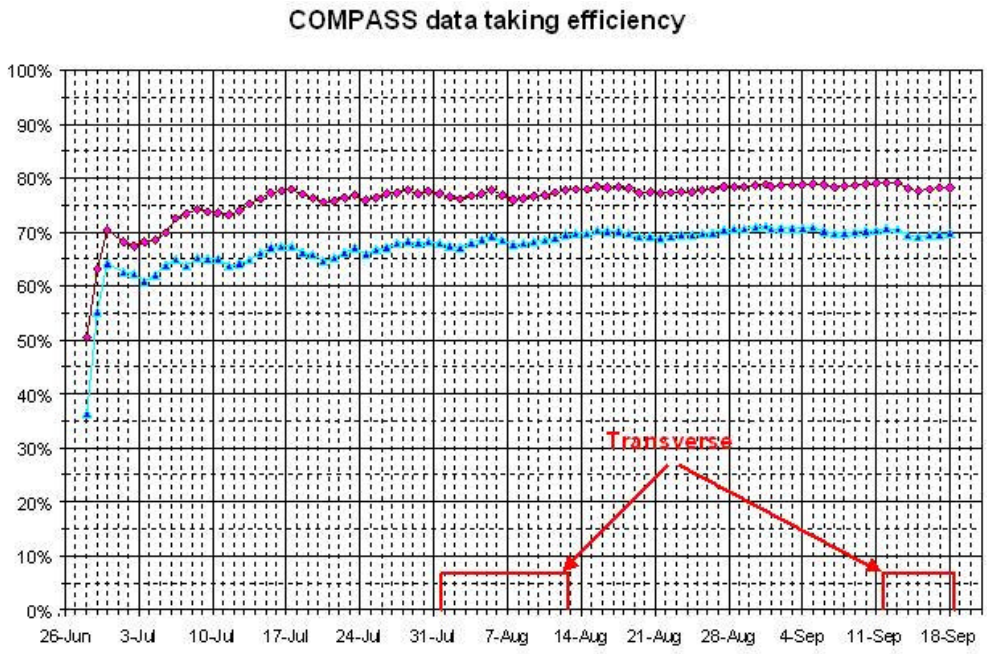

Fig. 36: COMPASS data-taking efficiency during the year 2002 run. The upper curve indicates the integral spectrometer efficiency, the lower curve the integral spectrometer efficiency folded with the SPS efficiency.

The present status can be summarised as follows: the system was started with heavy support from CERN/IT division, several sub-systems are included, but only basic functionality is presently implemented; system optimisation is certainly required to make it more stable and faster.

9.2 The on-line data monitoring system

An up-to-date on-line data monitoring system in COMPASS has been obtained with the COOOL software package written in C^{++} and built on ROOT libraries. The data decoding libraries are shared with the off-line data analysis package. The data, directly copied from the DAQ farm (more precisely from the event builder PCs), are analysed at a typical rate of ~ 150 (over $\sim 25\,000$) events per burst. Histograms, two-dimensional plots and tables are produced and information correlation as well as on-line cuts can be applied.

The data monitoring is complemented by the MurphyTV package which, by checking data rates and formats from the different hardware sources, allows the prompt diagnostic of the read-out systems.

9.3 The electronic log-book

The electronic log-book, filled on-line by the shift crew during the experiment run, completely replaces the old style paper log-book. Information and comments can be introduced; it is also possible to paste in plots and tables from the on-line monitoring system; data taking information (such as run number, target polarization, number of collected events, information from the SPS) is automatically transferred to the log-book for each 'run' (lasting typically 30 minutes) together with a basic set of monitoring histograms. Collaboration members at CERN can access the information at any time via the world-wide web.

10. CONCLUSIONS

It has been shown that the COMPASS initial lay-out is almost completely implemented and working, while some detector systems are richer than foreseen (scintillating fibres hodoscopes, MWPC stations

and SDC drift chambers). The access to the high Q^2 region, not possible with the foreseen initial set-up, has been opened with the installation of two large-sized W4-5 drift chamber stations (more stations are expected for the 2003 run) and two large-sized trigger hodoscopes.

A few days after the end of the 2002 run, the best summary of the spectrometer performances is given by the figures for the data taking efficiency, shown in Fig. 36. An inspection of the plot clearly indicates an increasing efficiency during the first weeks of data taking and fairly stable performance in the second part of the run period. The mean spectrometer efficiency over the 2002 run is almost 80%; this value, folded with the SPS accelerator efficiency, results in $\sim 70\%$ global efficiency of COMPASS data taking. These performances for efficiency, typical of experiments in operation for many years, demonstrate a largely successful 2002 run.

References

[1] The COMPASS Collaboration, *Common muon and proton apparatus for structure and spectroscopy*, Proposal to the CERN SPSLC, CERN/SPSLC/ 96-14, SPSC/P 297, March 1, 1996 and addendum, CERN/SPSLC/96-30, SPSLC/P 297 Add. 1, May 20, 1996.

[2] J. Ball *et al.*, "First results of the large COMPASS ^{6}LiD polarized target", Nucl. Instrum. Meth. A **498** (2003) 101.

[3] D. Adams *et al.*, Nucl. Instrum. Meth. A **437** (1999) 23.

[4] J. Bisplinghoff *et al.*, Nucl. Instrum. Meth. A **490** (2002) 101.

[5] H. Angerer *et al.*, "Present Status Of Silicon Detectors in COMPASS", Nucl. Instrum. Meth. **512** (2003) 229.

[6] D. Thers *et al.*, Nucl. Instrum. Meth. A **461** (2001) 29;
A. Magnon *et al.*, Nucl. Instrum. Meth. A **469** (2001) 133;
Ph. Abbon *et al.*, Nucl. Instrum. Meth. A **478** (2002) 210.

[7] F. Sauli *et al.*, Nucl. Instrum. Meth. A **386** (1997) 531.

[8] S. Bachmann *et al.*, Nucl. Instrum. Meth. A **470** (2001) 548;
B. Ketzer *et al.*, IEEE Trans. Nucl. Sci. **48** (2001) 1065;
B. Ketzer *et al.*, IEEE Trans. Nucl. Sci. **49** (2002) 2403;
C. Altunbas *et al.*, Nucl. Instrum. Meth. A **490** (2002) 177;
B. Ketzer *et al.*, Nucl. Instrum. Meth. A **494** (2002) 142.

[9] V.N. Bychkov *et al.*, Physics of Particles and Nuclei, Letters, **2**[111] (2002) 64.

[10] E. Albrecht *et al.*, "COMPASS RICH-1", Nucl. Instrum. Meth. A **504** (2003) 354;
G. Baum *et al.*, "RICHONE: a software package for the analysis of COMPASS RICH-1 data", Nucl. Instrum. Meth. A **502** (2003) 315–317;
E. Albrecht *et al.*, "The mirror system of COMPASS RICH-1", Nucl. Instrum. Meth. A **502** (2003) 236;
E. Albrecht *et al.*, "The radiator gas and the gas system of COMPASS RICH-1", Nucl. Instrum. Meth. A **502** (2003) 266.

[11] RD26 Collaboration, status reports: CERN/DRDC 93-36, 94-49, 96-20.

[12] The ALICE Collaboration, Technical Design Report of the High Momentum Particle Identification Detector, CERN/LHCC 98-19, ALICE TDR 1, 14 August, 1998.

[13] F. Piuz, “Rich imaging Cherenkov system based on gaseous photo-detectors: trends and limitations”, Nucl. Instrum. Meth. A **502** (2003) 76.

[14] A. Braem *et al.*, “Technology of photo-cathode production”, Nucl. Instrum. Meth. A **502** (2003) 205.

[15] H. Fischer *et al.*, IEEE Trans. Nucl. Sci., **49** (2002) 443.

[16] H. Fischer *et al.*, Nucl. Instrum. Meth. A **461** (2001) 507.

[17] G. Baum *et al.*, Nucl. Instrum. Meth. A **433** (1999) 426;
G. Baum *et al.*, “The COMPASS RICH-1 read-out system”, Nucl. Instrum. Meth. A **502** (2003) 246.

PROSPECTS FOR THE COMPASS 'MUON' PROGRAMME

Alain Magnon
CEA Saclay, SPhN-DAPNIA-DSM, F91191 Gif-sur-Yvette, France

Abstract
COMPASS started to take data in 2002 with a recently completed new spectrometer using the longitudinally polarized 160 GeV muon beam of the CERN SPS and a solid polarized target filled with ^{6}LiD. A preliminary look at data allows us to draw projections on the statistical errors which could be obtained in the near future for the gluon polarization $\Delta g/g$ and the transverse spin structure function h_1.

1. INTRODUCTION

The present objectives of the COMPASS experiment which has started with the muon beam programme are the measurement of the polarization of gluons $\Delta g/g$ within polarized nucleons, the measurement of the still unknown transverse spin structure function h_1, the measurement of lambda polarization, and the measurement of the inclusive and semi-inclusive longitudinal spin observables g_1 and Δq. The spectrometer was commissioned during 2001 and the first serious data taking started in 2002. Owing to some delays or technical difficulties, some major pieces of equipment were not available and back-up solutions were used, leading to a reduced angular acceptance. In addition, the financial difficulties which CERN has encountered with the LHC construction have a serious implication on the total amount of accelerator time available per year. This report gives an update on the overall figure of merit of the experiment based on recent simulations and also on a preliminary analysis of the 2002 data. The expected statistical errors on $\Delta g/g$ and h_1 are given. Expected progress but also handicaps are discussed. Finally, in view of the SPS shutdown in 2005, a possible strategy for data taking in 2003 and 2004 is presented.

2. PROGRAMME WITH POLARIZED MUONS

If one uses longitudinally polarized target and beam, the measurement of the longitudinal spin asymmetry in the production of D^0 or $\mathrm{D}^\star$ mesons [1] or in the production of a pair of hadrons with high transverse momentum P_T [2] allows the determination of $\Delta g/g$. The importance of the RICH detector performances should be underlined at this point since the RICH is essential to perform the K identification necessary to single out efficiently D^0 and $\mathrm{D}^\star$. The first spin structure function g_1 can be measured by detecting the scattered muon μ' only. If one detects in addition at least one produced hadron, one can reach the polarized parton distribution functions Δq. All these channels can be obtained simultaneously.

If one uses a transversely polarized target, the measurement of the azimuthal modulation of the single hadron cross-section can lead to the transverse spin structure function h_1, a yet unknown quantity.

3. COMPASS MODIFIED LAS SPECTROMETER

The year 2001 was almost entirely devoted to the commissioning of the present version of the spectrometer. All equipment was installed and their properties could be studied. However, two difficulties remained in 2002: the large bore radius superconducting magnet which matches the ≈ 250 mrad maximum opening angle of the spectrometer could still not be delivered to COMPASS; the construction of the straw trackers which provide the Large Area Tracking (LAT) downstream of the Large Acceptance Spectrometer (LAS) was delayed due to unexpected difficulties, consequently, only about one half of the straw trackers were available.

A backup solution was worked out, as shown in Fig. 1. It consists of using the SMC magnet which has similar properties but a reduced opening angle of ≈ 100 mrad instead of the COMPASS magnet

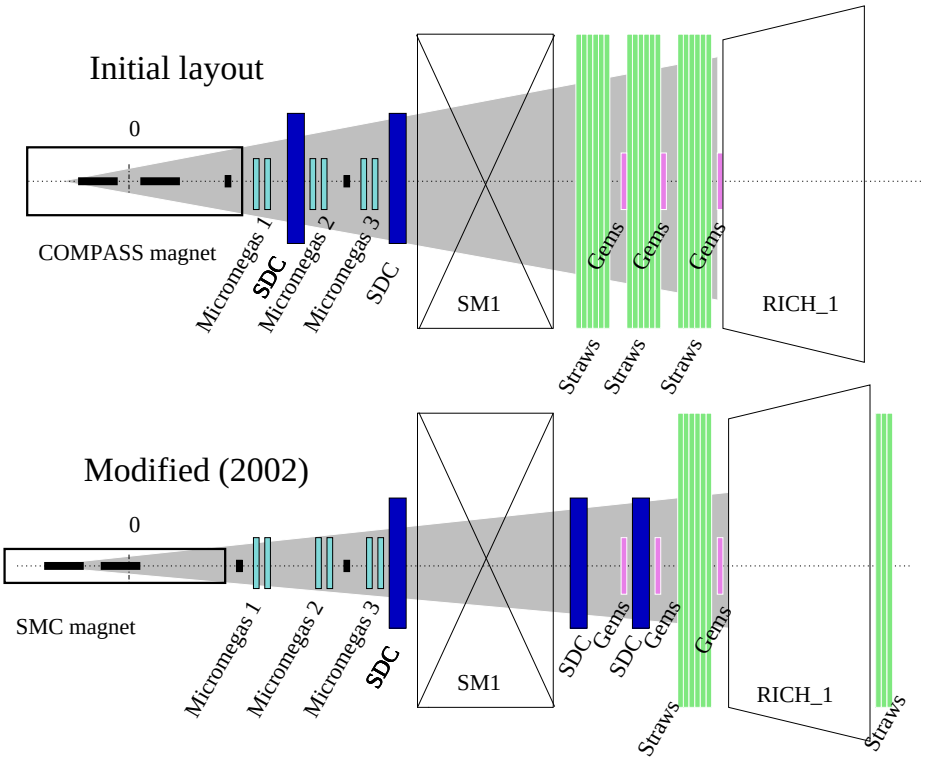

Fig. 1: The nominal and modified setups for the Large Acceptance Spectrometer.

and replacing the missing straws by the two larger-area Drift Chambers (DCs) foreseen for the upstream section of the LAS. This implied the construction of a third DC for the upstream section of the LAS. As shown in Fig. 1 it turns out that, in spite of their reduced area compared to the straws (DCs are $= 1.2 \times 1.2$ m^2, straws are $= 2.7 \times 3.2$ m^2), the DCs match the angular opening of the SMC magnet. Finally, due (mainly) to constraints in detector construction it was found that the total amount of material seen by the scattered particles was larger that initially foreseen. This resulted in a degradation of the mass resolution for both the D^0 and D^* channels and a proportional increase of the background-to-signal ratio for their detection. These changes had to be validated by a re-estimate of the overall figure of merit.

4. STATISTICAL ERROR ON $\Delta g/g$ AND OPTIMUM MUON ENERGY

As described in the COMPASS proposal [1] the gluon distribution is probed through the photon gluon fusion (PGF) process, $\gamma + g \rightarrow q + \bar{q}$. This process can be signed by the production of open charm and the spin asymmetry of that process provides a measurement of $\Delta g/g$. A new evaluation of the statistical uncertainty on $\Delta g/g$ using the $\mathrm{D}^0 \rightarrow \mathrm{K}\pi$ and $\mathrm{D}^\star \rightarrow \mathrm{D}^0\pi_s \rightarrow \mathrm{K}\pi\pi_s$ channels was performed [3]. The simulation has the following features:

1. Open charm events are produced using Aroma 2.4. Since Aroma is not supposed to predict correctly the absolute cross-section, a renormalization factor K is applied to the muon production cross-section. Using the measured photoproduction cross-sections, we estimate $K = 1.66$ for a mass of the charmed quark $m_c = 1.34$ GeV.
2. Combinatorial background events are produced using Pythia 6.1. This new version of Pythia allows the simulation of the whole Q^2 range from quasi real photoproduction to DIS. The rate of background is found compatible with the proposal within 20%.
3. The resolution in the D^0 mass and in the difference $\Delta M = M_{\mathrm{D}^\star} - M_{\mathrm{D}^0}$ between the $\mathrm{D}^\star$ and D^0 masses is evaluated analytically event by event using a procedure developed previously [4].

The average δM_{D^0} is 15.8, 17.5 and 18.1 MeV for an incident muon energy E_μ of 100, 160 and 190 GeV, respectively. The average $\delta\Delta M$ is 3.73, 3.83 and 3.89 MeV correspondingly. Note that the variation of $\delta\Delta M$ with beam energy is very weak since this resolution is dominated by the contribution of multiple scattering in the target.

4. In the standard asymmetry method one computes $A = (N^{\uparrow\downarrow} - N^{\uparrow\uparrow})/(N^{\uparrow\downarrow} + N^{\uparrow\uparrow})$, the raw asymmetry in the number of open charm events where the longitudinal polarizations of the beam and the target are either antiparallel or parallel. $\Delta g/g$ is obtained as:

$$\Delta g/g = A(1 + B/S)/(P_\mu P_T f\langle a_{LL}\rangle), \tag{1}$$

where B is the number of combinatorial background events, S the number of signal (D^0 or $\mathrm{D}^\star$), P_μ and P_T are the beam and target polarizations respectively, f is the dilution factor and $\langle a_{LL}\rangle$ the mean value of the PGF analysing power. The quantities a_{LL} and B/S have large variations over the spectrometer acceptance. In order to improve the statistical efficiency it is proposed to take these variations into account by weighting each event with the quantity $w = a_{LL}/(1 + B/S)$ which gives:

$$\Delta g/g = (1/P_T P_\mu f)(\sum_i^{\uparrow\downarrow} w_i - \sum_i^{\uparrow\uparrow} w_i)/(\sum_i^{\uparrow\downarrow} w_i^2 + \sum_i^{\uparrow\uparrow} w_i^2). \tag{2}$$

This weighting method is equivalent to gaining a factor $\langle w^2\rangle/\langle w\rangle^2$, in terms of the number of events. In our case, due to the fact that a_{LL} can even change sign over the acceptance, this factor is quite large, in the range of 1.5–2 depending on acceptance and beam energy.

A luminosity of 43 pb^{-1} per day corresponding to $\approx 2 \times 10^8\mu$/ 5 s spill ($\approx 1.4 \times 10^8\mu$ at 190 GeV) is assumed. The global data taking and reconstruction efficiency $\epsilon_{overall}$ is taken to be 0.25, as in the proposal. Since data analysis has just started, this critical factor is still poorly known. In order to derive estimates of the full duration of data taking for a given accuracy, it is convenient to use a time unit which incorporates $\epsilon_{overall}$ which we call $days@100\%$.

Table 1: Statistical error on $\Delta g/g$ for both D^0 and $\mathrm{D}^\star$ channels for different setups and beam energies. The luminosity corresponds to 100 days, and an overall efficiency of 25%. The number from the proposal does not involve the 'weighting method' and is rescaled to 100 days at 25%.

	$\sigma(\Delta g/g)$ D^0			$\sigma(\Delta g/g)$ $\mathrm{D}^\star$		
E_μ GeV	100	160	190	100	160	190
Proposal	0.31			0.26		
Nominal setup	0.30	0.22	0.25	0.25	0.20	0.24
idem + SMC magnet	0.38	0.24	0.26	0.31	0.22	0.25
Modified setup	0.39	0.24	0.26	0.32	0.23	0.26

Table 1 gives the statistical resolution on $\Delta g/g$, assuming 100 days running at nominal luminosity and $\epsilon_{overall} = 0.25$ equivalent to 25 $days@100\%$ and using the weighting method [3]. In the proposal E_μ was fixed to 100 GeV and the weighting method was not applied. Energies of 160 GeV and 190 GeV were considered also because the Lorentz boost, which favours smaller angles, helps to compensate for the loss in angular acceptance. The line labelled 'Nominal setup' corresponds to the setup shown in the upper part of Fig. 1. The next line shows the effect of replacing the large-aperture COMPASS magnet by the SMC magnet. The last line corresponds to the 'Modified setup', shown in Fig. 1. It has three stations of Micromegas and one station of drift chambers (DC) upstream of SM1; three stations of GEMs, two DCs and one station of straws (replacing the three foreseen stations of straws) downstream of SM1. Note that one half-station of straws is positioned after the RICH to re-inforce tracking in that region.

At 100 GeV, the statistical loss due to acceptance reduction is significant for both the D^0 and the $\mathrm{D}^\star$ channels. This effect is reduced at 160 GeV and 190 GeV as expected. However, at 190 GeV, the SPS can only deliver $\approx 70\%$ of its maximum flux which results in an increase of the error compared to 160 GeV. Therefore, a beam energy of 160 GeV is optimum for the present Modified setup. The resulting statistical uncertainties on $\Delta g/g$ of 0.24 (0.23) for the $\mathrm{D}^0(\mathrm{D}^\star)$ channels should be compared to the initial values from the proposal of 0.31 (0.26). We conclude that the reduction in acceptance along with the degradation of the mass resolution is compensated by running at $E_\mu = 160$ GeV and calculating the spin asymmetry using a weighting method.

5. 2002 AND BEYOND, EXPECTED STATISTICS

5.1 $\Delta g/g$ from D^0 and $\mathrm{D}^\star$

In the proposal, it is assumed that COMPASS runs for 1.5 years with a ^{6}LiD target with two assumptions: The SPS delivers ≈ 150 days/year of beam for physics and the overall efficiency of the experiment is 0.25. This translates into an effective total running time of:

$$T = 1.5 \times 150 \times 0.25 = 56\ days@100\%. \tag{3}$$

Using the error estimates from Table 1 (Modified setup, $E_\mu = 160$ GeV), we obtain:

$$\sigma(\Delta g/g) = 0.160\ (\mathrm{D}^0), \quad \sigma\Delta g/g = 0.154\ (\mathrm{D}^\star), \quad \sigma(\Delta g/g) = 0.11\ (\mathrm{D}^0\&\mathrm{D}^\star). \tag{4}$$

In 2002, the SPS delivered 112 days of beam out of which 36 days were used for preparing the spectrometer and the remaining time $T = 76$ days was shared between longitudinal and transverse data taking: $T = 76 = 57_L + 19_T$ days. The overall efficiency $\epsilon_{overall}$ can be decomposed as:

$$\epsilon_{overall} = \epsilon_{(data\_taking)} \times \epsilon_{(tracking)} \times \epsilon_{(RICH)}. \tag{5}$$

Where:

1. $\epsilon_{(data\_taking)}$ accounts for the beam availability and data taking efficiency. In 2002, we had $\epsilon_{(data\_taking)} = 0.59$.
2. $\epsilon_{(tracking)}$ accounts for detector and trigger efficiencies, track (including beam tracks) reconstruction efficiencies and data acquisition dead time. Given the preliminary status of data analysis we obtain $\epsilon_{(tracking)} \approx 0.1$ for events having a scattered muon and two hadrons originating from a D^0. For events having only a scattered muon, $\epsilon_{(tracking)}$ ranges from 0.3 to 0.4.
3. $\epsilon_{(RICH)}$ represents the fraction of kaons, identified as kaons by the RICH. The present number is ≈ 0.30.

Awaiting improved figures, we presently have: $\epsilon_{overall} \approx 0.015$. Note that this does not account for the presence of impurities in the RICH kaon sample which deteriorates the S/B ratio. When measuring spin asymmetries, data may be rejected because of instabilities which should be accounted for by a still unknown factor.

Given the present $\epsilon_{overall}$ we obtain $T_L = 0.85\ days@100\%$ for the 2002 longitudinal data taking which would lead, for $\Delta g/g$, to a result of **marginal** significance.

To illustrate the importance of $\epsilon_{overall}$ and set the goal for the near future, we assume the following scenario for 2003 and 2004: The SPS delivers 105 days each year, the preparation of data taking is restricted to 15 days of SPS beam and we run about 20% of the time with a transversely polarized target. Making the most pessimistic assumption that $\epsilon_{overall}$ does not change, the effective total running time for 2002, 2003 and 2004 would be:

$$T = (57 + 72 + 72) \times 0.015 = 3.0\ days@100\% \tag{6}$$

which translates into:

$$\sigma(\Delta g/g) = 0.48 \ (\mathrm{D}^0\&\mathrm{D}^\star). \tag{7}$$

To reach the proposal's error: $\sigma(\Delta g/g) = 0.11$, $\epsilon_{overall}$ **needs to be enlarged** by a factor of $\simeq 20$ which would correspond, for example, to having:

$$\epsilon_{(data\_taking)} \approx 0.8, \quad \epsilon_{(tracking)} \approx 0.7, \quad \epsilon_{(RICH)} \approx 0.6. \tag{8}$$

This shows the utmost necessity to **reduce** the spectrometer setup time, given the **already reduced** yearly beam allocation and to **improve by all possible means** $\epsilon_{(tracking)}$ and $\epsilon_{(RICH)}$.

5.2 $\Delta g/g$ from high P_T

The analysis of events containing a scattered muon and two hadrons with a high P_T is still in a primitive phase for the 2002 COMPASS data. However, an analysis of similar events obtained in the previous SMC experiment has almost been completed [5]. From these data, the statistical error on $\Delta g/g$ is about 0.5. It allows us, by normalizing to the number of reconstructed events with high P_T, to provide an estimate of the expected statistical error from the COMPASS data. With a cut $Q^2 > 1$ GeV$^2/c^2$ applied to the data, this procedure gives, for the 57 days of longitudinal data taking in 2002:

$$\sigma(\Delta g/g) \approx 0.4 \ (\text{high } P_T \text{ hadrons}, \ Q^2 > 1 \ \mathrm{GeV}^2/c^2). \tag{9}$$

Releasing this cut increases the statistics by a factor ≈ 10 which results in:

$$\sigma(\Delta g/g) \approx 0.13 \ (\text{high } P_T \text{ hadrons}). \tag{10}$$

5.3 Transversity

COMPASS plans to measure the transverse polarized parton distribution $\Delta_T q(x)$. This quantity can be viewed as the counterpart of the longitudinal polarized distribution $\Delta q(x)$ for a nucleon polarized perpendicular to the incoming lepton direction. Unlike $\Delta q(x)$, it cannot be accessed by inclusive DIS. However, semi-inclusive DIS provides the possibility to measure $\Delta_T q(x)$ via the azimuthal dependence of the hadron yield with the so-called Collins angle ϕ_c. This dependence involves the analysing power a_c which is still unmeasured. The measurement of transversity has been simulated using Lepto 6.5. Since nothing is known about $\Delta_T q(x)$, the simulation assumes $\Delta_T q(x) = \Delta q(x)$. For a_c, a linear dependence with the fraction z of the virtual photon energy transferred to the hadron is assumed, $a_c = 0.75 \times z$. In addition, the following kinematical cuts are applied, $Q^2 > 1 \ \mathrm{GeV}^2/c^2$, $0.1 \leq y \leq 0.95$ and $z \geq 0.3$.

Figure 2 shows the expected errors on the quantity $xh_1 = x\Sigma_q e_q^2 \Delta_T q(x)$, (the equivalent of $xg_1(x)$ for transversity) for 30 days of data taking, for both proton and deuteron, assuming $\epsilon_{overall} = 0.25$, i.e. $7.5 \ days@100\%$. The simulation was performed for both COMPASS and SMC target magnets. At high x, hadrons are produced at large angle and the reduced acceptance of the SMC magnet has a strong effect on the counting rate.

For events with only one hadron, our present estimate is $\epsilon_{(overall)} = \epsilon_{(datataking)} \times \epsilon_{(tracking)} = 0.59 \times 0.14 = 0.08$. Given the previous assumptions for both $\Delta_T q$ and a_c and assuming we still use the SMC magnet, a significant measurement of transversity (i.e. a $\simeq 6\sigma$ signal) could be performed if one spends 20% of the total allotted time with transverse spin.

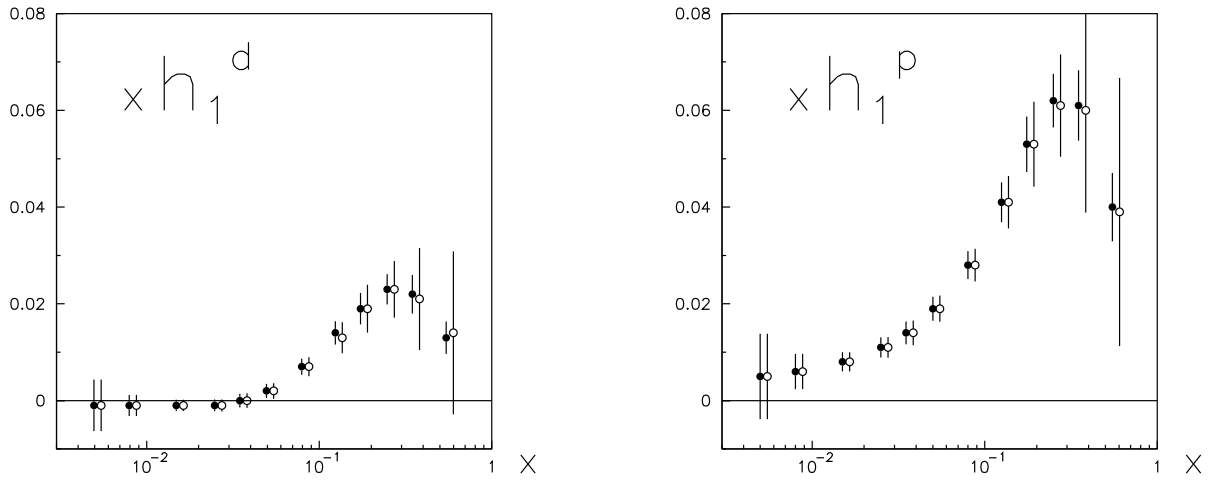

Fig. 2: Expected errors on $xh_1(x)$ for deuteron (left) and proton (right), for COMPASS (full circle) and SMC (open circle) polarized target magnets at $E_\mu = 160$ GeV.

6. CONCLUSION

COMPASS started to take data in 2002, using the 160 GeV polarized muon beam at the SPS and a polarized target which provided both longitudinal and transverse nucleon polarizations. The focus is presently the measurement of $\Delta g/g$, the gluon polarization within longitudinally polarized nucleons. Preliminary data were also taken with transverse polarization to access the yet unknown transverse polarized parton distribution $\Delta_T q$. The figure of merit of the experiment for the muon programme has been updated to account for modifications in the apparatus, mainly a reduction in the angular acceptance, and also a reduction in the SPS beam allocation compared to that of the proposal. It shows that a significant physics result on $\Delta g/g$ is within reach before the SPS shut down in 2005. However, this requires imperatively to improve the overall efficiency of our experiment by an order of magnitude if we compare to the present estimate which follows the 2002 data taking. The recent progress achieved in the data analysis gives an indication that such a goal is not unrealistic. However, it demands that both on the hardware and on the software side, all efforts are focused on understanding and improving, possibly to their ultimate limits, the many critical factors which enter in this figure of merit.

References

[1] CERN/SPSLC 96-14, SPSC/P 297.

[2] S. Bravar, D. von Harrach and A. Kotzinian, Phys. Lett. B **421** (1998) 349.

[3] J.-M. Le Goff, COMPASS note 2002-02.

[4] J.-M. Le Goff, COMPASS note 2000-13.

[5] E. Rondio *et al.*, COMPASS private communication.

[6] J.-M. Le Goff, Nucl. Phys. A **711** (2002) 56c.

THE PHENOMENOLOGY OF GLUEBALL AND HYBRID MESONS

Stephen Godfrey
Department of Physics, Carleton University, Ottawa K1S 5B6 CANADA
DESY, Deutsches Elektronen-Synchrotron, D22603 Hamburg, GERMANY

Abstract
The existence of non-$q\bar{q}$ hadrons such as glueballs and hybrids is one of the most important qualitative questions in QCD. The COMPASS experiment offers the possibility to unambiguously identify such states and map out the glueball and hybrid spectrum. In this review I discuss the expected properties of glueballs and hybrids and how they might be produced and studied by the COMPASS Collaboration.

1. INTRODUCTION

A fundamental qualitative question in the Standard Model is the understanding of quark and gluon confinement in Quantum Chromodynamics. Meson spectroscopy offers the ideal laboratory to understand this question which is intimately related to the question of "How does glue manifest itself in the soft QCD regime?" [1] Models of hadron structure predict new forms of hadronic matter with explicit glue degrees of freedom: Glueballs and Hybrids. The former is a type of hadron with no valence quark content, only glue, while the latter has quarks and antiquarks with an excited gluonic degree of freedom. In addition, multiquark states are also expected. With all these ingredients, the physical spectrum is expected to be very complicated.

Over the last decade there has been considerable theoretical progress in calculating hadron properties from first principles using Lattice QCD [2,3]. This approach gives a good description of the observed spectrum of heavy quarkonium and supports the potential model description, at least for the case of heavy quarkonium.

Lattice QCD now has reasonably robust predictions for glueball masses [2, 4, 5], albeit in the quenched approximation. Although there is growing evidence for the observation of glueballs it has required considerable theoretical analysis to argue that there is an extra isoscalar $J^{PC} = 0^{++}$ state in the meson spectrum. The problem is that a glueball with quantum numbers consistent with those of conventional $q\bar{q}$ mesons will mix with the $q\bar{q}$ states complicating the analysis of their couplings [6]. There is a strong need to unambiguously observe glueballs and perform detailed analysis of their properties as a rigorous test of QCD. A deeper reason for these studies is that lattice field theory has become an important tool for understanding strongly coupled field theories. QCD is the one place where we can test our calculations against experiment so that agreement with measurements will give us the confidence that we really can do nonperturbative field theory calculations.

Hybrid mesons pose another important test of our understanding of QCD. It is now clear that lattice QCD calculations support the flux tube picture of hadron dynamics, at least in the heavy quark limit [7]. Excitations of the flux tube are described by non-trivial representations of the flux tube symmetry [8]. A good analogy is that of the electron wavefunctions in diatomic molecules. In this picture, conventional mesons are described by a $q\bar{q}$ potential given by the lowest adiabatic surface and hybrids are described by a $q\bar{q}$ potential given by higher adiabatic surfaces arising from different flux tube symmetries. It is necessary to map out these higher adiabatic surfaces to test our understanding of 'soft QCD'. To do so requires the observation of enough states to map out these excited surfaces.

Although lattice calculations are maturing, giving more reliable results for masses, it will be some time before they can reliably describe decay and production couplings. We therefore rely on phenomenological models to describe their properties and build up a physical picture needed to help find these states.

[1] For a more detailed review on this subject see Ref. [1].

2. CONVENTIONAL MESONS

To search for glueballs and hybrids it is necessary to have reliable descriptions of conventional mesons [9–11]. Conventional mesons are composed of a quark–antiquark pair. The various quark flavours are combined with antiquarks to form the different mesons. The meson quantum numbers are characterized by a given J^{PC}. In the constituent quark model the quark and antiquark spins are combined to give a total spin with S =0, 1. S is then combined with the orbital angular momentum L to give total angular momentum $J = L + S$. Parity is given by $(-1)^{L+1}$ and charge conjugation by $C = (-1)^{L+S}$. This results in allowed quantum numbers, for example, $J^{PC} = 0^{-+}$, 1^{--}, 1^{+-}, 0^{++}, $2^{++}\ldots$ while $J^{PC} = 0^{--}$, 0^{+-}, 1^{-+}, 2^{+-} are forbidden by the quark model and are generally referred to as exotics.

Although the goal is to discover non $q\bar{q}$ states we can't ignore conventional mesons. We need to understand them quite well if we are to disentangle the non-$q\bar{q}$ states we seek from conventional $q\bar{q}$ mesons. We can do this because the couplings of states are sensitive to their internal structure. Strong decays are modelled by the $^3P_0$ model and by the flux-tube breaking model [10, 11] while electromagnetic couplings are quite well understood for heavy quarkonium and qualitatively for light quark mesons. The electromagnetic couplings can be measured in 2γ couplings and single photon transitions. The latter can be measured via Primakoff production by COMPASS.

3. GLUEBALLS

The predictions of glueball masses by Lattice QCD are becoming fairly robust [3]. The results of a Lattice QCD calculation of the glueball spectrum by Morningstar and Peardon [5] are given in Fig. 1. The lowest mass glueballs have conventional quantum numbers [4]: $M_{0^{++}} \sim 1.6$ GeV, $M_{2^{++}} \sim 2.3$ GeV $M_{0^{-+}} \sim 2.5$ GeV while the lowest lying glueballs with exotic quantum numbers, $J^{PC} = 0^{+-}$, 2^{+-}, and 1^{-+}, are much higher in mass. It is therefore difficult to produce glueballs with exotic quantum numbers. To disentangle glueballs with conventional quantum numbers from a dense background of conventional states is a painstaking task.

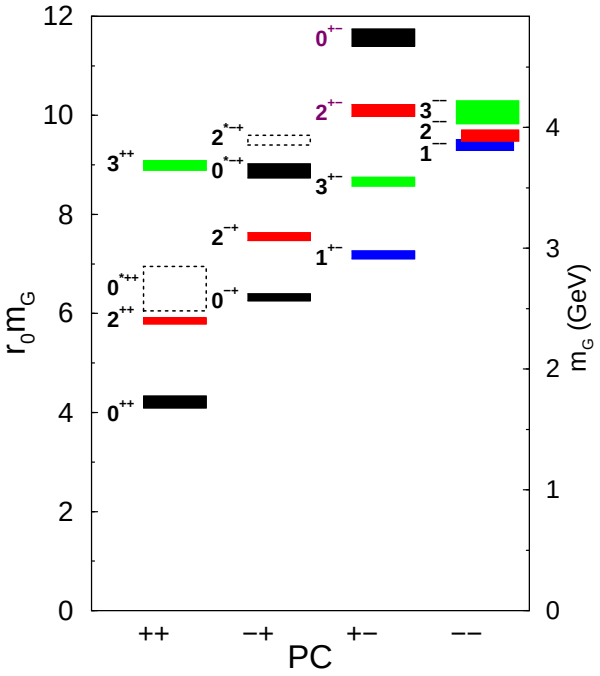

Fig. 1: The mass of the glueball states. The scale is set by r_0 with $1/r_0 = 410(20)$ MeV. From Morningstar and Peardon [5].

3.1 Glueball decays

We expect glueball decays to have flavour symmetric couplings to final-state hadrons:

$$\frac{\Gamma(G \to \pi\pi :\ K\bar{K} :\ \eta\eta :\ \eta\eta' :\ \eta'\eta')}{\text{Phase Space}} \simeq 3:4:1:0:1. \tag{1}$$

The situation is complicated by mixing with $q\bar{q}$ and $q\bar{q}q\bar{q}$ so the physical states are linear combinations:

$$|f_0\rangle = \alpha|n\bar{n}\rangle + \beta|s\bar{s}\rangle + \gamma|G\rangle + \delta|q\bar{q}q\bar{q}\rangle. \tag{2}$$

Mixing will both shift the unquenched glueball masses and distort the naive patterns of couplings given by Eq. (1) [6, 12].

Meson properties can be used to extract the mixings and understand the underlying dynamics. For example, central production of the isoscalar scalar mesons has found the ratio of partial widths $\Gamma(K\bar{K})/\Gamma(\pi\pi)$ to be [13]:

$$\begin{array}{lll} f_0(1370) & < 1 & (0.5 \pm 0.2) \\ f_0(1500) & \ll 1 & (0.3 \pm 0.1) \\ f_0(1710) & \gg 1 & (5.5 \pm 0.8) \end{array} \tag{3}$$

Relating this information to theoretical expectations, Close and Kirk find [12]:

$$\begin{array}{lcl} |f_0(1370)\rangle & = & -0.79|n\bar{n}\rangle - 0.13|s\bar{s}\rangle + 0.60|G\rangle \\ |f_0(1500)\rangle & = & -0.62|n\bar{n}\rangle + 0.37|s\bar{s}\rangle - 0.69|G\rangle \\ |f_0(1710)\rangle & = & +0.14|n\bar{n}\rangle + 0.9|s\bar{s}\rangle + 0.39|G\rangle. \end{array} \tag{4}$$

A similar analysis was done by Amsler [14]. The point is not the details of a specific mixing calculation but that mixing is an important consideration that must be taken into account in the phenomenology.

Before proceeding to hadronic production of glueballs we mention that two-photon couplings are a sensitive probe of $q\bar{q}$ content [12]. The L3 Collaboration at LEP sees the $f_0(1380)$ and $f_0(1710)$ in $\gamma\gamma \to K\bar{K}$ but not the $f_0(1500)$. Because gluons do not carry electric charge, glueball production should be suppressed in $\gamma\gamma$ collisions. Quite some time ago Chanowitz [15] quantified this in a parameter he called 'stickiness' given by the ratio of meson production in radiative J/ψ decay to two-photon couplings:

$$S = \frac{\Gamma(J/\psi \to \gamma X)}{PS(J/\psi \to \gamma X)} \times \frac{PS(\gamma\gamma \to X)}{\Gamma(\gamma\gamma \to X)} \tag{5}$$

where PS denotes phase space. A large value of S is supposed to reflect an enhanced glue content.

3.2 Glueball production

There are three processes which are touted as good places to look for glueballs:

1. $J/\psi \to \gamma X$
2. $p\bar{p}$ annihilation
3. $pp \to p_f(G)p_s$ central production

It is the latter process that is relevant to COMPASS. Central production is understood to proceed via gluonic pomeron exchange. It is expected that glueball production has to compete with $q\bar{q}$ production. However, a kinematic filter has been proposed which appears to suppress established $q\bar{q}$ states when in a P-wave or higher wave [16].

In the central production process:

$$pp \to p_f(G)p_s \tag{6}$$

p_s and p_f represent the slowest and fastest outgoing protons. Central production is believed to be dominated by double *pomeron* exchange. The pomeron is believed to have a large gluonic content. Folklore assumed that the pomeron has $J^{PC} = 0^{++}$ quantum numbers and therefore gives rise to a flat distribution. But the distribution turns out not to be flat and is well modelled assuming a $J = 1$ exchange particle [17]. In other words the pomeron transforms as a non-conserved vector current. Data from CERN experiment WA102 appears to support this hypothesis.

Close and Kirk [16] have found a kinematic filter that seems to suppress established $q\bar{q}$ states when they are in P and higher waves. The pattern of resonances depends on the vector difference of the transverse momentum recoil of the final-state protons:

$$dP_T = |\vec{k}_{T_1} - \vec{k}_{T_2}|. \tag{7}$$

For dP_T large, the well-established $q\bar{q}$ states are prominent while for dP_T small, the established $q\bar{q}$ states are suppressed and the $f_0(1500)$, $f_0(1710)$, and $f_0(980)$ survive.

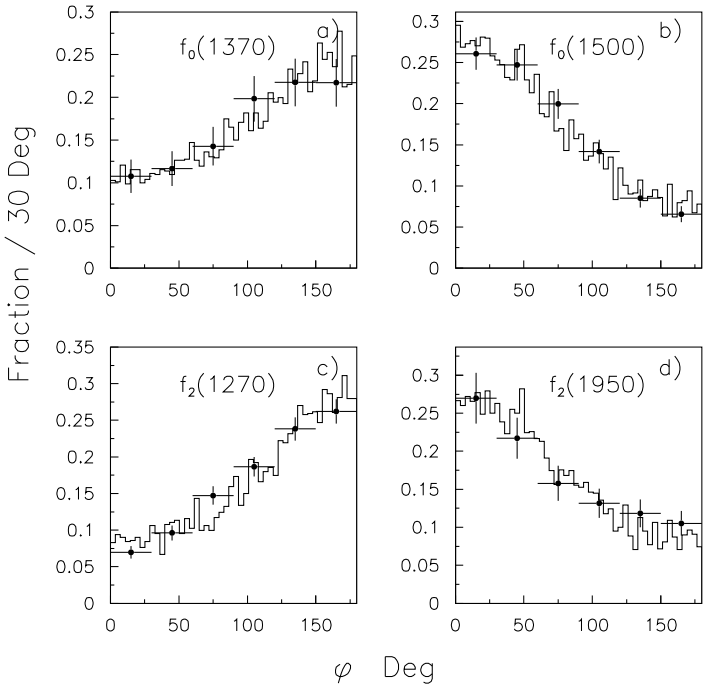

Fig. 2: The ϕ distributions for (a) $f_0(1370)$, (b) $f_0(1500)$, (c) $f_2(1270)$, (d) $f_2(1950)$ for the data (dots) and the Monte Carlo (histogram). From Close and Schuler [18].

Close, Kirk, and Schuler give a good account of the data by modelling the pomeron as a non-conserved vector exchange [18]. They find that the ϕ angular distribution, the angle between the k_T vectors, appears to distinguish between the production of different states [17, 18]. In particular:

0^{-+} Parity requires the vector pomeron to be transversely polarized. The distribution peaks at 90°.

1^{++} One pomeron is transverse and the other longitudinal and the distribution peaks at 180°.

2^{-+} Similar to the 0^{-+} case but peaks at 0°. Helicity 2 is suppressed by Bose statistics.

2^{++} Established states peak at 180° while the $f_2(1950)$ peaks at 0°.

0^{-+} Some states peak at 0° while others are spread out:

- $f_0(1500)$, $f_0(1710)$, and $f_0(980)$ peak at small ϕ.
- $f_0(1370)$ peaks at large ϕ.

The fact that the $f_0(1370)$ and $f_0(1500)$ have different ϕ dependence indicates that it is not just a J dependent phenomena [19, 20].

The 0^{++} and 2^{++} expect both TT and LL contributions. The differential cross-section is given by [18, 21]:

$$\frac{d\sigma}{d\phi} \sim \left[1 + \frac{\sqrt{t_1 t_2}}{\mu^2}\frac{a_t}{a_L}\cos\phi\right]^2 . \tag{8}$$

Differential cross-sections for scalar and tensor mesons are shown in Fig. 2 [18, 21]. Good fits to the distributions are obtained by varying $\mu^2 a_L/a_T$ with $\mu^2 a_L/a_T = -0.5\,\mathrm{GeV}^2$ for $f_0(1370)$, $= +0.7\,\mathrm{GeV}^2$ for $f_0(1500)$, $= -0.4\,\mathrm{GeV}^2$ for $f_2(1270)$, and $= +0.7\,\mathrm{GeV}^2$ for $f_0(1950)$. Thus, the ϕ distributions are fitted with only one parameter.

4. HYBRID MESONS

Hybrid mesons are defined as those in which the gluonic component is non-trivial. There are two types of hybrids; vibrational hybrids and topological hybrids. The hybrid spectrum is generated by generating effective potentials from adiabatically varying gluonic flux tubes. A given adiabatic surface corresponds to some string topology and excitation. This is illustrated in Fig. 3. In the flux-tube model the lowest excited adiabatic surface corresponds to transverse excitations of the flux tube.

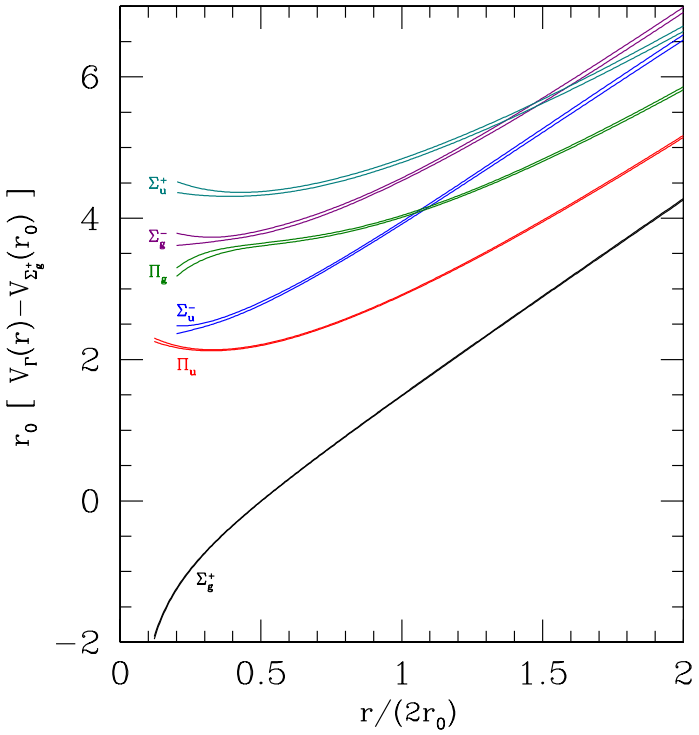

Fig. 3: A set of hybrid adiabatic surfaces for static central potentials. $\Lambda = \Sigma,\ \Pi,\ \Delta, \ldots$ corresponds to the magnitude of $J_{glue} = 0,\ 1,\ 2, \ldots$ projected onto the molecular axis. The superscript $= \pm$ corresponds to the even or oddness under reflections in a plane containing the molecular axis and the subscript u/g corresponds to odd/even charge conjugation plus spatial inversion about the midpoint. The familiar $q\bar{q}$ potential is labelled as Σ_g^+ and the first-excited potential is the Π_u so the lowest lying hybrid mesons should be based on this potential. The double lines on the excited surfaces indicate the calculational uncertainty in determining the potential. From Juge, Kuti and Morningstar [22].

While this picture is appropriate for heavy quarkonium it is not at all clear that it can be applied to light quark hybrids. Nevertheless, given that the constituent quark model works so well for light quarks, it is not unreasonable to also extend the flux tube description to light quarks. In the flux tube model the lowest mass hybrid mesons with light quark content have masses ~ 1.9 GeV [23–25]. There is a double degeneracy with $J^{PC} = 0^{+-}, 0^{-+}, 1^{+-}, 1^{-+}, 2^{+-}, 2^{-+}, 1^{++}, 1^{--}$ corresponding to the two transverse polarizations of the flux tube. The degeneracies are expected to be broken by the different excitation energies of the flux tube modes, spin dependent effects, and mixings with conventional $q\bar{q}$ states (and possibly $q\bar{q}q\bar{q}$). Lattice results are generally consistent with these predictions with $M(1^{-+}) \sim 1.9$ GeV, $M(0^{+-}) \sim 2.1$ GeV, and $M(2^{+-}) \sim 2.1$ GeV [26, 27].

4.1 Hybrid meson decays

Decay properties are a crucial tool in both directing exotic hybrid meson searches and distinguishing hybrids with conventional quantum numbers from conventional $q\bar{q}$ states. A general selection rule for hybrid decays, which appears to be universal to all models, is that to preserve the symmetries of quark and colour fields about the quarks, the Π_u hybrid must decay to a P-wave meson [28, 29]. In other words it cannot transfer angular momentum to relative angular momentum between final-state mesons but rather, to internal angular momentum of one of the final-state mesons. For the case of the 1^{-+} exotic the $\hat{\rho} \to b_1\pi,\ f_1\pi$ modes are expected to dominate.

To calculate hybrid properties we need to rely on models. We will use the results of the flux tube model [24, 30] which is based on strong coupling Hamiltonian lattice QCD. The degrees of freedom are quarks and flux-tubes. This model provides a unified framework for conventional hadrons, multiquark states, hybrids, and glueballs.

The flux-tube model predictions of Close and Page for the dominant decay widths of exotic hybrid mesons are given in Table 1 [30]. One can see that the $\hat{a}_0$ and $\hat{f}_0'$ are too broad to be observed as resonances. The $\hat{\omega}_1$ decays to $a_1\pi$ and K_1K as does the $\hat{\phi}_1$. These final states are notoriously difficult to reconstruct. Thus the best bets for finding exotic hybrids are the decays $\hat{\rho}_1 \to [b_1\pi]_S,\ [f_1\pi]_S$ with $\Gamma \simeq 170$ MeV. This is why the $\hat{\rho}$ is the focus of so much attention in hybrid searches. The narrow $f_1(1285)$ provides a particularly useful tag in $\hat{\rho} \to \pi f_1$. Although there is a general consensus among models with respect to the qualitative properties given here one should be aware that there is some disagreement in predictions. See, for example, the predictions of Page, Swanson and Szczepaniak [31, 32]. In particular, Page *et al.* [32] predict the $\hat{a}_2$ width to be very narrow so that it would be useful to search for $a_2\pi$ and $h_1\pi$ final states. If nothing else this would be a good test of the models.

Although hybrid mesons with exotic quantum numbers give a distinctive signature, hybrids with conventional quantum numbers are also expected in the meson spectrum. The situation is more complicated than simply looking for additional states because we expect strong mixing between non-spin exotic hybrids and conventional mesons with the same quantum numbers. Thus, to distinguish non-exotic hybrids from conventional states requires detailed predictions of properties [10, 30, 33, 34].

A first example is whether the $\pi(1800)$ is a conventional $3S$ isovector pseudoscalar meson (the 2nd radial excitation of the π) or a hybrid meson. Predictions for the partial width of a π_{3S} and π_H are given in Table 2. The flux tube model predicts that the π_{3S} decays to $\omega\pi$ but the π_H does not. Likewise, the π_H has a large partial width to $f_0(1300)\pi$ while for the π_{3S} this partial width is quite small. Therefore the $\rho\omega$ and $f_0(1300)\pi$ modes can be used as discriminators between the two possibilities. The π_{3S} has been observed in $\pi f_0(1300)$ lending support to its identification as a hybrid.

Another example is that of the ρ' and ω' mesons. One expects the physical vector mesons to be a linear combination

$$|V\rangle = \sum_n \alpha_n |n^3S_1\rangle + \sum_m \beta_m |m^3D_1\rangle + \gamma |V_H\rangle. \tag{9}$$

To disentangle the various components of the physical mesons we need to perform a detailed comparison between the observed states and the predictions for the unmixed $q\bar{q}$ and V_h states, much as was done

Table 1: Dominant decay widths of exotic hybrid mesons. From Close and Page [30].

Initial state	Final state	L	Γ
$\hat{\rho}(1^{-+})$	$b_1(1235)\pi$	S	100
		D	30
	$f_1(1285)\pi$	S	30
		D	20
$\hat{\omega}(1^{-+})$	$a_1(1260)\pi$	S	100
		D	70
	$K_1(1400)K$	S	100
$\hat{\phi}(1^{-+})$	$K_1(1270)K$	D	80
	$K_1(1400)K$	S	250
$\hat{a}_2(2^{+-})$	$a_2(1320)\pi$	P	450
	$a_1(1260)\pi$	P	100
	$h_1(1170)\pi$	P	150
$\hat{f}_2(2^{+-})$	$b_1(1235)\pi$	P	500
$\hat{f}'_2(2^{+-})$	$K_2^*(1430)K$	P	250
	$K_1(1400)K$	P	200
$\hat{a}_0(0^{+-})$	$a_1(1260)\pi$	P	800
	$h_1(1170)\pi$	P	100
$\hat{f}_0(0^{+-})$	$b_1(1235)\pi$	P	250
$\hat{f}'_0(0^{+-})$	$K_1(1270)K$	P	800
	$K_1(1400)K$	P	50

Table 2: Partial decay widths for the $\pi(3S)$ and π_H. From Barnes *et al.* [10].

State	Partial widths to final states						Total
	$\pi\rho$	$\omega\rho$	$\rho(1465)\pi$	$f_0(1300)\pi$	$f_2\pi$	K^*K	
$\pi_{3S}(1800)$	30	74	56	6	29	36	231
$\pi_H(1800)$	30	–	30	170	6	5	~ 240

for the scalar iso-scalar mesons. Partial width predictions are shown in Table 3 for the $\rho_{2S}(1465)$, $\rho_{1D}(1700)$, and $\rho_H(1500)$ states. For this example the πh_1 and πa_1 decay modes can discriminate between the ρ_{2S}, ρ_{1D} and ρ_H to disentangle the mixings.

A similar exercise can be applied to the isoscalar sector with the relevant partial widths given in Table 4. The decays $\omega(1420) \rightarrow \pi b_1$ and $\omega(1600) \rightarrow \pi b_1$ are both observed to be small so neither is likely to be a pure 1^3D_1 state. This implies that one is the 2^3S_1 and indicates that the other has significant ω_H content. It is clearly important to find the 3rd state in this set and determine some of the other branching ratios. The essential point is that although the two states may have the same J^{PC} quantum numbers they have different internal structure which will manifest itself in their decays. Unfortunately, nothing is simple and we once again point out that strong mixing is expected between hybrids with conventional quantum numbers and $q\bar{q}$ states with the same J^{PC} so that the decay patterns of physical states may not closely resemble those of either pure hybrids or pure $q\bar{q}$ states. With enough information one could perform an analysis similar to the one performed on the scalar meson sector by Close and Kirk [12].

Table 3: Partial decay widths for the ρ_{2S}, ρ_{1D} and ρ_H. From Barnes *et al.* [10].

State	Partial widths to final states								Total
	$\pi\pi$	$\omega\pi$	$\rho\eta$	$\rho\rho$	KK	K^*K	$h_1\pi$	$a_1\pi$	
$\rho_{2S}(1465)$	74	122	25	–	35	19	1	3	279
$\rho_{1D}(1700)$	48	35	16	14	36	26	124	134	435
$\rho_H(1500)$	0	5	1	0	0	0	0	140	~ 150

Table 4: Partial decay widths for the ω_{2S}, ω_{1D} and ω_H. From Barnes *et al.* [10].

State	Partial widths to final states					Total
	$\rho\pi$	$\omega\eta$	KK	K^*K	$b_1\pi$	
$\omega_{2S}(1419)$	328	12	31	5	1	378
$\omega_{1D}(1649)$	101	13	35	21	371	542
$\omega_H(1500)$	20	1	0	0	0	~ 20

4.2 Production of hybrid mesons

Hybrid mesons can be produced in a number of processes:

1. $J/\psi \to \gamma X$
2. $\bar{p}p$ annihilation
3. peripheral production
4. photoproduction

It is the latter two processes which are relevant to the COMPASS Collaboration. Peripheral production is discussed in more detail by Dorofeev [35] and photoproduction by Moinester [36] in these proceedings.

4.2.1 Hadronic peripheral production

In peripheral production the beam particle is excited and exchanges momentum and quantum numbers with the target nucleus via an exchange particle. The excited meson continues to move forward, subsequently decaying into the decay products which are detected by the experiment. This is shown schematically in Fig. 4. Examples of experiments which studied peripheral production are LASS at SLAC, E852 at Brookhaven, BENKEI at KEK, VES at IHEP/Serpukhov and GAMS at CERN.

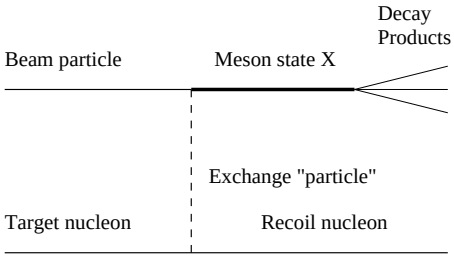

Fig. 4: Peripheral production of mesons.

Evidence for hybrid mesons has been seen by the VES collaboration [37] in $\rho^0\pi^-$, $\pi\eta$, and πb_1 final states in the reaction

$$\pi^- N \to (\eta\pi^+\pi^-)\pi^- N \text{ with a 37 GeV/}c\ \pi \text{ beam} \tag{10}$$

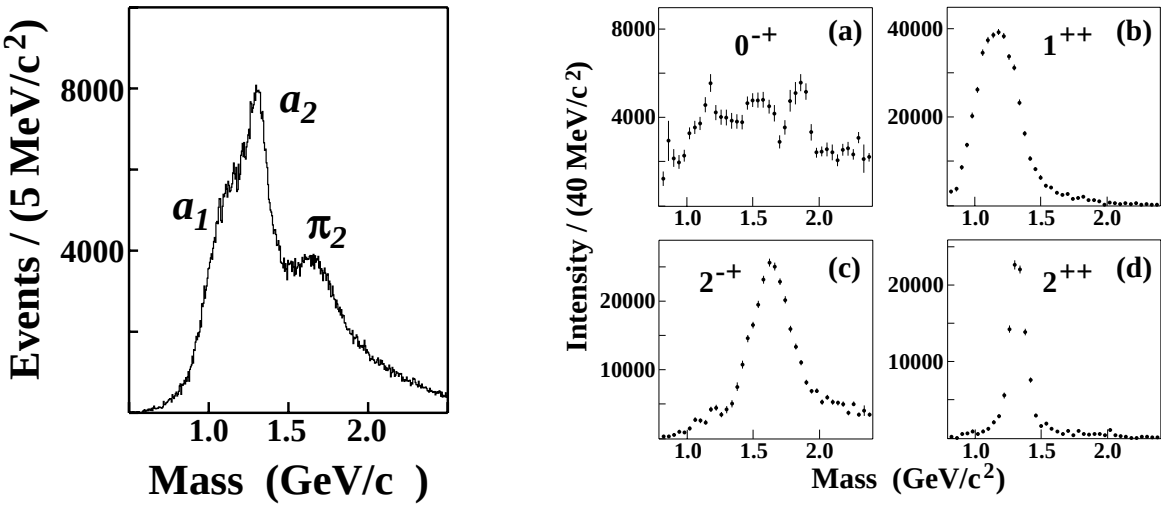

Fig. 5: Invariant mass distribution of $\pi^+\pi^-\pi^-$. The figure on the left shows the raw data and the figure on the right shows the results of a PWA. From Ref. [38].

and by BNL E852 [38] in the final state $\pi f_1(1285)$ in the reaction

$$\pi^- p \to (\pi^-\pi^+\pi^-)p \text{ with a 18 GeV/}c\,\pi \text{ beam.} \tag{11}$$

There is no reason a priori to expect that any type of hadron is preferred over any other in this mechanism. The π exchange mechanism only provides access to natural parity states. But the advantage of very high statistics is that with enough statistics one could use t-distributions to distinguish between different exchange particles which would allow one to study states other than the natural parity states.

Experiment E852 at Brookhaven provides a nice lesson in the advantages of high statistics [38]. In Fig. 5 the event rates for $\pi^- p \to \pi^+\pi^-\pi^- p$ at 18 GeV/c is shown as a function of $\pi^+\pi^-\pi^-$ invariant mass. Structure is seen corresponding to the a_1, a_2, and π_2 mesons although it would be difficult to draw conclusions from this figure alone. However, with the large data sample a partial wave analysis can be performed. The results are also shown in Fig. 5. One now sees clear resonances corresponding to the a_1, π_2 and a_2. These reference waves can be used to measure the phase shift of the exotic waves that are being looked for. This is shown in Fig. 6 where intensity and phase of the 1^{-+} exotic signal clearly stands out.

The lesson is that a PWA is a necessary component of any study of meson physics and that high statistics offer the opportunity to perform the necessary studies.

4.2.2 Photoproduction

COMPASS offers a unique opportunity in that it can also study hybrid meson production via photoproduction by way of initial muon beams. Photoproduction is qualitatively different from hadronic peripheral production so that the series of preferred excitations is likely to be different. Additionally, it is a strong source of $s\bar{s}$ states. Via vector meson dominance one can view the photon as a linear combination of the ρ, ω, ϕ and other vector mesons. In vector mesons the quark spins are aligned in a $S = 1$ triplet state. As hybrid mesons with exotic quantum numbers are also in a spin triplet state it is believed that exotic hybrid mesons are favoured by this process. At the present time there is virtually no photoproduction data available. Some time ago the OMEGA Photon Collaboration studied the process $\gamma p \to (b_1\pi)p$ at 25–50 GeV incident energy with the specific intention of seeking hybrids [39]. The most recent photoproduction experiment was done at SLAC studying $\gamma p \to \pi^+\pi^+\pi^- n$ at 19 GeV [40]. It showed hints

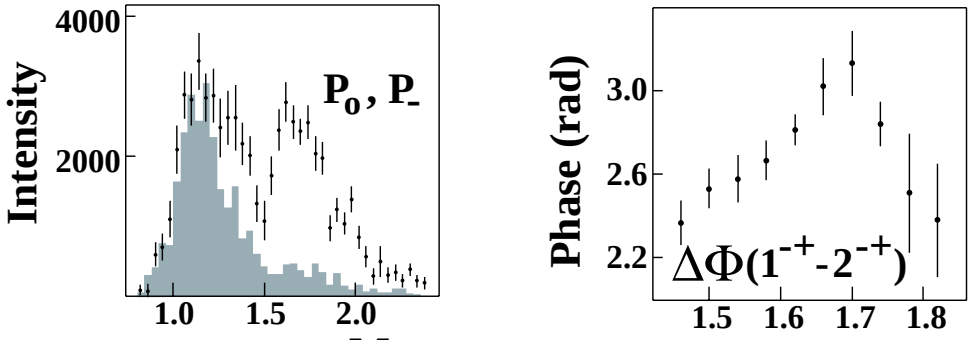

Fig. 6: The figure on the left shows the wave intensities of the 1^{-+} exotic waves. The PWA fit to the data is shown as the points with error bars and the shaded histograms show estimated contributions from all nonexotic waves due to leakage. The figure on the right shows the phase difference between the 1^{-+} and 2^{-+} waves from a coupled mass-dependent Breit–Wigner fit. From Ref. [38].

of exotics but, unfortunately, the statistics were rather low. A dedicated high-statistics experiment with the power of modern detection and analysis should re-examine this process [41]. This is almost virgin territory and an area to which the COMPASS Collaboration could make important contributions.

5. MULTIQUARK MESONS

In addition to conventional $q\bar{q}$ mesons, hybrids and glueballs, multiquark mesons are also expected to exist. It was noted in the discussions of glueballs and hybrids that they contribute to the physical spectrum.

While there is no room to discuss this topic in any detail I mention it as an additional ingredient that one should be aware of when studying meson spectroscopy. Several examples exist of multiquark candidates. It has long been believed that the $f_0(980)$ and $a_0(980)$ are multiquark states although their exact nature, a compact $q\bar{q}q\bar{q}$ object or an extended $K\bar{K}$ molecule, is the focus of vigorous debate. The nature of the $f_1(1430)$ is a longstanding puzzle and is part of our lack of understanding of what is known as the E/ι puzzle. There is speculation that it is a K^*K bound state.

Multiquark states can also have exotic quantum numbers. The best bets along this line of study would be fractional or doubly charged mesons although it has been speculated that at least one of the $J^{PC} = 1^{-+}$ exotic candidates is a $\bar{q}q\bar{q}q$ object.

6. SUMMARY

The existence of non-$q\bar{q}$ mesons is the most important qualitative open question in QCD. The discovery and mapping out of the glueball and hybrid meson spectrum is a crucial test of QCD. It will help validate lattice QCD as an important computational tool for non-perturbative field theory. It will take detailed studies to distinguish glueball and hybrid candidates from conventional $q\bar{q}$ states. This will require extremely high statistics experiments to measure meson properties such as partial widths and production mechanisms. COMPASS is unique. It has numerous tools to do this via π, K, p, and μ beams. COMPASS can make important advances in this field. I strongly encourage you to do so.

Acknowledgements

The author thanks Frank Close for helpful comments in preparing this manuscript, the organizers of the workshop for providing a stimulating environment for the discussion of these issues, and the DESY

theory group for their warm hospitality where this was written up. This work was partially funded by the Natural Sciences and Engineering Research Council of Canada.

References

[1] For a recent review of meson spectroscopy see S. Godfrey and J. Napolitano, Rev. Mod. Phys. **71** (1999) 1411. See also F.E. Close, Int. J. Mod. Phys. A **17** (2002) 3239, [hep-ph/0110081].

[2] G.S. Bali, Phys. Rep. **343** (2001) 1, [hep-ph/0001312]; C. Davies in Proceedings *55th Scottish Universities Summer School in Physics: Heavy Flavor Physics*, St. Andrews, Scotland, 2001, C.T.H. Davies and S.M. Playfer, eds. (*Heavy Flavor Physics*, Scottish Graduate Textbook Series, Institute of Physics 2002) p. 105, [hep-ph/0205181].

[3] C. Michael in Proceedings *4th International Conference on Quark Confinement and the Hadron Spectrum*, Vienna, Austria, 2000, p. 197, [hep-ph/0009115].

[4] G. Bali, K. Schilling, A. Hulsebos, A. Irving, C. Michael and P. Stephenson, Phys. Lett. B **309** (1993) 378; C. Morningstar and M. Peardon, Phys. Rev. D **60** (1999) 034509, [hep-lat/9901004]; W. Lee and D. Weingarten, [hep-lat/9805029]; K. Chen, J. Sexton, A. Vaccarino and D. Weingarten, Nucl. Phys. B (Proc. Suppl) **34** (1994) 357; C. Michael in Proceedings *Seventh International Conference on Hadron Spectroscopy*, Brookhaven National Laboratory, New York, 1997, S.-U. Chung and H.J. Willutzki, eds. (AIP Conference Proceedings 432, Woodbury New York, 1998) p. 657.

[5] C. Morningstar and M. Peardon, Phys. Rev. D **56** (1997) 4043; Phys. Rev. D **60** (1999) 034509.

[6] C. Amsler and F.E. Close, Phys. Rev. D **53** (1996) 295; Phys. Lett. B **353** (1995) 385.

[7] G.S. Bali, K. Schilling and C. Schlichter, Phys. Rev. D **51** (1995) 5165, [hep-lat/9409005].

[8] K.J. Juge, J. Kuti and C.J. Morningstar, Phys. Rev. Lett. **82** (1999) 4400; Nucl. Phys. B (Proc. Suppl.) **63A-C** (1998) 326.

[9] A detailed account of conventional meson properties is given by: S. Godfrey and N. Isgur, Phys. Rev. D **32** (1985) 189; Phys. Rev. D **34** (1986) 899; S. Godfrey, Phys. Rev. D **31** (1985) 2375; S. Godfrey and R. Kokoski, Phys. Rev. D **43** (1991) 1679.

[10] T. Barnes, F.E. Close, P.R. Page and E.S. Swanson, Phys. Rev. D **55** (1997) 4157.

[11] T. Barnes, N. Black and P.R. Page, Phys. Rev. D **68** (2003) 054014, [nucl-th/0208072].

[12] F. Close and A. Kirk, Phys. Lett. B **483** (2000) 345; Eur. Phys. J. C **21** (2001) 531.

[13] B. Barberis *et al.*, Phys. Lett. B **479** (2000) 59.

[14] C. Amsler, Phys. Lett. B **541** (2002) 22.

[15] M. Chanowitz in Proceedings *6th International Workshop on Photon–Photon Collisions*, Lake Tahoe, Canada, 1984, R.L. Lander, ed. (World Scientific, 1985).

[16] F. Close and A. Kirk, Phys. Lett. B **397** (1997) 333.

[17] B. Barberis *et al.*, Phys. Lett. B **467** (1999) 165.

[18] F.E. Close and G.A. Schuler, Phys. Lett. B **458** (1999) 127; Phys. Lett. B **464** (1999) 279.

[19] B. Barberis *et al.*, Phys. Lett. B **474** (2000) 423.

[20] B. Barberis *et al.*, Phys. Lett. B **462** (1999) 462.

[21] F. Close, A. Kirk and G. Schuler, Phys. Lett. B **477** (2000) 13.

[22] K.J. Juge, J. Kuti and C. Morningstar, Nucl. Phys. (Proc. Suppl.) **63A-C** (1998) 326.

[23] N. Isgur and J. Paton, Phys. Rev. D **31** (1985) 2910.

[24] N. Isgur, R. Kokoski and J. Paton, Phys. Rev. Lett. **54** (1985) 869.

[25] T. Barnes, F.E. Close and E.S. Swanson, Phys. Rev. D **52** (1995) 5242.

[26] C. Michael, *8th International Symposium On Heavy Flavor Physics*, Southampton, England, 1999, [hep-ph/9911219].

[27] P. Lacock, C. Michael, P. Boyle and P. Rowland, Phys. Rev. D **54** (1996) 6997; Phys. Lett. B **401** (1997) 308; C. Bernard *et al.*, Phys. Rev. D **56** (1997) 7039; Nucl. Phys. B (Proc. Suppl.) **73** (1999) 264; P. Lacock and K. Schilling, Nucl. Phys. B (Proc. Suppl.) **73** (1999) 261.

[28] P. Page, Phys. Lett. B **402** (1997) 183.

[29] C. McNeile, C. Michael and P. Pennanen, Phys. Rev. D **65** (2002) 094505.

[30] F. Close and P. Page, Nucl. Phys. B **443** (1995) 233.

[31] E. Swanson and A. Szczepaniak, Phys. Rev. D **56** (1997) 5692.

[32] P.R. Page, E. Swanson and A. Szczepaniak, Phys. Rev. D **59** (1999) 034016.

[33] F. Close and P. Page, Phys. Rev. D **56** (1997) 1584.

[34] A. Donnachie and Yu.S. Kalashnikova, Phys. Rev. D **60** (1999) 114011.

[35] V. Dorofeev, these proceedings.

[36] M. Moinester, these proceedings.

[37] G.M. Beladidze *et al.* (VES Collaboration), Phys. Lett. B **313** (1993) 276.

[38] G. Adams *et al.* (E852 Collaboration), Phys. Rev. Lett. **81** (1998) 5760.

[39] M. Atkinson *et al.* (Omega Photon Collaboration), Z. Phys. C **34** (1987) 157.

[40] G.T. Condo *et al.*, Phys. Rev. D **48** (1993) 3045.

[41] F. Close and P. Page, Phys. Rev. D **52** (1995) 1706.

EXOTICS AND GLUEBALLS ON THE LATTICE

C. McNeile
Dept. of Math Sci., University of Liverpool, L69 3BX, UK

Abstract
I review the results from lattice gauge theory for the properties of the light 1^{-+} exotic state and 0^{++} glueball.

1. INTRODUCTION

High-energy experiments have confirmed that QCD is a simple elegant theory that contains quarks and gluons. At low energy the states observed in experiments are messy hadrons. It is hard to relate the world of quarks and gluons to the 'real-world' practicalities of hadrons, because QCD is such a hard theory to solve. A particularly good test of our understanding of the non-perturbative aspects of QCD is to study particles where the gauge field is excited somehow, and hence playing a more important dynamic role than in 'standard' hadrons. Examples of such particles are glueballs (particles made out of the gauge fields) and hybrid mesons ($\overline{q}q$ and excited glue).

Quantities, such as masses, depend on the coupling (g) like $M \sim e^{-1/g^2}$ [1], hence perturbation theory can't be used to compute the masses of hadrons such as the proton. The only technique that offers any prospect of computing masses and matrix elements non-perturbatively, from first principles, is lattice QCD. I review the results from the lattice for the glueballs and mesons with exotic quantum numbers, Other recent reviews [2–4] of lattice results for hybrids and glueballs focus on different aspects of the subject.

2. LATTICE QCD CALCULATIONS

In this section, I briefly describe the formalism for lattice QCD calculations. The lecture notes by Gupta [5] provide specific details about lattice QCD calculations.

Many bound state properties of QCD can be determined from the path integral

$$c(t) \sim \int dU \int d\psi \int d\overline{\psi} \sum_{\underline{x}} O(\underline{0},0) O(\underline{x},t)^{\dagger} e^{-S_F - S_G} \tag{1}$$

where S_F is the fermion action (some lattice version of the continuum Dirac action) and S_G is the pure gauge action. The path integral in Eq. (1) is put on the computer using a clever finite difference formalism [1], due to Wilson, that maintains gauge invariance. The path integral in Eq. (1) is evaluated using algorithms that are generalizations of the Monte Carlo methods used to compute low-dimensional integrals. The algorithms produce samples of gauge fields, that are essentially snapshots of the vacuum. The physical picture for Eq. (1) is that a hadron is created at time 0 using an interpolating operator. The quarks then propagate to time t in the background of the gauge fields, where the hadron is destroyed. The physics from the calculation is extracted using a fit model [1]:

$$c(t) = a_0 e^{-m_0 t} + a_1 e^{-m_1 t} + \cdots \tag{2}$$

where m_0 (m_1) is the ground (first excited) state mass and the dots represent higher excitations. Although in principle excited state masses can be extracted from a multiple exponential fit, in practise this is a numerically non-trivial task, because of the noise in the data from the Monte Carlo calculation. More sophisticated fitting techniques are starting to be used to extract masses from the data. For example the CP-PACS Collaboration have used maximum entropy fitting techniques [6] to look at excited states of the rho and pion in quenched QCD. CP-PACS obtained the masses of the first excited rho and pion to be

1540 (570) MeV and 660 (590) MeV respectively [6]. More experience is needed with these 'advanced fitting' methods before they can be used to make physical predictions.

Any gauge invariant combination of quark fields and gauge links can be used as interpolating operators ($O(\underline{x}, t)$) in Eq. (1). Interpolating operators that are similar to the state will couple strongly to the state. For example, a $\overline{qq}qq$ state may not couple strongly to an interpolating operator with only a valence content of $\overline{q}q$.

The fermion integration can be done exactly in Eq. (1) to produce the quark determinant. The determinant describes the dynamics of the sea quarks. In quenched QCD calculations, the quark determinant is set to a constant. Quenched calculations are roughly 1000 times computationally cheaper than the calculations that include the dynamics of the sea quarks.

There are a variety of heuristic ways of understanding quenched QCD. One way is to view quenched QCD as QCD with infinitely heavy sea quarks. The connection between quenched QCD and the large N_c (number of colours) limit of QCD has recently been discussed by Chen [7]. Perhaps, surprisingly quenched QCD gives quite a reasonable description of experiment. For example, the most accurate quenched calculation of the hadron spectrum, to date, has been completed by the CP-PACS Collaboration [8]. CP-PACS [8] found that the masses of 11 light hadrons disagree with experiment by at most 11%. Quenched QCD is not a consistent theory and problems with the formalism have been found in calculations [9].

In an individual lattice calculation there are errors from the finite size of the lattice spacing and the finite lattice volume. State-of-the-art lattice calculations in quenched QCD run at a number of different lattice spacings and physical volumes and extrapolate the results to the continuum and infinite volume [8] limit. The increased computational costs of unquenched calculations means that most calculations are currently done at fixed lattice spacings [10] or an extrapolation to the continuum limit is attempted from coarse lattice spacings [11]. One of the most interesting unquenched calculations is being performed by the MILC Collaboration [12]. MILC's calculations include 2+1 flavours of sea quarks with a lattice spacing of 0.09 fm, box size of 2.6 fm, and the lightest ratio of the pseudo-scalar to vector mass is 0.4.

3. RESULTS FOR GLUEBALLS IN QUENCHED QCD

Interpolating operators for glueballs are constructed for Eq. (1) from closed loops of gauge links with specific J^{PC} quantum numbers. Some highlights of the results are that the lightest glueball is the 0^{++} state with a mass of 1.611(30)(160) GeV [2, 13] (where the second error is systematic). The next lightest glueball is 2^{++}. The ratio of the tensor to scalar glueball mass is $M_{2^{++}}/M_{0^{++}}$ = 1.42(6) [13]. The spectrum of glueball states for other J^{PC} quantum numbers with masses under 4 GeV has been comprehensively mapped out by Morningstar and Peardon [14].

In the real world glueballs will decay to two mesons, hence they will have a decay width. Lattice QCD calculations are performed in Euclidean space, for convergence of the path integral in Eq. (1). The Euclidean nature of lattice calculations makes the computation of inherently complex quantities such as decay widths more involved [15].

The GF11 lattice group computed the decay widths for the decay of the 0^{++} glueball to two pseudoscalars [16] to be 108(28) MeV. Although the error is only statistical, it is encouraging that the width was small relative to the mass, so the 0^{++} glueball may exist as a well-defined state. The calculation was done at a coarse lattice spacing. The decay widths for individual meson pairs [17] did not agree with the predictions from the 'flavour democratic' assumption.

The experimental situation [18] for light 0^{++} scalars is very interesting, because there are too many states to put into SU(3) nonets, as other particles with different J^{PC} quantum numbers, such as the pseudoscalars, can be. The $f_0(1370)$, $f_0(1500)$, and $f_0(1710)$ hadrons have masses close to the mass of the 0^{++} glueball from quenched QCD. Potentially one way of identifying one of the f_0's with a quenched glueball would be to reduce the errors on the value of the mass of the 0^{++} glueball until

the value agrees with one of the experimental masses and the error is at least 3σ away from the other masses. This requires the error on the 0^{++} glueball mass to be below 50 MeV. The detailed error for the mass of the 0^{++} mass from Morningstar and Peardon [14] is 1730(50)(80) MeV. The second error is from the different ways of choosing the lattice spacing in quenched QCD calculations and reflects the fact the quenched QCD is not the real world. As the 80 MeV systematic error can not be reduced in quenched QCD, the quenched glueball spectrum is known as accurately as it will ever be. There are some preliminary indications that this ambiguity in the choice of lattice spacing has been reduced in the unquenched calculations from the MILC Collaboration [12, 19].

In unquenched QCD interpolating operators with 0^{++} can be constructed from quarks and anti-quarks, such as $\overline{q}q$. In full QCD, the pure glue 0^{++} operators will mix with the fermionic 0^{++} operators. If the mixing is very strong, then the final 0^{++} masses will have little to do with the glueball masses from quenched QCD.

Weingarten and Lee [20] studied the effect of mixing between the glueball and $\overline{q}q$ states in quenched QCD. They measured the correlation between the 0^{++} glueball states and $\overline{q}q$ states in Eq. (1). The results were expressed as a mixing matrix

$$\begin{pmatrix} m_g & E(s) \\ E(s) & m_\sigma(s) \end{pmatrix} \tag{3}$$

where m_g is the glueball mass, $m_\sigma(s)$ is the mass of the non-singlet 0^{++} state at the strange quark mass, and $E(s)$ is the mixing energy. Weingarten and Lee measured: m_g = 1648(58) MeV, $m_\sigma(s)$ = 1322(42) MeV, and $E(s)$ = 61(58) MeV in the continuum limit. The qualitative picture that emerges is that the $f_0(1710)$ is 'mostly' 0^{++} glueball, and the $f_0(1500)$ is 'mostly' $\overline{s}s$. It is not clear whether $f_0(1500)$ being $\overline{s}s$ is consistent with its decay width [21]. The mixing energy $E(s)$ has large lattice spacing errors. For example at a lattice spacing of $a^{-1} \sim 1.2$ GeV, the Weingarten and Lee [20] result is $E(s) \sim 0.36$ GeV. This has been checked by another group's result [22] of $E(s) \sim 0.44$ GeV.

The analysis of Weingarten and Lee [20] depends on the 0^{++} states being well defined in quenched QCD. Bardeen [9] *et al.* have shown that there is a problem with the non-singlet 0^{++} correlator in quenched QCD. The problem can be understood using quenched chiral perturbation theory. The non-singlet 0^{++} propagator contains an intermediate state of $\eta' - \pi$. The removal of fermion loops in quenched QCD has a big effect on the η' propagator. The result is that a ghost state contributes to the scalar correlator, that makes the expression in Eq. (2) inappropriate to extract masses from the calculation. Eichten *et al.* [9] predict that the ghost state will make the a_0 mass increase as the quark mass is reduced below a certain point. This behaviour was observed by Weingarten and Lee [20] for small box sizes ($L \leq 1.6$ fm) for quark masses below strange. It is not clear how the problem with the non-singlet 0^{++} correlator in the quenched approximation affects the results of Weingarten and Lee [20], however, their most important results come from masses above the strange quark mass where the ghost diagram will make a smaller contribution that may be negligible.

Lattice QCD calculations are sometimes criticized for just producing numbers, but no insight. Increasingly, lattice QCD methods are used to provide intuition about hadronic physics. For example the large N_c limit of QCD has been a place where analytical calculations are possible, however, the calculation of the $1/N_c$ corrections has turned out to be hard.

Teper and Lucini [23] have systematically studied the glueball spectrum for N_c = 2,3,4 and 5. They found that the dependence of the glueball spectrum on N_c is weak. To determine the N_c dependence of the glueball masses, the systematic errors, such as lattice spacing errors, had to be quantified and controlled. This type of lattice study is very useful to the attempts to compute the glueball spectrum using the ADS super-gravity duality (for example see Brower *et al.* [24] and the references within), as the glueball spectrum is obtained in the large N_c limit.

The light scalar mesons seem to be full of surprises. There are lighter 0^{++} states, such as the $f_0(980)$ and the $a_0(980)$, and the enigmatic $f_0(400-1200)$. The $f_0(980)$ and $a_0(980)$ states are consid-

ered by some people to be kaon molecules or $\overline{qq}qq$ states, although there are dissenting opinions. There has been some recent work by Alford and Jaffe [25] on $\overline{qq}qq$ quark states.

4. RESULTS FOR GLUEBALL MASSES IN TWO-FLAVOUR QCD

The Weingarten and Lee [20] analysis predicted that the mixing of the 0^{++} glueball and $\overline{q}q$ states is small. Parts of their calculation have been criticized in Ref. [22], however, the problems with the non-singlet 0^{++} correlator [9] in the quenched QCD will make further progress in mixing in the quenched QCD difficult. There are attempts to take into account the quenched artifact in the a_0 correlator [26].

A lattice QCD calculation that included the dynamics of the sea quarks should just reproduce the physical spectrum of 0^{++} states. Some insight into the composition of individual 0^{++} states, such as whether a physical particle couples to $\overline{q}q$ or pure glue operators, could be studied by looking at the effect of decreasing the sea quark mass. For very heavy sea quark masses the theory is more like quenched QCD, where glueballs are distinct from $\overline{q}q$ operators.

Figure 1 shows a compendium of recent results for the mass of singlet 0^{++} states from two-flavour unquenched QCD versus the square of the lattice spacing.

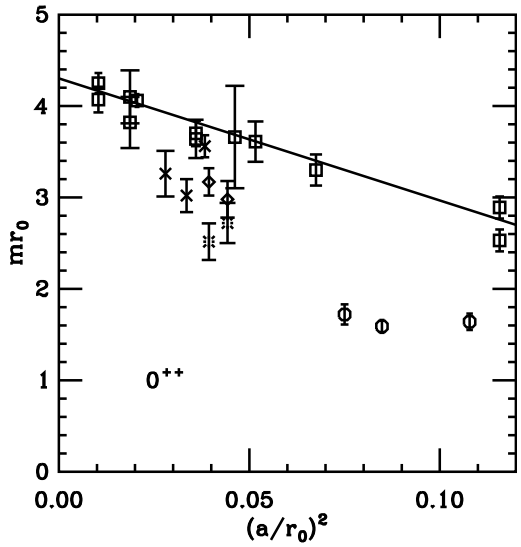

Fig. 1: Singlet 0^{++} mass in units of r_0 as a function of lattice spacing. The crosses are from SESAM [27]. The octagons are from UKQCD's [22] first $n_f = 2$ data set. The diamonds are the results from Hart and Teper [28]. The bursts are from a combined analysis of glueball and $\overline{q}q$ interpolating operators. The squares are the results from quenched calculations (see Ref. [22] for references).

Hart and Teper [28] found that the ratio of the 0^{++} glueball mass in $n_f = 2$ QCD to the quenched QCD result was: $M^{0^{++}}_{n_f=2}/M^{0^{++}}_{quenched}$ = 0.84 ± 0.03 at a fixed lattice spacing of 0.1 fm. The n_f = 2 results [28] for the mass of the 2^{++} were consistent with the quenched value. As the lattice spacing dependence of the mass of the singlet 0^{++} state in two-flavour QCD and quenched QCD could be different, a definitive result will only come after a continuum extrapolation of the unquenched masses. In quenched QCD [13], the difference between the continuum extrapolated mass of the 0^{++} glueball and the mass at 0.1 fm is of the order of 200 MeV. This is the same magnitude of the mass splittings between the masses of the experimentally observed particles $f_0(1500)$ and $f_0(1710)$. Although the current results for singlet 0^{++} states are starting to be interesting, the lattice spacing used in unquenched calculations must be reduced before direct contact can be made to phenomenology.

Traditionally, glueball calculations have been done with Wilson loop type operators. However, singlet quark operators of the form $\overline{q}q$ also have the quantum numbers of 0^{++}. The UKQCD Collaboration were the first to attempt a joint analysis of 0^{++} states that included glueball and $\overline{q}q$ operators [22]. Preliminary results are now available for a finer lattice spacing [29]. In Fig. 1 we plot the masses from the calculation by Hart and Teper (diamonds) with the masses obtained in this analysis (bursts). The value of $1/r_0$ is ~ 373 MeV from the string tension [2]. The inclusion of the $\overline{q}q$ operators with the Wilson loop operators has produced a further suppression of the mass of the singlet 0^{++} state at the lattice spacing used.

The mass of the 0^{++} singlet meson on the lightest UKQCD data set are degenerate with the mass of two pions [28]. As the mass of the sea quarks is reduced, two-pion states may affect the physics of singlet 0^{++} states. Two-pion interpolating operators may also need to be included in the basis of interpolating operators.

5. RESULTS FOR LIGHT 1^{-+} EXOTIC MESONS

The quark model predicts the charge conjugation (C = $(-1)^{L+S}$) and parity (P= $(-1)^{L+1}$) of a meson with spin S and orbital angular momentum L. States with quantum numbers not predicted by the quark model, such as J^{PC}_{exotic} = 1^{-+}, 0^{+-}, 2^{+-}, 0^{--} are known as exotics [30]. Exotic states are allowed by QCD. Morningstar and Peardon [14] claim that there are no glueballs with exotic quantum numbers with masses less than 4 GeV in quenched lattice QCD.

There are a number of different possibilities for the structure of an exotic state. An exotic state could be a hybrid meson, that is a quark and anti-quark with excited glue, or bound state of two quarks and two anti-quarks ($\overline{qq}qq$).

One possible interpolating operator [31], that can be used in Eq. (1), for a hybrid 1^{-+} particle is

$$O_{1^{-+}}(\underline{x},t) = \overline{q}(\underline{x},t)\gamma_j F_{ij}(\underline{x},t)q(\underline{x},t) \tag{4}$$

where F is the QCD field strength tensor. If F is removed from Eq. (4), the operator creates the ρ particle. In this formalism a gauge invariant interpolating operator, for any possible exotic hybrid particle or four-particle state can be constructed. The dynamics then determines whether the resulting state has a narrow decay width, hence it can be detected experimentally. In the large N_c (number of colours) limit [30, 32] both exotic hybrid mesons and non-exotic mesons have widths that are small compared to their masses.

There have not been many new calculations of the mass of the light 1^{-+} hybrid recently. All the results from the various lattice QCD calculations, by UKQCD [33, 34], MILC [31, 35] and SESAM [36] are essentially consistent with the mass of the 1^{-+} state around $1.9(2)$ GeV [2]. The interpolating operators used to create the exotic meson states in the MILC calculations [31] are different from those used in the UKQCD [33] and SESAM simulations [36], hence giving confidence that the systematic errors are under control. The results for the hybrid masses reported by Lacock and Schilling [36], include some effects from dynamical sea quarks. The recent results for the 1^{-+} mass from calculations that used an asymmetric [37] lattice in time (for a better signal to noise ratio) are consistent with the older results.

The MILC Collaboration have started the first serious study of the exotic meson spectrum in unquenched QCD [38]. The MILC Collaboration use a formalism called improved staggered fermions for the quarks. This formulation can study much lighter quarks than competitive fermion actions. The main disadvantage of this formalism is that flavour symmetry is broken. The preliminary result from MILC for the mass of the lightest 1^{-+} state is consistent with (or perhaps slightly lower than) earlier estimates from MILC and UKQCD. MILC found problems extracting the 1^{-+} state from the lightest unquenched calculations [38]. Their preliminary speculation is that this is due to mixing with $\overline{qq}qq$ states. Further work is required to test this.

There are a number of experimental candidates for light 1^{-+} states [18]. The E852 Collaboration have reported [39] a signal for 1^{-+} state around 1.6 GeV. There is also an experimental signal for a 1^{-+} state at 1.4 GeV [18].

There has been some recent work [40] on the quark mass dependence of the 1^{-+} states. The lattice calculations are usually done at large quark masses and the results extrapolated to the physical quark masses. The conclusion of Ref. [40] was that the inclusion of the decay of the hybrid in the quark mass dependence of the exotic mass could reduce the final answer by 100 MeV. The predictions in Ref. [40] will be tested as the quark masses used in lattice calculations are reduced. The 1^{-+} state at 1.4 GeV seems low relative to the lattice results.

It is possible that the states seen experimentally are really $\overline{q}\overline{q}qq$ states, in which case the operators used in the lattice simulations [Eq. (4)] might not couple strongly to them. Alford and Jaffe [25] studied $\overline{q}\overline{q}qq$ operators with $J^{PC} = 0^{++}$ in a recent lattice calculation. The motivation was to gain insight into states such as the $f_0(980)$ that some people believe is not a $\overline{q}q$ meson, but a $\overline{q}\overline{q}qq$ state. A similar lattice calculation could in principle be done for the $J^{PC} = 1^{-+}$ exotic.

To definitely identify a particle requires both the calculation of the mass as well as the decay widths. There has been very little work on strong decays on the lattice. The most obvious hadronic process to study using lattice gauge theory is the $\rho \to \pi\pi$ decay, however, there have only been a few attempts to calculate the $g_{\rho\pi\pi}$ coupling [41, 42]. Michael discusses the problems with the formalism for hadronic decays on the lattice [15].

In the static quark limit the exotic states on the lattice are described by adiabatic potentials. The ground state of the static potential (A_{1g}) is the familiar Coulomb plus linear potential. The excited potential (E_u) is a very flat potential, that can be used with Schrödinger's equation to predict the spectrum of heavy-heavy hybrids [2]. UKQCD [43] have investigated the de-excitation of the E_u potential to the A_{1g} potential by the emission of a light quark loop. In the real world, the decays would correspond to $1^{-+} \to \chi_b\eta$ and $1^{-+} \to \chi_b S$ with S a scalar and η a pseudo-scalar. The decay width of $1^{-+} \to \chi_b\eta$ and $1^{-+} \to \chi_b S$ transitions were less than 1 MeV and around 80 MeV respectively. The various approximations in the static limit mean that these widths have no direct relevance to experiment.

The MILC Collaboration [31] have investigated the mixing between the operator in Eq. (4) and the operator ($\pi \otimes a_1$) Eq. (5).

$$\overline{q}^a\gamma_5 q^a \overline{q}^b \gamma_5\gamma_i q^b \tag{5}$$

that has the quantum numbers 1^{-+}. This type of correlator is part of the calculation required to compute the decay width of the 1^{-+} state to ρ, and a_1. The more complicated part is to use Eq. (5) in Eq. (1) which requires some clever numerical work.

6. CONCLUSIONS

The glueball spectrum from quenched QCD has been stable for a number of years and has provided useful hints to experiments that are trying to find experimental evidence for glueballs. The mixing between glueball and $\overline{q}q$ states has been studied by Lee and Weingarten [20] and the UKQCD Collaboration [22]. Further checks on the seminal calculations of Lee and Weingarten [20] will be hampered by formalism problems in quenched QCD [9]. It is better to study the mixing using unquenched QCD calculations [22].

Progress in glueball and hybrid meson spectroscopy will be dependent on how close the masses of the sea quarks are to their physical values. The physical mass of the singlet 0^{++} in unquenched QCD is obscured by lattice artefacts. To reduce the systematic errors on the mass of the singlet 0^{++} requires lattice calculations at finer lattice spacings. This is computationally expensive, but possible.

The computation of decay widths from a Euclidean lattice calculation is a tough problem. The UKQCD Collaboration have recently computed the coupling for the rho to decay to two pions [44]. This formalism may be able to compute couplings for decays relevant to scalar and exotic meson decays.

There is a sizeable community of lattice people in the UKQCD Collaboration who are interested in glueball and exotic meson physics. At the end of 2003 the UKQCD Collaboration will get a QCDOC [45] (QCD On a Chip) computer that has essentially the computational power of 10 000 PCs. So the COMPASS Collaboration may expect improved lattice calculations of pertinent hadronic masses from the UKQCD Collaboration in the next few years.

Acknowledgements

I thank Chris Michael and Doug Toussaint for discussions.

References

[1] I. Montvay and G. Munster, Quantum fields on a lattice, Cambridge, UK: Univ. Pr. (1994) 491 p. (Cambridge monographs on mathematical physics).

[2] C. Michael, Glueballs, hybrid and exotic mesons (2001), hep-ph/0101287.

[3] C. Morningstar, Gluonic excitations in lattice QCD: A brief survey (2001), nucl-th/0110074.

[4] G. S. Bali, 'Glueballs': Results and perspectives from the lattice (2001), hep-ph/0110254.

[5] R. Gupta, Introduction to lattice QCD (1997), hep-lat/9807028.

[6] T. Yamazaki *et al.*, Spectral function and excited states in lattice QCD with maximum entropy method, Phys. Rev. D **65** (2002) 014501.

[7] J.-W. Chen, Connecting the quenched and unquenched worlds via the large n(c) world, Phys. Lett. B **543** (2002) 183–188.

[8] S. Aoki *et al.*, Quenched light hadron spectrum, Phys. Rev. Lett. **84** (2000) 238–241.

[9] W. Bardeen, A. Duncan, E. Eichten, N. Isgur and H. Thacker, Chiral loops and ghost states in the quenched scalar propagator, Phys. Rev. D **65** (2002) 014509.

[10] C. R. Allton *et al.*, Effects of non-perturbatively improved dynamical fermions in QCD at fixed lattice spacing, Phys. Rev. D **65** (2002) 054502.

[11] A. Ali Khan *et al.*, Light hadron spectroscopy with two flavors of dynamical quarks on the lattice, Phys. Rev. D **65** (2002) 054505.

[12] C. W. Bernard *et al.*, The QCD spectrum with three quark flavors, Phys. Rev. D **64** (2001) 054506.

[13] M. J. Teper, Glueball masses and other physical properties of su(n) gauge theories in d = 3+1: A review of lattice results for theorists (1998), hep-th/9812187.

[14] C. J. Morningstar and M. J. Peardon, The glueball spectrum from an anisotropic lattice study, Phys. Rev. D **60** (1999) 034509.

[15] C. Michael, Particle decay in lattice gauge theory, Nucl. Phys. B **327** (1989) 515.

[16] J. Sexton, A. Vaccarino and D. Weingarten, Numerical evidence for the observation of a scalar glueball, Phys. Rev. Lett. **75** (1995) 4563–4566.

[17] L. Burakovsky and P. R. Page, Scalar glueball mixing and decay, Phys. Rev. D **59** (1999) 014022.

[18] D. E. Groom *et al.*, Review of particle physics, Eur. Phys. J. C **15** (2000) 1–878.

[19] A. Gray *et al.*, The upsilon spectrum from lattice QCD with 2+1 flavors of dynamical quarks (2002), hep-lat/0209022.

[20] W.-J. Lee and D. Weingarten, Scalar quarkonium masses and mixing with the lightest scalar glueball, Phys. Rev. D **61** (2000) 014015.

[21] F. E. Close and A. Kirk, Scalar glueball q anti-q mixing above 1-GeV and implications for lattice QCD, Eur. Phys. J. C **21** (2001) 531–543.

[22] C. McNeile and C. Michael, Mixing of scalar glueballs and flavour-singlet scalar mesons, Phys. Rev. D **63** (2001) 114503.

[23] B. Lucini and M. Teper, Su(n) gauge theories in four dimensions: Exploring the approach to n = infinity, JHEP **06** (2001) 050.

[24] R. C. Brower, S. D. Mathur and C.-I. Tan, Glueball spectrum for QCD from ads supergravity duality, Nucl. Phys. B **587** (2000) 249–276.

[25] M. G. Alford and R. L. Jaffe, Insight into the scalar mesons from a lattice calculation, Nucl. Phys. B **578** (2000) 367–382.

[26] S. Prelovsek and K. Orginos, Quenched scalar meson correlator with domain wall fermions (2002), hep-lat/0209132.

[27] G. S. Bali *et al.*, Static potentials and glueball masses from QCD simulations with wilson sea quarks, Phys. Rev. D **62** (2000) 054503.

[28] A. Hart and M. Teper, On the glueball spectrum in O(a)-improved lattice QCD, Phys. Rev. D **65** (2002) 034502.

[29] A. Hart, C. McNeile and C. Michael, Masses of singlet and non-singlet 0++ particles (2002), hep-lat/0209063.

[30] T. H. Burnett and S. R. Sharpe, Nonquark model mesons, Annu. Rev. Nucl. Part. Sci. **40** (1990) 327–356.

[31] C. Bernard *et al.*, Exotic mesons in quenched lattice QCD, Phys. Rev. D **56** (1997) 7039–7051.

[32] T. D. Cohen, Quantum number exotic hybrid mesons and large n(c) QCD, Phys. Lett. B **427** (1998) 348.

[33] P. Lacock, C. Michael, P. Boyle and P. Rowland, Hybrid mesons from quenched QCD, Phys. Lett. B **401** (1997) 308–312.

[34] P. Lacock, C. Michael, P. Boyle and P. Rowland, Orbitally excited and hybrid mesons from the lattice, Phys. Rev. D **54** (1996) 6997–7009.

[35] C. McNeile *et al.*, Exotic meson spectroscopy from the clover action at beta = 5.85 and 6.15, Nucl. Phys. Proc. Suppl. **73** (1999) 264–266.

[36] P. Lacock and K. Schilling, Hybrid and orbitally excited mesons in full QCD, Nucl. Phys. Proc. Suppl. **73** (1999) 261–263.

[37] Z.-H. Mei and X.-Q. Luo, Exotic mesons from quantum chromodynamics with improved gluon and quark actions on the anisotropic lattice (2002), hep-lat/0206012.

[38] C. Bernard *et al.*, Exotic hybrid mesons from improved kogut-susskind fermions (2002), hep-lat/0209097.

[39] G. S. Adams *et al.*, Observation of a new j(pc) = 1-+ exotic state in the reaction pi- p → pi+ pi- pi- p at 18-GeV/c, Phys. Rev. Lett. **81** (1998) 5760.

[40] A. W. Thomas and A. P. Szczepaniak, Chiral extrapolations and exotic meson spectrum, Phys. Lett. B **526** (2002) 72–78.

[41] S. Gottlieb, P. B. Mackenzie, H. B. Thacker and D. Weingarten, The rho- pi pi coupling constant in lattice gauge theory, Phys. Lett. **134B** (1984) 346.

[42] R. D. Loft and T. A. DeGrand, Vector meson decay into pseudoscalars from quenched lattice QCD, Phys. Rev. D **39** (1989) 2692.

[43] C. McNeile, C. Michael and P. Pennanen, Hybrid meson decay from the lattice, Phys. Rev. D **65** (2002) 094505.

[44] C. McNeile and C. Michael, Hadronic decay of a vector meson from the lattice (2002), hep-lat/0212020.

[45] P. A. Boyle *et al.*, Status of and performance estimates for QCDOC (2002), hep-lat/0210034.

EXPERIMENTAL STATUS OF EXOTICS

W. Dünnweber
Sektion Physik, Universität München

Abstract
A short introduction to exotic mesons is given and the experimental evidence for mesons with the non-$q\bar{q}$ quantum number combination $J^{PC} = 1^{-+}$ is scrutinized. From studies of annihilation reactions and of peripheral production, evidence for at least two 1^{-+} resonances is accumulating.

1. INTRODUCTION

CERN has a great tradition in meson spectroscopy. Much of today's knowledge is descended from the bubble chamber and LEAR eras. The constituent quark model is a very useful tool to systemize the experimental data. As a result, the $q\bar{q}$ nonets for q = u,d,s with given $J^{PC}(C = (-1)^{L+S})$ are mostly established up to $L = 3$ and many radial excitations are identified as well. As an example, Fig. 1 shows the $J^{PC} = 2^{++}$ nonet.

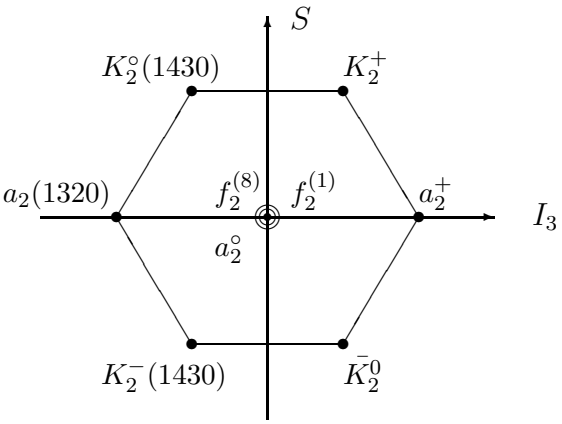

(1)/(8) mixing:
$f_2(1270) \approx n\bar{n}$
$f_2(1525) \approx s\bar{s}$

Fig. 1: The $J^{PC} = 2^{++}$ nonet.

Exotics can be grouped into a) $qg\bar{q}$, b) $gg(g)$ and c) $q\bar{q}q\bar{q}$:

a) hybrids
The excitation of the gluonic string that binds quark and antiquark in an ordinary meson is a natural degree of freedom. Our understanding of QCD and of confinement demands the existence of states formed by coupling string excitations to $q\bar{q}$. These may have non-$q\bar{q}$ quantum numbers, i.e. quantum numbers forbidden for $q\bar{q}$ by the generalized Pauli principle[1]. The lowest hybrid states expected by flux tube or lattice calculations [1] have $J^{PC} = 1^{-+}, 0^{-+}$, and 1^{--}, the first of which is a non-$q\bar{q}$ quantum number combination. For charged mesons C-parity must be replaced by G-parity and the non-$q\bar{q}$ combination is $J^{PG} = 1^{--}$ for isospin $I = 1$.

[1] Allowed quantum number combinations of the $q\bar{q}$ system are $P = (-1)^{L+1}$, $C = (-1)^{L+S}$, with $\vec{L}$ and $\vec{S}$ coupling to the total spin $\vec{J}$ of the meson.

b) glueballs
Gluon self-interaction is inherent to QCD. Building states from constituent gluons has been part of the QCD game since its introduction [2]. Although non-$q\bar{q}$ quantum numbers, e.g. 0^{--}, are to be expected in the glueball spectrum, the lowest lying states come in the order 0^{++}, 2^{++}, 0^{-+} in lattice and other calculations [1]. Thus supernumerary states intrude into the $q\bar{q}$ scheme. Indeed, some $q\bar{q}$ nonets appear to be overpopulated [3]. Configuration mixing will take place and this sets the difficult task to decifer the gluonic nonet from characteristic decay branchings or production strengths [4].

c) quartets and molecules
By flavour coupling a large number of $q\bar{q}q\bar{q}$ multiplets can be created, but it is expected [5, 6] that these are not bound except for the $(q\bar{q})$x$(q\bar{q})$ S-wave. It is tempting to identify the narrow f_0 and a_0 states near the $K\bar{K}$ threshold, close to 1 GeV, with such configurations. A unique signature of quartet states would be flavour exotics. The only recent claim is an isospin 2 resonance in the $\pi^+\pi^+$ and $\rho^0\rho^0$ S-waves produced in the annihilation process $\bar{n}p \to \pi^+\pi^+\pi^-$ and $\rho^0\rho^0\pi^+$ [7].

The present text provides a review of the recent experimental results on resonances with the exotic quantum numbers $J^{PC} = 1^{-+}$ which are of prime importance for the initial stage of the COMPASS hadron program. For a more extensive review on ordinary and exotic mesons, and on glueballs in particular, excellent recent articles [4, 6, 8] are recommended.

2. ANNIHILATION AT REST

The $\eta\pi$ system is attractive for the exotics search since its P-wave must carry non-$q\bar{q}$ quantum numbers $J^{PC} = 1^{-+}$ ($G = -$). It cannot form a glueball, however, because of its isospin 1. Resonances with these quantum numbers are designated here as $\hat{\rho}$, although π_1 appears to become prevailing [3].

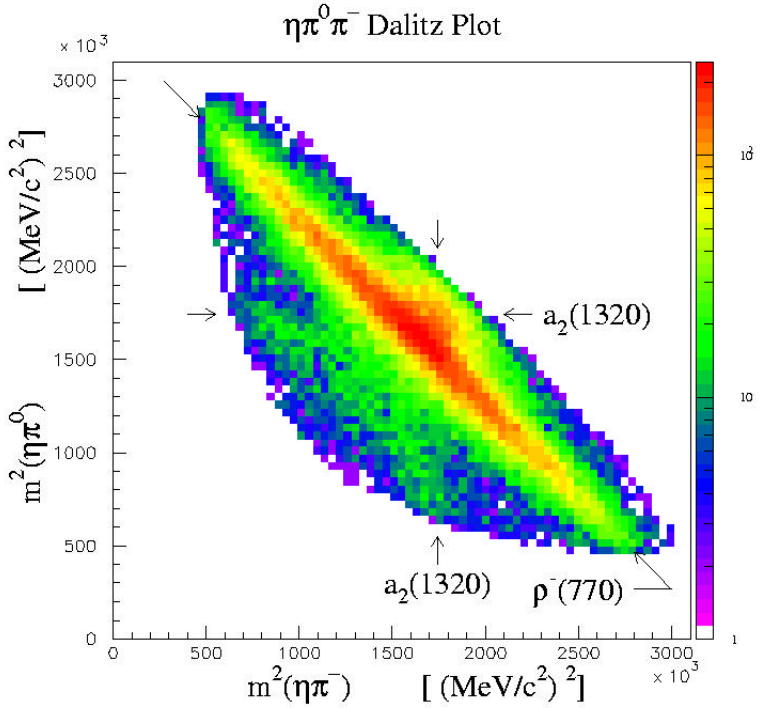

Fig. 2: Experimental intensity distribution (binned and acceptance corrected).

The reaction $\bar{p}n \rightarrow \eta\pi^-\pi^0$, with antiprotons from the LEAR facility stopped in a liquid deuterium target, was studied [9] with the Crystal Barrel detector which was equipped for charged particle and photon spectroscopy with close-to-4π geometry. A sample of 5×10^4 events of the type $\bar{p}d \rightarrow \pi^-\pi^0(\gamma\gamma)\eta(\gamma\gamma)p$ with a proton spectator momentum < 100 MeV/c was fully reconstructed and kinematically selected. The momentum cut was chosen to guarantee the spectator role of the proton, i.e. the negligibility of final-state interactions with the produced mesons. The experimental intensity distribution is displayed as a Dalitz plot in Fig. 2. A simple pattern is observed which is dominated by a diagonal $\rho^-(770)$ band and two broad orthogonal bands in the region of the $a_2(1320)$. The latter show large modulations indicative of interference between odd- and even-L $\eta\pi$ waves.

The partial-wave analysis assumes intermediate states of $\pi^-\pi^0$ resonances with a recoiling η or $\eta\pi$ resonances with a recoiling π:

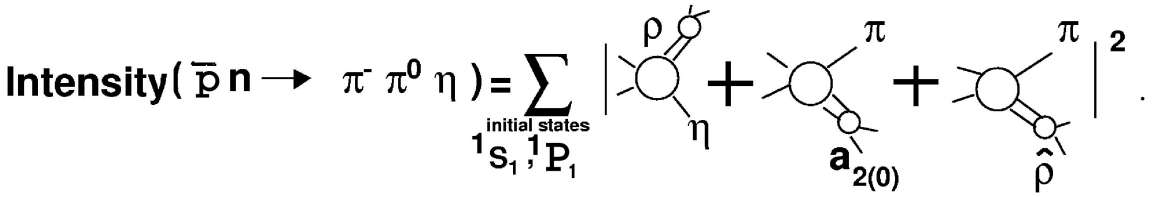

All allowed (see above) known or candidate resonances with nominal mass inside or close to the phase space boundary were tried. The isobar transition amplitude is expressed by use of the Zemach formalism (see Ref. [9] and references given there). A simple model space containing only the $\rho^-(770)\eta$, $a_2(1320)\pi$ and $(\eta\pi)_{P-wave}\pi$ intermediate states is sufficient for a good fit ($\chi^2/N_{dof} = 506/391$). The contribution of the exotic $\eta\pi$ resonance amounts to 11% (without the interferences with the other two resonances), which is almost as much as the a_2 contribution. Without the $\eta\pi$ P-wave no satisfactory fits are obtained and the χ^2 distribution gives evidence for missing interference structure (Fig. 3). Inclusion of the $\eta\pi$ P-wave yields a flat χ^2 distribution with only statistical fluctuations [9].

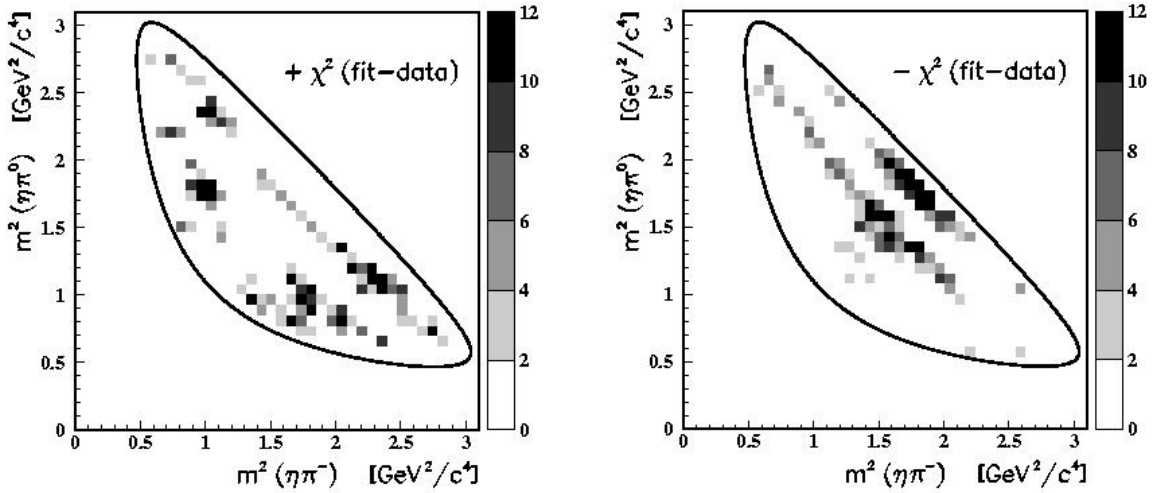

Fig. 3: Deviations between the data and a fit that does not include the $\eta\pi$ P-wave but all other allowed resonances. Left panel: fit exceeds data, right panel: the reverse.

The interference of the $\eta\pi$ P-wave with both the ρ^- and the a_2 resonances pins down the resonance characteristics. The relative phase of the latter two resonances is fixed by their crossing in the Dalitz plot. Both probe the $\eta\pi$ phase motion in different regions. Constructive and destructive interference on opposite sides of the ρ^- band centre is visible in Fig. 4 which shows the intensity distribution of the exotic

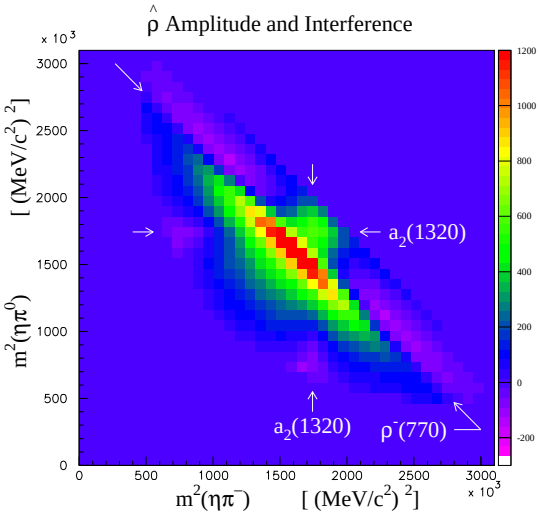

Fig. 4: Intensity distribution of the $\eta\pi$P-wave, as obtained by subtracting from the experimental intensity the ρ^- and a_2 contributions according to the partial-wave analysis.

resonance including the interferences. Moving along a parallel just below the position of the ρ^- band, one observes the rise and fall of the constructive term, which reflects the almost complete phase rotation of the $\eta\pi$ resonance. Close to the phase space boundaries, one finds at $m^2(\eta\pi)$ =(1.7–1.8) GeV^2/c^4 the interference maximum and minimum arising from the overlap with the a_2.

The fitted parameters of the exotic resonance are

$$M = (1400 \pm 20_{stat} \pm 20_{syst})\ \mathrm{MeV}/c^2, \qquad \Gamma = (310 \pm 50_{stat} + 50/-30_{syst})\ \mathrm{MeV}/c^2.$$

These values are not inconsistent with the results for pion-induced reactions (see below). In those cases the relative contribution from the $\eta\pi$ wave is smaller and the evidence is based only on interferences with the a_2.

As an alternative model of the $\eta\pi$ P-wave, an effective range amplitude is found to yield convergent or divergent fits in the range of scattering parameters that characterize resonant or non-resonant behaviour, respectively. The resonant solution is practically identical to the Breit–Wigner fit amplitude.

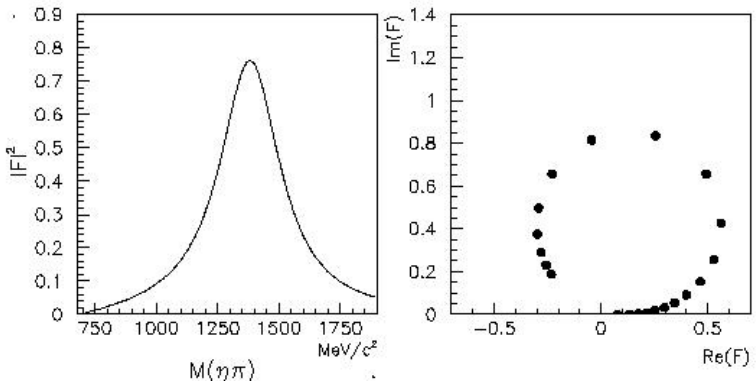

Fig. 5: Left: $(\eta\pi)_P$ effective range amplitude (squared absolute value) fitted to the data. Right: Corresponding Argand plot, showing the imaginary versus the real part of the effective range amplitude. The range from M = 690 to 1800 MeV/c^2 is divided into equal Δm steps. An almost complete anti-clockwise phase rotation is observed.

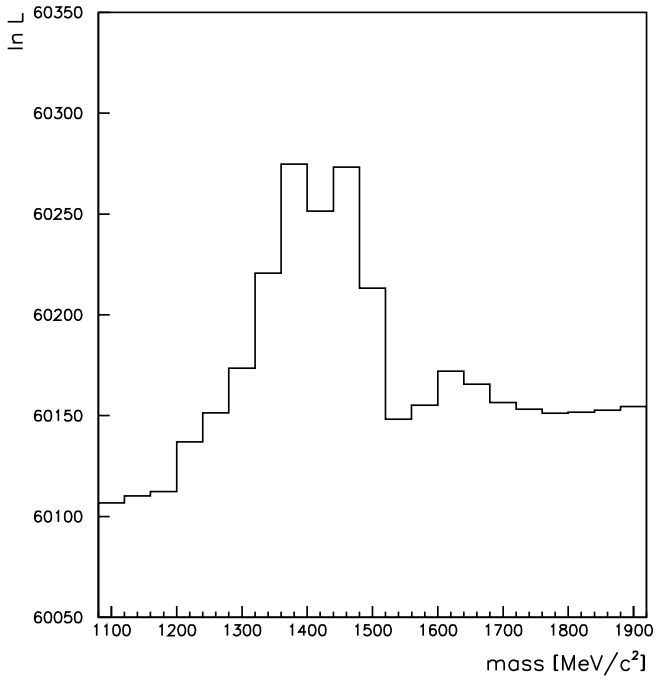

Fig. 6: Mass scan of the ln *Likelihood* for a $(\rho\pi)$ resonance with $J^{PC} = 1^{-+}$ in $\bar{p}n$ (at rest) $\rightarrow (\rho\pi)\pi$.

Its phase motion shows the typical resonance behaviour in an Argand diagram (Fig. 5). It is evident from this representation that the complete phase motion is probed in the present Dalitz plot.

The results of exotics hunting in other annihilation channels may be summarized as follows:

- $\mathbf{\bar{p}p \rightarrow \hat{\rho}(\rightarrow \eta\pi^0)\pi^0}$
  Supportive evidence for the $\hat{\rho}(1400)$ was obtained, with resonance parameters as above, but the observed rate was much smaller than for $\bar{p}n$ annihilation [10]. The difference in the relative rates points to an interesting angular momentum selectivity. For the incoming S-wave the $\hat{\rho}\pi$ channel is accessible only from the singlet spin configuration of $\bar{p}p$ and the triplet configuration of $\bar{p}n$.
- $\mathbf{\bar{p}p \rightarrow \hat{\rho}(\rightarrow \eta'\pi^0)\pi^0}$
  The $\hat{\rho}(1400)$ is not seen but evidence ($\Delta \ln$ *Likelihood* = 20) is obtained for $\hat{\rho}(1600)$ [11].
- $\mathbf{\bar{p}n \rightarrow \hat{\rho}(K^*K)\pi}$
  No evidence for the $\hat{\rho}(1400)$ is found [12], which disfavours a $\mathrm{K}^*\mathrm{K}$ molecular picture [13] for this resonance.
- $\mathbf{\bar{p}n \rightarrow \hat{\rho}(\rightarrow \rho\pi)\pi}$
  A high-statistics study [14] of this 4π final state yields evidence for complex 1^{-+} resonance structure in the m =1400–1700 MeV/c^2 region (Fig. 6), including the above $\hat{\rho}(1400)$. The full partial-wave analysis also yields evidence for the hybrid candidate $\pi(1800)$, with ordinary $\bar{q}q$ quantum numbers 0^{+-}, decaying mainly to $\sigma(\rightarrow \pi^0\pi^0)\pi$.

3. DIFFRACTIVE PROCESSES

The $\eta\pi$ spectrum from π-induced peripheral processes (Fig. 7) is dominated by the $a(1320)$ which is produced mainly by ρ exchange. An additional 1^{-+} resonance becomes visible by its interference with the a_2. After the early claim of the GAMS Collaboration [15] the clearest evidence came from a study of 18 GeV/c $\pi^- p \rightarrow \eta\pi^- p$ at BNL [16]. The analyses differ in the quantum numbers of the exchange

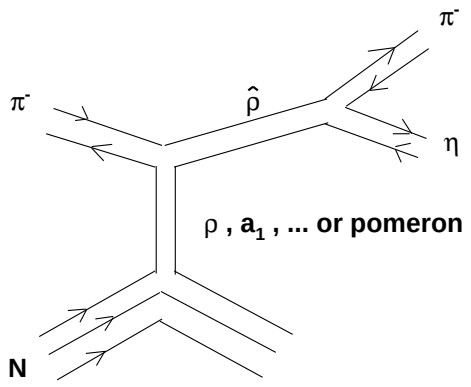

Fig. 7: Quark line diagram of exotics production in a peripheral process.

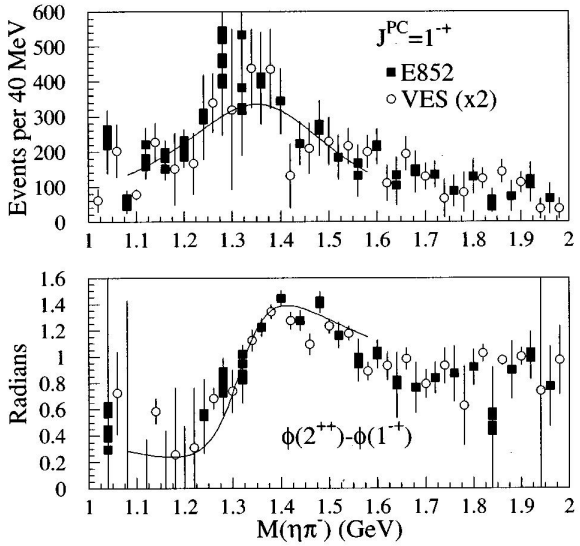

Fig. 8: The exotic 1^{-+} signal as extracted from $\pi^- p \to \eta\pi^- p$ data at $p(\pi^-) = 18$ GeV/c from BNL [16] and from $\pi^- N \to \eta\pi^-$X data at 37 GeV/c from VES [17]. The solid line shows the resonance fit of BNL.

particle which were claimed to be unnatural (a_1-like) in one case [15] and natural (ρ- or pomeron-like) in the other [16]. The 1^{-+} intensity and the phase motion with respect to the a_2 as extracted by the BNL group is in good agreement with corresponding results from VES [17] (Fig. 8). However, recent work from VES which uses better statistics and a new analysis technique shows that a non-resonant $\eta\pi$ P-wave may account equally well for the data [18].

While peripheral production of $\hat{\rho}(1400)$ has only been seen in $\eta\pi$, the evidence for $\hat{\rho}(1600)$ comes from three channels: $b_1\pi, \eta'\pi$ and $\rho\pi$. Consistent resonance parameters, $m = 1600$ and $\Gamma \approx 300$ MeV/c^2, were reported by VES [19] and BNL [20]. The $\hat{\rho}$ branchings of the observed three decay channels are of similar strength. However, as in the case discussed above, in the more recent work from VES [18] the resonant solution appears to be not unique in their new partial-wave analysis of $\eta'\pi$ and $\rho\pi$. It is possible to tune different non-resonant background amplitudes in the alternative analysis to mimic the phase motion of an exotic resonance with respect to the dominant a_2 and π_2 resonances, respectively, in these two channels. However, in the case of $b_1\pi$, the exotic $\hat{\rho}(1600)$ was resistent against any such conspiracy of background amplitudes [18].

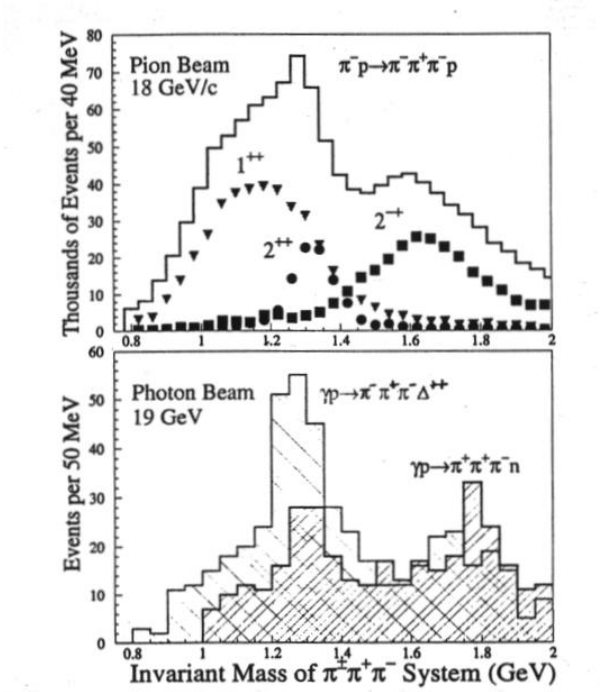

Fig. 9: Comparison of the 3π invariant mass spectra from π^- and γ-induced peripheral photoproduction [21].

Photoproduction can be regarded as a special peripheral production process where the photon interacts like a vector meson. Selective production of hadrons with aligned q and $\bar{q}$ spins, as in the 1^{-+} hybrid model configuration, is expected because of the spin triplet $q\bar{q}$ configuration of a vector meson. Indeed a comparison of the 3π invariant mass spectra (which are mainly $\rho\pi$ spectra) from π and γ-induced production (Fig. 9) shows a dramatic difference in the selectivity. In the former case, the exotic resonance hides, as a 5% contribution, below a dominant $2^{-+}(\pi_2)$ peak. In the latter case [22] π_2 production is not observed. Above the $a_2(1320)$ broad structure appears, peaking at 1.8 GeV/c^2, with most probably $J^P = 1^-$ which would imply the exotic quantum number combination in this case, since $\pi^+\pi^-\pi^-$ couple to isospin 1 and G-parity -1, see Ref. [22]. Because of limited statistics, no full partial-wave analysis is possible for these data, and any other photoproduction data collected so far. The Hall D project at Jefferson Lab will change this situation [21].

At present one can only speculate whether the resonance at 1.8 GeV/c^2, indicated in the lower part of Fig. 9, will turn out to be the third exotic. Possibly the same resonance was seen in the $b_1\pi$ system in a photoproduction experiment at CERN [23]. In π-induced reactions a corresponding peak was found in the $f_1\pi$ spectrum [24] and, with less significance, in the $\rho\pi$ spectrum [20].

4. CONCLUSION

There is hard evidence for exotic resonances with exotic $J^{PC} = 1^{-+}$ at 1400 and 1600 MeV/c^2. The lower one was observed in $\eta\pi$ and probably in $\rho\pi$ but not in $\eta'\pi$, $b_1\pi$ and $f_1\pi$, the upper one in $b_1\pi$ and probably in $\eta'\pi$ and $\rho\pi$ but not in $\eta\pi$. The strongest case for the lower one is $\bar{p}n$ annihilation into $(\eta\pi)_{1^{-+}}\pi$, and for the upper one peripheral production of $(b_1\pi)_{1^{-+}}$. There are indications of a third 1^{-+} resonance, decaying into $b_1\pi$, $f_1\pi$ and $\rho\pi$, at 1800–1900 MeV/c^2 in peripheral production induced by pions or photons. One expects a $qg\bar{q}$ hybrid configuration to branch preferably into $b_1\pi$ and $f_1\pi$ and not into $\eta\pi$, and $q\bar{q}q\bar{q}$ flavour decouplet or octet configurations to branch preferably into $\eta\pi$ or $\eta'\pi$, respectively [25–27]. These expectations suggest a labelling of the above three resonances. However, configuration mixing of exotica is to be expected. Exotica with different isospin and flavour, demanded by the hybrid and quartet schemes, still await experimental discovery.

References

[1] S. Godfrey, these proceedings.

[2] H. Fritzsch and P. Minkowski, Nuovo Cim. **30A** (1975) 393.

[3] Particle Data Group, Eur. Phys. J. C **15** (2000) 1.

[4] S. Godfrey and J. Napolitano, Rev. Mod. Phys. **71** (1999) 1311.

[5] J. Weinstein and N. Isgur, Phys. Rev. Lett. **48** (1982) 659.

[6] F.E. Close and N.A. Törnqvist, J. Phys. G **28** (2002) R249.

[7] A. Filippi, Proc. 9th Int. Conf. on Hadron Spectroscopy, AIP Vol. 619 (2002) 582.

[8] E. Klempt, Proc. Meson 2000, Acta Phys. Polon. **B31** (2000) 2587.

[9] A. Abele *et al.*, Phys. Lett. B **423** (1998) 175.

[10] A. Abele *et al.*, Phys. Lett. B **446** (1999) 349.

[11] J. Reinnarth, Proc. 9th Int. Conf. on Hadron Spectroscopy, AIP Vol. 619 (2002) 792.

[12] F. Meyer-Wildhagen, Diploma thesis (Universität München 1999).

[13] M.S. Chanowitz, Phys. Lett. B **187** (1987) 409.

[14] F. Meyer-Wildhagen, Proc. PANIC 2002 (in press).

[15] D. Alde *et al.*, Phys. Lett. B **205** (1988) 397.

[16] D.R. Thompson *et al.*, Phys. Rev. Lett. **79** (1997) 1630.

[17] G.M. Beladidze *et al.*, Phys. Lett. B **313** (1993) 276.

[18] V. Dorofeev, Proc. 9th Int. Conf. on Hadron Spectroscopy, AIP Vol. 619 (2002) 143.

[19] Yu. Khokhlov, Nucl. Phys. A **663** (2000) 596c.

[20] A.V. Popov, Proc. 9th Int. Conf. on Hadron Spectroscopy, AIP Vol. 619 (2002) 135.

[21] C.A. Meyer, Proc. 9th Int. Conf. on Hadron Spectroscopy, AIP Vol. 619 (2002) 408.

[22] G.T. Condo *et al.*, Phys. Rev. D **43** (1991) 2787.

[23] M. Atkinson *et al.*, Z. Physik C **34** (1987) 157.

[24] J.H. Lee *et al.*, Phys. Lett. B **323** (1994) 227.

[25] S.U. Chung, E. Klempt and J. Körner, preprint BNL-QGS-01-0501 (2002).

[26] F.E. Close and H.J. Lipkin, Phys. Lett. B **196** (1987) 245.

[27] P.R. Page, Phys. Lett. B **415** (1997) 205.

CENTRAL PRODUCTION OF EXOTICS

S.V. Donskov
Institute for High Energy Physics, Protvino, Russia

Abstract
The availability of glueball studies with the COMPASS setup is presented. Central production of X^0 decaying into $\eta\eta$ was used to estimate the registration efficiency. A few scenarios of the possible setup geometry are compared.

1. PHYSICS MOTIVATION

Spectroscopy of light quark systems and glueballs is one of the goals of the COMPASS programme. Since the experiment proposal was published six years ago new experimental data and theoretical descriptions have appeared. But still there are a lot of open questions in this field, high-statistics detailed data are needed to clarify the picture. A detailed review of this subject was made by S. Godfrey at this workshop, so my presentation will be short. QCD predicts the existence of non-$q\bar{q}$ mesons such as glueballs and hybrids. The best glueball mass estimates come from lattice gauge theory calculations. The lightest glueball has $J^{PC} = 0^{++}$ and its mass should be in the range 1.45–1.75 GeV.
Special methods based on production characteristics, decay patterns and relations to other mesons could be applied for a glueball search, namely:

- search for the states with J^{PC} not allowed for normal $q\bar{q}$ states, for example 1^{-+};
- a study of the extra states, that is states that have the quantum numbers of already completed nonets, with low masses (to exclude radially excited nonet members);
- a detailed study and look for the states with unusual branching ratios;
- search for the states preferentially produced in gluon-rich processes (Fig. 1): Pomeron–Pomeron scattering, J/ψ decays, proton–antiproton annihilation, special hadronic reactions.

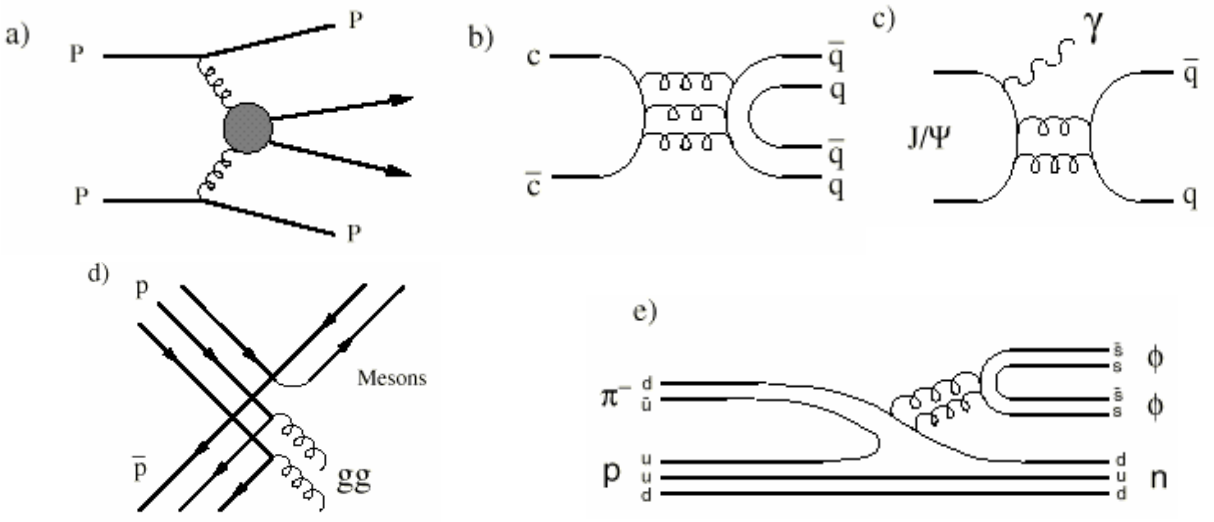

Fig. 1: Gluon-rich processes: a) Pomeron–Pomeron exchange; b) and c) J/ψ decays; d) $p\bar{p}$ annihilation; e) reactions involving disconnected quark lines.

According to lattice inspired models, glueballs will mix strongly with nearby $q\bar{q}$ states with the same J^{PC}. The three states in the glueball mass range are: $f_0(1370)$, $f_0(1500)$ and $f_0(1710)$**.** The WA102 Collaboration published, for the first time in a single experiment, a complete data set for the decay branching ratios of these mesons to all pseudoscalar meson pairs: $\pi\pi$, $K\bar{K}$, $\eta\eta$, $\eta\eta'$, 4π. Based on this data, an analysis of the scalar glueball-$q\bar{q}$ mixing was done by A. Kirk and F. E. Close [1]. They identify a systematic correlation between glueball mass, mixing, and flavour symmetry breaking and conclude that the glueball may be rather lighter than some quenched lattice QCD computations have suggested.
A result that is more general than any specific mixing scheme is that no pair out of the three $f_0(1370)$, $f_0(1500)$, $f_0(1710)$ can be in the same pure $q\bar{q}$ nonet; other degrees of freedom are required. The WA102 data and world averages lead to the summary for the favoured results

	$f_{i1}^{(G)}$	$f_{i2}^{(S)}$	$f_{i3}^{(N)}$
$f_0(1700)$	0.39 ± 0.03	0.91 ± 0.02	0.15 ± 0.02
$f_0(1500)$	-0.65 ± 0.04	0.33 ± 0.04	0.70 ± 0.07
$f_0(1370)$	-0.69 ± 0.07	0.15 ± 0.01	0.07 ± 0.07

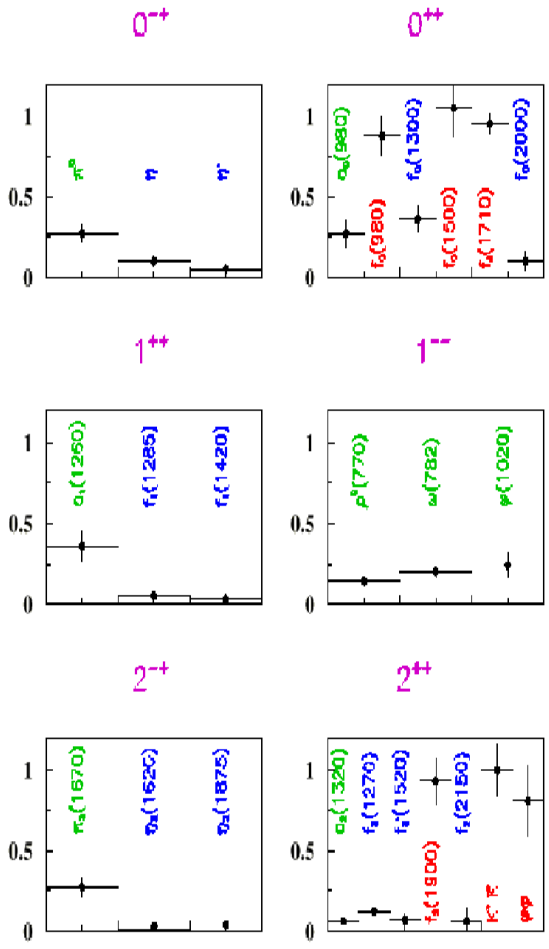

Fig. 2: Gluon filter.

for which m_G = 1443 ± 24 MeV, m_N = 1377 ± 20 MeV and m_S = 1674 ± 10 MeV. The solution is compatible with the relative production strength in pp central production, $p\bar{p}$-annihilations and J/ψ radiative decays.
An interesting empirical observation of a different topology for central production of glueball candidates and $q\bar{q}$ mesons was done [2]. It was observed, that the ratio

$$R = \frac{N(\Delta P_T < 0.2\,\mathrm{GeV})}{N(\Delta P_T > 0.5\,\mathrm{GeV})}$$

for the number of events N with small and large ΔP_T is sensitive to the resonance nature. ΔP_T here is the absolute value of the momentum transfer difference for fast and slow hadrons. For undisputed $q\bar{q}$ mesons produced by Double Pomeron Exchange (DPE) $R < 0.1$, $R \approx 0.25$ for the states which cannot be produced by DPE ($I = 1$ or $G = -$); $R \approx 1$ for the states with a rich gluon component. The results of the WA102 experiment are presented in Fig. 2.

2. EXPERIMENTAL LAYOUT

The COMPASS spectrometer setup for the central production measurements (Fig. 3) is described in the original experiment proposal. I will concern myself with few detectors only which are essential for the hadron part of the programme. The spectrometer consists of a large and a small angle spectrometer stage. The standard COMPASS tracking system is the same as for the muon setup. Two RICH detectors are used for charged particle identification. A 40 cm long liquid hydrogen target is installed in the RPDS [3]. Guard lead scintillator sandwiches were placed after the RPDS. The 30 × 30 cm^2 scintillator counter was installed at the end of the setup to register the fast hadron produced in the central production reaction. This counter has a hole of 5.2 cm in diameter to transport the non-interacting beam. The RPDS will select events consistent with only one particle coming from the target. Measurements of this slow particle velocity will be done. An essential part of the hadron setup is the electromagnetic calorimeters ECAL1 and ECAL2.

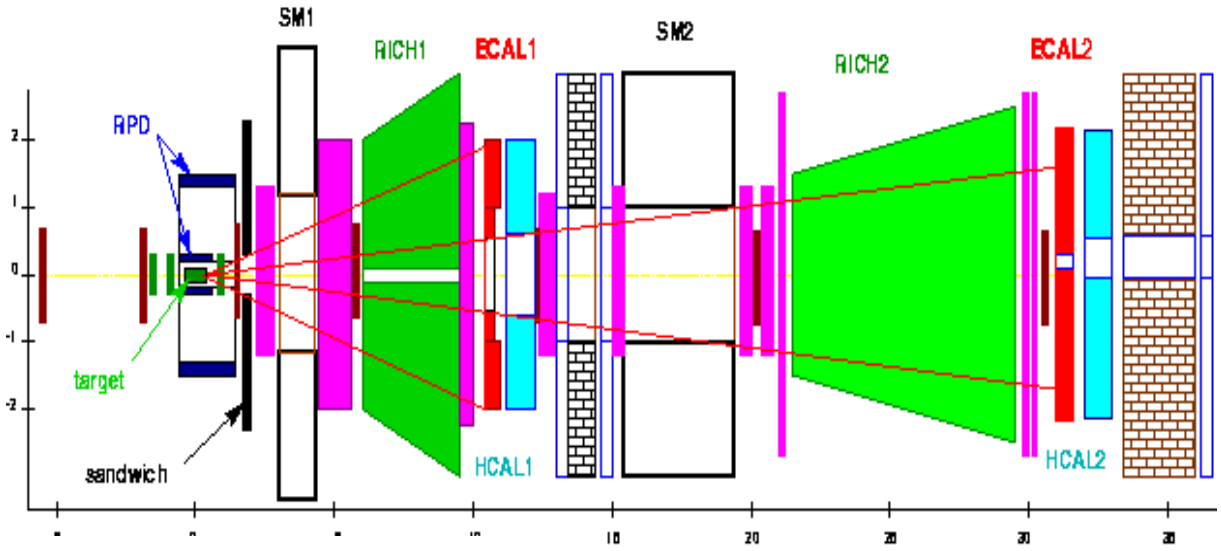

Fig.3: COMPASS Cental Production layout.

The main characteristics of the detectors are:

- ECAL1:
  - Total number of channels: 3216
  - Size: 4 × 2.9 m^2
  - $\sigma(E)/E = 5–6\%/\sqrt{E} \otimes 2\%$
- ECAL2:
  - Total number of channels: 3436
  - Size: 4.4 × 2 m^2
  - $\sigma(E)/E = 5–6\%/\sqrt{E} \otimes 2\%$
- Liquid H_2 target:
  - Length: 40 cm, 2.83 g/cm^2, 0.046 X_0
- RPDS
  - Total number of channels: 60
  - Time measurements
    - TOF resolution: 350 ps for MIP
    - Space resolution: A layer: 1.8 cm, B layer: 2.7 cm
  - Amplitude measurements:
    - Space measurements based on light attenuation
    - dE/dx
  - Measurement accuracy (P_{slow},) for time and amplitude are comparable.

3. MONTE CARLO SIMULATION

To understand the COMPASS spectrometer performance for the central production process a Monte Carlo simulation was made for the most pessimistic version of the setup with an ECAL2 size that was half that of the basic setup. Due to this change ECAL1 was placed at 15 m from the target instead of 11 m.

To study the setup operation for registration of the central production event the reaction

$$h\,p \to h_{fast}\,p_{slow}\,M_{centr}$$

was used, where h is the beam hadron, h_{fast} the fast secondary hadron, p_{slow} the slow recoil proton, M_{centr} the produced central system.

Two decay channels of the central system were studied:

$$M_{centr} \to \eta\eta \to 4\gamma \qquad \text{(the neutral decay channel)}$$

$$M_{centr} \to \eta\eta \to 2\gamma,\ \eta \to \pi^0\pi^+\pi^-,\ \pi^0 \to 2\gamma \qquad \text{(the mixed decay channel)}$$

The program COMGEANT was used to generate the Monte Carlo events. The generator for the central production events was analogous to that used in the WA102 experiment. The range of the generated events on M_{centr} was 1.2–4 GeV. The beam energy was 180 GeV, the beam size 1.2×1.2 mm^2, the beam divergence 0.3 mrad for both coordinates.

At the event generation the following trigger requirements were imposed:
1) a hit of only one counter in both the A and B layers of the RPDS;
2) absence of hits in the guard sandwiches;
3) a hit in the counter for fast hadron detection.

The generated events were reconstructed using the CDRA2 program and the following events were taken for further analysis:

a) neutral mode:
   1) one primary vertex with one secondary track with an energy of more than 140 GeV was reconstructed in the setup target;
   2) four photons found with energy more than 0.4 GeV in ECAL1 or more than 0.8 GeV in ECAL2.

b) mixed mode:
   1) one primary vertex with three secondary tracks, one of which with an energy of more than 140 GeV;
   2) four photons in ECAL1 and ECAL2 with the same energy cuts as above.

Then the events passed through the kinematics fit and the events with the probability of more than 1% for a corresponding hypothesis were selected (C3-fit for the neutral mode and C4-fit for the mixed mode).

The energy distribution for h_{fast} is shown in Fig. 4. As seen in this figure, the energy of h_{fast} is generally higher than 150 GeV and close to the beam energy.

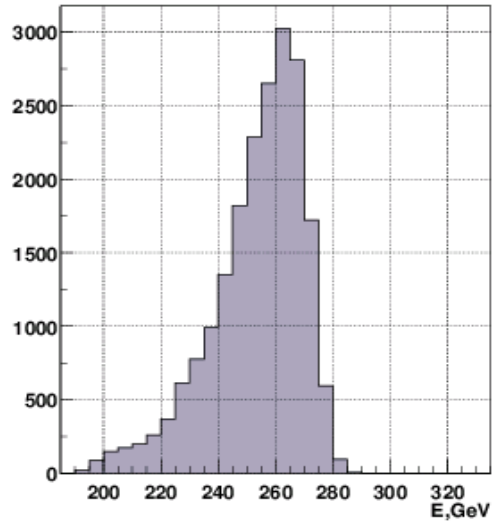

Fig. 4: Fast hadron energy.

In Fig. 5 one can see the momentum distribution of generated p_{slow} as well as that satisfying the trigger requirements. The threshold due to proton absorption in liquid hydrogen and RPDS material is clearly seen. The energy distribution of the M_{centr} versus its mass is shown in Fig. 6. It is seen that the mean energy of M_{centr} is growing with the mass.

Mass resolution of the reconstructed events appeared to be about 12 MeV (Fig. 7), and it is approximately the same for both decay modes.

In Fig. 8 one can see the x_F distribution of reconstructed events.

The setup registration efficiency as a function of M_{centr} is presented in Fig. 9 (the neutral mode) and Fig. 10 (the mixed mode). This efficiency includes the geometrical efficiency, the CORAL reconstruction efficiency and the influence of the selection criteria used.

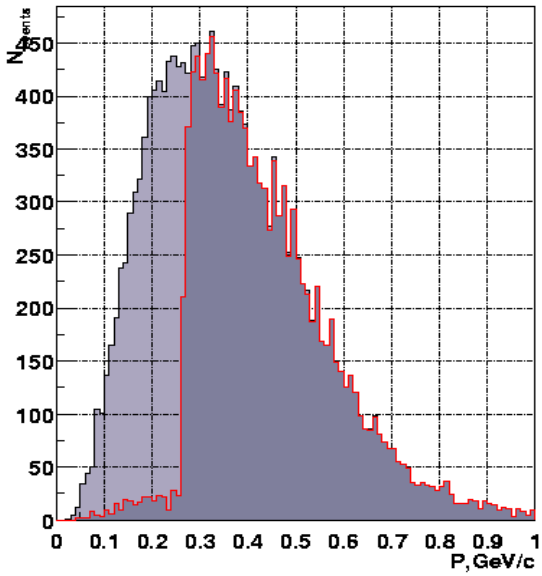

Fig. 5: Slow proton momentum.

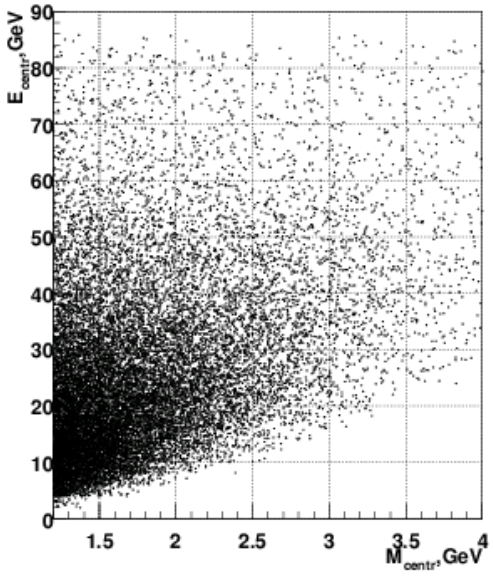

Fig. 6: Central system energy vs mass.

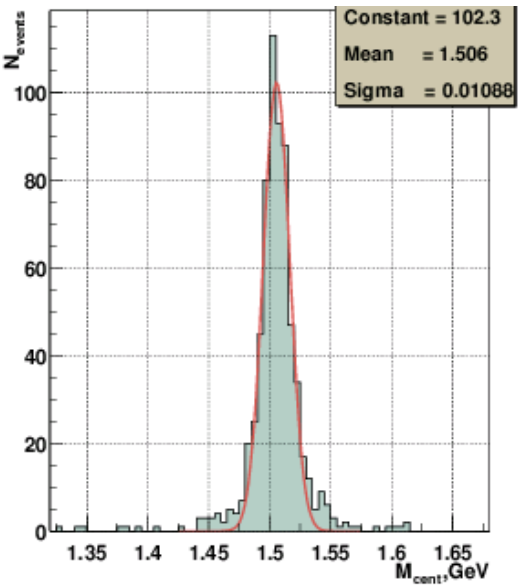

Fig. 7: Mass resolution, $\eta\eta \to 4\gamma\pi^+\pi^-$, C4-fit.

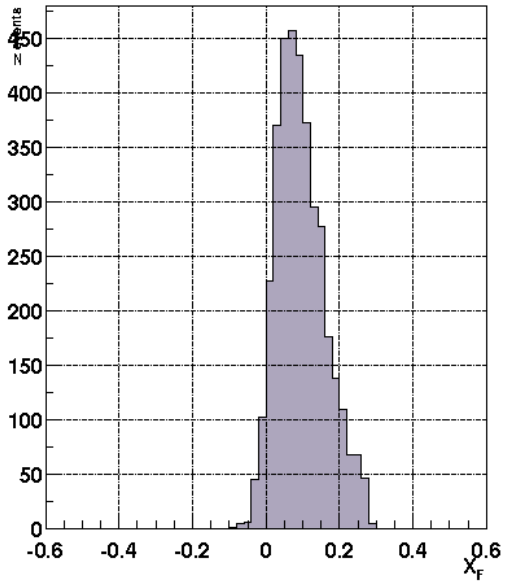

Fig. 8: x_F, $\eta\eta$ (4γ) central system.

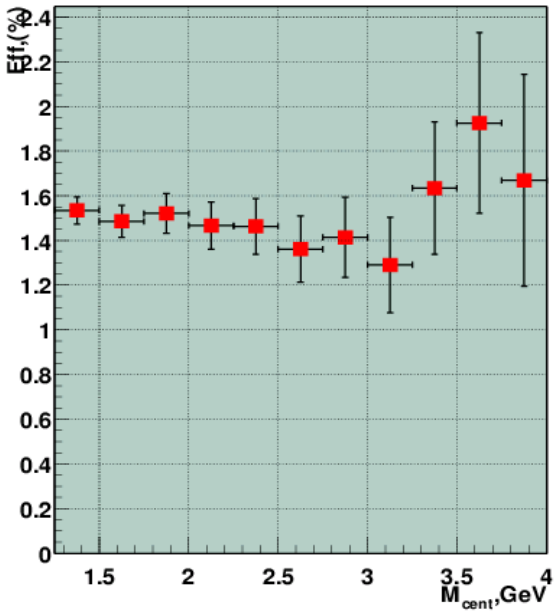

Fig. 9: Efficiency, $\eta\eta \to 4\gamma\pi^+\pi^-$, ECAL2 at 34 m.

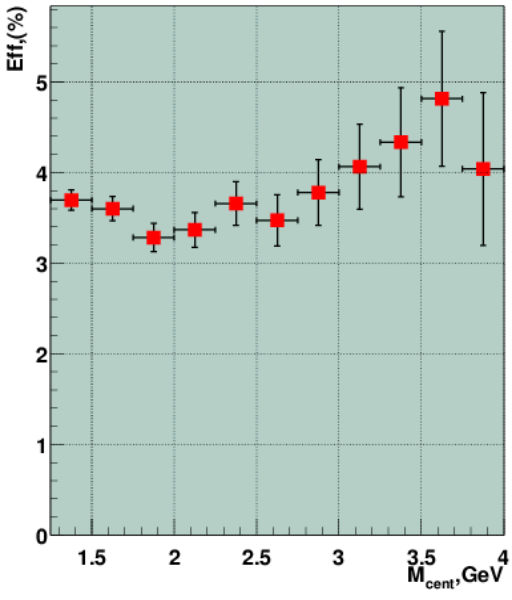

Fig. 10: Efficiency, $\eta\eta \to 4\gamma$, ECAL2 at 34 m.

The WA102 result for the cross section of the $f_0(1500)$ central production in pp interaction at 450 GeV is 2914±301 nb [4]. To estimate the COMPASS counting rate of the centrally produced $f_0(1500)$ in the $\eta\eta$ decay mode a value of 3 μb was used. With beam intensity 2.5×10^7 particles/spill (limited by the radiation hardness of the ECAL2 calorimeter) one can expect 450 events/day. The total statistics of WA102 for $f_0(1500)$ in the $\eta\eta$ decay mode is 3351 events [5].

There are evident recommendations to increase the counting rate. The nominal COMPASS setup with the proposed ECAL2 improves by a factor two in γ acceptance (18% for the simulated pessimistic setup), moreover the use of the sandwich type electromagnetic calorimeter in place of the sandwich counter (Fig. 3) gives the possibility to increase this value up to 95%. The acceptance cuts for different geometries are presented in Fig. 11. Another possibility is to produce a radiation-resistant ECAL2 central part to increase the acceptable beam intensity.

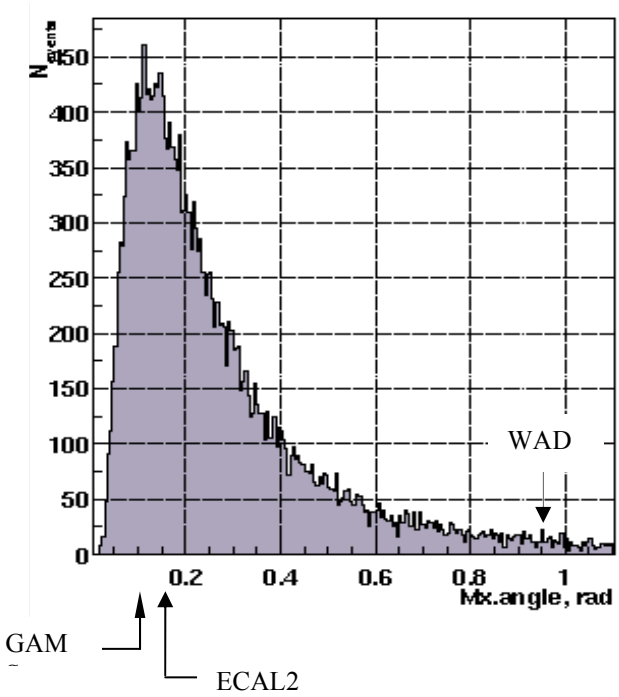

Fig. 11: γ acceptance for centrally produced $\eta\eta$ system decaying into 4γ.

4. CONCLUSION

The features of the COMPASS spectrometer are large geometrical acceptance, high mass, energy and angular resolution for the decay products, good particle identification, powerful data acquisition system, availability to operate in high-intensity beams. The estimated value of the registration efficiency calculated with COMGEANT is one order of magnitude higher then that for the WA102 setup. All this opens the possibility to use COMPASS for precise high statistics measurements of the centrally produced mesons decaying particularly into $\eta\eta$, $\eta\eta'$, $\eta'\eta'$, in which one may expect a manifestation of the gluonic component.

REFERENCES

[1] F. E. Close and A. Kirk, Scalar glueball-$q\bar{q}$ mixing above 1 GeV and implications for lattice QCD, Eur. Phys. J. C **21** (2001) 531–543.

[2] F. E. Close and A. Kirk, A Glueball-$q\bar{q}$ filter in Central Hadron Production, Phys. Lett. B **397** (1997) 333–338.

[3] D. Alde *et al.,* Nucl. Instrum. Methods A **342** (1994) 389.

[4] A. Kirk, Resonance production in central pp collisions at the CERN Omega Spectrometer, Phys. Lett. B **489** (2000) 29–37.

[5] D. Barberis *et al.,* A study of $\eta\eta$ channel produced in central pp interactions at 450 GeV/*c*, Phys. Lett. B **479** (2000) 59–66.

SIMULATION OF THE $\eta\pi^-$ DIFFRACTIVE PRODUCTION AND DETECTION AT COMPASS

*Valery Dorofeev**
Institute for High Energy Physics, Protvino, Russia

Abstract
We present preliminary results of simulation of the $\eta\pi^-$ system production, detection and reconstruction at the COMPASS hadron set-up.

1. INTRODUCTION

At present several groups have evidence for $J^{PC} = 1^{-+}$ meson production (Tab. 1), which is forbidden for ordinary quarkonia and hence might be a good candidate for a hybrid [1,2]. Here J is the total angular momentum, P is the parity, C is the charge parity. The $\pi_1(1400)$ meson shows up in the $\eta\pi$ final state in two experiments [3–5]. The VES group found that the results of the $\eta'\pi^-$ and $b_1\pi$ system Partial-Wave Analysis (PWA) at 37 GeV/c agree with the production of the higher mass $\pi_1(1600)$ [6], evidence for which in the $\eta'\pi^-$ has been also confirmed by E852 at BNL [7,8]. The latest analysis by VES of the 2.5 times larger data sample collected at 28 GeV/c [9] confirmed in general the results of the $\eta\pi^-$, $\eta'\pi^-$ and $b_1\pi$ system PWA of the 37 GeV beam data.

However, they pointed to the possible non-resonant nature of the 1^{-+} state in the $\eta\pi^-$ and $\eta'\pi^-$ systems.

A PWA of the diffractively produced $\eta\pi^-$ state shows that two partial waves are significant:

- the $J^P M^\eta = 2^+1^+$ with the intensively produced $a_2(1320)$ meson, denoted by D_+,
- the $J^P M^\eta = 1^-1^+$ with exotic quantum numbers, denoted by P_+,

where M is an absolute value of the total angular momentum z projection, η reflectivity [10]. The result of the $\eta\pi$ PWA is intensities and a relative phase of the P_+ and the D_+ partial waves. The issue is: Does the phase of the P_+ wave show a resonant behaviour?

Table 1: Evidence for $J^{PC} = 1^{-+}$ exotics.

Exp.	Mass (MeV)	Width (MeV)	Reaction
BNL	1359^{+16+10}_{-14-24}	314^{+31+9}_{-29-66}	$\pi^- p \to \eta\pi^- p$
CBar	$1400 \pm 20 \pm 20$	$310 \pm 50^{+50}_{-30}$	$\bar{p}n \to \pi^-\pi^0\eta$
CBar	1360 ± 25	220 ± 90	$\bar{p}p \to \pi^0\pi^0\eta$
VES	(1316 ± 12)?	(287 ± 25)?	$\pi^- Be \to \eta\pi^- Be$

2. EVENT PROCESSING SCHEMA

To get an answer to the question whether COMPASS can collect a much larger data sample, the following scheme of event processing has been carried out (see Fig. 1). An event was generated by a stand-alone program. Simulated momenta and a vertex were passed to the input of the COMGEANT program. COMGEANT is a standard COMPASS tool for simulation of the set-up response to a transversing particle. Then tracks were reconstructed by a standard COMPASS reconstruction program CORAL, slightly fitted to the hadron set-up. Physical quantities (energy and intercept with a calorimeter) of the detected gammas were smeared, according to the calorimeter resolution taken from the proposal [11]

*) e-mail: dorofeev@cern.ch

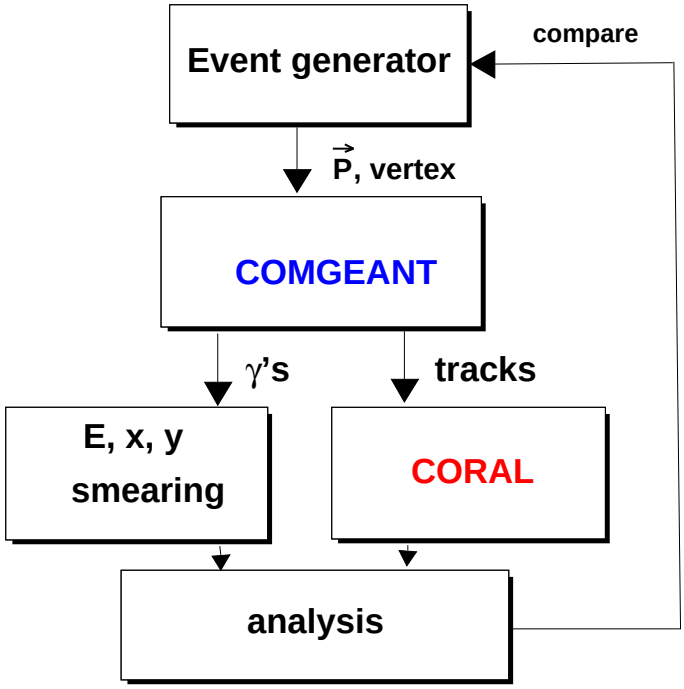

Fig. 1: An event processing scheme.

$\sigma_E/E = 1.5\% + 5.5\%/\sqrt{(E)}$, and $\sigma_{XY} = 6$ mm$/\sqrt{(E)}$, (E in GeV). The $ECAL_2'$ option of the COMPASS hadron set-up was studied. Description of the $ECAL_2'$ option can be found in Ref. [12]. Trigger requirements have not been studied in this work. A procedure of a physical analysis was applied to the reconstructed event and the results were compared to Monte Carlo simulations.

3. SIMULATION OF THE PRODUCTION AND DECAY PROCESSES

An exclusive diffractive process $\pi^- p \to Xp$ was simulated as a first step. A monochromatic pin-like beam $P_x = P_y = 0$, and $P_z = 190$ GeV and a rotational symmetry about the beam were assumed. A vertex is always in the centre of the target. A momentum transfer squared distribution was taken in the form $\frac{d\sigma}{t'} \sim \exp(-bt')$, where $t' = t - t_{min}$ and $b = 8$ GeV^{-2} is a typical slope value for diffractive production on the hydrogen target. It is essential for the PWA to measure not only a partial wave under study (P_+ wave in our case), but a relative D_+ wave too. Therefore two options of the X state have been studied:

- the $D_+(\eta\pi)$ with mass in the range $[0.92 \div 2.12\ \mathrm{GeV}]$ with 0.2 GeV step,
- the $P_+(\eta\pi)$ produced with intensity as was presented by VES at Hadron2001 [9].

The following X decay chain was selected: a decay $X \to \eta\pi^-$ in the P or D wave, is followed by the $\eta \to \pi^+\pi^-\pi^0$ and the $\pi^0 \to \gamma\gamma$. Therefore we finally have the reaction $\pi^- p \to \pi^+\pi^-\pi^-\gamma\gamma + p$ with three forward moving charged pions and two gammas and a recoil proton.

The $D_+(\eta\pi)$ state kinematics with $M_{\eta\pi} = 1.32$ GeV is shown as an example in Fig. 2 and Fig. 3. The recoil proton is soft, according to the diffractive nature of the production process. The $\cos\Theta_{GJ}$ distribution of the D wave decay has two peaks, corresponding to the mainly forward or backward production of the η meson, where Θ_{GJ} is a polar angle of the η meson in the Gottfried–Jackson reference frame. The Gottfried–Jackson reference frame is a rest frame of the $\eta\pi^-$ system with the z-axis in the

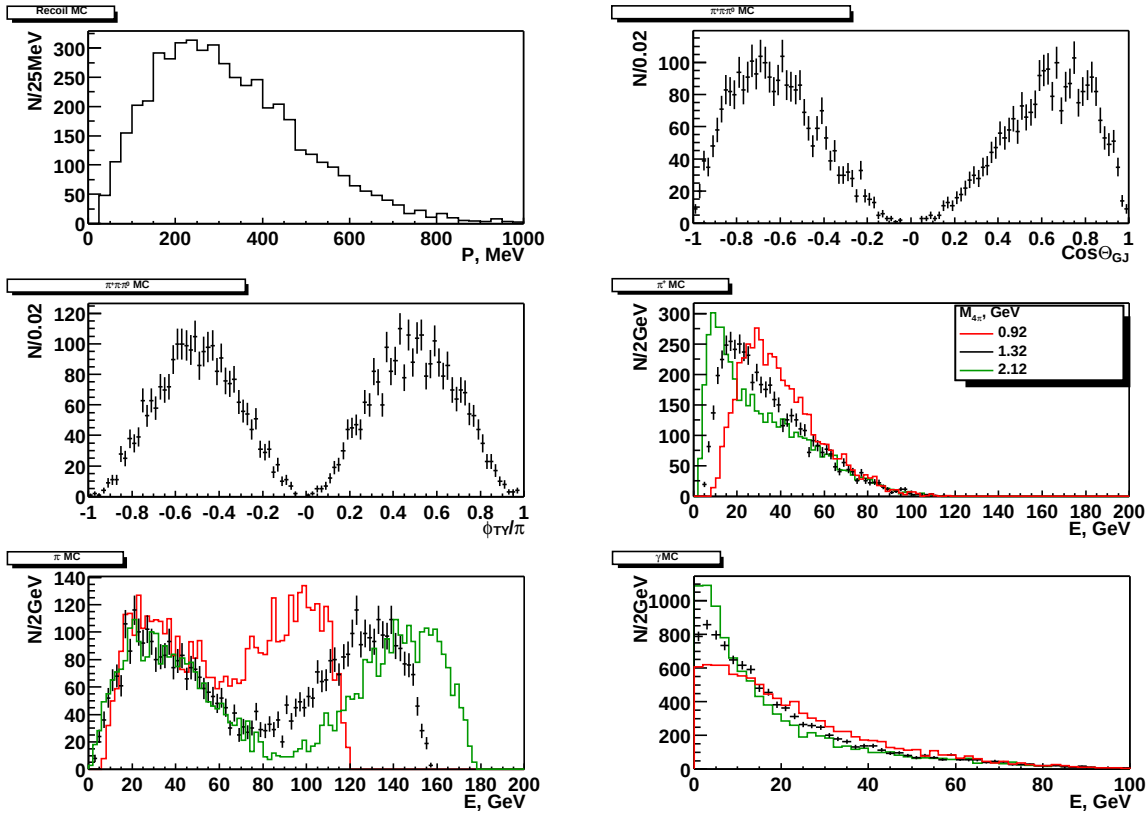

Fig. 2: Kinematical properties of the $D_+(\eta\pi)$ events.

direction of the beam and the y-axis perpendicular to the production plane. A superimposed plot shows a more spherical feature of the P_+ wave $\eta\pi^-$ system decay. An axial angle of the η in this frame the ϕ_{TY} is called a Treiman–Young angle and has a $\sin^2\phi_{TY}$ form, which stands for the $\eta\pi^-$ production with $M = 1$. Plots for three different $\eta\pi$ mass values show the mass dependence of the final state particles' momenta. The distribution shown in Fig. 3 reflects the spatial dispersion of tracks and gammas. A fact that only a small tail of the maximal laboratory γ polar angle distribution is greater than 30 mrad means, that nearly almost all γ's move through the hole in the $ECAL_1$ and strike the $ECAL_2'$. One might expect to have a large γ acceptance. An angular distance $\Delta = \sqrt{(\delta\frac{P_x}{P_z})^2 + (\delta\frac{P_y}{P_z})^2}$ is a distance between particles in a plane divided by a distance to the vertex. The distribution for tracks of it's minimal value peaks near 3 mrad. The angular distance between γ's is in general greater than the angle size of a $ECAL_2'$ cell and therefore means a rare π^0 meson loss caused by the unseparated γ's.

4. EFFICIENCIES

A capability of the $\eta\pi^-$ system detection is expressed by an efficiency, which is a product of the track and the γ detection efficiency and the track reconstruction efficiency. The γ reconstruction efficiency was assumed to be equal to 1 in our work. The sources of inefficiency can be exemplified by Fig. 4, where the efficiencies of the $D_+(\eta\pi)$ events with the relatively high-mass $M_{\eta\pi} = 2.12$ GeV are shown. A low track reconstruction efficiency is due to the poor reconstruction procedure in the presence of a background, originating from the particle interaction with the material of the set-up. One observes a sharp decrease for soft tracks ($E_{track} < 10$ GeV). A fall is observed in the Δ_{min} dependence of the efficiency of events with narrow tracks and of very dispersed ones. These track inefficiencies cause the objectionable fall of the event efficiency for the backward moving η meson in the Gottfried–Jackson

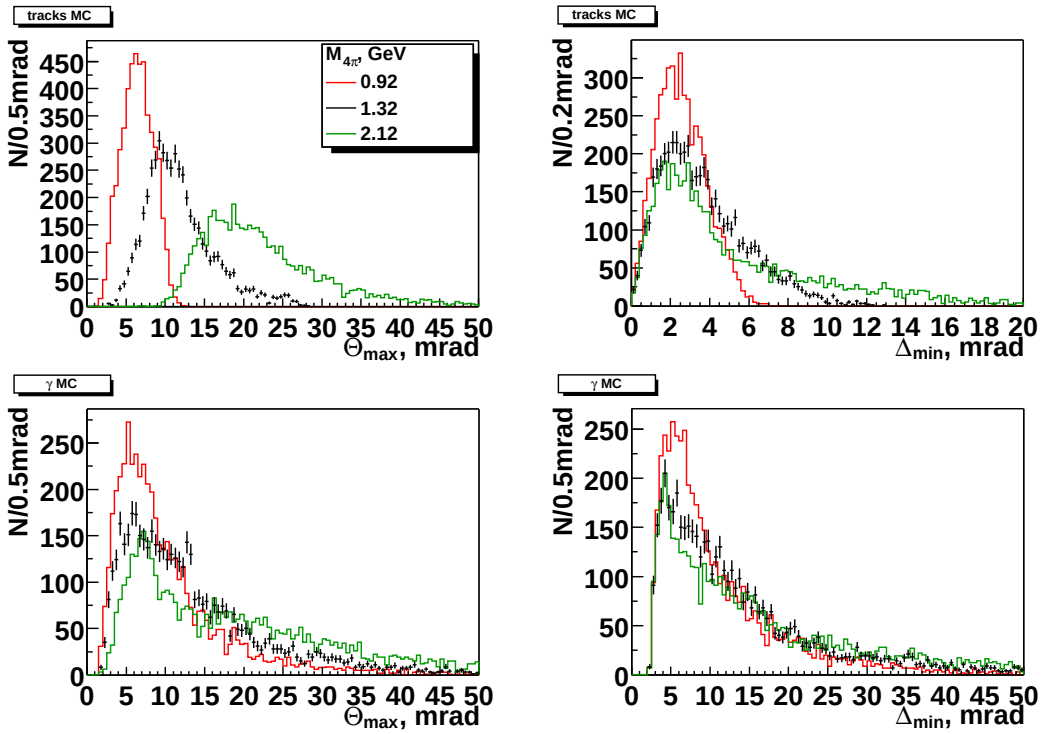

Fig. 3: Spatial dispersion of the $D_+(\eta\pi)$ events.

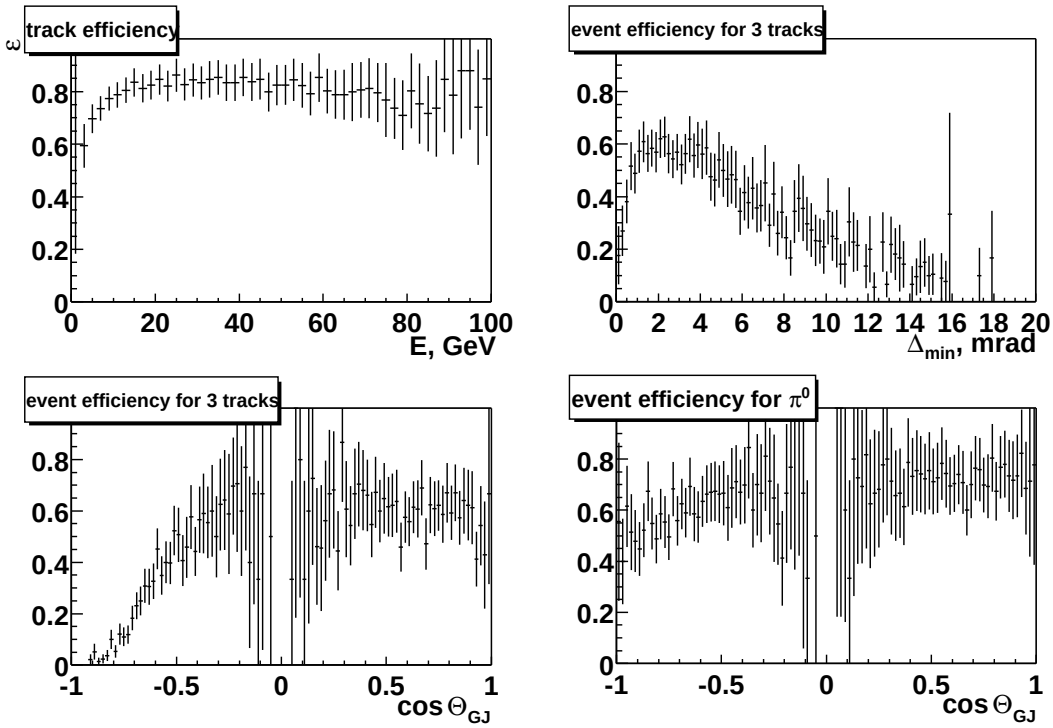

Fig. 4: Efficiency of the $D_+(\eta\pi)$ events with $M_{\eta\pi} = 2.12$ GeV.

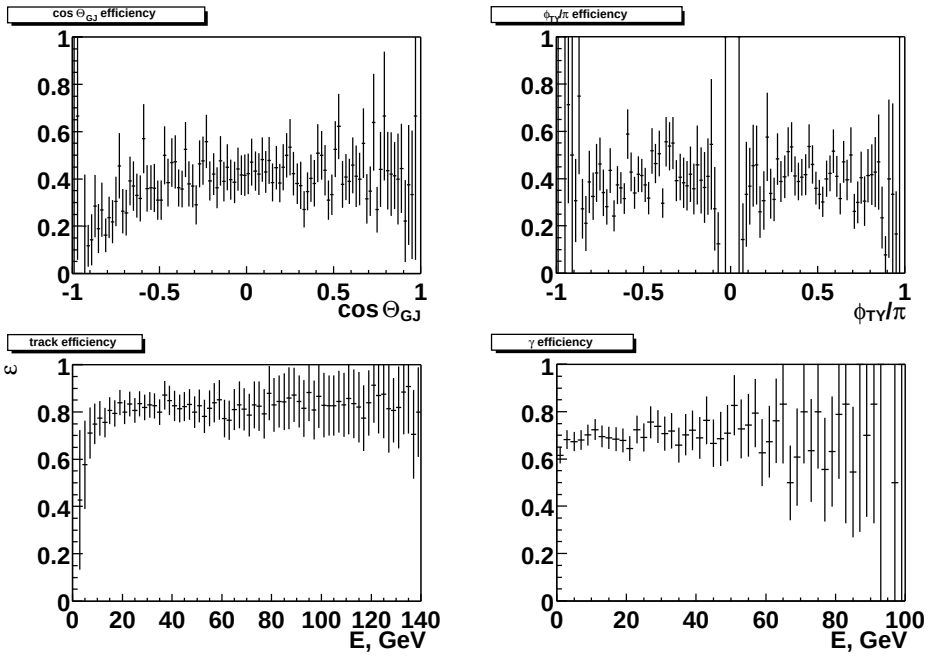

Fig. 5: The detection and reconstruction efficiency of the $P_+(\eta\pi)$ events.

reference frame and hence an asymmetry in the cosine of the Gottfried–Jackson angle distribution (see Fig. 4). There is also a weak dependence of the event efficiency upon the detection of the π^0. The γ acceptance is large enough thus making the γ absorption in the material of the set-up the dominant contribution to the event inefficiency. However, the absorption in the target, which is $\approx 5\%$ of the radiation length, is relatively small.

Integral efficiencies of the $P_+(\eta\pi)$ events over the whole range are shown in Fig. 5. There are no strong mass dependence of the event efficiency, which decreases by $\approx 25\%$ with the mass increasing for both states under study, as shown in Fig. 6 and Fig. 7. The individual contributions of the track and γ efficiencies to the total efficieny are nearly equal (see Fig. 6).

5. RESOLUTIONS

The $D_+(\eta\pi)$ mass resolution at $M_{\eta\pi} = 1.32$ GeV is shown in Fig. 8. The lower histogram and curve show the difference between generated and reconstructed Monte Carlo events for the 4π invariant mass for the case that the reconstructed momenta of the charged pions are coupled to the Monte Carlo momentum of the π^0 meson. The upper histogram and curve are for the case that the reconstructed momenta of the charged pions are coupled to the reconstructed momentum of the π^0 meson after a $1C$ fit to the π^0 mass has been applied to the γ energies. An approximate equality of the widths means that the dominant contribution to the 4π mass resolution is the charged track resolution. To which, in turn, a multiple scattering in the material of the set-up gives a major contribution.

The $\eta\pi$ mass dependence of the resolution is shown in Fig. 9. A σ_M/M ratio is $\approx 0.5\%$, which slightly increases when M becomes larger.

Resolutions of the $\pi^+\pi^-\pi^0$ mass, the cosine of the Gottfried–Jackson angle, the Treiman–Young angle, the axial angle and the transverse momentum of the recoil proton in the laboratory frame are presented in Table 2. It is worth pointing to a nice $\pi^+\pi^-\pi^0$ mass resolution, which is only 2.7 MeV.

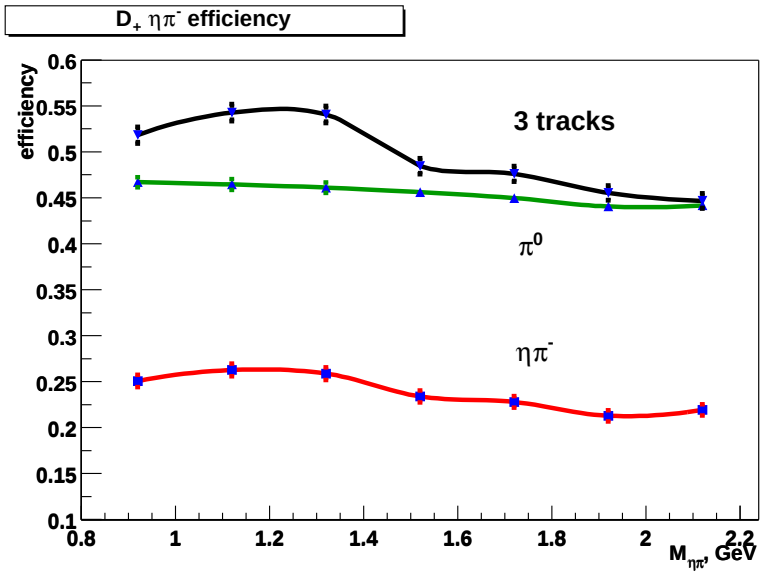

Fig. 6: Mass dependence of the $D_+(\eta\pi)$ events efficiencies.

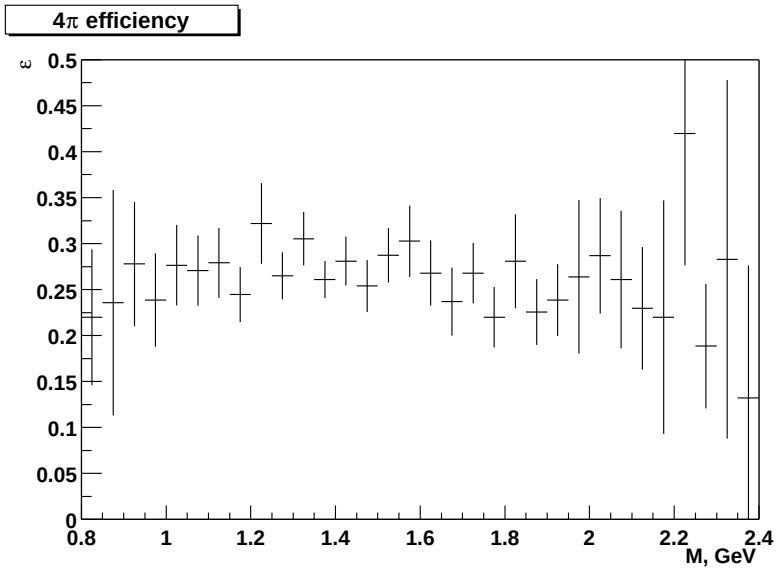

Fig. 7: Mass dependence of the $P_+(\eta\pi)$ events efficiency.

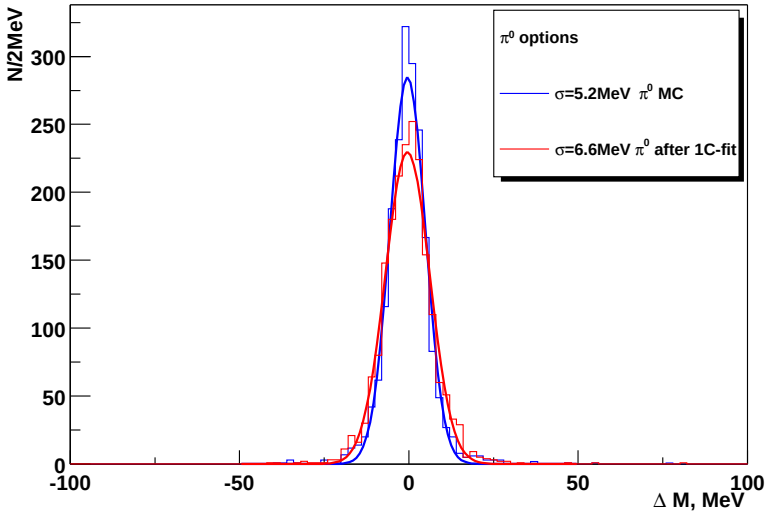

Fig. 8: The $D_+(\eta\pi)$ mass resolution at $M_{\eta\pi} = 1.32$ GeV.

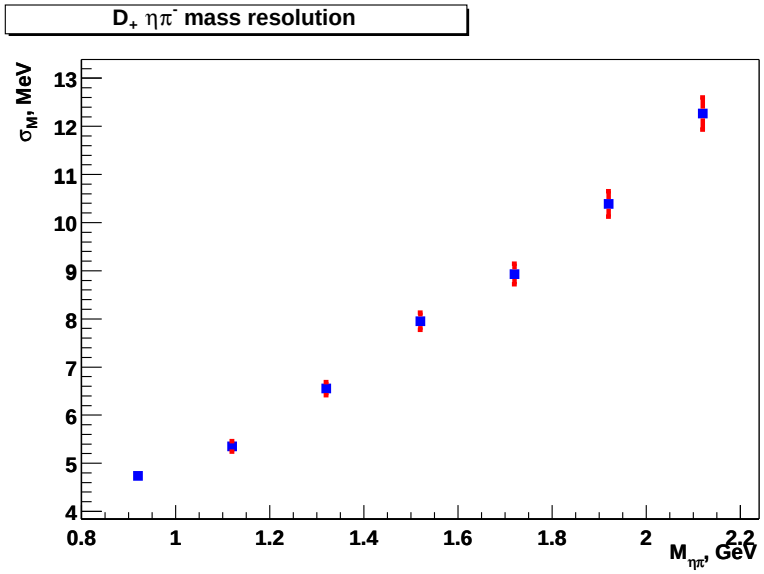

Fig. 9: The $\eta\pi$ mass dependence of resolution.

Table 2: Parameters of the $\pi^+\pi^-\pi^0$ process

Quantity	1σ resolution
$M(\pi^+\pi^-\pi^0)$	~ 2.7 MeV
$\cos(\Theta_{GJ})$	(9.5–5.5) 10^{-3}
ϕ_{TY}/π	(8.2–11.5) 10^{-3}
recoil ϕ/π	(1.2–1.5) 10^{-2}
recoil P_T	(6.8–8.2) MeV

6. ESTIMATION OF RATES

The obtained efficiency allowed us to estimate the $a_2(1320) \to \eta\pi^-$ event rate according to: $N_{\eta\pi} = N_0 \frac{N_A}{A} \rho l \sigma_{a_2} BR(a_2 \to \eta\pi) BR(\eta \to \pi^+\pi^-\pi^0)\epsilon$, where:

- N_0 is the beam flux;
- $N_A = 6 \times 10^{23}$ /mol the Avogadro number;
- $A = 1.01$ g/mol the atomic number of the target material [13];
- $\rho = 0.0708$ g/cm^3 the target density [13];
- $l = 40$ cm the target length;
- $\sigma_{a_2} = 25$ μb the $a_2(1320)$ production cross-section [14];
- $BR(a_2(1320) \to \eta\pi) = 0.145$ [13];
- $BR(\eta \to \pi^+\pi^-\pi^{0)} = 0.226$ [13];
- $\epsilon = 0.25$ the detection and reconstruction efficiency.

Substitution of these values results in the $a_2(1320) \to \eta\pi^-$ rate being $N_{\eta\pi} = N_0 \cdot 34 \times 10^{-8}$. If we assume a beam flux to be equal to $N_0 = 10^8/\text{min}$, then we will have $N_{a_2 \to \eta\pi} \approx 50\,000$/day. This value can be converted using the ratio from Ref. [3] into the P_+ state $\eta\pi^-$ system production rate, which then will be equal to $N_{P_+(\eta\pi)} \approx 2500/\text{day}$

7. CONCLUSION

The detection, track reconstruction procedure and a physical analysis of the $\eta\pi^-$ system were simulated. As a result the production rate of the $J^{PC} = 1^{-+}$ $\eta\pi^-$ events was found to be ≈ 2500/day. This allows one to conclude that:

- COMPASS can measure the shape of the exotic $J^{PC} = 1^{-+}$ $\eta\pi^-$ wave with the best precision.
- COMPASS can collect simultaneously the largest data samples to study the exotic wave production not only in the $\eta(\pi^+\pi^-\pi^0)\pi^-$, but also in the $\eta(2\gamma)\pi^-$, $\eta'\pi^-$, $\rho^0\pi^-$ and $b_1(1235)(\omega\pi)\pi$.

Acknowledgements

I would like to thank the organizers F. Bradamante, S. Paul and G. Mallot; my colleagues of the COMPASS project, in particular, G. Khaustov and Yu. Khokhlov for fruitful discussions; V. Alexakhin, Y. Bedfer, A. Korzenev for help. My special thanks go to S. Paul for his comments.

References

[1] N. Isgur and J. Paton, Phys. Rev. D **31** (1985) 2910.

[2] F. E. Close and P. R. Page, Nucl. Phys. B **443** (1995) 233.

[3] S. U. Chung *et al.*, Phys. Rev. D **60** (1999) 092001.

[4] A. Abele *et al.*, Phys. Lett. B **423** (1998) 175.

[5] A. Abele *et al.*, Phys. Lett. B **446** (1999) 349.

[6] Y. Khokhlov *et al.*, Nucl. Phys. A **663** (2000) 596.

[7] E. I. Ivanov *et al.*, Phys. Rev. Lett. **85** (2001) 3977.

[8] A. V. Popov *et al.*, "Recent Results from Brookhaven E852 Experiment", in CP619, Hadron Spectroscopy: Ninth International Conference, edited by D. Amelin and A. M. Zaitsev, 2002, pp. 135–142.

[9] V. A. Dorofeev *et al.*, "The $J^{PC} = 1^{-+}$ hunting season at VES", in CP619, Hadron Spectroscopy: Ninth International Conference, edited by D. Amelin and A. M. Zaitsev, 2002, pp. 143–154.

[10] J. D. Hansen, G. Jones, G. Otter and G. Rudolph, Nucl. Phys. B **81** (1974) 403.

[11] COMPASS Collaboration, "Common Muon and Proton Apparatus for Structure and Spectroscopy", CERN/SPSLC, 96-14, (1996).

[12] S. V. Donskov, these proceedings (2002).

[13] D. E. Groom *et al.*, Eur. Phys. J. C **15** (2000) 1–878.

[14] C. Bromberg *et al.*, Phys. Rev. D **29** (1984) 2469–2475.

HYBRID MESON PRODUCTION VIA PION SCATTERING FROM THE NUCLEAR COULOMB FIELD

Murray Moinester
R. and B. Sackler Faculty of Exact Sciences, School of Physics and Astronomy, Tel Aviv University, 69978 Tel Aviv, Israel; e-mail: murraym@tauphy.tau.ac.il

Abstract
The CERN COMPASS experiment can use 100–280 GeV pion and kaon beams and magnetic spectrometers and calorimeters to measure Hybrid (mixed quark–gluon) meson production cross sections in the Primakoff scattering of high-energy pions and kaons from virtual photons in the Coulomb field of high-Z targets. There are many advantages to studying such processes via the Primakoff reactions $\pi^-\gamma \rightarrow Hybrid \rightarrow \rho\pi, \eta\pi, \eta'\pi, \pi b_1, \pi f_1$, and similar reactions with a K^- beam. Such data should provide significant input for gaining a better understanding of non-perturbative QCD. A brief description and update of this programme is presented.

1. PIONIC HYBRID MESONS

The CERN COMPASS experiment focuses on issues in the physics of strong interactions pertaining to the structure of hadrons in terms of valence quarks and gluons. This report deals with the COMPASS Hybrid meson programme. The Hybrid (quark–antiquark–gluon, $q\bar{q}g$) mixed quark–gluon mesons are particles predicted by QCD [1–4]. The unambiguous discoveries of these meson states will provide a major landmark in hadron spectroscopy. Of course, the Fock state of a meson is represented as an infinite expansion of different quark and gluon configurations, but in a Hybrid meson, the $q\bar{q}g$ component dominates. The force between quarks in QCD is mediated by the exchange of coloured gluons. In ordinary quark–antiquark mesons, the exchanged gluons localize within a narrow string-like tube connecting the quarks: a non-vibrating flux-tube of coloured flux lines. In the flux-tube description of a Hybrid meson, a quark–antiquark pair couples directly to the vibrational degrees of freedom of the gluonic flux-tube. Hybrid mesons therefore contain explicit valence gluons, as opposed to the hidden gluons in ordinary mesons [3]. Understanding such valence gluons is critical to understanding the origin of hadron mass. Establishing the existence of Hybrid mesons and studying their properties can provide insight into colour confinement.

Input from experiments is needed to provide better understanding of the current situation, especially to show that the present evidence [5] is not just the result of some artifice. GSI Darmstadt [6] proposes an exotic meson programme via a new facility for $p\bar{p}$ reactions. The planned \$150M 12 GeV JLab upgrade focuses on Hybrid meson studies at JLab Hall D [7]. Future experiments at Fermilab CDF and D0 may measure double-Pomeron production of exotic mesons [8]. More results from BNL, VES, Crystal Barrel [9–11] (from analysis of completed experiments), and further theoretical calculations, are becoming available. COMPASS has a multi-faceted Hybrid meson research programme [12, 13], which includes this proposal for Primakoff production of Hybrids. COMPASS [14] is well positioned to collect significantly cleaner data, and at lower cost, and using complementary methods, compared to the other planned efforts. The Primakoff production of Hybrids in COMPASS is part of a more global Primakoff physics programme, involving studies of pion and kaon polarizabilities, and studies of the chiral anomaly [14, 15].

The COMPASS Hybrid meson searches [15–17] will focus on 'oddballs'—mesons with quantum numbers not allowed for ordinary $q\bar{q}$ states, such as $I^G\,J^{PC} = 1^-\,1^{-+}$ Hybrids. Unlike Glueballs, these cannot mix with normal $q\bar{q}$ mesons. However, since such oddballs could also be four-quark states, the

spin assignment is not sufficient to make the Hybrid identification [18]. In certain cases, there are other theoretical interpretations [19, 20] for such experimental signals. Previous experimental efforts have reported several 1^{-+} resonant signals [9–11] at masses between 1.4 and 1.9 GeV, in a variety of decay channels, including the $\rho\pi$ channel. The signature for such an exotic state is that a detailed partial-wave analysis (PWA) of a large data sample requires a set of quantum numbers inconsistent with a normal ($q\bar{q}$) meson. To increase confidence in a Hybrid interpretation, complementary evidence is sorely needed. The path to understanding requires that different experiments, such as the important input from COMPASS Primakoff studies, provide a large database of candidate Hybrid states, and their properties.

Barnes and Isgur, using the flux-tube model [21, 22], calculated the mass of the lightest pionic hybrid with quantum numbers of $J^{PC} = 1^{-+}$ to be around 1.9 GeV, higher than the experimental claims. Close and Page [23] predict that such a high-lying pionic hybrid should decay into the following channels:

$\mathrm{b}_1\pi$	$\mathrm{f}_1\pi$	$\rho\pi$	$\eta\pi$	$\eta'\pi$
170	60	$5 \rightarrow 20$	$0 \rightarrow 10$	$0 \rightarrow 10$

where the numbers refer to the partial widths in MeV. They expect the total width to be larger than 235–270 MeV, since the $s\bar{s}$ decay modes were not included. Recent updates on hybrid meson structure are given in Refs. [3, 24, 25]. The lower lying Hybrids of recent experiments have significantly different branching ratios. This may reflect that the structure of these experimental low-mass Hybrids is different than that of the theoretical high-mass Hybrids, and considering the high thresholds of the $\mathrm{b}_1\pi$ and $\mathrm{f}_1\pi$ decay channels for decay of a low-mass Hybrid.

From over a decade of experimental efforts at IHEP [26–28], CERN [9, 29], KEK [30], and BNL [10], several hybrid candidates have been identified. BNL E852 [10] reported two $J^{PC} = 1^{-+}$ resonant signals at masses of 1.4 and 1.6 GeV in $\eta\pi^-$ and $\eta\pi^0$ systems, as well as in $\pi^+\pi^-\pi^-$, $\pi^-\pi^0\pi^0$, $\eta'\pi^-$ and $\mathrm{f}_1(1285)\pi^-$. The VES Collaboration presented [11] the results of a coupled-channel analysis of the $\pi 1(1600)$ meson in the channels $\mathrm{b}_1(1235)\pi$, $\eta'\pi$, and $\rho\pi$, with a total width of 290 MeV, and relative branching ratios: $1 : 1 \pm 0.3 : 1.6 \pm 0.4$. They did not include the $\mathrm{f}_1\pi$ channel in this analysis. The resonant nature of the 1.6 GeV state was observed in the $\mathrm{b}_1\pi$ mode, by a combined fit of the 2^{++} and 1^{-+} waves. Then an assumption was made that in the $\eta'\pi$ and $\rho\pi$ channels, they observed the same state, considering the similar shapes. Therefore, their coupled-channel analysis result of a $\rho\pi$ partial width of 130 MeV, and a total width of 290 MeV, should be taken with some caution, considering also that the $\mathrm{f}_1\pi$ channel is not included. Still, for the 1.6 GeV region, the VES $\rho\pi$ partial width is consistent with the BNL $\rho\pi$ width of 168 MeV. For count rate estimates below, we will use an average value of 150 MeV for the $\rho\pi$ width at 1.6 GeV.

The kinematic variables for the $\pi\gamma \rightarrow$ Hybrid $\rightarrow \pi^-\eta$ Primakoff process in COMPASS are shown in Fig. 1. A virtual photon from the Coulomb field of the target nucleus interacts with the pion beam. At 200 GeV π beam energy, nuclear (meson-exchange) amplitudes in the Primakoff production of the ρ meson were shown to be very small [31] in the kinematic region of Primakoff production. This is very encouraging for the COMPASS studies. Still, COMPASS can carry out data analysis of Hybrid data with and without meson-exchange amplitudes, to test to what extent their presence affects the extraction of the Primakoff cross section. For a given Hybrid ($\pi 1$) partial decay width $\Gamma(\pi 1 \rightarrow \pi\rho)$, the Vector Dominance Model (VDM) gives an associated radiative width $\Gamma(\pi 1 \rightarrow \pi\gamma)$ [32, 33]. As the Primakoff cross section is proportional to $\Gamma(\pi 1 \rightarrow \pi\gamma)$ [32–34], all Hybrids that decay to the $\pi\rho$ channel should also be produced in the Primakoff reaction. In contrast to the $\pi 1(1600)$, the $\pi 1(1400)$ 1^{-+} state should be only weakly populated in the Primakoff reaction, as it has a very small $\pi\rho$ partial decay width. For the $\pi 1(1600)$ radiative width, we use the standard VDM expression [31–33] with a $\rho\gamma$ coupling $g^2_{\rho\gamma}/\pi = 2.5$, which correctly relates the corresponding widths for the ρ meson decay. We obtain $\Gamma(\pi 1 \rightarrow \pi\gamma) = 6.6 \times 10^{-3}\Gamma(\pi 1 \rightarrow \pi\rho)$, which gives the VDM estimate $\Gamma(\pi 1 \rightarrow \pi\gamma) \approx 1000$ keV.

In Fig. 1, a Hybrid meson (other than $\pi 1(1400)$) is produced and decays to $\pi^-\eta$ at small forward

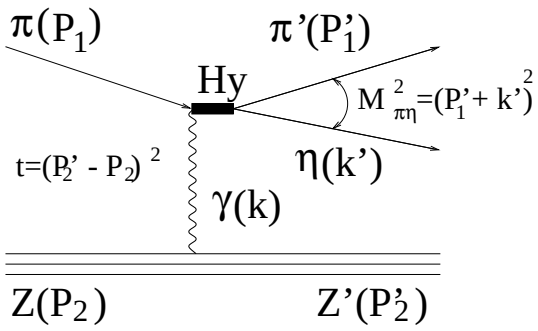

Fig. 1: Primakoff Hybrid-meson production process and kinematic variables (4-momenta): P1, P1′ = for initial/final pion, P2, P2′ = for initial/final target, k = for initial γ, k′ = for final η.

angles in the laboratory frame, while the target nucleus (in the ground state) recoils coherently with a small transverse p_T. The corresponding small p_T of the exchanged photon means that it is essentially real and transverse. Consequently, the helicities of incident and Primakoff produced mesons differ by unity. The peak at small target p_T used to identify [32, 33] the Primakoff process is observed by using the beam and vertex and other COMPASS detectors to measure the beam-pion and final-state Hybrid momenta. Primakoff scattering is a large impact-parameter, ultra-peripheral reaction on a virtual photon target. The initial-state pion and final-state Hybrid interact at very small t-value (four-momentum transfer to the target nucleus), where the nuclear form factor is essentially unity, and there are no final-state interactions [35].

It is important to note that in addition to Primakoff production of excited meson states, one also expects diffractive production. It is necessary to separate the Primakoff forward peak from these underlying sometimes large diffractive yields [32, 34]. The strength of the diffractive cross section depends on angular momentum conservation at zero degrees; and therefore on which decay mode is studied: $\mathrm{b}_1\pi$, $\mathrm{f}_1\pi$, $\rho\pi$, $\eta\pi$, $\eta'\pi$. The potentially large diffractively produced waves with spin projection $M = 0$ and $J^P = 1^+$ can complicate the PWA of $\rho\pi$, but not $\pi\eta$. Of course, although the $\pi\eta$ channel may be cleaner, it may not necessarily have a large 1^- Hybrid contribution.

The t-distribution of the diffractive yield depends on whether there is helicity flip at zero degrees. The t-dependence of these dominant (no helicity-flip) diffractive waves is $\exp(-bt)$. The accuracy with which one can subtract this background depends on the fraction of the projective helicity-flip ($M = \pm 1$) diffractive waves associated with 2^+ states, which have a t-dependence $t \times \exp(-bt)$. All the waves have phases and can interfere, so that subtracting only an exponential would ignore these effects. However, as the Coulomb waves have Gottfried–Jackson helicity $M = \pm 1$, while strong production occurs dominantly with $M = 0$, the interference should be zero to lowest order [36].

Such subtraction was done, even for a large diffractive cross section [36], as in the recent measurement of the radiative decay width of the $\mathrm{a}_2(1320)$ meson [34] via its decay to the $\pi\rho$ channel. The subtraction was done by extrapolation of the data away from the forward Primakoff peak, assuming an $\exp(-bt)$ dependence of the diffractive yields. Such theoretical assumptions on the t-dependence of the background should have a small effect on narrow resonances (104 MeV width) such as the a_2. This appears to be the case, considering the consistency of the a_2 radiative widths determined via Primakoff production and their decay via the $\pi\rho$ and $\pi\eta$ channels [34]. But an exponential subtraction may cause larger uncertainties for Hybrids with large (300–500 MeV) widths. The Hybrid data analysis therefore should test the sensitivity of the results to such exponential background assumptions.

In the recent Primakoff study of the a_2 radiative width by decay to $\pi\rho$, following subtraction of the diffractive yield, due in part to poor statistics, the resulting Primakoff mass spectrum does not show significant structure above the clearly observed $\mathrm{a}_2(1320)$. Also, for this high mass region, a PWA is not

available. Considering the subtraction and statistical uncertainties discussed above, this does not rule out the possibility that the $\pi\rho$ width is nonetheless large in the region of the expected 1.6 GeV Hybrid. And with improved statistics and resolution and acceptance, and by studying all decay modes in the same experiment, COMPASS can potentially do a significantly better Hybrid analysis. High-lying excited meson states certainly couple to the $\pi\rho$ channel, as shown clearly in the work of photoproduction of excited mesons, observed by their $\pi\rho$ decay mode [37].

Consider some typical angular distributions from Primakoff scattering, such as those for the $\pi^-\gamma \to \eta\pi$ scattering, for different values of $\eta\pi$ invariant mass. If these are associated with the production and decay of a $J^{PC} = 1^{-+}$ $(d\bar{u}g)$ Hybrid state, with quantum numbers not available to $q\bar{q}$ mesons, then a detailed partial-wave analysis (PWA) of a large data sample would indicate the need for these quantum numbers. The partial-wave analysis (PWA) of systems such as $\eta\pi$ or $\eta'\pi$ in the mass region below 2 GeV requires high statistics and minimum background. This region is dominated by strong resonances (e.g., a_2(1320) near the 1.4 GeV Hybrid candidate and π_2(1670) near the 1.6 GeV Hybrid candidate), and the PWA can yield ambiguous results [27] for the weaker 1^{-+} wave. For the Primakoff yield, following subtraction of the diffractive yield, the cross section for 1.6 GeV hybrid production ($\pi 1$), in all decay channels, should be larger than the background. This is so because $\Gamma(\pi_2 \to \pi\gamma) \approx 300$ keV, smaller than the expected $\Gamma(\pi 1 \to \pi\gamma) \approx 1000$ keV. In contrast, the BNL experiment [10] for this decay channel has a background from π_2(1670) some 10 times stronger than the Hybrid signal. Primakoff data with reduced backgrounds should significantly diminish uncertainties in the partial wave analysis compared to the non-Primakoff production experiments. It might allow the Hybrid to be observed in the mass spectrum in some of the decay modes, not only via PWA. Furthermore, in Primakoff (photon-exchange) production experiments, besides the absence of final-state interactions, meson-exchange and diffractive backgrounds can be largely eliminated. Most of these backgrounds occur at larger values of the four-momentum transfer t, and are easily removed by an analysis cut on the t-value. The part of these backgrounds that extends to small-t can be largely removed by extrapolation to small-t of the large-t data. These are important advantages compared to previous $\pi^-\mathrm{p} \to$Hybrid production experiments [16, 17].

Preliminary low-statistics Hybrid production data [32, 33] at Fermilab E272 via Primakoff scattering provide encouraging initial results for production of a 1.6 GeV 1^{-+} Hybrid. The data for decay to the $\pi\mathrm{f}_1$ channel shows signs of Primakoff enhancement (excess of 25 events) at small-t. This gives $\Gamma(\pi 1 \to \pi\gamma) \times B(\pi 1 \to \pi\mathrm{f}_1) \approx 250$ keV. If $B(\pi 1 \to \pi\mathrm{f}_1) \approx 0.25$, that corresponds to $\Gamma(\pi 1 \to \pi\gamma) \approx 1000$ keV, close to the value deduced using VDM with a 150 MeV partial width in the $\pi\rho$ channel. For $\pi\rho$ decay of a 1.6 GeV state, FNAL E272 had insufficient statistics to separate a Coulomb enhancement from the diffractive background. As their data was for the combined spectra, their estimate of the upper limit to the Primakoff Hybrid yield has large uncertainties. FNAL SELEX measured the a_2 radiative decay via the $\pi\rho$ mode. The SELEX Primakoff spectrum, after subtraction of diffractive background, shows the a_2 peak clearly. The E272 $\pi\rho$ data for diffractive plus Primakoff production does not even show the a_2 peak. It is difficult to use E272 data to get Primakoff limits in the $\pi\rho$ channel near 1.6 GeV. For a 150 MeV $\pi\rho$ partial width of a 1.6 GeV Hybrid, the E272 data gives an upper limit for $\Gamma(\pi 1 \to \pi\gamma)$ close to 100 keV. Since this limit value has a huge error bar, the E272 estimate using the cleaner $\pi\mathrm{f}_1$ data is certainly more reliable. E272 also shows via the $\eta\pi$ decay mode, that $\Gamma(\pi 1 \to \pi\gamma) \times B(\pi 1 \to \pi\eta)$ is at most 100 keV for a $\pi 1$ near 1.6 GeV, for a $\pi 1$ with a total width of 400 MeV. But the $\pi 1$ branching B($\pi 1 \to \pi\eta$) from VES and BNL is very small, so this is still consistent with $\Gamma(\pi 1 \to \pi\gamma)$ near 1000 keV. Consequently, one may estimate from the E272 $\pi\mathrm{f}_1$ data that $\Gamma(\pi 1 \to \pi\gamma)$ is close to 1000 keV. This is consistent with $\Gamma(\pi 1 \to \pi\gamma) \approx 1000$ keV, which we obtain by applying VDM to the experimental $\Gamma(\pi 1 \to \pi\rho)$ width, as described above.

One can summarize the situation as follows. For Primakoff scattering, the Hybrid-meson production cross section depends on the strength of its $\pi\rho$ coupling, and via vector dominance to its $\pi\gamma$ coupling. Both BNL and VES claim this decay mode for the 1.6 GeV Hybrid candidate. A low-statistics $\gamma p \to$ Meson photoproduction experiment [37] also observed resonances (including near 1.9 GeV) in the

$\pi\rho$ channel, suggesting possible Hybrid interpretations. Based on previous data from FNAL E272 and VES, we estimate $\Gamma(\pi 1 \rightarrow \pi\gamma) \approx 1000$ keV for a 1.6 GeV Hybrid. The relevant Primakoff reactions $\pi^-\gamma \rightarrow$ Hybrid $\rightarrow \rho\pi, \eta\pi, \eta'\pi, \mathrm{b}_1(1235)\pi, \pi\mathrm{f}_1$, etc., can therefore be studied in COMPASS potentially in the 1.4–3.0 GeV mass region, which includes all previous Hybrid candidates.

2. KAONIC HYBRID MESONS

The quark content of the hybrid meson ($q\bar{q}g$) nonet should be identical to the quark content of the regular meson ($q\bar{q}$) nonet, with identical SU(3) decomposition in the plane of isospin I_3 and hypercharge Y, for the 1^- and other spin-parity states. Thus, for every pionic $(d\bar{u}g)$ 1^{-+} Hybrid, there should be a flavour excited kaonic $(s\bar{u}g)$ 1^- Hybrid, at an excitation energy roughly 100–140 MeV higher than its pionic Hybrid cousin, possibly narrower because of phase space. COMPASS can observe the kaonic Hybrids via $\mathrm{K}^-\mathrm{Z} \rightarrow$ Hybrid $\rightarrow \mathrm{K}^-\rho^0\,\mathrm{Z}$, as well as other decay modes: $\mathrm{b}_1\mathrm{K}^-$, $\mathrm{f}_1\mathrm{K}^-$, $\eta\mathrm{K}^-$, $\eta'\mathrm{K}^-$. The backgrounds should be low from Primakoff excitation of normal kaonic excited mesons, as in the case of the pionic Hybrids; and also if the kaonic hybrids are narrower. The first ever measurement of the kaonic Hybrids via Primakoff scattering would be of inherent interest, but would also provide valuable support that the analogous pionic signals are properly identified as Hybrids. Searches for $s\bar{s}g$ Hybrids via $\mathrm{K}^-\mathrm{p} \rightarrow$ Hybrid have also been proposed recently [38].

3. MESON RADIATIVE TRANSITIONS

COMPASS will also study Primakoff radiative transitions leading from the pion to the ρ^-, $\mathrm{a}_1(1260)$, and $\mathrm{a}_2(1320)$, and for the kaon to K^*. The data can be obtained with a particle-multiplicity trigger [17]. Theoretical predictions for radiative transition widths are available from vector dominance and quark models. Independent and higher precision data for these and higher resonances would provide a useful check of the COMPASS apparatus, and would allow a more meaningful comparison with theoretical predictions. For example, the $\rho \rightarrow \pi\gamma$ width measurements [31, 39, 40] range from 60 to 81 keV; the $\mathrm{a}_1(1260) \rightarrow \pi\gamma$ width measurement [41] is 0.64 ± 0.25 MeV; and the $\mathrm{a}_2(1320) \rightarrow \pi\gamma$ width is is $\Gamma = 295\pm$ 60 keV [42] and $\Gamma = 284 \pm 25 \pm 25$ keV [34]. For $\mathrm{K}^* \rightarrow \mathrm{K}\gamma$, the widths obtained previously are 48 ± 11 keV [43] and 51 ± 5 keV [44]. The above references indicate that the formalism of Primakoff production provides an excellent description of excited mesons, the same formalism that we use to search for Primakoff production of Hybrids.

These as well as polarizability and chiral anomaly [14, 15] Primakoff measurements are important for a variety of reasons: (1) COMPASS can significantly improve their precision, (2) COMPASS can get data for other $q\bar{q}$ meson excited states, (3) these measurements with sufficient statistics test our methodologies and help calibrate our apparatus for the Hybrid studies.

4. DETAILED DESCRIPTION OF APPARATUS

COMPASS is a fixed-target experiment that uses a 160 GeV polarized muon beam, and pion, kaon, and proton beams. In order to achieve good energy resolution within a wide energy range, COMPASS has a two-stage spectrometer with 1.0 Tm and 5.2 Tm conventional magnets. The tracking stations contain different detector types to cover a large area, and to achieve good spatial resolution in the vicinity of the beam. Most of the tracking detectors operate on the principle of gas amplification, while some are silicon strip detectors. At the end of each stage, an electromagnetic and a hadronic calorimeter detect energies of photons, electrons and hadrons. The calorimeters in the first stage and the EM calorimeter of the second stage have holes through which the beam passes.

In COMPASS, two beam Cherenkov detectors (CEDAR), far upstream of the target, provide $\pi/\mathrm{K}/p$ particle identification (PID). The incoming hadron momentum is measured in the beam spectrometer. Before and after the target, charged particles are tracked by high-resolution silicon tracking detectors. The measurement of both initial and final-state momenta provides constraints to identify the

reaction. The final-state meson momenta are measured downstream in the magnetic spectrometer and in the γ calorimeter. These provide a precise determination of the p_T transfer to the target nucleus, the main signature of the Primakoff process, and the means to separate Primakoff from meson-exchange scattering events.

We considered in detail previously the beam, target, detector, and trigger requirements for Hybrid studies [15, 17]. A brief description is given below of some important components of the apparatus for Primakoff studies. The September 2002 status of the full COMPASS apparatus is described in Ref. [35].

4.1 Beam requirements

We can obtain good statistics for the pion study by using the high beam intensities of the CERN SPS. We can take data at different beam energies and use different targets, with both positive and negative beams, as part of efforts to control systematic uncertainties.

For the 120–300 GeV hadron beams, particle identification (PID) is needed to provide pion, kaon, and proton beam tagging for positive and negative beams. For the COMPASS beam, one expects [14] a beam intensity of 100 MHz, with beam composition [45] roughly: 120–300 GeV/c, negative, 87–98% pions, 7–1% kaons, 2–1% antiprotons; 120–300 GeV/c, positive, 43–2% pions, 7–1% kaons, 49–97% protons. PID is accomplished at CERN with the CEDAR detectors, a Cherenkov differential counter with achromatic ring focusing. There are two CEDAR detectors (in series) in the COMPASS beamline [46]. They each have eight large-area PMTs arranged in a circle, preceded by a single light diaphragm (LD) to finely fix a ring radius. A six-fold coincidence is required for the PID. The gas pressure is varied to set the ring radius for pions or kaons or protons at the LD location. The narrow diaphragm mounted in CEDAR-N separates kaons from pions up to 300 GeV/c, and can tag protons down to 12 GeV/c.

4.2 Target and target detectors

The target platform is movable and allows easy insertion of a solid target, e.g., a cylindrical lead plate 40 mm in diameter and 1.4 mm thick. We use silicon tracking detectors before and immediately after the targets. These are essential for Primakoff reactions as the angles have to be measured with a precision of order 100 μrad. We veto target break-up events via a target recoil detector, and by selecting low-t events in the off-line analysis.

4.3 The γ calorimeter ECAL2

The COMPASS γ detector is equipped with 3.8 by 3.8 cm^2 GAMS lead-glass for a total active area of order 2 m diameter. The central area is already completely instrumented with ADC readouts. For the precise monitoring of energy calibration of the photon calorimeters, COMPASS will use LED and laser monitor systems, as described in Ref. [47]. The position resolution in the second γ calorimeter ECAL2 for the photon is 1.0 mm, corresponding to an angular resolution of 30 μrad. In the interesting energy range, the energy resolution is 2–3%. The photon acceptance is 98% due to a beam hole of ECAL2, while the reconstruction efficiency is 58%, as a result of pair production within the spectrometer.

As can be seen from Fig. 1, COMPASS requires reconstructed η's for the hybrid study. The two γ's from η decay have half-opening angles $\theta^h_{\gamma\gamma}$ for the symmetric decays of $\theta^h_{\gamma\gamma} = m/E_\eta$, where m is the mass (η) and E_η is the η energy. (Opening angles are somewhat larger for asymmetric decays.) In order to catch most of the decays, it is necessary to subtend a cone with about double that angle, i.e., $\pm 2m/E_\eta$, neglecting the angular spread of the original η's around the beam direction. For the ECAL2 γ detector, with a circular active area of 2 m in diameter, the acceptance for the $\pi\eta$ channel at 30 m from the target for η's above $E_\eta = 33$ GeV is therefore excellent. At half this energy, however, the acceptance becomes quite poor. The acceptance depends of course on the Hybrid mass, which is taken between 1.4 and 3.0 GeV for the planned COMPASS study. Detailed Monte Carlo studies are needed for different Hybrid decay modes, for a range of assumed masses. For the $\pi \mathrm{f}_1$ channel, for example, $\mathrm{f}_1 \to \pi\pi\eta$, the

η's will have low energy, and therefore large γ angles. To maintain good acceptance for low-energy η's, the ECAL2 diameter should be about 2 m.

The available COMPASS ECAL does not have radiation hardened blocks near the beam hole. If those were available, it would allow increasing the beam intensity by a factor of five, to allow substantially more statistics for the same run time. This would clearly be a cost-effective improvement.

4.4 The magnetic spectrometer and the t-resolution

The p_T impulses of the COMPASS magnets are 0.3 GeV/c for SM1 (4 metres from target) and 1.56 GeV/c for SM2 (16 metres from target). The fields of both magnets are set in the same direction for maximum deflection of the beam. We achieve good momentum resolution for the incident and final-state charged and neutral mesons, and therefore good resolution in t. The relative momentum resolution for charged π, with all interactions accounted for, is 1% for energies above 35 GeV and up to 2.5% below this mark. The angular resolution in a single coordinate for a charged-pion of momentum p is 7.9 mrad-GeV/p. The reconstruction efficiency for pions with energy greater than 2 GeV is 92%.

The angular resolution for a final-state charged meson is controlled by minimizing the multiple scattering in the targets and detectors. With a lead target of 0.8% interaction length (1.6 g/cm^2, 24% radiation length), multiple Coulomb scattering (MCS) of the beam and outgoing pion in the target gives an rms angular resolution of order 32 μrad, small compared to the intrinsic tracking-detector angular resolution. The target contributes to the resolution in the transverse momentum p_T through MCS. For $t = p_T^2$, including all other effects [15, 17], we aim for a p_T resolution of less than 15 MeV, corresponding to Δt smaller than $\approx 2.5 \times 10^{-4}$ GeV^2.

This resolution will provide good separation for contributions from diffractive and meson-exchange processes. Minimum material (radiation and interaction lengths) in COMPASS will also yield a higher acceptance, since the γ's will not be converted before the ECAL2, and the result is minimum e^+e^- backgrounds.

4.5 The COMPASS Primakoff trigger

We design [15, 16, 48] the COMPASS Primakoff trigger to enhance the acceptance and statistics. We minimize target break-up events via veto scintillators around the target. The trigger uses the characteristic decay pattern: one or three charged mesons with accompanying γ hits, or three charged mesons and no γ hits. The trigger [15, 16, 48] for the $\pi\eta$ hybrid decay channel (charged particle multiplicity = 1) is based on a determination of the pion energy loss (via its characteristic angular deflection), correlated with downstream scintillator hodoscopes stations (H1 versus H2) with the aid of a fast matrix chip, as shown in Fig. 2. This trigger is a copy of the currently running muon-beam energy-loss trigger [35]. We will use the Beam Kill detectors BK1/BK2 as veto only during low-intensity tests. These detectors are positioned in the pion-beam trajectory, as shown in Fig. 2, but they cannot handle the full 100 MHz beam rate.

5. OBJECTIVES AND EXPECTED SIGNIFICANCE

COMPASS can study pionic hybrid-meson candidates between near 1.4–1.9 GeV, produced by the ultra-peripheral Primakoff reaction. But COMPASS may also be sensitive to pionic and kaonic hybrids for the 1.9–3.0 GeV mass range, if they also couple to the $\pi\rho$ and Kρ channels. We can then potentially obtain superior statistics for hybrid states via a production mechanism that is not complicated by hadronic final-state interactions. We can also get important data on the different decay modes in both pionic and kaonic channels.

We make initial rough estimates of the statistics attainable for hybrid production in the COMPASS experiment. Monte Carlo simulations will refine these estimates. We assume a 1.6 mb cross section per Pb nucleus for production of a 1.6 GeV Hybrid meson. We use the radiative width of

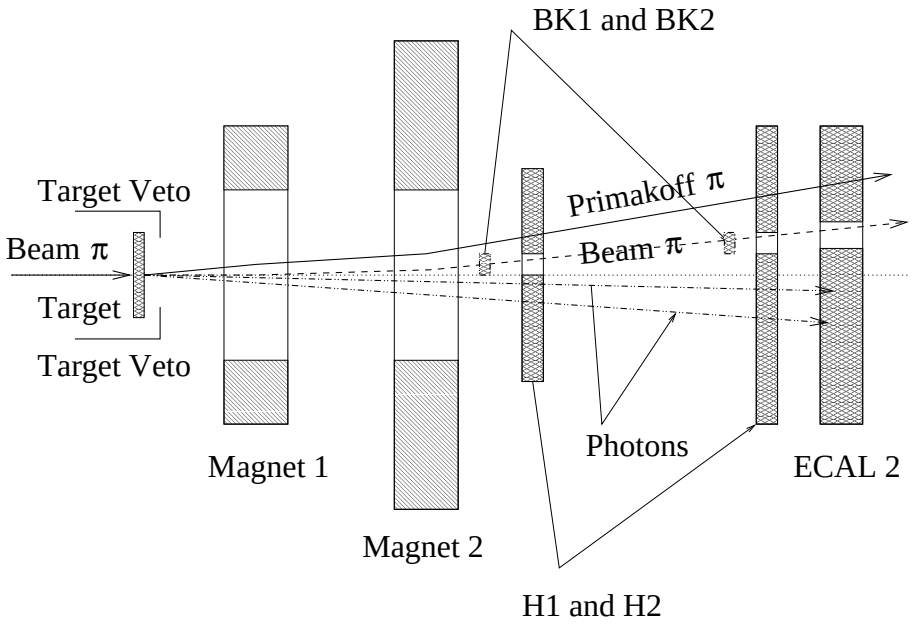

Fig. 2: Detector layout for the COMPASS Primakoff Hybrid trigger, $\pi^- Z \to Hybrid \to \pi^- \eta$. BK1,BK2: beam killer system; H1,H2: hodoscope system for charged particle detection; ECAL2: second photon calorimeter. For η decay, one observes the two γ's shown. For polarizability, there is only one γ to detect.

$\Gamma(\pi 1(1600) \to \pi\gamma) \approx 1000$ keV, as described above, and also for the 1.9–3.0 GeV mass region. Integrating the Primakoff Hybrid production differential cross section for a 280 GeV pion beam, and using this radiative width, gives 1.6 mb [16, 32, 33].

We consider a beam flux of 2×10^7 pions/s, with a spill structure that provides a 5-second beam every 16 seconds. In two months of running at 100% efficiency, we obtain $3.2\times\ 10^{13}$ beam pions. Prior to the data production run, time is also needed to calibrate ECAL2, to make the tracking detectors operational, to bring the DAQ to a stable mode, and for other contingencies. We use a 0.8 % interaction length target, or 1.4 mm lead plate with target density $N_t = 10^{22}\ \mathrm{cm}^{-2}$. The Primakoff interaction rate is then $R = \sigma(Pb) \cdot N_t = 1.6\times\ 10^{-5}$. In a two-month run period, we therefore obtain $5.1\times\ 10^8$ Hybrid events at 100% efficiency. Considering efficiencies for tracking (92%), γ detection (58% for each γ), accelerator and COMPASS operation (70%), analysis cuts to reduce backgrounds (75%), branching ratio for the $\eta \to 2\gamma$ and $\eta \to \pi^+\pi^-\pi^0$ decay modes ($\approx$ 62%), trigger efficiency ($\approx$ 60%), geometrical acceptances ($\approx$ 90%), π^0 and η reconstruction from two γ hits ($\approx$ 45%), and event reconstruction efficiencies ($\approx$ 60%), we estimate a global efficiency of ϵ(total) = 1.5%. We will assume here the same average detection efficiency for all Hybrid decay modes, via $\rho\pi, \eta\pi, \eta'\pi, \pi b_1, \pi f_1$. Therefore, we can expect to observe a total of 7.7 $\times 10^6$ Hybrid decays in all decay channels for the 1.6 GeV Hybrid. For example, following theory and VES branching ratios, we expect for the 1.6 GeV state, most data in the πf_1, $\pi\rho$, $\pi\eta'$, and $b_1\pi$ channels.

For 2, 2.5, 3.0 GeV mass Hybrids, assuming that they have the same radiative width, the number of useful events decreases by factors of 6, 25, and 100, respectively. But even in these cases, assuming again a global 1.5% efficiency, that would represent a very interesting potential of samples of 13×10^5, 3.1×10^5, and 0.77 $\times 10^5$ Hybrid meson detected events, with masses 2.0, 2.5, and 3.0 GeV, respectively.

Taking into account the very high beam intensity, fast data acquisition, high acceptance and good resolution of the COMPASS set-up, one can expect from COMPASS the highest statistics and a 'systematics-free' data sample that includes many tests to control possible uncertainties. Comparison between COMPASS and past and new experiments [6, 8], with complementary methodologies, should

allow fast progress on understanding Hybrid meson structure, their production and decay characteristics, and on establishing systematic uncertainties.

Acknowledgements

This work was supported in part by the Israel Science Foundation funded by the Israel Academy of Sciences and Humanities. Thanks are due to T. Ferbel, V. Dorofeev, and S. Paul for a critical reading of this manuscript. Thanks are due also to R. Bertini, F. Bradamante, A. Bravar, D. Casey, S. U. Chung, M. Colantoni, N. d'Hose, S. Donskov, W. Dunnweber, M. Faessler, M. Finger, L. Frankfurt, S. Godfrey, H. Hahn, D. von Harrach, T. Hasegawa, Y. Khokhlov, K. Königsmann, R. Kuhn, F. Kunne, L. Landsberg, J. Lichtenstadt, A. Magnon, G. Mallot, V. Molchanov, J. Nassalski, A. Olchevski, E. Piasetzky, J. Pochodzalla, S. Prakhov, A. Sandacz, L. Schmitt, C. Schwarz, H. W. Siebert, V. Sougoniaev, T. Walcher, and M. Zielinski for valuable discussions. Thanks are due to the Johannes Gutenberg Universitaet (Mainz, Germany) for hospitality during the writing of this report, during a sabbatical leave from Tel Aviv University, as a visiting Mercator Professor.

References

[1] N. Isgur and A. Dzierba, CERN Courier **40** (2000) 23; http://www.cerncourier.com/main/article/40/7/16.

[2] A. Dzierba *et al.*, Amer. Sci. **88** (2000) 406; http://www.americanscientist.org/articles/00articles/dzierba.html; QCD Confinement and the Hall D Project at Jefferson Lab, hep-ex/0106010.

[3] S. Godfrey and J. Napolitano, Rev. Mod. Phys. **71** (1999) 1411; hep-ph/0211464, these proceedings.

[4] S. U. Chung, Nucl. Phys. B **86** (2000) 341.

[5] W. Dünnweber, these proceedings.

[6] U. Wiedner, Exotic Meson Prospects via a New Facility for $p\bar{p}$ reactions, www.gsi.de/GSI-Future/program.html, Darmstadt, Germany, Oct. 2000, Light-Quark Spectroscopy with Anti-Proton Proton Annihilation, Workshop on Low-Energy Pbar Storage Ring (Pbar2000), Aug. 2000, Chicago, Illinois, http://www.iit.edu/ bcps/hep/pbar2000.html.

[7] A. Dzierba *et al.*, The Hall D project Design Report, Searching for QCD Exotics with a Beam of Photons, Nov. 2000; http://dustbunny.physics.indiana.edu/HallD/.

[8] S. U. Chung, Exotic Meson Prospects via FNAL CDF/D0 and BNL RICH double-Pomeron production, private communication.

[9] A. Abele *et al.*, Phys. Lett. B **423** (1998) 175.

[10] D. R. Thompson *et al.*, Phys. Rev. Lett. **79** (1997) 1630; G. S. Adams *et al.*, Phys. Rev. Lett. **81** (1998) 5760; S. U. Chung *et al.*, Phys. Rev. D **65** (2002) 072001.

[11] V. Dorofeev (VES Collaboration), hep-ex/9905002, hep-ex/0110075; I Kachaev, hep-ex/0111067; A. Zaitsev, Nucl. Phys. A **675** (2000) 155c.

[12] S. Donskov, these proceedings.

[13] V. Dorofeev, these proceedings.

[14] CERN Proposal COMPASS, http://wwwcompass.cern.ch/, CERN/SPSLC 96-14, SPSC/P297; CERN/SPSLC 96-30, SPSC/P297, Addendum 1;
http://www_nuclear.tau.ac.il/∼murraym/primaphysreps.html

[15] M. A. Moinester, V. Steiner and S. Prakhov, Hadron-Photon Interactions in COMPASS, hep-ph/9910039.

[16] M. A. Moinester and S. U. Chung, Hybrid Meson Structure at COMPASS, hep-ex/0003008.

[17] M. A. Moinester, Pion Polarizabilities and Hybrid Meson Structure at COMPASS, hep-ex/0012063.

[18] S. U. Chung, E. Klempt and J. Koerner, hep-ph/0211100.

[19] A. Donnachie and P. R. Page, Phys. Rev. D **58** (1998) 114012.

[20] S. Bass, hep-ph/0210018.

[21] T. Barnes, Photoproduction of Hybrid Mesons, nucl-th/9907020;
Hadron 2001 Conference Summary, hep-ph/0202157.

[22] N. Isgur, Phys. Rev. D **60** (1999) 114016.

[23] F. Close and P. Page, Nucl. Phys. B **443** (1995) 233.

[24] N. Isgur, Spectroscopy - An Introduction and Overview, JLAB-THY-99-03-A, Feb 1999,
in Proceedings of the 8th International Conference on the Structure of Baryons (Baryons 98), Bonn, Germany, Sept. 1998, Eds. D. W. Menze, B. Metsch, World Scientific, 1999.

[25] K. Peters, Meson Spectroscopy and Exotic Quantum Numbers, in Proceedings of the 8th International Conference on the Structure of Baryons (Baryons 98), Bonn, Germany, Sept. 1998, Eds. D. W. Menze, B. Metsch, World Scientific, 1999; Physics of Exotic and Non-Exotic Mesons at HESR, Workshop on Gross Properties of Nuclei and Nuclear Excitations, Hirschegg, Austria, Jan 2001, http://theory.gsi.de/hirschegg/.

[26] D. Alde *et al.*, Proc. of HADRON-97, BNL, August 1997.

[27] Yu.D. Prokoshkin and S.A. Sadovsky, Phys. At. Nucl. **58** (1995) 606.

[28] G. M. Beliadze *et al.*, Phys. Lett. B **313** (1993) 276–282; A.Zaitsev, Proc. of HADRON-97, BNL, August 1997.

[29] D. Alde *et al.*, Phys. Lett. B **205** (1988) 397; Phys. Atom. Nucl. **62** (1999) 1993.

[30] H. Aoyagi *et al.*, Phys. Lett. B **314** (1993) 246.

[31] T. Jensen *et al.*, Phys. Rev. **27D** (1983) 26.

[32] M. Zielinski *et al.*, Z. Phys. C **31** (1986) 545;
Z. Phys. C **34** (1987) 255; M. Zielinski (in BNL 88, Glueballs, Hybrids, and Exotic Hadrons); M. Zielinski, Acta Phys. Polon. B **18** (1987) 455.

[33] T. Ferbel *et al.*, Proceedings of the XVIth Rencontre de Moriond on New Flavors and Hadron Spectroscopy, Les Arcs, Savoie, 1981, p. 373; Acta Phys. Polon. B **12** (1981) 1129.

[34] V. Molchonov *et al.* (SELEX Collaboration), Phys. Lett. **B521** (2001) 171.

[35] CERN Workshop on Future Physics at COMPASS, Sept. 2002, Proceedings and Transparencies, http://compass-cw2002.web.cern.ch/compass-cw2002/programme.htm.

[36] M. Zielinski *et al.*, Z. Phys. C, Particles and Fields **16** (1983) 197.

[37] G. T. Condo *et al.*, Phys. Rev. **43D** (1991) 2787.

[38] S. U. Chung, Future Prospects for Exotic Mesons, Workshop on Gross Properties of Nuclei and Nuclear Excitations, Hirschegg, Austria, Jan 2001, http://theory.gsi.de/hirschegg/.

[39] J. Huston *et al.*, Phys. Rev. **33** (1986) 3199.

[40] L. Capraro *et al.*, Nucl. Phys. B **288** (1987) 659.

[41] M. Zielinski *et al.*, Phys. Rev. Lett. **52** (1984) 1195.

[42] S. Cihangir *et al.*, Phys. Lett. **117B** (1982) 119; ibid., p.123;
Phys. Rev. Lett. **51** (1983) 1.

[43] D. Berg *et al.*, Phys. Lett. B **98** (1981) 119.

[44] C. Chandlee *et al.*, Phys. Rev. Lett. **51** (1983) 168.

[45] H. W. Atherton *et al.*, Precise Measurements of Particle Production by 400 GeV/c Protons on Beryllium Targets, report CERN 80-07, 1980.

[46] M. Benot *et al.*, Nucl. Instr. Meth. **105** (1972) 431; C. Bovet, S. Milner and A. Placci, CERN/Lab. II/EA/74-4, (Rev. Aug 1975), The CEDAR Project; CErenkov Differential counters with Achromatic Ring focus; C. Bovet *et al.*, CERN-SPS/EBP/77-19, The CEDAR Project, IEEE Trans. Nucl. Sci. **25** (1978) 572; C. Bovet *et al.*, CERN report CERN 82-13, The CEDAR counters for particle identification in the SPS secondary beams: a description and operation manual.

[47] M. Moinester, http://www-nuclear.tau.ac.il/∼murraym/COMPASS/laser_monitor_techrep.html.

[48] M. A. Moinester and V. Steiner, Pion and Kaon Polarizabilities and Radiative Transitions, Proc. 'Chiral Dynamics Workshop' U. Mainz, Sept. 1997, hep-ex/9801008.

DOUBLY CHARMED BARYONS

Peter S. Cooper
on behalf of the SELEX Collaboration
Fermi National Accelerator Laboratory
P.O. Box 500, MS 122, IL 60510

Abstract
Candidates for several new high-mass states which include a cleanly-identified daughter Λ_c^+ baryon are seen in data from the SELEX experiment at Fermilab. These states are candidates for doubly charmed baryons: a Ξ_{cc}^{++} state and a Ξ_{cc}^{+} state. These candidates are more than 5σ signals in each case at masses of 3520 and 3460 MeV respectively.

1. INTRODUCTION

The SELEX experiment, of which I am a spokesman, reports evidence for three new high-mass states decaying into $\Lambda_c^+ K^- \pi^+ (\pi^+)$. These states are consistent with some expectations of the doubly charmed baryons predicted by the broken SU(4) symmetry of a system with four quark flavors [1]. This work is presently being published in the refereed journals with one paper already in print [2] and others in preparation. I shall only briefly summarize this work here.

2. DOUBLY CHARMED BARYON CANDIDATES FROM SELEX

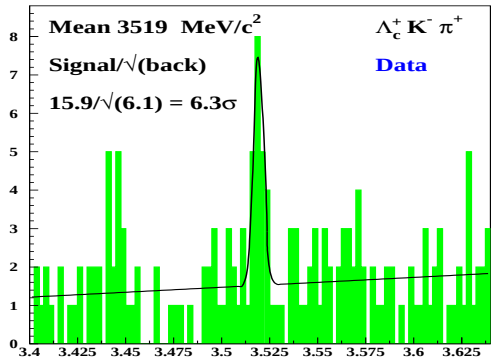

Fig. 1: SELEX $\Xi_{cc}^{+}(3519)$ signal.

SELEX reports [2] a Ξ_{cc}^{+} state at 3519 MeV with a statistical significance of 6.3σ (Figure 1) and an apparent iso-partner Ξ_{cc}^{++} state at 3460 MeV with a statistical significance of 4.8σ (Figure 2). Both of these states have a width consistent with resolution and a very short lifetime (<30 fs). SELEX also sees a broad state at 3783 MeV (Figure 3) which looks like a Ξ_{cc}^{*++} with evidence for the strong decay mode $\Xi_{cc}^{*++}(3783) \rightarrow \Xi_{cc}^{+}(3519)\pi^+$.

The FOCUS experiment has shown [3] their search for states like SELEX observes. Starting with 10 times more Λ_c^+ events they have no evidence for any signals, and few entries in general, in a long list of decay modes, including those where SELEX sees signals. Whatever SELEX observes in hadro-production with baryon beams is not observed in photo-production.

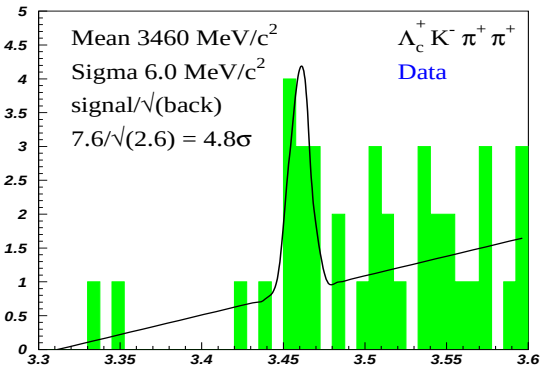

Fig. 2: SELEX $\Xi_{cc}^{++}(3460)$ signal.

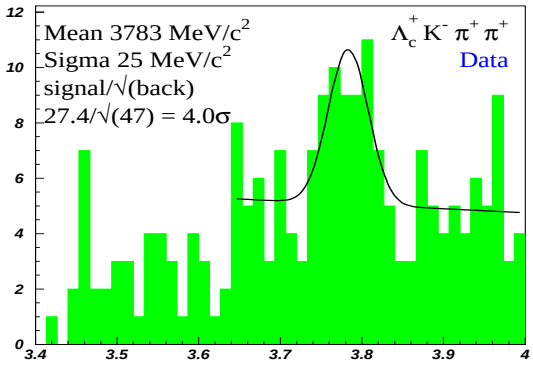

Fig. 3: SELEX $\Xi_{cc}^{*++}(3783)$ signal.

The SELEX signals do not constitute a clear and unambiguous picture as doubly charmed baryons. The production cross-section of these states, in the forward region where SELEX is sensitive, is considerably higher than expected; lifetimes as short as 30 fs are less than models predict and a 60 MeV mass difference between $\Xi_{cc}^{+}(3519)$ and $\Xi_{cc}^{++}(3460)$ is hard to understand as an isospin splitting. With evidence for three inter-related new states we can only guess, at this time, what fraction and pieces of the total picture we are now seeing.

What is abundantly clear it that these signals are not statistical fluctuations; they are something. The only alternative interpretation consistent with the observed properties of these states is as decays of very high mass, singly charmed baryon excited states with absurdly narrow strong decay widths.

3. FUTURE PROSPECTS

We can look forward to further measurements from SELEX, and hopefully others, to confirm (or contradict) these signals. New work on the phenomenology and models of doubly charmed baryons can also be expected in order to more fully understand these observations.

References

[1] Particle Data Group, K. Hagiwara *et al.*, Phys. Rev. D **66** (2002) 010001.

[2] SELEX Collaboration, M. Mattson *et al.*, Phys. Rev. Lett. **89** (2002) 112001.

[3] FOCUS Collaboration, S. Ratti, Proceedings of the 5th International Conference on Hyperons, Charm, and Beauty Hadrons, Vancouver, BC, Canada, 25–29 July 2002.

DOUBLE CHARM PHYSICS

Jean-Marc Richard[*]
Institut des Sciences Nucléaires, Université Joseph Fourier–CNRS-IN2P3
53, avenue des Martyrs, F-38026 Grenoble cedex

Abstract
We review the weak-decay and spectroscopy properties of baryons with two charmed quarks. We also present the convergent speculations on exotic mesons $(QQ\bar{q}\bar{q})$ with two heavy quarks and two light antiquarks.

1 INTRODUCTION

The discovery of the $(b\bar{c})$ ground state [1], and that of the (ccd) baryon [2–4] demonstrates that new sectors of hadron physics are becoming accessible to experiments.

There are several good reasons to study hadron systems with two c quarks:

- Double charm baryons provide tests of mechanisms proposed to describe the weak decays of charmed mesons and single-charm baryons.
- The dynamics of confinement in (QQq) baryons combine the slow relative motion of two heavy quarks with the fast motion of a light quark.
- $(QQ\bar{q}\bar{q})$ multiquark states have been predicted, whose stability results from the flavour-independent character of quark forces at short distances and from pion-exchange between two heavy mesons at large distances.

These aspects will be reviewed in the next sections. Details will be skipped. Many references will be provided for further reading.

2 WEAK DECAY OF CHARM

2.1 General considerations

It was a surprise in our community when the ratio of lifetimes $r = \tau(D^{\pm})/\tau(D^0)$ was announced to significantly differ from unity. The preliminary value $r \simeq 4$ even amplified the shock. Still, the stabilised value $r \simeq 2.5$ [1] is impressive. With only spectator diagrams such as those of Fig. 1, all lifetimes would be equal (up to minor phase-space effects) and all semileptonic widths comparable. $r \neq 1$ reveals

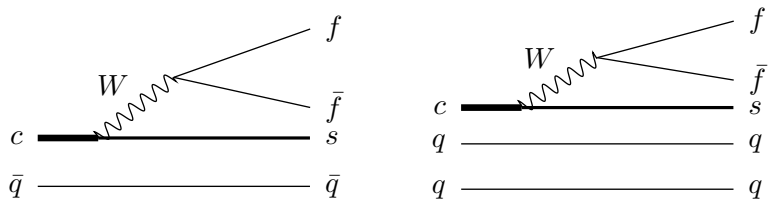

Fig. 1: Spectator diagram, for charmed mesons (left) and single-charm baryons (right).

important non-spectator effects: interferences between a constituent quark or antiquark, and another coming from c or W decay; W exchange between c and d or s; to a lesser extent, W formation in the s-channel. Further refinements such as penguin diagrams might also be included.

[*]e-mail: jean-marc.richard@isn.in2p3.fr

2.2 Charmed mesons

There are many data on charmed mesons. In particular, the semileptonic widths are comparable [1]

$$\Gamma_{\rm SL}(D^{\pm}) \sim \Gamma_{\rm SL}(D^0) \sim \Gamma_{\rm SL}(D_s) \sim 0.3\,{\rm ps}^{-1}\,. \tag{1}$$

There is no major interference effect. So the mechanism of Fig. 1 (left) with $(f,\bar{f}) = (e^+,\nu_e)$ or (μ^+,ν_μ) provides all mesons with a similar semi-leptonic rate. The differences in lifetimes come from the hadronic part. The results [1]

$$\tau(D^0) \sim 400\,{\rm fs}\,, \quad \tau(D_s) \sim 500\,{\rm fs}\,, \quad \tau(D^+) \sim 1000\,{\rm fs}\,, \tag{2}$$

indicate that the light antiquark is not a mere spectator. When $\bar{f} = \bar{d}$ in $W \to f\bar{f}$ decay, this $\bar{d}$ interferes with the $\bar{d}$ of D^+. For D^0 and D_s, a W boson can be exchanged. For D_s, there is a small contribution of W formation. Some effects are pictured in Fig. 2.

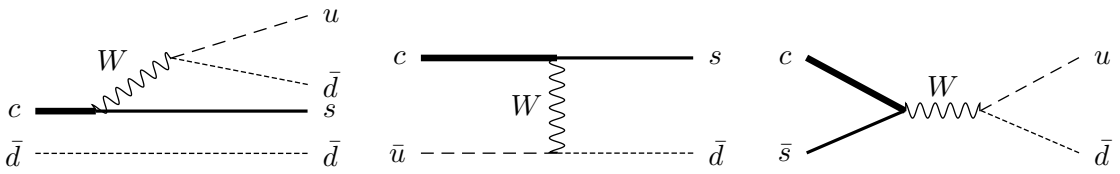

Fig. 2: Some mechanisms contributing to differences among the lifetimes of charmed mesons: interferences (left), W exchange (centre), fusion into W (right).

2.3 Baryons with single charm

The above mechanisms have been applied to charmed baryons: $\Lambda_c^+(cud)$, $\Xi_c^+(csu)$, $\Xi_c^0(csd)$ and $\Omega_c(css)$. A new interference appears with respect to the meson case: the s-quark coming from the decaying c might "feel" the presence of another s. The W-exchange contribution receives a larger strength. Annihilation becomes negligible, since requiring an antiquark from the sea. Some typical contributions are shown in Fig. 3. The mechanisms can be tested in subclasses of decays, once the statistics becomes sufficient for such filtering. An example is the last diagram of Fig. 3 showing a W-exchange contribution to doubly-Cabbibo-suppressed decay.

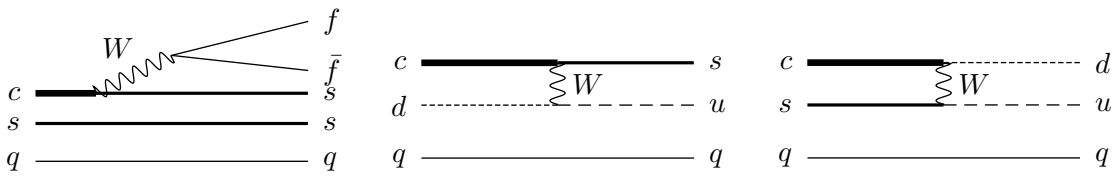

Fig. 3: Some diagrams differentiating the weak decay properties of various single-charm baryons: ss interferences, W exchange for ordinary hadronic decay, W exchange for suppressed decay.

.

The main *predictions* [5, 6] are that

- there are differences in the semileptonic partial widths $\Gamma_{\rm SL}$, namely

$$\Gamma_{\rm SL}(\Lambda_c^+) < \Gamma_{\rm SL}(\Xi_c^+) < \Gamma_{\rm SL}(\Xi_c^0) < \Gamma_{\rm SL}(\Omega_c^0)\,, \tag{3}$$

- the lifetimes are ordered as

$$\tau(\Omega_c) < \tau(\Xi_c^0) < \tau(\Lambda_c^+) < \tau(\Xi_c^+)\,. \tag{4}$$

Present data do not enable one to check the prediction (3). The ordering (4) of lifetimes is remarkably verified by the data, but the spread of values seems always underestimated in theoretical calculations, at least to my knowledge. This is hopefully just a matter of using more realistic values of some model-dependent parameters, such as the probability to find two quarks at the same location, which enters the contribution of W exchange.

There are many predictions for exclusive rates, at least for their relative values. See, for example, Ref. [7] for a flavour of this rich physics.

2.4 Weak decays of baryons with double charm

The same mechanisms have been further applied to baryons with double charm. Examples are drawn in Fig. 4. There is an overall agreement that the hierarchy of lifetimes is [6, 8]

$$\tau(\Xi_{cc}^+) \lesssim \tau(\Omega_{cc}^+) \ll \tau(\Xi_{cc}^{++}) \,, \tag{5}$$

with, perhaps, an underestimate of the magnitude of the effect. For instance, Kiselev *et al.* [9, 10] predicted $\tau(\Xi_{cc}^+) \sim 400\,\text{fs}$, as compared to the value $\tau \lesssim 30\,\text{fs}$ suggested by SELEX data [2, 4]. This is one of the reasons leading Kiselev *et al.* [11] to cast some doubt about the Fermilab result. See, also, Ref. [12]. But, again, the lifetime of other charmed baryons was also overestimated by theorists. In the plot of lifetimes, Fig. 5, a value as low as 30 fs does not look too extravagant an extrapolation.

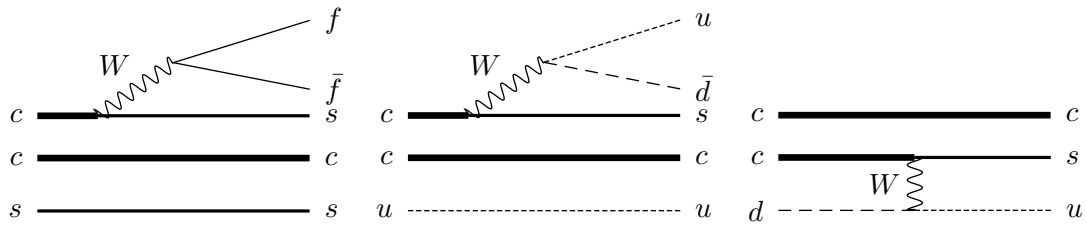

Fig. 4: Some diagrams leading to differences among the lifetimes of baryons with double charm.

3 SPECTROSCOPY OF DOUBLE-CHARM BARYONS

In the 1960s, the flavour group SU(3)_F was immediately extrapolated to SU(4) or higher. A better motivation for a fourth quark came from the GIM mechanism [13]. At the time where charm was discovered, in the hidden form of $(c\bar{c})$, some classic papers were written on hadrons with charm, including a section on (ccq) states [14, 15].

More detailed studies of (QQq) baryons came in the 1980s and later [6, 16–23]. No doubt the recent discovery at SELEX will stimulate further works.

(QQq) baryons are perhaps the most interesting of ordinary hadrons, as they combine in a single bag two extreme regimes:

1. the slow relative motion of two heavy quarks, as in charmonium,
2. the fast motion of a light quark. Remember that the electron moves faster in hydrogen than in positronium. Similarly, a light quark is likely more relativistic in heavy-light hadrons than in light mesons.

Hence, (QQq) baryons offer a very interesting laboratory to study confinement.

3.1 Diquark clustering and excitations

In the (QQq) wave function, the average QQ separation is smaller than the Qq one. This leads to envisage approximations, such as a quark–diquark picture, to be discussed shortly. The diquark is,

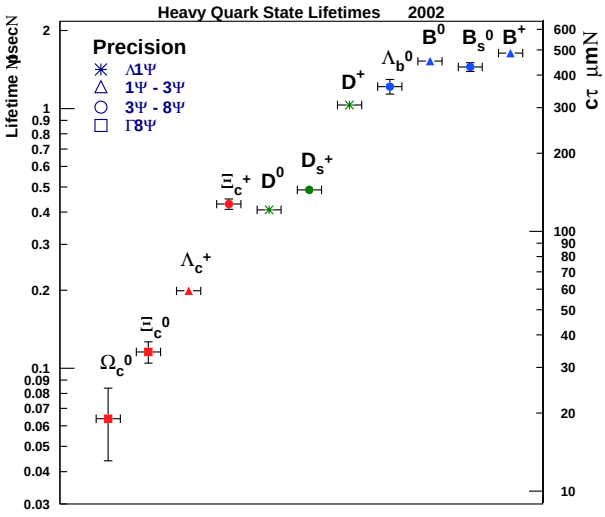

Fig. 5: Lifetimes of heavy baryons, borrowed from the slides of P. Cooper at the last Hyperon Conference [3].

however, not frozen. The first excitations arise in the QQ relative motion, i.e., the (QQq) ground state, and its first orbital excitation $(QQq)^*$ are built out of different diquarks.

3.2 The two-step approximation

It is rather legitimate to replace the full three-body calculation by a two-step procedure where one

1. calculates the QQ mass, by solving a two-body problem,
2. calculates the $QQ - q$ mass by solving another two-body problem.

The second step is rather safe. The finite-size corrections are small. For instance, they cancel out exactly for the harmonic oscillator.

As for the first step, one should be aware that the QQ potential is *effective*, since it contains both the direct QQ interaction and a contribution from the light quark. For instance, in the harmonic oscillator model, the identity

$$r_{12}^2 + r_{23}^2 + r_{31}^2 = \frac{3}{2} r_{12}^2 + 2\, r_{12-3}^2 \,, \tag{6}$$

demonstrates that 1/3 of the QQ interaction comes from the light quark. Replacing 3/2 by 1 results in an underestimate of energies and spacings by a factor $\sqrt{3/2}$.

3.3 The Born–Oppenheimer approximation

It was used, for example, by Fleck and Richard [16]. For a given QQ separation r_{12}, the two-centre problem is solved for the light quark, with proper reduced mass. The ground-state energy $E_0(r_{12})$, supplemented by the direct QQ interaction, provides the adiabatic potential V_{QQ}. Solving the 2-body problem with this potential gives the first levels. The adiabatic potential built out of the second "electronic" energy $E_1(r_{12})$ leads to a second series of levels. This is very similar to the spectroscopy of H_2^+ in atomic physics.

Within explicit potential models, the Born–Oppenheimer approximation can be checked against an accurate solution of the 3-body problem, using for instance a systematic hyperspherical expansion. The approximation is excellent for (bbq) and (ccq), with $q = u$, d or s, or even for (ssu) or (ssd).

3.4 Typical results

In Ref. [16], (ccq) masses were estimated from a specific variant of the bag model, already used for charmed mesons. The results turn out to be rather sensitive to details such as centre-of-mass corrections, value of the bag constant, etc. Other bag-model calculations have been performed [24].

Potential models, on the other hand, tend to give very stable results, when the parameters are varied while maintaining a reasonable fit of lighter hadrons. Typically

- a ground state near or slightly above $3.6\,\mathrm{GeV}$ for the (ccu) or (ccd) ground state,
- a hyperfine splitting of about $80\,\mathrm{MeV}$ between the spin 3/2 and spin 1/2 states,
- the first orbital excitation about $300\,\mathrm{MeV}$ above the ground state,
- the first (ccs) state near $3.7\,\mathrm{GeV}$.

Note that models tuned to (cqq) or lighter baryons might underestimate the short-range QQ attraction. If models are adjusted to $(c\bar{c})$ spectroscopy, there is an ambiguity on how to translate it to cc. The usual recipe stating that

$$V_{QQ} = \frac{1}{2} V_{Q\overline{Q}}\,, \tag{7}$$

implies pairwise forces mediated by colour-octet exchanges. Small, non-confining, colour-singlet exchanges, as well as three-body forces might complicate the issue.

3.5 Towards better estimates

Most existing calculations are of a rather exploratory nature, since made when double charm was considered as science fiction, or far future. Meanwhile, the art of QCD has made significant progress.

One could retain from simple potential models that the Born–Oppenheimer approximation provides an adequate framework. The effective QQ potential could be estimated from relativistic models or from lattice calculations, similar to those of the $Q\overline{Q}$ potential or the effective QQ potential in exotic $(QQ\bar{q}\bar{q})$ mesons, on which more shortly. It is hoped that the new experimental results will stimulate such calculations.

The literature already contains approaches somewhat more ambitious than simple bag or potential models: QCD sum rules [19], string picture [25, 26], etc.

4 EXOTIC MESONS WITH DOUBLE CHARM?

4.1 Minireview on advertised exotics

The famous H dibaryon proposed by Jaffe [27], and the less notorious pentaquark P proposed independently by Lipkin [28] and the Grenoble group [29], owe their tentative stability to *chromomagnetic* forces. Other mechanisms might lead to stable multiquarks: *chromoelectric* forces and long-range *Yukawa* interaction. These mechanisms were first proposed with crude approximations for the overall dynamics. It is important to examine to which extent multiquark binding survives all refinements brought in model calculations.

4.1.1 Hexaquark

The chromomagnetic interaction [15]

$$H_{cm} = -C \sum_{i<j} \frac{\vec{\sigma}_i.\vec{\sigma}_j\, \tilde{\lambda}_i.\tilde{\lambda}_j}{m_i m_j} \delta^{(3)}(\vec{r}_{ij})\,, \tag{8}$$

or its bag model analogue [30], successfully describes the observed hyperfine splittings such as $\Delta - N$ or $J/\Psi - \eta_c$. The astute observation by Jaffe [27] is that this operator provides a binding

$$(ssuudd) - 2(sud) \sim -150\,\mathrm{MeV} \tag{9}$$

to the $H = (ssuudd)$ dibaryon with spin and isospin $J = I = 0$. This estimates, however, relies on:

1. $\mathrm{SU(3)_F}$ flavour symmetry,
2. $\langle \delta^{(3)}(\vec{r}_{ij}) \rangle$ independent of (i, j) pair and borrowed from the wave function of ordinary baryons.

Relaxing these hypotheses, and introducing kinetic energy and spin-independent forces in the 6-body Hamiltonian usually spoils the stability of H [31–33]. The existence of H is nowadays controversial. It has been searched for in many experiments, without success so far. For instance, the doubly-strange hypernucleus ${}^{6}_{\Lambda\Lambda}\mathrm{He}$ is not observed to decay into $H + \alpha$ [34].

4.1.2 Pentaquark

If the calculation made for the H is repeated in the limit where $m(Q) \to \infty$, the same binding

$$(\overline{Q}qqqq) - (\overline{Q}q) - (qqq) \sim -150\,\mathrm{MeV} \tag{10}$$

is obtained for the pentaquark $(\overline{Q}qqqq)$, $qqqq$ being in a $\mathrm{SU(3)_F}$ triplet [28, 29]. All corrections, again, tend to weaken this binding [33, 35] so it is not completely sure that the actual pentaquark is stable. See, also, Ref. [36].

For the case where the chromomagnetic term (8) is replaced by Goldstone-boson exchange, see, for example, the review by Stancu [37] and references therein.

4.2 Tetraquark

Twenty years ago, it was pointed out that current confining potentials bind $(QQ\bar{q}\bar{q})$ below its dissociation threshold into $(Q\bar{q}) + (Q\bar{q})$, provided the mass ratio $m(Q)/m(q)$ is large enough [38]. This *chromoelectric* binding was studied by several authors, in the context of flavour-independent potentials [39–47] or with lattice QCD [48, 49] (see, also, [50, 51]), with a remarkable convergence towards the same conclusion. This somewhat contrasts with the confusion in other sectors of multiquark spectroscopy.

4.2.1 Favourable symmetry breaking

Let us consider the limit of a purely flavour-independent potential V for $(QQ\bar{q}\bar{q})$. The situation becomes similar to that of exotic four-body molecules (M^+, M^+, m^-, m^-), which all use the very same Coulomb potential. The hydrogen molecule with $M \gg m$ is much more stable than the positronium molecule Ps_2 with $M = m$. If one decomposes the 4-body Hamiltonian as

$$\mathcal{H}_4 = \left[\frac{M^{-1} + m^{-1}}{4} \left(\vec{p}_1^{\,2} + \vec{p}_2^{\,2} + \vec{p}_3^{\,2} + \vec{p}_4^{\,2} \right) + V \right] + \frac{M^{-1} - m^{-1}}{4} \left(\vec{p}_1^{\,2} + \vec{p}_2^{\,2} - \vec{p}_3^{\,2} - \vec{p}_4^{\,2} \right) \ , \tag{11}$$

the first term, even under charge conjugation, corresponds to a rescaled equal-mass system with *the same threshold* as $\mathcal{H}_4$. The second term, which breaks charge conjugation, improves the energy of $\mathcal{H}_4$ (one can applies the variational principle to $\mathcal{H}_4$ using the symmetric ground state of the first term as a trial wave function). In the molecular case, the second term changes the marginally bound Ps_2 (or rescaled copy) into the deeply bound H_2. In quark models, an unbound $(qq\bar{q}\bar{q})$ becomes a stable $(QQ\bar{q}\bar{q})$.

The effective QQ potential has been estimated by Rosina *et al.* [46] in the framework of empirical potential models, and by Mihaly *et al.* [48] and Michael *et al.* (UKQCD) [49], who used lattice simulations of QCD.

The question is obviously: is the c quark heavy enough to make $(cc\bar{q}\bar{q})$ bound when $q = u$ or d? At this point, the answer is usually negative, most authors stating that b is required to bind $(QQ\bar{q}\bar{q})$ below its $(Q\bar{q}) + (Q\bar{q})$ threshold.

4.3 Deuterium-like binding

There is, however, another mechanism: pion-exchange or, more generally, nuclear-like forces between hadrons containing light quarks or antiquarks. This effect was studied by several authors, in particular Törnqvist [52], Manohar and Wise [53], and Ericson and Karl [54]. In particular a D and D^* can exchange a pion, thus inducing an attractive potential. It is weaker than in the nucleon–nucleon case, but what matters for a potential $gV(r)$ to bind, is the product gm of the strength g and reduced mass m.

It is found that (DD^*) is close to being bound, while binding is better established for (BB^*). The result depends on how sharply the long-range potential is empirically regularised at short distances.

4.4 Combining long- and short-range forces

A lattice calculation such as those of Refs. [48, 49] contains in principle all effects. In practice, space is truncated, so long-range forces are perhaps not entirely included. Explicit quark models such as [46] make specific assumptions about interquark forces, but do not account for pion exchange.

In our opinion, a proper combination of long- and short-range forces should lead to bind (DD^*), since each component is almost sufficient by itself. This is presently under active study.

4.5 Borromean binding

There is a further possibility to build exotic, multicharmed systems. If the interaction between two charmed mesons cannot lead to a bound state (this is presumably the case for (DD), since pion exchange does not contribute here), it is likely that the very same meson–meson interaction binds three or more mesons. This is known as the phenomenon of 'Borromean' binding.

For instance, in atomic physics, neither two ^{3}He atoms nor a ^{3}He atom and a ^{4}He atom can form a binary molecule, even at vanishing temperature, but it is found that $^3\mathrm{He}^3\mathrm{He}^4\mathrm{He}$ is bound [55]. Similarly, in nuclear physics, the isotope ^{6}He is stable against evaporating two neutrons, or any other dissociation process, while ^{5}He is unstable. In a 3-body picture, this means that (α, n, n) is stable, while neither (α, n) nor (n, n) have a stable bound state. In short, binding three constituents is easier than two.

5 CONCLUSIONS AND OUTLOOK

The results by the SELEX [2] and BELLE [56] groups show that we are now able to produce and identify two units of charm in hadron or electron collisions.

Double charm opens unique perspectives for studying new aspects of weak decays and confining forces, and for producing heavy exotic states.

A step further is triple-charm. The Ω_{ccc} family was named by Bjorken [57] the "ultimate goal of baryon spectroscopy". It will reveals a 'pure' baryon spectrum, without light quark complications. Comparing $(c\bar{c})$ and (ccc) ordering and spacing pattern will be crucial to check current ideas on the gluon strings picture leading to linear confinement.

Acknowledgements

I would like to thank my collaborators on the spectroscopy of charmed particles, in particular J.-P. Ader, S. Fleck, M. Genovese, A. Martin, S. Pepin, B. Silvestre-Brac, Fl. Stancu, P. Taxil and S. Zouzou. I am also grateful to P. Fayet and X.Y. Pham for informative discussions on weak decays.

References

[1] Particle Data Group, K. Hagiwara *et al.*, "Review of particle physics", Phys. Rev. D **66** (2002) 010001.

[2] SELEX, M. Mattson *et al.*, "First observation of the doubly charmed baryon Ξ_{cc}^{+}", Phys. Rev. Lett. **89** (2002) 112001, hep-ex/0208014.

[3] P. Cooper, *Heavy Baryons- Recent and Very New Results, Doubly Charmed Baryons?*, Talk at BEACH 2002, Vancouver, June 2002, http://beach2002.physics.ubc.ca/talks/Peter_Cooper.pdf.

[4] P. S. Cooper, Contribution to this Workshop.

[5] B. Guberina, R. Ruckl and J. Trampetic, "Charmed baryon lifetime differences", Z. Phys. C **33** (1986) 297.

[6] S. Fleck and J.M. Richard, "Charmed baryons", Part. World **1** (1990) 67.

[7] M.J. Savage and R.P. Springer, "SU(3) Predictions for charmed baryon decays", Phys. Rev. D **42** (1990) 1527.

[8] B. Guberina, B. Melic and H. Stefancic, "Inclusive decays and lifetimes of doubly charmed baryons", Eur. Phys. J. C **9** (1999) 213, hep-ph/9901323, Erratum: Eur. Phys. J. C **13** (2000) 551.

[9] V.V. Kiselev, A.K. Likhoded and A.I. Onishchenko, "Lifetimes of doubly charmed baryons: Ξ_{cc}^{+} and Ξ_{cc}^{++}", Phys. Rev. D **60** (1999) 014007, hep-ph/9807354.

[10] V.V. Kiselev, A.K. Likhoded and A.I. Onishchenko, "Lifetimes of doubly charmed baryons: Ξ_{cc}^{+} and Ξ_{cc}^{++}", Phys. Atom. Nucl. **62** (1999) 1940.

[11] V.V. Kiselev and A.K. Likhoded, "Comment on first observation of doubly charmed baryon Ξ_{cc}^{+}", (2002), hep-ph/0208231.

[12] J. Yelton, "Charmed particles at the double", Phys. World **15N10** (2002) 19.

[13] S.L. Glashow, J. Iliopoulos and L. Maiani, "Weak interactions with lepton–hadron symmetry", Phys. Rev. D **2** (1970) 1285.

[14] M.K. Gaillard, B.W. Lee and J.L. Rosner, "Search for charm", Rev. Mod. Phys. **47** (1975) 277.

[15] A. De Rujula, H. Georgi and S.L. Glashow, "Hadron masses in a gauge theory", Phys. Rev. D **12** (1975) 147.

[16] S. Fleck and J.M. Richard, "Baryons with double charm", Prog. Theor. Phys. **82** (1989) 760.

[17] M.J. Savage and M.B. Wise, "Spectrum of baryons with two heavy quarks", Phys. Lett. B **248** (1990) 177.

[18] M.J. Savage and R.P. Springer, "Very charming baryons", Int. J. Mod. Phys. A **6** (1991) 1701.

[19] E. Bagan *et al.*, "Hadrons with charm and beauty", Z. Phys. C **64** (1994) 57, hep-ph/9403208.

[20] R. Roncaglia, D.B. Lichtenberg and E. Predazzi, "Predicting the masses of baryons containing one or two heavy quarks", Phys. Rev. D **52** (1995) 1722, hep-ph/9502251.

[21] B. Silvestre-Brac, "Spectrum and static properties of heavy baryons", Few-Body Syst. **20** (1996) 1.

[22] V.V. Kiselev and A.E. Kovalsky, "Doubly heavy baryons $\Omega_{QQ'}$ vs. $\Xi_{QQ'}$ in sum rules of NRQCD", Phys. Rev. D **64** (2001) 014002, hep-ph/0005019.

[23] S.P. Tong *et al.*, "Spectra of baryons containing two heavy quarks in potential model", Phys. Rev. D **62** (2000) 054024, hep-ph/9910259.

[24] W. Ponce, "Heavy quarks in a spherical bag", Phys. Rev. D **19** (1979) 2197.

[25] S.S. Gershtein *et al.*, "Spectroscopy of doubly charmed baryons: Ξ_{cc}^{+} and Ξ_{cc}^{++}", Mod. Phys. Lett. A **14** (1999) 135, hep-ph/9807375.

[26] S.S. Gershtein *et al.*, "Spectroscopy of doubly heavy baryons", Phys. Rev. D **62** (2000) 054021.

[27] R.L. Jaffe, "Perhaps a stable dihyperon", Phys. Rev. Lett. **38** (1977) 195, ibid. **38** (1977) 617 (E).

[28] H.J. Lipkin, "New possibilities for exotic hadrons: Anticharmed strange baryons", Phys. Lett. B **195** (1987) 484.

[29] C. Gignoux, B. Silvestre-Brac and J.M. Richard, "Possibility of stable multiquark baryons", Phys. Lett. B **193** (1987) 323.

[30] A. Chodos *et al.*, "A new extended model of hadrons", Phys. Rev. D **9** (1974) 3471.

[31] J.L. Rosner, "SU(3) breaking and the H dibaryon", Phys. Rev. D **33** (1986) 2043.

[32] G. Karl and P. Zenczykowski, "H dibaryon spectroscopy", Phys. Rev. D **36** (1987) 2079.

[33] S. Fleck *et al.*, "The dilambda and the pentaquark in the constituent quark model", Phys. Lett. B **220** (1989) 616.

[34] A. Gal, "To bind or not to bind: $\Lambda\overline{\Lambda}$ hypernuclei and Ξ hyperons", (2002), nucl-th/0211070.

[35] G. Karl and P. Zenczykowski, "SU(3) flavor symmetry breaking in $(\bar{c}suud)$ bound state", Phys. Rev. D **36** (1987) 3520.

[36] J. Leandri and B. Silvestre-Brac, "Systematics of $\overline{Q}q^4$ systems with a pure chromomagnetic interaction", Phys. Rev. D **40** (1989) 2340.

[37] F. Stancu, "Stability of multiquark systems," International Workshop on Hadron Physics: Effective Theories of Low Energy QCD, Coimbra, Portugal, 10-15 Sep 1999, hep-ph/9910547.

[38] J.P. Ader, J.M. Richard and P. Taxil, "Do narrow heavy multiquark states exist?", Phys. Rev. D **25** (1982) 2370.

[39] L. Heller and J.A. Tjon, "On bound states of heavy $Q^2\bar{q}^2$ systems", Phys. Rev. D **32** (1985) 755.

[40] L. Heller and J.A. Tjon, "On the existence of stable dimesons", Phys. Rev. D **35** (1987) 969.

[41] J. Carlson, L. Heller and J.A. Tjon, "Stability of dimesons", Phys. Rev. D **37** (1988) 744.

[42] S. Zouzou *et al.*, "Four quark bound states", Z. Phys. C **30** (1986) 457.

[43] H.J. Lipkin, "A model independent approach to multiquark bound states", Phys. Lett. B **172** (1986) 242.

[44] D.M. Brink and F. Stancu, "Role of hidden color states in $q^2\bar{q}^2$ systems", Phys. Rev. D **49** (1994) 4665.

[45] D.M. Brink and F. Stancu, "Tetraquarks with heavy flavors", Phys. Rev. D **57** (1998) 6778.

[46] D. Janc and M. Rosina, "A phenomenological estimate of the binding energy of heavy dimesons", Few-Body Syst. **31** (2001) 1, hep-ph/0007024.

[47] B.A. Gelman and S. Nussinov, "Does a narrow tetraquark $cc\bar{u}\bar{d}$ state exist?, preprint hep-ph/0209095.

[48] A. Mihaly *et al.*, "Interactions between heavy - light mesons in lattice QCD", Phys. Rev. D **55** (1997) 3077.

[49] UKQCD, M. Foster and C. Michael, "Hadrons with a heavy colour-adjoint particle", Phys. Rev. D **59** (1999) 094509, hep-lat/9811010.

[50] A.M. Green and P. Pennanen, "A model for multiquark systems", Phys. Lett. B **426** (1998) 243, hep-lat/9709124.

[51] A.M. Green and P. Pennanen, "An interquark potential model for multiquark systems", Phys. Rev. C **57** (1998) 3384, hep-lat/9804003.

[52] N.A. Törnqvist, "Possible large deuteron - like meson-meson states bound by pions", Phys. Rev. Lett. **67** (1991) 556.

[53] A.V. Manohar and M.B. Wise, "Exotic $QQ\bar{q}\bar{q}$ states in QCD", Nucl. Phys. B **399** (1993) 17, hep-ph/9212236.

[54] T.E.O. Ericson and G. Karl, "Strength of pion exchange in hadronic molecules", Phys. Lett. B **309** (1993) 426.

[55] D. Bressanini, G. Morosi, L. Bertini, and M. Mella, Stability of Few-Body Quantum Systems and Quantum Monte-Carlo Methods, Few-Body Syst. **31** (1002) 199.

[56] Belle, K. Abe *et al.*, "Observation of double c-$\bar{c}$ production in e^+e^- annihilation at $s^{1/2} \approx 10.6$ GeV", Phys. Rev. Lett. **89** (2002) 142001, hep-ex/0205104.

[57] J.D. Bjorken, "Is the ccc a new deal for baryon spectroscopy?", Int. C onf. on Hadron Spectroscopy, College Park, MD, Apr 20-22, 1985, Proc. Ed. by S. Oneda. N.Y., American Inst. Phys., 1985. 485p. (AIP Conference Proceedings, 132).

DOUBLY CHARMED BARYONS IN COMPASS

L. Schmitt, S. Paul, R. Kuhn
TU-München, Physik-Department E18, Munich, Germany
M. A. Moinester
School of Physics and Astronomy, Tel Aviv University, Ramat Aviv, Israel

Abstract
The search for doubly charmed baryons has been a topic for COMPASS from the beginning. Requiring, however, a complete spectrometer and highest possible trigger rates, this measurement has been postponed. The scenario for such a measurement in the second phase of COMPASS is outlined here. First studies of triggering and simulation of the setup have been performed. New rate estimates based on recent measurements from SELEX at FNAL are presented.

1. INTRODUCTION

The COMPASS collaboration was founded in 1996 to perform a number of measurements in hadron physics ranging from polarized structure functions examined with deep-inelastic muon scattering to topics like light meson spectroscopy and the study of exotic hadrons [1]. After the first phase of the COMPASS experiment focusing on the contribution of gluons to the polarized structure function of the nucleon, a second phase is planned to address more topics with hadron beams. One of these topics, the search for doubly charmed baryons, is described in this report.

The quantum chromodynamics hadron spectrum includes doubly charmed baryons (DCBs): Ξ_{cc}^{+} (ccd), $\Xi_{cc}^{++}(ccu)$, and Ω_{cc}^{+} (ccs), as well as the triply charmed Ω_{ccc}^{++} (ccc). A 1996 DCB review [2] collected information on masses, lifetimes, internal structure, production cross sections, decay modes, branching ratios, yields, and experimental requirements for optimizing the signal and minimizing the backgrounds. DCB works published since then are given in Refs. [3, 4, 5, 6, 7, 8, 9, 10, 11]. The doubly and triply charmed baryons provide a new window for understanding the structure of all baryons. As pointed out by Bjorken [12], one should strive to study the triply charmed (ccc) baryon. Its excitation spectrum, including several narrow levels above the ground state, should be closer to the perturbative regime than is the case for the DCBs. The (ccq) studies are a valuable prelude to such (ccc) efforts.

Hadron structures with size scales much less than $1/\Lambda_{qcd}$ should be well described by perturbative QCD. The tightly bound colour antitriplet $(cc)_{\bar{3}}$ diquark in (ccq) may satisfy this condition. But the DCB radius may be large, if it is dominated by the low mass q orbiting the tightly bound (cc) pair. The study of such configurations and their weak decays can help to set constraints on models of quark–quark forces [13, 14]. Stong [15] emphasized how the QQq excitation spectra can be used to phenomenologically determine the QQ potential, to complement the approach taken for $Q\bar{Q}$ quarkonium interactions.

Savage and Wise [16] discussed the (ccq) excitation spectrum for the q degree of freedom (with the (cc) in its ground state) via the analogy to the spectrum of $\bar{Q}q$ mesons, where the (cc) pair plays the role of the heavy $\bar{Q}$ antiquark. Fleck and Richard [13] calculated excitation spectra and other properties of (ccq) baryons for a variety of potential and bag models, which describe successfully known hadrons. In contrast to heavy mesons, the descriptions of light quark (qqq) and singly charmed (cqq) baryons are less successful. We need to better understand how the proton and other baryons are built from quarks. The investigation of the (ccq) system should help put constraints on baryon models, including light quark (qqq) and singly charmed (cqq) baryons, since the (ccq) has a quark structure intermediate between (qqq) proton and $\bar{Q}q$ meson structures.

In the double-charm system, there have been many predictions for the masses of the J=1/2 states and the J=3/2 hyperfine excitations [10]. Most results are consistent with expectations of a ground state

mean mass around 3.6 GeV/c^2. The (cc) colour antitriplet diquark has spin S=1. The spin of the third quark is either parallel (J=3/2) or anti-parallel (J=1/2) to the diquark. For (ccq), the J=1/2 states are expected to be lower than the J=3/2 states by around 80 MeV/c^2 [10, 11, 13, 17].

Bjorken [12] and also Fleck and Richard [13] suggest that internal W exchange diagrams in the Ξ_{cc}^+ decay could reduce its lifetime to around 100 fs, roughly half the lifetime of the Λ_c^+. Considering possible constructive interference between the W-exchange and two c-quark decay amplitudes, it is possible that this state should have an even shorter lifetime.

We describe qualitatively the perturbative production mechanism for DCBs. One must produce two c quarks (and associated antiquarks), and they must join to a tightly bound, small size anti-triplet pair. The pair then joins a light quark to produce the final (ccq). The two c-quarks may be produced (initial state) with a range of separations and relative momenta (up to say tens of GeV/c). In the final state, if they are tightly bound in a small size (cc) pair, they should have relative momentum lower than roughly 1 GeV/c. The overlap integral between initial and final states determines the probability for the (cc)-q fusion process. Such cross sections may be smaller by as much as 10^{-2}–10^{-3} compared to single-charm production. Aoki *et al.* [18] reported a low statistics measurement at $\sqrt{s} = 26$ GeV/c^2 for the ratio of double to single open charm pair production, of 10^{-2}. This $D\bar{D}D\bar{D}$ to $D\bar{D}$ cross section ratio was for all central and diffractive events. This high ratio is encouraging for (ccq) searches. Cross section guestimates are given in Ref. [2].

Brodsky and Vogt [19] suggested that there may be significant intrinsic charm (IC) $c\bar{c}$ components in hadron wave functions, and therefore also $cc\bar{c}\bar{c}$ components. The double intrinsic charm component can lead to (ccq) production, as the (cc) pairs pre-exist in the incident hadron. Intrinsic charm (ccq) production, with its expected high X_f distribution, would therefore be especially attractive. When a double charm IC state is freed in a soft collision, the charm quarks should also have approximately the same velocity as the valence quark. Thus, coalescence into a (ccq) state is likely. Cross section guestimates are given in Ref. [2].

The semi-leptonic and non-leptonic branching ratios of (ccq) baryons were estimated by Bjorken [12] in 1986. He uses a statistical approach to assign probabilities to different decay modes. He first considers the most significant particles in a decay, those that carry baryon or strangeness number. Pions are then added according to a Poisson distribution. The Bjorken method and other approaches for charm baryon decay modes are described by Klein [20]. For the Ξ_{cc}^{++}, Bjorken [12] estimated the $\Lambda_c^+\pi^+K^-\pi^+$ final state to have 5% branching ratio; while for the Ξ_{cc}^+, he estimated the $\Lambda_c^+\pi^+K^-$ final state to have 3% branching ratio. One expects [2] that roughly 80% of the (ccq) decays are hadronic, with as many as one-third of these leading to final states with all charged hadrons.

Recently the SELEX experiment at Fermilab has reported the first observation of the doubly charmed baryon Ξ_{cc}^+ in the channel to $\Lambda_c\mathrm{K}^-\pi^+$ [21]. Evidence for other states was found as well. The forward production seems to be strongly enhanced in baryon beams. Effectively, a large fraction of their observed Λ_c are daughters of doubly charm baryons [22]. This requires new mechanisms of charm- or even di-charm generation. Therefore much larger yields of doubly charmed baryons could be expected at the high-rate COMPASS experiment.

2. EXPERIMENTAL SETUP

To measure doubly charmed baryons with the COMPASS spectrometer several modifications have to be made and some detector systems have either to be built from scratch or upgraded. This section outlines the hardware requirements for a DCB measurement.

It is foreseen to run the double charm measurement with a proton beam of 280 GeV (the maximum of the present beamline setup) and an intensity of up to 10^8 during the 5-s SPS spill every 16.8 s.

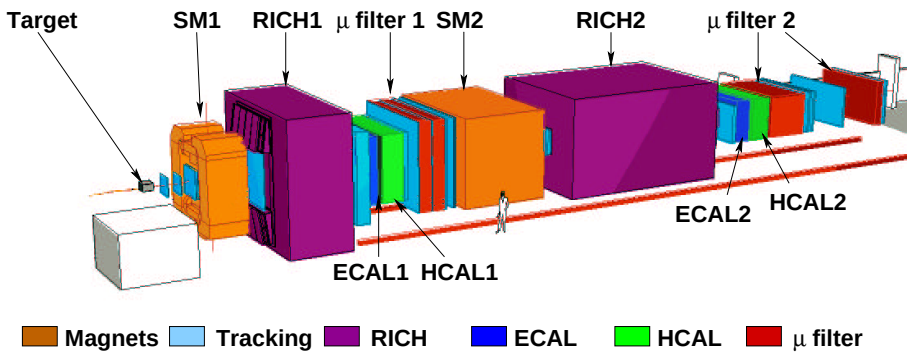

Fig. 1: General setup of the COMPASS spectrometer.

2.1 Spectrometer

COMPASS uses a double magnetic spectrometer with tracking, electromagnetic and hadronic calorimetry and particle identification in each section: the first stage detects low-momentum particles with large angles (± 180 mrad). High-momentum particles are analysed in the second part (± 25 mrad) using a large lever arm and a higher magnetic field than in the first stage. In this way an angular resolution down to 10 μrad (for small scattering angles) and a transverse resolution down to 7 μm can be achieved. A schematic view of the spectrometer is given in Fig. 1. For the double charm setup the gap of the first spectrometer magnet should be reduced from the present 1.72 m to 0.82 m, which is possible by removing some of the modular yoke pieces. This provides a higher field for the higher beam energy and also a smaller stray field in the tracking zones.

The tracking system is built up from a set of **L**arge **A**ngle **T**rackers (**LAT**) covering the outer region with lowest track density and **S**mall **A**ngle **T**rackers (**SAT**) for the inner regions. So-called *tracking stations* are distributed all over the spectrometer and consist of three different detector types staggered, each smaller one having finer granularity and rate capability and covering with some overlap a central hole in the next larger one. For the innermost part, directly in the beam, silicon detectors [23] and scintillating fibres are used. The LAT are small cell size drift chambers, straw chambers [24] and further downstream MWPC and large cell size drift chambers. The very important inner trackers between the beam region and the LAT consist of Micromegas [25] before the first magnet and GEM detectors [26] after that.

The compatibility of the tracking system with the high-intensity hadron beam, however, still has to be proven. In particular the inner trackers may run at a higher risk of discharges, which could make a partial revision of the setup necessary.

Particle identification is first of all given by RICH 1. A second RICH is currently under planning and should be able to cover the high momentum part of the spectrum passing through the second magnet. It is foreseen to have a fast readout which could make particle identification at the second trigger level possible. In addition two upgraded Cherenkov counters of CEDAR type will provide particle identification in the beamline to be able to obtain clean cross section measurements.

Further downstream electromagnetic and hadronic calorimeters provide the energy measurement needed to form a first level trigger based on transverse energy. Thereafter two muon filters allow muons from semi-leptonic charm decays to be identified. In addition to the existing muon walls the first muon filter has to be augmented by a muon hodoscope for triggering. Only a small fraction of muons from semi-leptonic decays would reach the present muon hodoscopes put far downstream for DIS measurements.

2.2 Target setup

The target setup as described in the present simulation is shown in Fig. 2. Beam definition is provided as in the present setup by scintillating fibres and silicon microstrips. The beam impinges on a segmented target of in total 2% of a nuclear interaction length. It is foreseen to use different materials for the thin target plates to study the A-dependence of charm production. The segmentation allows charm hadrons to decay mostly outside the target material to allow a cleaner vertex separation.

After the target a silicon microstrip telescope is needed to allow precise vertex determination. A clear separation of primary production vertex and secondary decay vertex is the cleanest signature for a weak charm decay. As a minimum setup, 16 microstrip planes arranged in four projections are foreseen. Depending on resolution, acceptance and possible stray fields a fifth station might be needed. A further consideration is the possibility to fully reconstruct semi-leptonic decays by using a densely packed decay detector right after the target as shown in Fig. 3. In the order of 16 planes are spaced within 2 cm along the beam and have a pitch of 10–15 μm. This setup would allow one to see a fraction of charm tracks (mostly D-mesons) still in the detector before their decay. Both resolution and the benefit of a charm decay detector still have to be studied carefully in simulations.

After the target a scintillating fibre detector will be used to obtain the track multiplicity at the trigger level and provide precise timing for all vertex tracks.

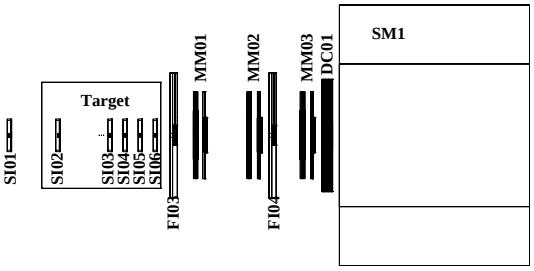

Fig. 2: Target region as used in the simulation.

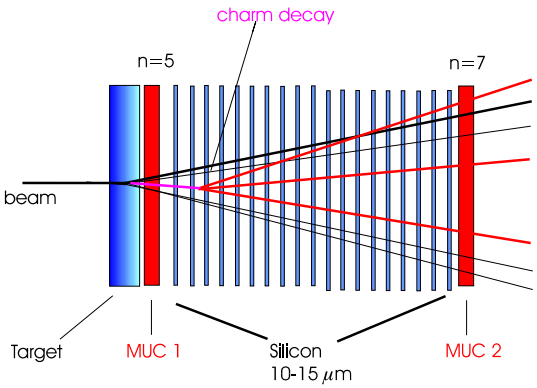

Fig. 3: Charm decay detector. 16–20 planes are spaced by 2 mm and have a pitch of 10–15 μm.

In COMPASS no precision vertex detector is present yet. The design of this detector has to fulfil a number of strict requirements:

- The detector has to stand fluences up to 5×10^{14} particles/cm^2.
- The spatial resolution in beam direction should be better than 100 μm to provide sufficient resolving power for charm decay vertices.
- Finally, at the very high particle rates foreseen, a good timing resolution is needed to recognize interaction pileup and disentangle multiple beam tracks.

It is foreseen to make use of the Lazarus effect [27] by operating silicon detectors at cryogenic temperatures so that they can survive larger fluences.

During the process of detector optimization we have to investigate the design of a monolithic target-vertex-cryostat, determine the best pitch size, and determine the effects of a larger lever arm vs. acceptance and mechanical design.

Finally the readout has to run at a speed of up to 100 kHz. ADCs are needed to obtain better space resolution, a good timing of the signal, and discrimination of secondary interactions.

3. TRIGGER SCENARIO

One of the most important problems to solve is to reduce the vast number of inelastic interactions to the interesting ones showing signatures for charm hadron decays. This is discussed in this section.

The starting point are 2×10^6 interactions per SPS spill. The first-level trigger has to reduce this to a rate of not more than 100 kHz, i.e. by at least a factor 4. Owing to the constraints of the readout system of existing detectors per event, 1 μs is available for the trigger decision at this level.

Three types of triggers can be envisaged at this trigger level, of which a combination should be able to reach the desired rejection level at a reasonable efficiency:

- Requiring simple charged track multiplicities bigger than 4 is a safe cut, in particular when searching for double charm. This removes a large part of the diffractive inelastic reactions and all elastic ones.
- A large transverse energy detectable by the calorimeters can indicate charm decays.
- A rather high fraction (up to 17%) of D-mesons decay semi-leptonically, mostly producing a muon. This can be selected by the muon filters of the spectrometer.

These trigger types shall be discussed in the following.

The rate coming from the first level trigger is still far too high to be written to mass storage. Therefore a second and/or third trigger level is required. The features exploited at these further levels are described below:

- Hit multiplicity, suppression of secondary interactions and a possible multiplicity jump in the vertex detector can already be performed in an intelligent detector frontend.
- Track prototypes can be formed within a super ROB, a particularly powerful readout buffer computer which reads the entire vertex detector. With these track angles, track multiplicity and possibly high track impacts can be investigated.
- Vertex reconstruction needs the power of a third-level trigger farm with many CPUs or high power co-processor cards for the super ROB. Here vertices can be searched, and separated production and decay vertices can be identified.
- Finally, particle identification can be performed from the information of the RICH detectors, and secondary vertices of hyperons and strange mesons can be tagged.

The final rate should be in the order of 10–20 000 triggers per spill.

3.1 Transverse energy

The high charm quark mass of around 1.5 GeV opens up a large number of decay channels. At the same time the Q value of the decay is large and therefore also the transverse momenta of the decay products. Enriching events with high p_T tracks will therefore also enhance charm decays. Experiments E791 and E831 already used this type of cut successfully. Typical values are 3–5 GeV reducing the number of triggers by a factor of 3–5 at efficiencies between 70 and 55%. The simulation of doubly charmed baryons shows an even higher transverse energy due to the two charm quarks and rather long decay chains. Figures 4 and 5 illustrate this trigger.

3.2 Multiplicities and muon trigger

Owing to the large Q value of the double charm decay and the long decay chains, the charged track multiplicity is very high. For example, looking at the decay $\Xi_{cc}^{+} \rightarrow \Lambda_c \mathrm{K}^{-}\pi^{+}$ with some associated D mesons, basically no events with less than 10 charged tracks are seen. A simple cut of at least four tracks would already cut down the events by half with 100% charm efficiency. Higher reduction factors at still very high double charm efficiencies can be reached. Technically this trigger would be implemented by means of a fast scintillating fibre detector at the end of the vertex region. Multiplicities of double-charm events and minimum-bias events are compared in Figs. 6 a) and b).

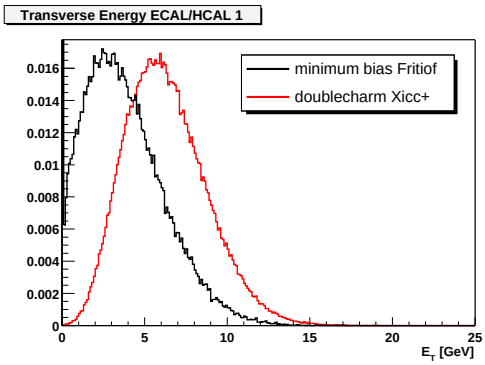

Fig. 4: Distribution of transverse energy of minimum-bias events and double charm events.

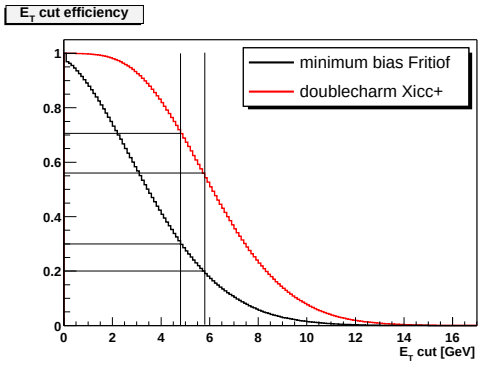

Fig. 5: E_T-cut efficiency. Shown are curves for minimum-bias and double charm. Intersections for a background reduction to 20% and 30% are drawn.

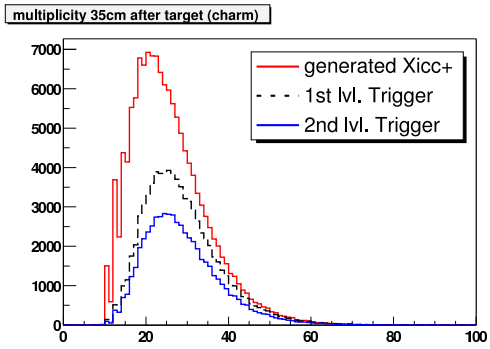

a) Multiplicities from double charm

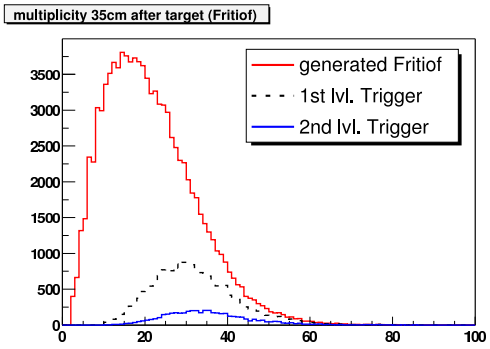

b) Multiplicities from minimum-bias

Fig. 6: Multiplicities for all generated events, events passing a first-level trigger consisting of a multiplicity cut plus a minimum transverse energy and events requiring a reconstructible secondary vertex are compared.

Another clean signature is the production of muons in semi-leptonic decays of charm mesons. The branching ratios are

$$BR(D^0 \to \mu X) = 7\% \,, \quad \text{and} \quad BR(D^+ \to \mu X) = 10\%$$

whereas background from pion and kaon decays is small due to their much longer lifetimes compared to the charm mesons. Therefore a reduction factor of 30 from σ_{tot} can be reached at an efficiency which is basically equivalent to the semi-leptonic branching ratio. In addition, background can be further reduced by requiring a minimum transverse momentum of the muon.

3.3 Online filter

Coming to an acceptable data rate requires online filtering of the events. In the present COMPASS DAQ system with its 12 (to max. 16) eventbuilder computers (with 2 processors each) there is little room for complicated tasks, since at 40 kHz only 2–3 ms are available to process one event. Therefore other, additional or alternative ways of filtering and data processing have to be implemented. The various possible options will be briefly discussed here.

A very resource-efficient first approach is to improve the frontend electronics of detectors relevant to further trigger decisions with more processing power by means of fast Field Programmable Gate Array (FPGA) chips. This allows the preprocessing of data at an early stage saving CPU power on the actual filtering stage for mostly physics-oriented data treatment. Possible tasks for frontend preprocessing are:

- correlation and cut on the signal time,
- data reduction by forming clusters from adjacent channels including time cuts and amplitude weighting,
- determination of hit multiplicities,
- rejection of secondary interactions by means of a second threshold for too large signals.

As a second-level trigger a special readout buffer computer (Super-ROB) could be developed for the vertex detector. A large part of physically relevant data arrives at this single computer and equipping it with extra CPU power (4–8 CPUs) and, in addition, with powerful DSP or FPGA co-processor cards can yield a high selectivity based on simple criteria. It is mainly the forming of track prototypes that can be performed here from which selections on

- track multiplicities,
- track angles (partly correlated to transverse momenta),
- a preliminary interaction vertex and
- high track impact parameters

can be derived easily. This can be nicely embedded in the COMPASS DAQ system by also making this special machine the event distribution manager which directs the data flow from ROB computers to eventbuilders (Fig. 7). A large fraction of events would be simply flagged by the EDM after processing on the Super ROB to be discarded on all other ROBs.

The final filtering of events can be done in a dedicated filter farm consisting of densely packed CPUs, either as flat rack servers or better server blades with CPUs with low power consumption in racks with high integration and built-in network, power and cooling infrastructure. These systems can attack complicated filtering tasks like

- secondary vertex reconstruction,
- tagging of daughter decays (hyperons, K^0_s, D mesons),
- reconstruction of RICH rings.

In a system with 300–600 CPUs processing time of up to 25–50 ms per event is available.

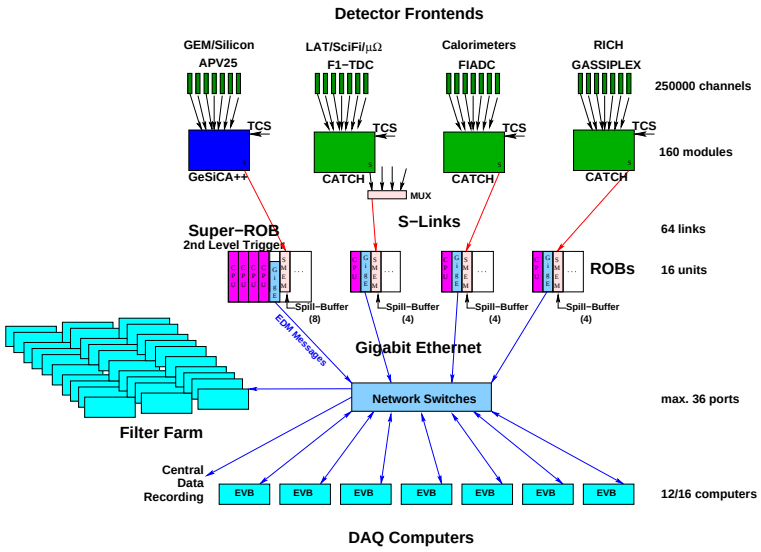

Fig. 7: Improved DAQ system for the second phase of COMPASS.

An alternative approach can be the implementation of a more homogeneous system of networked compute nodes which in a first layer address directly buffered detector data and then pass on data to

further levels [28]. This approach in its full reach can even accomplish a readout system without dedicated hardware trigger signals that samples data at a constant frequency and performs data reduction, feature extraction and filtering in parallel as the data is transported and combined. This, however, also puts strong requirements on the frontends which actively have to perform hit-detection and data reduction before transferring any data. Although this might not be fully realizable in COMPASS, the compute node network can be a cost-effective alternative to an expensive CPU farm.

4. SIMULATIONS

In preparation for the COMPASS Future Workshop in September 2002 a number of simulation studies were performed. Their results are summarized here. Further studies to address a number of open questions are under way.

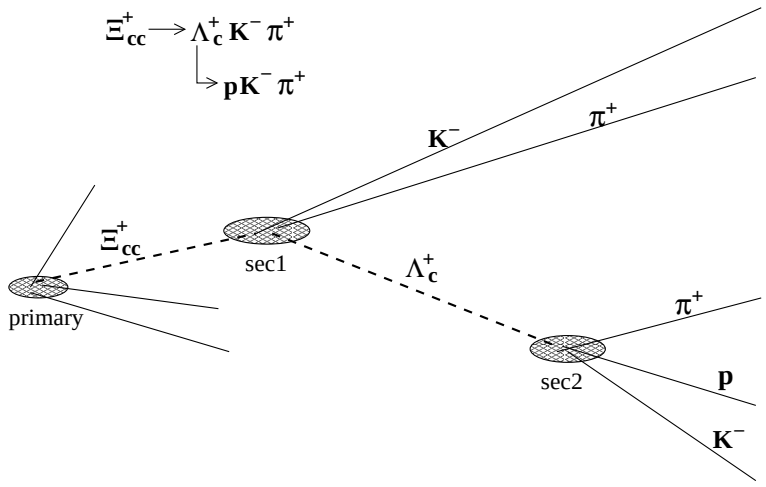

Fig. 8: Schematic decay chain of the Ξ_{cc}^{+} in the SELEX channel.

The first set of simulations of doubly charmed baryons in COMPASS was based on the decay channel $\Xi_{cc}^{+} \rightarrow \Lambda_c \mathrm{K}^{-}\pi^{+}$ (Fig. 8) observed by SELEX at FNAL [21]. Together with the baryon two anti-D- mesons are generated. The production parameters are assumed to follow

$$\sigma \sim (1 - x_F)^3$$
$$\sigma \sim \exp(-1.2 p_T^2) \ .$$

The remaining energy is given to the Fritiof event generator to add further light hadrons.

For the detector simulation COMGEANT, a Monte Carlo program based on GEANT 3.14 is used. The detector geometry used here is from the first spectrometer magnet SM1 onwards identical to the present DIS setup. The target area before this magnet was already shown in Fig. 2 but there is further room for optimization. Currently only fieldmaps for magnet gaps of 1.72 m and 1.32 m are available. However, a more favourable gap of 82 cm should be studied in the near future.

The following assumptions and cuts are implied in this simulation study.

- The doubly charmed baryon was simulated with a lifetime of 25 fs corresponding to a value as favoured by the SELEX observations.
- The main cuts in GEANT were set to 100 MeV for faster processing.
- There was no detailed simulation of the RICH, only momentum thresholds for the various particles were applied. Positive identification of all kaons and protons was required.

- Any secondary charm vertex was required to be outside the target material to be reconstructible.

The following sections illustrate the results of these simulations.

4.1 Acceptance and resolution

The overall geometrical acceptance and tracking capability of the simulated setup was found to be 5%. Detector efficiencies were not yet applied, but the present reconstruction program CORAL was used.

The mass resolution for the reconstructed Λ_c was found to be 8 MeV whereas the resolution of Ξ_{cc} turned out to be 13 MeV as shown in Fig. 9.

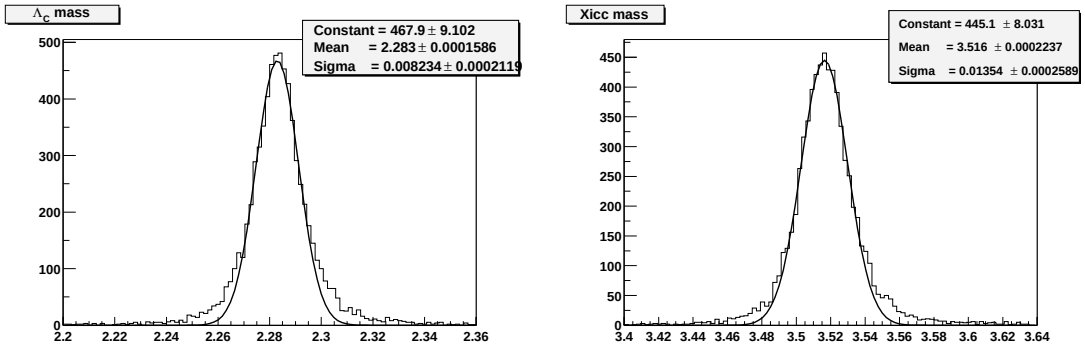

a) $\sigma(\Lambda_c) = 8$ MeV

b) $\sigma(\Xi_{cc}) = 13$ MeV

Fig. 9: Mass resolutions of Λ_c and $\Xi_c c$ after reconstruction.

4.2 Momenta and track efficiencies

Figure 10 summarizes the distribution of momenta of the various particles simulated in the Ξ_{cc} events. It is notable that only very few particles reach momenta above 40 GeV/c. This underlines the importance of the first spectrometer magnet. Presently a relatively poor average momentum resolution of 2% in this region is found, indicating that a reduced gap of SM1 leading to a higher field would be beneficial. Figure 11 shows that for particles above 5 GeV/c a reasonable tracking efficiency above 80% can be reached with the present setup.

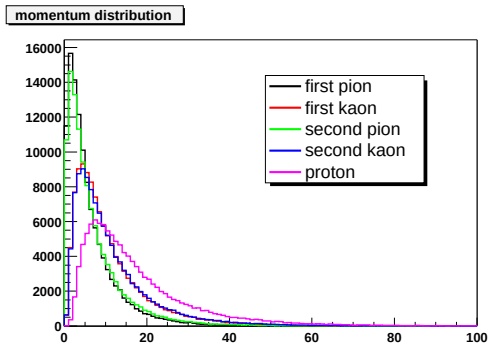

Fig. 10: Distribution of momenta of particles arising form the Ξ_{cc} decay.

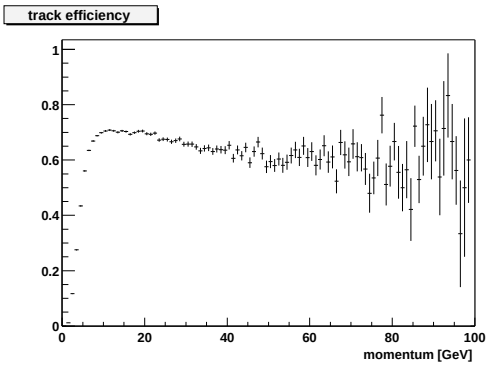

Fig. 11: Tracking efficiency vs. momentum for the present setup.

4.3 Trigger efficiencies

Finally, it was also possible to derive estimates for trigger efficiencies from the simulations in a simplified way. Note, however, that in the following exclusive double charm events are only compared to events generated by Fritiof as a kind of minimum-bias hadronic background. A large part of the total cross section constituted by elastic and diffractive scattering events are not treated here. They should be strongly suppressed by a hard multiplicity cut.

Trigger type	**Ratio Charm/Fritiof**
Muon trigger ($p(\mu) > 2$ GeV/c)	29.5% / 11.7%
Multiplicity trigger	100% / 85%
(more than 10 charged tracks)	
1st level trigger	57.7% / 20 %
(*Multiplicity* $\wedge$ $((E_T > 5.8$ GeV$) \vee (E_T > 3$ GeV $\wedge \mu))$)	
2nd level trigger	41.5% / 4.6%
(some vertex activity)	

These values show that in comparison to the relatively hard spectrum of products from Fritiof, the discussed trigger scenario would work, i.e. provide a sufficient reduction at the first trigger level and good selectivity at the second.

In addition Fig. 12 shows the absolute x_F-acceptance of reconstruction and triggers and Fig. 13 the efficiency distribution normalized to all generated events. Here also the effect of RICH cuts was included. These cuts are based simply on acceptance and momentum cuts according to the operating thresholds of the employed RICH detectors. It turns out that the second RICH detector does not contribute a lot, mostly due to the fact that the fraction of tracks with momenta above 40 GeV/c is rather low. Nevertheless, the high-momentum part is of particular interest for the highly forward produced subsample which is of biggest relevance in the comparison with the SELEX results. In any case RICH cuts in the end would clean up the data substantially and reduce ambiguous interpretations.

The figures show as well that a reasonable reconstruction efficiency is reached already at $x_F > -0.1$.

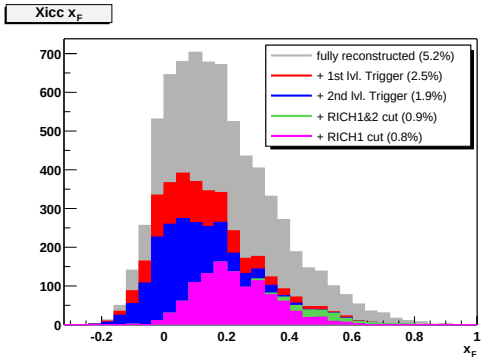

Fig. 12: Accepted events vs. x_F for the various steps in the triggering process. In addition the effect of RICH cuts based on simple acceptance and momentum thresholds are shown.

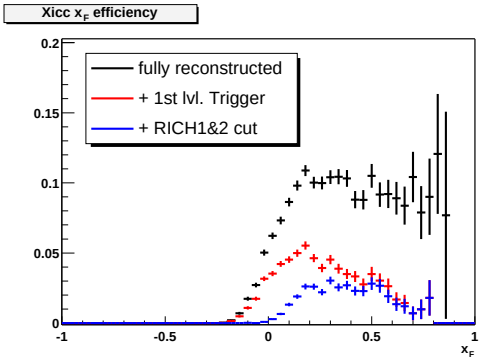

Fig. 13: Reconstruction and trigger efficiencies normalized to all simulated events.

5. RATE ESTIMATES

Rate estimates can be obtained from the conducted simulations. Further input are the nominal beam rate of up to 10^8 protons per spill and the assumed target with a thickness of 2% of an interaction length.

This leads to a total of 10^{12} interactions in a run of 100 effective days which corresponds to an integrated luminosity of $\int \mathcal{L} = 25$ pb^{-1}, based on a total cross section of 40 mb per nucleon.

The SELEX observations [22, 29] point to an unexpectedly large fraction of double charm production: From roughly 1600 reconstructed Λ_c they obtain about 50 doubly charmed baryons. If one then takes into account all cuts and branching ratios of the observed channels one comes to the conclusion that about half of all Λ_c in fact come from doubly charmed baryons. Assuming therefore a double charm production cross section in the order of the singly charmed baryon production cross section of about 2 μb (cf. results from WA89 [30] at a similar energy to COMPASS), this would mean for COMPASS that 50 million doubly charmed baryons would be produced.

Taking into account now the results of the simulation (acceptance $\times$ reconstruction $\times$ trigger $\times$ RICH = 0.8% as from Fig. 12) and estimates for branching ratios ($BR(CCQ) \times BR(CQQ) = 30\% \times 20\% = 6\%$) and assuming an additional factor for the overall detection and vertexing efficiency of 40 to 70%, one arrives at 10 000 to 17 000 reconstructed doubly charmed baryons. Here $BR(CCQ)$ already includes an estimated sum of all measurable CCQ channels, not only the simulated channel $\Xi_{cc}^{+} \to \Lambda_c \mathrm{K}^{-}\pi^{+}$, and $BR(CQQ)$ denotes the fraction of reconstructible daughter baryon decays. This result is quite remarkable aside from the simple numbers in the sense that this would bring the highly interesting field of CCQ spectroscopy into reach.

But even a more conservative cross section estimate along the lines of $\sigma(CCQ) \sim \sigma_{tot} \times (10^{-3})^2$, i.e. a factor 10^{-3} down from charm production giving in the order of 10 nb would still correspond to 250 000 produced or 100 to 170 reconstructed doubly charmed baryons. This number nevertheless would constitute a solid observation.

6. CONCLUSIONS

In this report the hardware requirements for the measurement of doubly charmed baryons in COMPASS were outlined and the results of first simulations were presented. It was shown that sufficient suppression factors for the first trigger level could be reached by a combination of multiplicity and transverse energy cuts enhanced by identifying muons from semi-leptonic decays. Based on these results, rate estimates for a COMPASS measurement were obtained. With the exciting SELEX observations in view, doubly charmed baryons could be produced so abundantly that CCQ-spectroscopy would be in reach for COMPASS.

Simultaneously to the search for doubly charmed baryons valuable high-statistics data on singly charmed baryons can be obtained. Here one has to choose between a single charm measurement with double charm as bonus or a strict orientation of setup and triggers toward double charm. This choice is essentially determined by data rates and the desired selectivity.

However, there is still a lot of work to be done. An optimized setup has to be found for the vertex detector, the spectrometer layout and the trigger detectors. In particular there is substantial design work needed for the vertex detector. Further simulation studies of trigger efficiencies and reduction factors are needed. It would be interesting to obtain a better handle on the rejection of minimum-bias events from real hadron beam data. Then the best filter algorithm has to be found and coded. Further question marks lie in lifetimes, cross sections and production mechanisms of doubly charmed baryons.

References

[1] The COMPASS Collaboration, COMPASS proposal, CERN /SPSLC 96-14, SPSC/P297 (Geneva, March 1996); CERN/SPSLC 96-30 (Geneva, May 1996),
WWW: `http://wwwcompass.cern.ch/` .

[2] M. A. Moinester, *How to Search for Doubly Charmed Baryons and Tetraquarks*, Z. Phys. A **355** (1996) 349 and references therein;
http://link.springer.de/link/service/journals/00218/bibs/6355004/63550349.htm .

[3] V.V.Kiselev, A.K.Likhoded, O.N.Pakhomova and V.A.Saleev Phys. Rev. D **66** (2002) 034030; V. V. Kiselev and A. K. Likhoded, hep-ph/0103169;
A. V. Berezhnoi, V. V. Kiselev, A. K. Likhoded and A. I. Onishchenko, Phys. Rev. D **57** (1998) 4385; V. V. Kiselev and A. K. Likhoded, hep-ph/0208231; V. V. Kiselev, A. K. Likhoded and A I. Onishchenko, Phys. Rev. D **60** (1999) 014007;
S. S. Gershtein, V. V. Kiselev, A. K. Likhoded and A. I. Onishchenko, Phys. Rev. D **62** (2000) 054021; Heavy Ion Phys. **9** (1999) 133; Phys. Atom. Nucl. **63** (2000) 274; hep-ph/9811212; Mod. Phys. Lett. A **14** (1999) 135.

[4] D. Ebert, R. N. Faustov, V. O. Galkin and A. P. Martynenko, Phys. Rev. D **66** (2002) 014008.

[5] D. A. Gunter and V. A. Saleev, Phys. Rev. D **64** (2001) 034006; Phys. Atom. Nucl. **65** (2002) 299.

[6] A. I. Onishchenko, hep-ph/0006295, hep-ph/0006271; A. K. Likhoded and A. I. Onishchenko, hep-ph/9912425.

[7] B. Guberina, B. Melic and H. Stefancic, Eur. Phys. J. C **9** (1999) 213; Eur. Phys. J. C **13** (2000) 551, hep-ph/9911241.

[8] D. A. Gunter and V. A. Saleev, Phys. Rev. D **64** (2001) 034006.

[9] C. Itoh, T. Minamikawa, K. Miura and T. Watanabe, Phys. Rev. D **61** (2000) 057502.

[10] K. Anikeev *et al.*, B Physics at the Tevatron, hep-ph/0201071, see pp 499–508 and references 111–124.

[11] I. M. Narodetskii and M. A. Trusov, Phys. Atom. Nucl. **65** (2002) 917, hep-ph/0209044, hep-ph/0204320.

[12] J. D. Bjorken, FERMILAB-CONF-85/69, *Is the ccc a New Deal for Baryon Spectroscopy?*, Int. Conf. on Hadron Spectroscopy, College Park, MD, Apr. 1985;
Unpublished Draft, *Estimates of Decay Branching Ratios for Hadrons Containing Charm and Bottom Quarks*, July 22, 1986;
Unpublished Draft, *Masses of Charm and Strange Baryons*, Aug. 13, 1986.

[13] S. Fleck and J. M. Richard, Prog. Theor. Phys. **82** (1989) 760; J. M. Richard, Nucl. Phys. Proc. Suppl. **50** (1996) 147; J. M. Richard, Nucl. Phys. A **689** (2001) 235.

[14] J. L. Rosner, Comments in Nucl. Part. Phys. **21** (1995) 369, hep-ph/9501291.

[15] M. L. Stong, hep-ph/9505217; M. A. Doncheski *et al.*, Phys. Rev. D **53** (1996) 1247.

[16] M. J. Savage, M. B. Wise, Phys. Lett. B **248** (1990) 177.

[17] D. B. Lichtenberg, R. Roncaglia and E. Predazzi, Phys. Rev. D **53** (1996) 6678; D. B. Lichtenberg and R. Roncaglia, Phys. Lett. B **358** (1995) 106.

[18] S. Aoki *et al.*, CERN WA75 collaboration, Phys. Lett. B **187** (1987) 185.

[19] R. Vogt and S.J. Brodsky, Nucl. Phys. B **478** (1996) 311; Phys. Lett. B **349** (1995) 569.

[20] S. R. Klein, Int. Jour. Mod. Phys. A **5** (1990) 1457.

[21] M. Mattson *et al.*, [SELEX Collaboration], *First Observation of the Doubly Charmed Baryon* Ξ_{cc}^{+}, Phys. Rev. Lett. **89** (2002) 112001.

[22] J. S. Russ *et al.*, [SELEX Collaboration], *First Observation of a Family of Double Charm Baryons*, Proceedings of 31st International Conference on High Energy Physics (ICHEP 2002), Amsterdam, The Netherlands, July 2002, hep-ex/0209075;
M. Moinester *et al.*, [SELEX Collaboration], *First Observation of Doubly Charmed Baryons*, Proceedings of "Symmetries and Spin" workshop, Prague, July 2002, hep-ex/0212029.

[23] H. Angerer *et al.*, *Present Status Of Silicon Detectors in COMPASS*, Proceedings of the 9th European Symposium on Semiconductor Detectors, Schloss Elmau, June 23–27, 2002, to appear in Nucl. Instr. and Meth. in Phys. Res. A.

[24] V. N. Bychkov *et al.*, *Construction and Manufacture of Large Size Straw-Chambers of the COMPASS Spectrometer Tracking System*, Particles and Nuclei Letters, **2** (111) June 2002.

[25] Y. Giomataris *et al.*, Nucl. Instrum. Meth. A **376** (1996) 29; Y. Giomataris, *Development of fast gaseous detector "Micromegas"*, DAPNIA-98-01, presentation at WCC'98, Vienna, Nucl. Instrum. Meth. A **419** (1998) 239–250.

[26] F. Sauli *et al.*, Nucl. Instrum. Meth. A **386** (1997) 531; F. Sauli, *Gas detectors: Recent developments and future perspectives*, CERN-EP/98-51, invited opening presentation at WCC'98, Vienna, Nucl. Instrum. Meth. A **419** (1998) 189–201.

[27] RD39 Collaboration, *Charge Collection Efficiency of Irradiated Silicon Detectors Operated at Cryogenic Temperatures*, Nucl. Instr. and Meth. in Phys. Res. A **440** (2000) 5–16.
G. Ruggiero *et al.*, *Silicon detectors irradiated in situ at cryogenic temperatures*, Nucl. Instr. and Meth. in Phys. Res. A **476** (2002) 583–587.

[28] L. Schmitt *et al.*, *S-DAQ - A High Rate Sampling Data Acquisition System*, COMPASS Note 2002-13, CERN, December 2002,
WWW: `http://wwwcompass.cern.ch/compass/notes/2002-13/2002-13.pdf` .

[29] P. Cooper, *Double Charmed Baryons in SELEX*, these proceedings, and Future Physics at COMPASS, CERN Workshop, Sept. 2002, http://compass-cw2002.web.cern.ch/compass-cw2002/programme.htm .

[30] M. I. Adamovich *et al.* (WA89 Collaboration), *Determination of the total c anti-c production cross section in 340 GeV/c Sigma- nucleus interactions*, Eur. Phys. J. C **13** (2000) 247.

RECENT CALCULATIONS IN CHIRAL PERTURBATION THEORY

J. Gasser
Institute for Theoretical Physics, University of Bern, Sidlerstr. 5, CH-3012 Bern, Switzerland
e-mail:gasser@itp.unibe.ch

Abstract
There are several processes that can be measured at COMPASS and that are of relevance for chiral perturbation theory. I discuss, in particular, pion polarizabilities and photon–meson transition amplitudes. In addition, I point out that more precise experimental information on the $I = 2$ S-wave phase shift in elastic $\pi\pi$ scattering would be very welcome.

1. INTRODUCTION

At low energies, it is useful to replace QCD by an effective quantum field theory that has the same physical content as QCD but is formulated in terms of asymptotically observable fields. This method to calculate physical observables in QCD is called chiral perturbation theory (ChPT) [1, 2, 3].

At COMPASS, one can test several ChPT predictions. This concerns in particular the electric and magnetic polarizabilities of the charged pions and kaons, and photon–meson transition amplitudes like γ + meson $\to$ meson + meson. The relation of the latter process to the chiral anomaly makes it particularly attractive. Furthermore, in case that COMPASS can provide precise data on low-energy S-wave phase shifts in elastic $\pi\pi$ scattering, or information on $\pi K \to \pi K$, one should not miss the opportunity to measure these processes.

In the following, I concentrate on

$$\begin{aligned} \pi X &\to \pi\gamma X' \\ K X &\to K\gamma X' \\ \pi X &\to \pi\pi X', K\bar{K}X' \\ K X &\to K\pi X' \\ K X &\to K X\,. \end{aligned}$$

These processes are generated in the COMPASS experiment through the Primakoff reaction or through one-pion exchange. I shall not discuss

$$K_{l3}, K_{l4}, K \to 2\pi, 3\pi, \ldots\,,$$

because these are (will be) investigated, for example, at NA48.

2. CHIRAL PERTURBATION THEORY

Chiral perturbation theory [1, 2, 3] has been developed over the last two decades into a method that allows one to calculate several hadronic quantities with high precision. The method can be summarized as follows. One replaces the original Lagrangian of QCD by a Lagrangian that contains the asymptotically observable fields like pions, kaons, etas, ...,

$$\begin{array}{ll} \mathcal{L}_{QCD} & \to \quad \mathcal{L}_{eff} \\ \text{quarks, gluons} & \qquad \pi, K, \eta, p, n, ... \end{array} \tag{1}$$

$$\mathcal{L}_{eff} = \mathcal{L}_2 + \mathcal{L}_4 + \mathcal{L}_6 + \cdots\,. \tag{2}$$

Here, $\mathcal{L}_n$ generates terms of order (external momentum)^n in the low-energy expansion of S-matrix elements.

Comments on this construction:

- chiral symmetry determines the structure of $\mathcal{L}_n$
- the low-energy coupling constants (LECs) in $\mathcal{L}_n$ must be determined from experiment or lattice calculations, they are in general not determined by chiral symmetry alone
- for appropriately chosen LECs, the effective theory reproduces the S-matrix elements of QCD at low energies [4]

I illustrate the method with the $I = 0$ S-wave scattering length of elastic $\pi\pi$ scattering. The result of the χ calculation is

$$a_0^0 \quad = \quad \frac{7x}{32\pi}\left[1 + c_1 x + c_2 x^2 + O(x^3)\right] \tag{3}$$

where

$$x \quad = \quad M_\pi^2/F_\pi^2 \; ; \; c_{1,2} = \text{numbers + } \chi\text{logs + LECs}\,,$$

and where $F_\pi = 92.4$ MeV is the pion decay constant. The symbol χlogs stands for non-analytic terms in the chiral expansion, of the form $\log M_\pi^2$, and powers thereof. A similar expression holds for the $I = 2$ S-wave scattering length a_0^2. The leading terms in the scattering length expansion were determined by Weinberg [5] in 1966, whereas the coefficients c_1 and c_2 and the analogous ones for a_0^2 have been worked out algebraically at a later stage [6, 7]. Recently, the relevant LECs have been determined numerically, such that [8]

$$a_0^0 - a_0^2 = 0.265 \pm 0.004\,. \tag{4}$$

Note that the uncertainty is less than two per cent in this case. Once $a_0^0 - a_0^2$ is known, one can predict the lifetime of the ground state of the $\pi^+\pi^-$ atom [9],

$$\tau = (2.9 \pm 0.1) \times 10^{-15}\text{s}\,. \tag{5}$$

Needless to say, we anxiously await the result of the lifetime measurement at DIRAC [10].

This is obviously not the place to review ChPT. I refer the interested reader to one of the many reviews available, for example, one may search at *arXiv:hep-ph* with *find title chiral perturbation theory*.

3. PHOTON-INDUCED REACTIONS

3.1 Pion polarizabilities

We consider Compton scattering

$$\gamma\pi^\pm \to \gamma\pi^\pm$$

and expand the amplitude in powers of photon momenta. The quadratic terms contain the polarizabilities $\bar{\alpha}_\pi, \bar{\beta}_\pi$. I refer the reader to Bürgi's article [11] for further notation. Here, I note that

a) The Compton amplitude and hence the polarizabilities are known to one [12] and two loops [11] in the chiral expansion.

b) Once the Compton amplitude is known, the polarizabilities may be expanded in powers of the pion mass – the structure of this expansion is very similar to the expansion (3) for the scattering length,

$$\bar{\alpha}_\pi \pm \bar{\beta}_\pi = \frac{\alpha}{16\pi^2 M_\pi F_\pi^2} \left\{ a_\pm + b_\pm x + O(x^2) \right\} , \tag{6}$$

where $\alpha = 1/137.036$ is the fine structure constant of QED. The quantities $a_\pm$ and $b_\pm$ denote the one- and two-loop contributions, respectively [the tree contributions vanish]. The coefficients $a_\pm, b_\pm$ again contain pure numbers, χlogs and LECs. At one loop, the sum of the polarizabilities vanishes, whereas the difference is given by a particular combination $\bar{l}_6 - \bar{l}_5$ of two LECs from the effective Lagrangian $\mathcal{L}_4$ [11, 13],

$$a_+ = 0 \, , \; a_- = \frac{2}{3} (\bar{l}_6 - \bar{l}_5) \, . \tag{7}$$

At two-loop order, both the sum and the difference receive a non-vanishing contribution $b_\pm \neq 0$. *Chiral symmetry does not, therefore, predict that* $\bar{\alpha}_\pi + \bar{\beta}_\pi = 0$. For an explicit expression of $b_\pm$ in terms of χlogs and LECs, I refer the reader to Ref. [11].

c) The two-loop coefficients $b_\pm$ contain LECs from $\mathcal{L}_6$. They had been estimated in Ref. [11] by use of resonance saturation. Bürgi's final result is

$$\begin{aligned} \bar{\alpha}_\pi + \bar{\beta}_\pi &= (0.3 \pm 0.1) \times 10^{-4} \, \mathrm{fm}^3 \, , \\ \bar{\alpha}_\pi - \bar{\beta}_\pi &= (4.4 \pm 1.0) \times 10^{-4} \, \mathrm{fm}^3 \, . \end{aligned} \tag{8}$$

The uncertainties stem from the uncertainties in the low-energy constants and do not contain estimates of the higher order terms (three loops and beyond).

d) The knowledge of LECs has improved over the last years, e.g., the structure of $\mathcal{L}_6$ is now known [14], and some of the low-energy constants at order p^4 have been reevaluated [15, 16, 17]. To illustrate the effect on (8), I consider the one-loop contribution (7). The combination $\bar{l}_6 - \bar{l}_5$ can be determined from the decay $\pi \to e\nu\gamma$. Its value depends on the data, and on the accuracy to which the chiral expansion is carried out. Here I compare the values used in Ref. [11] with the more recent determination by Bijnens and Talavera [15],

$$\bar{l}_6 - \bar{l}_5 = \begin{cases} 2.7 \pm 0.4 & [11] \\ 3.0 \pm 0.3 & [15] \end{cases} . \tag{9}$$

Evaluating $\bar{\alpha}_\pi - \bar{\beta}_\pi$ at one-loop order with the two central values displayed in Eq. (9) generates a difference of 0.6×10^{-4} fm^3. Furthermore, the constants $\bar{l}_{5,6}$ also enter the coefficients $b_\pm$ at two-loop order, which in addition contain $\bar{l}_{1,2,3,4}$ from $\mathcal{L}_4$. These observations make it evident that an update of (8) is needed before firm conclusions from a comparison with new data from the COMPASS experiment can be drawn [18].

3.2 Kaon polarizabilities

Kaon polarizabilities have been worked out to one loop in Ref. [19]. I am not aware of a calculation at two-loop order. Since the chiral expansion now also contains an expansion in powers of the strange quark mass, the predictions will be less precise. However, it is clear that one should perform such an analysis in view of the fact that the kaon polarizabilities will be measured at COMPASS [20].

The motivations for measuring the meson polarizabilities are for example

i) Polarizabilities start being nonzero at one-loop order–one explores chiral loop effects directly.

ii) In general, a comparison of the data with the chiral expansion is of similar interest as the $\pi\pi$ scattering lengths.

3.3 Kaon electromagnetic form factor

If COMPASS can measure kaon electromagnetic form factors [21] to larger values of $|q^2|$ than exist at present and more precisely, this will probably be useful also in constraining the theory for V_{us} via K_{l3} decays [22].

4. THE ANOMALY

The word *anomaly* refers to anomalous Ward identities for the Green functions of quark currents.

4.1 $\pi^0 \to \gamma\gamma$

The amplitude for $\pi \to \gamma\gamma$ has been evaluated [23] in the framework of $U(3) \times U(3)$ at order e^2, including one chiral loop. Recently, higher order terms in isospin breaking effects have been taken into account, both, in $U(2) \times U(2)$ [24], and in $U(3) \times U(3)$ [25]. The predictions are

$$\Gamma_{\pi^0\to\gamma\gamma} = \begin{cases} 8.06 \pm 0.02 \pm 0.06 \text{ eV } [24] \\ 8.10 \pm 0.08 \text{ eV } [25] \ , \end{cases} \tag{10}$$

whereas the PDG [26] quotes $\Gamma_{\pi^0\to\gamma\gamma}$ = 7.74 $\pm$ 0.55 eV. The measurement of this decay is in progress at JLAB (PRIMEX) [27].

4.2 $\gamma\pi^\pm \to \pi^\pm\pi^0$

We write the matrix element for the process $\gamma\pi \to \pi\pi$ in the form [28]

$$F^{3\pi}(s,\cos\theta) = F_0^{3\pi}\left\{f^{(0)}(s,\cos\theta) + f^{(1)}(s,\cos\theta) + f^{(2)}(s,\cos\theta) + \cdots\right\} \ ,$$

where $f^{(0)}, f^{(1)}$ and $f^{(2)}$ denote the tree, one-loop [29] and two-loop [30] contribution in the chiral expansion, and where $s, \cos\theta$ are the standard kinematic variables. The constant $F_0^{3\pi}$ is fixed by the chiral anomaly. Recently, electromagnetic corrections have been calculated to $f^{(0)}$ and $f^{(1)}$ [28, 24]. Interestingly, the correction to $f^{(0)}$ in the $\gamma\pi^\pm \to \pi^\pm\pi^0$ channel is sizeable, for the following reason. This term is generated by the two graphs a) and b) in Fig. 1, and is given [28] by $f^{(0)} = 1 - 2e^2F_\pi^2/t$, where t denotes the (momentum transfer)^2 of the virtual photon in graph b). As t may become small, this contribution can be sizeable. In addition, it is rather sensitive to the scattering angle, see Fig. 2 in Ref. [28].

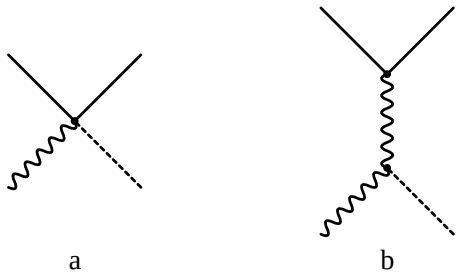

Fig. 1: Leading order contributions to the process $\gamma\pi^\pm \to \pi^\pm\pi^0$. The solid (dashed) lines denote charged (neutral) pions, a wiggly line the photon. Graph a) displays the standard anomalous vertex, and b) contains both, an ordinary vertex $\gamma\pi^\pm\pi^\pm$ and an anomalous one $\gamma\gamma\pi^0$. The two vertexes in b) are connected by the exchange of a virtual photon in the t-channel. Both graphs occur at order p^4 in the chiral expansion.

Remarks:

i) Including electromagnetic interactions in the chiral Lagrangian requires the charge to be counted as a quantity of order p for consistency. In this case, the two graphs a) and b) are algebraically of the same order in the low-energy expansion, because the propagator in b) contributes at order p^{-2}.

ii) In graph b), an ordinary vertex ($\pi^{\pm}\pi^{\pm}\gamma$) as well as an anomalous one ($\pi^0\gamma\gamma$) are present.

iii) Both graphs change sign under $\pi^+ \leftrightarrow \pi^-$.

At one-loop order, infrared divergences occur – these are cancelled in the standard manner by including [28] also the process

$$\gamma\pi \to \pi\pi\gamma\,.$$

The authors of Ref. [28] find that the result is rather insensitive to the photon energy of the outgoing photon. For explicit formulas for the cross sections, I refer the reader to this reference. All in all, after including electromagnetic interactions in the manner just described, theory agrees with the available experimental information according to Ref. [28].

4.3 $\gamma K \to \pi K$

This process is again dominated by anomalous terms in the effective Lagrangian (SU(3) version of anomaly). The calculations are yet to be performed. Since the chiral expansion also involves expansions in m_s, the prediction will be less precise than in the pion case discussed above. Note that for the process $\gamma K^0 \to K^0\pi^0$, the t-channel singularity is absent. Therefore, at leading order, this reaction gives direct access to the chiral anomaly.

4.4 N_c-dependence

The N_c dependence of anomalous processes has been investigated in the framework of the standard model in [31, 32, 33]. These authors find the following N_c dependence for the amplitudes:

$\pi^0 \to \gamma\gamma, \gamma\pi \to \pi\pi$	independent of N_c	[31, 32, 33]
$\gamma K^{\pm} \to \pi^0 K^{\pm}$	$N_c + 1$	[33]
$\gamma K^0 \to \pi^0 K^0$	$N_c - 1$	[33] .

5. STRONG INTERACTIONS

5.1 $\pi K \to \pi K$

Recent calculations that involve the reaction $\pi K \to \pi K$ include

i) a dispersive analysis of available data to determine LECs in $\mathcal{L}_4$ [34]

ii) a relation between the spectrum of $\pi^- K^+$ atoms and the elastic πK scattering amplitude [35].

What is the motivation for having more precise data on this reaction?

a) to pin down LECs

b) to get information on the character of chiral symmetry breakdown: is the vacuum affected by heavy $\bar{s}s$ pairs [36] ?

It would be useful to have data that allow one to separate isospin 1/2 and 3/2 amplitude. Furthermore, information on $\pi\pi \to K\bar{K}$ in the region of $K\bar{K}$ threshold and beyond would be very welcome [37].

5.2 $\pi\pi \to \pi\pi$

Elastic $\pi\pi$ scattering is an ideal observable to access the chiral structure of QCD vacuum for the following reason. The quark mass expansion of the pion mass reads

$$M_\pi^2 = M^2 - M^4 \bar{l}_3/(32\pi^2 F_\pi^2) + O(M^6) \qquad (11)$$

where M^2 is proportional to the quark condensate and to the quark mass, and $\bar{l}_3$ is a low-energy constant from $\mathcal{L}_4$. Standard chiral perturbation theory assumes that the first term in this expansion is dominant, and that further terms induce small corrections. This assumption has been put in question by Stern and collaborators [36] who pointed out that there is no experimental evidence for the quark condensate to be different from zero. The LEC $\bar{l}_3$ also occurs in the elastic $\pi\pi$ scattering amplitude and has recently been determined from high precision data on K_{e4} decays [38, 39]. It has turned out that indeed the first term in Eq. (11) is dominant – a rearrangement of the chiral expansion as proposed in [36] is not needed (see also Ref. [40]).

The point I wish to make concerning the COMPASS experiment and $\pi\pi$ scattering is the following. The Roy-equation analysis of $\pi\pi$ scattering [41], together with chiral symmetry requirements, predicts the $I = 2$ S-wave phase shift below 800 MeV, to within rather small uncertainties, see Fig. 9 in Ref. [17]. *It would therefore be very instructive to have more precise experimental information on this phase shift.*

6. SUMMARY

The following table reflects my personal view of the theoretical and experimental status of some of the processes described above.

	Ref. theory	Status of theory	Status of experiment
photons:			
$\gamma\pi \to \gamma\pi$	[11, 13]	**(*)	*
$\gamma K \to \gamma K$	[19]	*	
anomaly:			
$\pi^0 \to \gamma\gamma$	[23, 24, 25]	***	**
$\gamma\pi \to \pi\pi$	[28, 24]	***	*
$\gamma K \to K\pi$			
strong interactions:			
$\pi K \to \pi K$	[34]	**	*
$\pi\pi \to \pi\pi$	[17, 38, 39, 40, 41]	****	***

Acknowledgments

I thank the organizers of the COMPASS workshop for the invitation to give this talk and for giving me the opportunity to express the interest of the chiral community in low-energy experiments carried out at COMPASS. In addition, I thank A. Ananthanarayan, J. Bijnens, P. Büttiker, M. Knecht, B. Moussallam and M.E. Sainio for correspondence, J. Bijnens and M. Knecht for useful comments concerning the manuscript, and G. Colangelo and H. Leutwyler for informative discussions on the $I = 2$ S-wave phase shift. This work was supported in part by the Swiss National Science Foundation, and by RTN, BBW-Contract No. 01.0357 and EC-Contract No. HPRN-CT-2002-00311 (EURIDICE).

References

[1] S. Weinberg, Physica A **96** (1979) 327.

[2] J. Gasser and H. Leutwyler, Annals Phys. **158** (1984) 142.

[3] J. Gasser and H. Leutwyler, Nucl. Phys. B **250** (1985) 465.

[4] H. Leutwyler, Annals Phys. **235** (1994) 165 [arXiv:hep-ph/9311274].

[5] S. Weinberg, Phys. Rev. Lett. **17** (1966) 616.

[6] J. Gasser and H. Leutwyler, Phys. Lett. B **125** (1983) 325.

[7] J. Bijnens, G. Colangelo, G. Ecker, J. Gasser and M. E. Sainio, Phys. Lett. B **374** (1996) 210 [arXiv:hep-ph/9511397]; Nucl. Phys. B **508** (1997) 263 [Erratum-ibid. B **517** (1998) 639] [arXiv:hep-ph/9707291].

[8] G. Colangelo, J. Gasser and H. Leutwyler, Phys. Lett. B **488** (2000) 261 [arXiv:hep-ph/0007112].

[9] J. Gasser, V. E. Lyubovitskij, A. Rusetsky and A. Gall, Phys. Rev. D **64** (2001) 016008 [arXiv:hep-ph/0103157].

[10] B. Adeva *et al.*, CERN proposal CERN/SPSLC 95-1 (1995).

[11] U. Burgi, Phys. Lett. B **377** (1996) 147 [arXiv:hep-ph/9602421]; Nucl. Phys. B **479** (1996) 392, [arXiv:hep-ph/9602429].

[12] J. Bijnens and F. Cornet, Nucl. Phys. B **296** (1988) 557.

[13] J.F. Donoghue and B.R. Holstein, Phys. Rev. D **40** (1989) 2378;
B.R. Holstein, Comm. Nucl. Part. Phys. **19** (1990) 221.

[14] J. Bijnens, G. Colangelo and G. Ecker, JHEP **9902** (1999) 020 [arXiv:hep-ph/9902437]; Annals Phys. **280** (2000) 100 [arXiv:hep-ph/9907333].

[15] J. Bijnens and P. Talavera, Nucl. Phys. B **489** (1997) 387 [arXiv:hep-ph/9610269].

[16] J. Bijnens, G. Colangelo and P. Talavera, JHEP **9805** (1998) 014 [arXiv:hep-ph/9805389];
G. Amoros, J. Bijnens and P. Talavera, Nucl. Phys. B **585** (2000) 293 [Erratum-ibid. B **598** (2001) 665] [arXiv:hep-ph/0003258];
L. Girlanda, M. Knecht, B. Moussallam and J. Stern, Phys. Lett. B **409** (1997) 461 [arXiv:hep-ph/9703448].

[17] G. Colangelo, J. Gasser and H. Leutwyler, Nucl. Phys. B **603** (2001) 125 [arXiv:hep-ph/0103088].

[18] J. Gasser and M.E. Sainio, work in progress.

[19] J. F. Donoghue and B. R. Holstein, Phys. Rev. D **40** (1989) 3700.

[20] M. Colantoni, *Measurements of π and K polarizability @ COMPASS*, talk given at "Workshop on Future Physics @ COMPASS", CERN, Sept. 26 - 27, 2002.

[21] J. Bijnens and P. Talavera, JHEP **0203** (2002) 046 [arXiv:hep-ph/0203049].

[22] I thank J. Bijnens for pointing out to me this connection between the electromagnetic form factors and K_{l3} decays. See also J. Bijnens and P. Talavera, to be published.

[23] J. Bijnens, A. Bramon and F. Cornet, Phys. Rev. Lett. **61** (1988) 1453.

[24] B. Ananthanarayan and B. Moussallam, JHEP **0205** (2002) 052 [arXiv:hep-ph/0205232].

[25] J. L. Goity, A. M. Bernstein and B. R. Holstein, Phys. Rev. D **66** (2002) 076014 [arXiv:hep-ph/0206007].

[26] K. Hagiwara *et al.*, Phys. Rev. D **66** (2002) 010001.

[27] A. Gasparian *et al.*, Conceptual design report for PRIMEX, url: www.jlab.org/primex

[28] L. Ametller, M. Knecht and P. Talavera, Phys. Rev. D **64** (2001) 094009 [arXiv:hep-ph/0107127].

[29] J. Bijnens, A. Bramon and F. Cornet, Phys. Lett. B **237** (1990) 488.

[30] T. Hannah, Nucl. Phys. B **593** (2001) 577 [arXiv:hep-ph/0102213].

[31] S. Rudaz, Phys. Rev. D **41** (1990) 2619.

[32] A. Abbas, arXiv:hep-ph/0009242.

[33] O. Bar and U. J. Wiese, Nucl. Phys. B **609** (2001) 225 [arXiv:hep-ph/0105258].

[34] B. Ananthanarayan, P. Buttiker and B. Moussallam, Eur. Phys. J. C **22** (2001) 133 [arXiv:hep-ph/0106230].

[35] H. Sazdjian, *Relevance of the $K-\pi$ atom measurements*, talk given at the workshop "HadAtom02", Oct. 14 and 15, 2002, CERN, and work in progress;
J. Gasser and J. Schweizer, work in progress.

[36] M. Knecht, B. Moussallam, J. Stern and N. H. Fuchs, Nucl. Phys. B **457** (1995) 513 [arXiv:hep-ph/9507319]; Nucl. Phys. B **471** (1996) 445 [arXiv:hep-ph/9512404];
L. Girlanda, M. Knecht, B. Moussallam and J. Stern, Phys. Lett. B **409** (1997) 461 [arXiv:hep-ph/9703448].

[37] B. Ananthanarayan, P. Buttiker and B. Moussallam, Eur. Phys. J. C **22** (2001) 133 [arXiv:hep-ph/0106230], and private communication.

[38] G. Colangelo, J. Gasser and H. Leutwyler, Phys. Rev. Lett. **86** (2001) 5008 [arXiv:hep-ph/0103063].

[39] S. Pislak *et al.* [BNL-E865 Collaboration], Phys. Rev. Lett. **87** (2001) 221801 [arXiv:hep-ex/0106071].

[40] S. Descotes, N. H. Fuchs, L. Girlanda and J. Stern, Eur. Phys. J. C **24** (2002) 469 [arXiv:hep-ph/0112088].

[41] B. Ananthanarayan, G. Colangelo, J. Gasser and H. Leutwyler, Phys. Rept. **353** (2001) 207 [arXiv:hep-ph/0005297].

MEASUREMENTS OF π AND K POLARIZABILITY @ COMPASS

Marialaura Colantoni[1], *F. Balestra*[1], *R. Bertini*[1], *M.P. Bussa*[1], *O. Denisov*[1], *A. Dolgopolov*[2], *M. Faessler*[3], *A. Ferrero*[1], *L. Ferrero*[1], *J. Friedrich* [4], *V. Frolov*[1], *R. Garfagnini*[1], *N. Grasso*[1], *V. Kolossov*[2], *R. Kuhn*[4], *A. Maggiora*[1], *M. Maggiora*[1], *A. Manara*[1], *Y. Mikhailov*[2], *M. Moinester*[6], *V. Obraztsov*[2], *A. Olchevski*[7], *D. Panzieri*[1*], *S. Paul*[4], *G, Piragino*[1], *J. Pochodzalla*[5], *V. Poliakov*[2], *A. Sadovski*[7], *M. Sans, L. Schmitt*[4], *H. Siebert*[8], *A. Skachkova*[1], *T. Walcher*[5], *A. Zvyagin*[3]
[1] Univ. Torino-INFN, Italy, [1*] Univ. Piemonte Orientale-INFN, Italy [2] IHEP Protvino, Russia, [3] LU Munich, Germany, [4] TU Munich, Germany, [5] Univ. Mainz, Germany, [6] Univ. Tel Aviv, Israel, [7] JINR, Dubna, Russia, [8] Univ. Heidelberg, Germany,

Abstract
The COMPASS spectrometer is specially suited to perform a precise measurement of the pion-polarizabilities through the Primakoff reaction $\pi + Z \rightarrow \pi + Z + \gamma$. The results of a simulation are presented. An overall error of the measured polarizabilities comparable with the theoretical uncertainty can be obtained, making possible a clean test of the chiral symmetry polarizability prediction.

1. INTRODUCTION

The response of a particle, thought of as a composite structure of quarks, to an external electromagnetic field is described by its electric $\overline{\alpha}$ and magnetic $\overline{\beta}$ polarizabilities. These are fundamental quantities whose understanding is of great importance in any model or theory of the strong interactions, because the knowledge of these two quantities is an essential piece of information to check fundamental symmetry relations like the chiral symmetry.

The Chiral Perturbation Theory, χPT, based on the assumption of the chiral symmetry conservation, predicts for the two pion polarizabilities the values [1]:

$$\begin{aligned} \overline{\alpha_\pi} &= (\ \ 2.4 \pm 0.5) \cdot 10^{-4} \ \mathrm{fm}^3 \\ \overline{\beta_\pi} &= (-2.1 \pm 0.5) \cdot 10^{-4} \ \mathrm{fm}^3. \end{aligned}$$

The error on $\overline{\alpha_\pi}$ and $\overline{\beta_\pi}$ is due to the uncertainty in the knowledge of the axial and vector coupling constants that were measured in the radiative pion decay, where the polarizability can be expressed [2] as:

$$\overline{\alpha_\pi} = \frac{4\alpha_F}{m_\pi f_\pi^2}(L_r^9 - L_r^{10}),$$

where L_r^i are the chiral Lagrangian renormalization coupling constants.

Different experimental approaches have been used to deduce the pion polarizabilities. An approach involves the production of a $\pi^+\pi^-$ pair in e^+e^- collisions as a way to study the reaction $\gamma\gamma \rightarrow \pi^+\pi^-$, as shown in Fig. 1. The result [3]:

$$\overline{\alpha_\pi} = (2.2 \pm 1.6_{stat+sys}) \cdot 10^{-4} \ \mathrm{fm}^3$$

is obtained using dispersion relation. This result is, however, based on some model-dependent assumption and has, therefore, not to be considered as a pure experimental result.

Polarizabilities can also be measured via pion Compton scattering. Since a pion target is not available, the Compton scattering is only indirectly accessible through the radiative pion photoproduction and the pion radiative scattering.

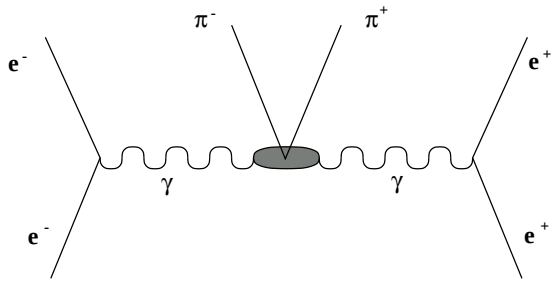

Fig. 1: Photon–photon collision.

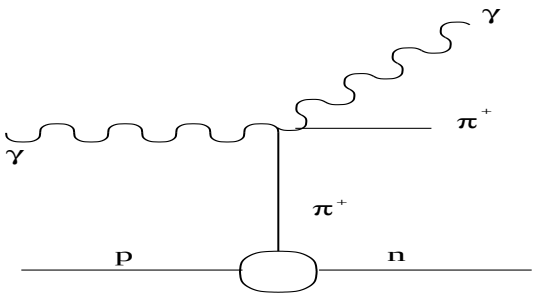

Fig. 2: Radiative pion photoproduction.

In the pion photoproduction a real photon scatters on a virtual pion $\gamma p \to \gamma \pi^+ n$ (see Fig. 2). With this process the following result was obtained [4]:

$$\overline{\alpha_\pi} = (20 \pm 12_{stat}) \cdot 10^{-4}\ \mathrm{fm}^3$$

The problem with such an approach is how to handle the final-state interaction between the produced pion and the scattered neutron.

Another way to deduce the pion polarizability is to make use of the radiative pion scattering $\pi^- Z \to \pi^- Z \gamma$, where the problem of final-state interactions, discussed before, is not present, because of the different interaction lengths of the strong and electromagnetic interactions. In the process considered here, also called Primakoff reaction, a real pion scatters on a virtual photon provided by the nuclear field (see Fig. 3). This approach allows for a simultaneous measurement of $\overline{\alpha_\pi}$ and $(\overline{\alpha_\pi} + \overline{\beta_\pi})$, therefore a check of the chiral symmetry relation between ($\overline{\alpha_\pi}$ and $\overline{\beta_\pi}$). This reaction has been used by the Serphukov group [5–7], studying the scattering of 40 GeV/c pion on a ^{12}C target. The result obtained is:

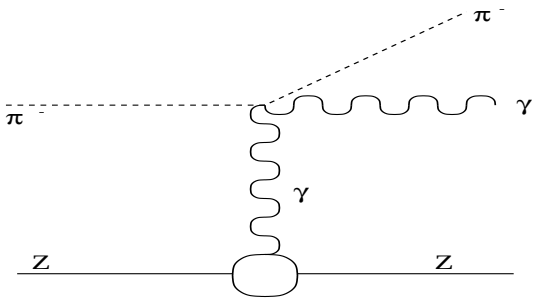

Fig. 3: Radiative pion scattering.

$$\overline{\alpha_\pi} = (6.8 \pm 1.4_{stat} \pm 1.2_{sys}) \cdot 10^{-4}\ \mathrm{fm}^3$$

assuming $(\overline{\alpha_\pi} + \overline{\beta_\pi}) = 0$ [5] and

$$(\overline{\alpha_\pi} + \overline{\beta_\pi}) = (1.4 \pm 3.1_{stat} \pm 2.5_{sys}) \cdot 10^{-4}\ \mathrm{fm}^3$$

without this assumption [6]. The value of $(\overline{\alpha_\pi} + \overline{\beta_\pi})$, here obtained as an independent measurement, is compatible with zero. The value of $\overline{\alpha_\pi} = 6.8 \cdot 10^{-4}\ \mathrm{fm}^3$ substantially differs from the χPT prediction $\overline{\alpha_\pi} = 2.4 \cdot 10^{-4}\ \mathrm{fm}^3$.

The experimental results of different experiment given here are very different and disagree with the χPT predictions, with the exception of [3], where the error bar is significantly larger than the theoretical uncertainty. Therefore new experiments are needed to measure $\overline{\alpha_\pi}$ and $\overline{\beta_\pi}$ with a statistical significance comparable with the uncertainty estimated by the theory. The COMPASS spectrometer is specially suited to perform a precise measurement of these two quantities, as part of the global Primakoff programme [8]. For this purpose we plan to measure the polarizabilities $\overline{\alpha_\pi}$ and $\overline{\beta_\pi}$ with a 190 GeV pion beam scattered on a lead target. The choice of the energy and the target will be discussed in Section 2.

2. THE PRIMAKOFF REACTION

A characteristic of the Coulomb scattering is the sharp dependence of the cross section on t, the four-momentum transfer from the incoming pion to the target nucleus. The t-dependence of $d\sigma/dt$, measured at the Serphukov experiment [7], is presented in Fig. 4. The dominance of the Coulomb amplitude for $t \leq 10^{-3}(\mathrm{GeV}/c)^2$ is evident, while the background coming from the strong interactions remains small.

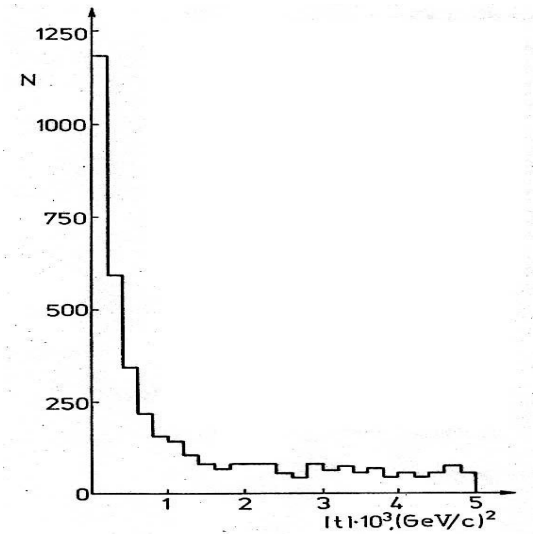

Fig. 4: t-dependence of $d\sigma/dt$ measured at Serphukov.

The Primakoff differential cross section for a pion scattering on a nucleus in the anti-laboratory frame (alab), the pion rest frame, is described by this formula:

$$\frac{d^3\sigma}{dt d\omega d\cos\theta} = \frac{\alpha_f Z^2}{\pi\omega}\frac{t - t_0}{t^2}\frac{d\sigma_{\gamma\pi}(\omega,\theta)}{d\cos\theta}|F_A(t)|^2 \qquad (1)$$

where t is the four-momentum transfer, $t_0 = (\frac{m_\pi \omega}{p_{beam}})^2$, m_π is the pion mass, ω is the energy of the virtual photon in the alab system, p_{beam} is the momentum of the incoming pion in the laboratory frame, θ is the

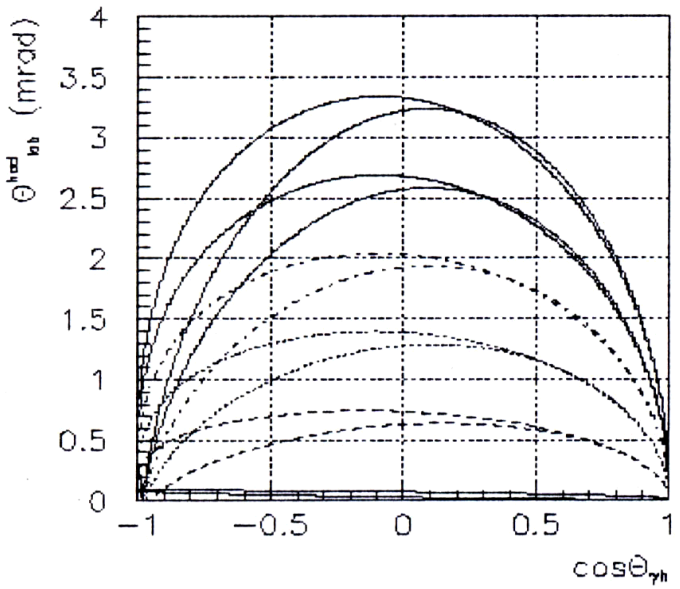

Fig. 5: Pion scattering angle in the lab system vs pion-photon angle in the alab system. The different curves correspond to increasing photon energies in the alab system from the lowest (dashed curve) to the highest value (full curve).

scattering angle of the real photon relative to the incident virtual photon direction in the alab system, α_f is the fine structure constant, Z is the charge of the nuclear target, $F_A(t)$ is electromagnetic form factor of the nucleus ($F_A(t) \approx 1$ in the range of $t < 10^{-3}(\mathrm{GeV}/c)^2$). In Eq. (1) the dependence on the pion polarizability is included in the cross section $\frac{d\sigma_{\gamma\pi}}{d\cos\theta}$, given by:

$$\frac{d\sigma_{\gamma\pi}(\omega,\theta)}{d\cos\theta} = \frac{2\pi\alpha_f^2}{m_\pi^2} \cdot \left(F_{\pi\gamma}^{Th} + \frac{m_\pi \omega^2}{\alpha_f} \cdot \frac{\overline{\alpha_\pi}(1+\cos^2\theta) + \overline{\beta_\pi}\cos\theta}{(1+\frac{\omega}{m_\pi}(1-\cos\theta))^3} \right) \ . \tag{2}$$

The first term in the parenthesis represents the Thomson cross section for the γ scattering on a point-like particle given by:

$$F_{\pi\gamma}^{Th} = \frac{1}{2} \cdot \frac{1+\cos^2\theta}{\left(1+\frac{\omega}{m_\pi}(1-\cos\theta)\right)^2} \ . \tag{3}$$

The second term expresses the correction for a non-pointlike particle. It describes the structure of the pion through the polarizabilities $\overline{\alpha_\pi}$ and $\overline{\beta_\pi}$.

The general behaviour of this cross section is characterized by the dependence on $(\overline{\alpha_\pi} + \overline{\beta_\pi})$ at forward angles and on $(\overline{\alpha_\pi} - \overline{\beta_\pi})$ at backward angles in the alab system.

In the COMPASS experiment this measurement will be performed at the beam momentum of 190 GeV/c, higher than that used at Serphukov. This choice allows for lower t values, where the cross section is higher. For the first measurement we have chosen a lead target, instead of carbon, because of the Z^2 dependence in the cross section. We can also use an higher beam intensity (up to 2×10^7 π's per second) and therefore collect a statistics significantly larger than that collected in the Serphukov experiment.

The kinematics of the scattering of a 190 GeV/c pion beam on a lead target shows the existence of a limit angle for the pion. In Fig. 5 the relation between the pion angle in the laboratory system versus the angle between the scattered pion and photon in the alab system is shown. The different lines correspond

to different energies for the virtual photon hitting the pion in the alab system. The limit angle is about 3.5 mrad.

For small t values the scattered pion is close to the non-scattered pion beam, therefore to identify the Primakoff reaction it is mandatory to reconstruct the complete final state, measuring simultaneously the pion momentum components, the energy and the emission angle of the photon. A good resolution on the reconstructed momentum transfer is one of the most stringent experimental requirements in order to well separate this reaction from the background due to the strong interactions.

3. TRIGGER

The COMPASS experimental setup has already been described in detail in other contributions. Therefore we give here in Fig. 6 a schematic view of the apparatus as needed to study $\overline{\alpha_\pi}$ and $\overline{\beta_\pi}$ polarizabilities. To select the Primakoff reaction, we need to identify and reconstruct the complete final state, detecting and measuring both the pion and the photon.

The total cross section for the Primakoff scattering is small, if compared to the total inelastic cross

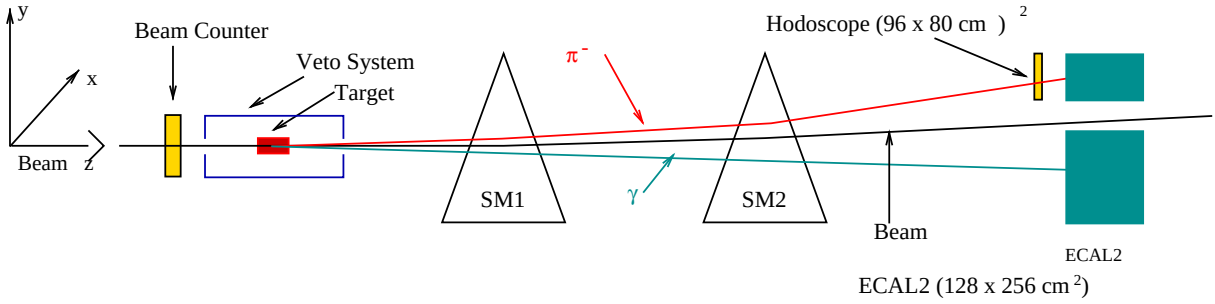

Fig. 6: The trigger.

section. Therefore, to get the high statistics needed to extract the polarizabilities, a high-intensity beam and a good acceptance are required. This implies for the trigger system, that it should act as a beam killer by accepting only the Primakoff scattered pions, and suppressing the large background associated with the non-interacting pions of the beam. In addition it should not cut the acceptance for the photon emitted at backward angles in the alab system, where the effects of the polarizabilities are more evident.

Trigger studies were performed during the test runs. The setup is illustrated in Fig. 6. It consists of a beam counter upstream of the target, a veto system around the target, a beam veto counter (beam killer) in front of ECAL2, and a hodoscope situated in front of ECAL2, displaced by 20 cm from the centre of the deflected beam. The trigger used was the coincidence of a signal in the beam counter with a photon that left an energy larger than $((0.2 \div 0.3) \times E_{beam})$ in ECAL2 and with a charged particle in the hodoscope.

From the test runs, with a beam intensity of $6 \cdot 10^6$ π/spill on a 3 mm lead target, the trigger rate was 2.5×10^5 events/spill [9]. This result is obtained without the beam killer and the veto counter. Their inclusion in the trigger does not decrease significantly the trigger rate. A further reduction of the number of events will be done offline using the target veto to reject background reactions with large momentum transfer to the target. The trigger rate reached is fully compatible with the capability of the data taking.

4. MONTE CARLO SIMULATION

To check the feasibility of our experiment, we [8, 10–12] made a Monte Carlo simulation with the following assumption: the pion and photon pass through the setup simulating the response of the apparatus to their interactions. The hits produced in the detectors are then used by the track reconstruction software to get the pion momentum components and the photon energy and emission angle at the target. The event

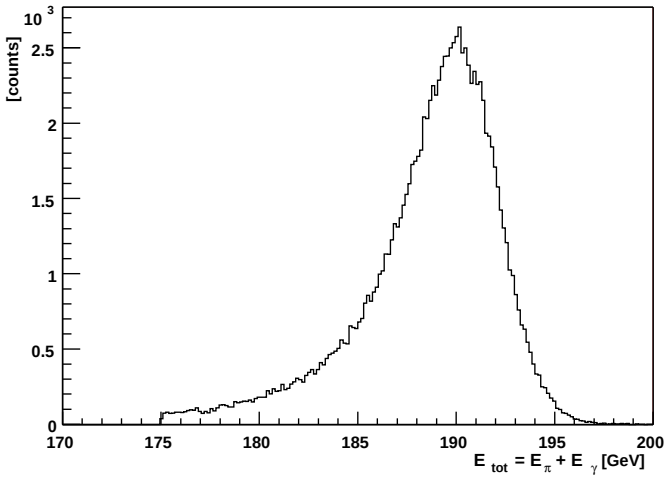

Fig. 7: Total energy of the $\pi\gamma$ pair.

generator was the program POLARIS [13] that produced Primakoff events according to the cross section given in Eq. (1) with $p_{beam} = 190$ GeV/c and with a lead target 1.7 mm thick. Only the events satisfying that, the photon energy $E_\gamma > 90$ GeV, were kept. With this cut the contribution of the polarizability term [see Eq. (1)] is emphasized versus the pointlike term $F_{\pi\gamma}^{Th}$.

These events were then processed by the POLTOGEA interface to adapt the database configuration to that required as an input to COMGEANT. COMGEANT [14] is a simulation software based on GEANT 3.21 [15] and developed according to the COMPASS Initial Layout requirements. This code traces the pion and the photon throughout the whole apparatus taking into account all the possible interactions with the detectors and with any other material they cross. The hits corresponding to the interaction points in the sensitive detectors were stored in a ZEBRA file that is the input for the reconstruction program CORAL: COMPASS Reconstruction and AnaLysis program [16], developed using object-oriented techniques. In CORAL, this input is digitized taking into account the proper experimental resolution of each detector. Then the retracking of the pion and the photon is performed to get at the target their kinematics variables. The sets of the generated (MC) and the reconstructed (RC) variables are then compared to evaluate the performance of our apparatus for the study of this specific reaction.

A first consistency check was made on the energy conservation. The energy E_γ of the photon detected in the electromagnetic calorimeter ECAL2 and the energy of the pion E_π obtained through the retracking were summed up and compared to the beam energy. The result is shown in Fig. 7. It can be seen that the peak is correctly centred at the beam energy of 190 GeV. The asymmetric tail on the low-energy side reflects the energy loss in the interactions with the apparatus. We selected only the events following the (180÷196) GeV cut. The reconstruction efficiency versus the four-momentum transfer squared for these events is plotted in Fig. 8.

The efficiency distribution is flat in the region of interest of t. There is no need for a t-dependent correction where the Primakoff cross-section varies very rapidly with t, as show in Fig. 4. So any cut on the t variable will not affect the detection efficiency.

To distinguish the Coulomb scattering from the strong interaction and in particular from the diffractive scattering $\pi Z \to \pi Z\gamma\gamma$, a good resolution on the transverse transfer momentum is necessary. A good selection between the single and multiple photons is also required by ECAL2. Typical values of the transverse momentum are: 0.1 GeV/c for the Primakoff reaction and 1 GeV/c for the diffractive scattering.

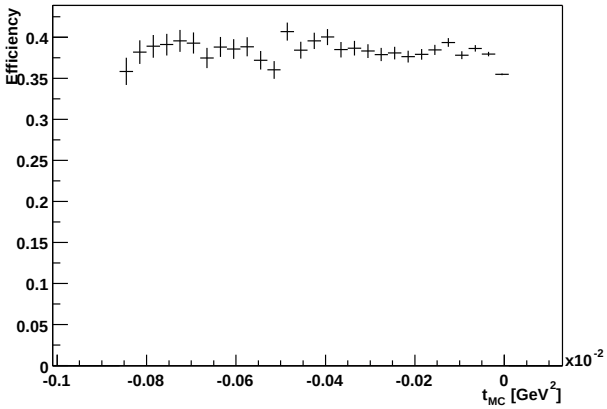

Fig. 8: Total efficiency vs t.

The transverse transfer momentum can be expressed in the following way:

$$p_T = \sqrt{(p_{x_\pi} + p_{x_\gamma})^2 + (p_{y_\pi} + p_{y_\gamma})^2} \tag{4}$$

id est

$$p_T = \sqrt{(p_X)^2 + (p_Y)^2} \ . \tag{5}$$

In Figs. 9, 10 are reported the resolution for the transverse component of the four-momentum transfer. The resolution found on p_T was $\sigma(p_T) \approx 18\ \mathrm{MeV}/c$. This resolution is sufficient to clearly distinguish the Primakoff and the diffractive process. The effect of this resolution on p_T on the t dependence in the cross section is shown in Fig. 11.

5. CONCLUSION

If we compare our results with the corresponding data obtained by the Serphukov experiment, we can infer the expected precision of the polarizabilities. In that experiment the statistical precision in $\overline{\alpha_\pi}$ was $\pm 1.4 \cdot 10^{-4}\ \mathrm{fm}^3$ with the total flux of $2 \cdot 10^{11}$ pions. Assuming a lead target, a beam momentum of 190 GeV/c and a pion flux of $2{\cdot}10^7\ \pi/\mathrm{s}$ we expect to measure $\overline{\alpha_\pi}$ with an overall error of $\approx 0.4{\cdot}10^{-4}\ \mathrm{fm}^3$. This error is comparable with the theoretical error computed for pion polarizability. We hope to get a similar error also for the sum $(\overline{\alpha_\pi} + \overline{\beta_\pi})$. To get this number we made the following assumption: an overall flux of $3.2 \cdot 10^{11}$ pions per day, an interaction probability $R = \sigma N_T = 5 \cdot 10^{-6}$, computed

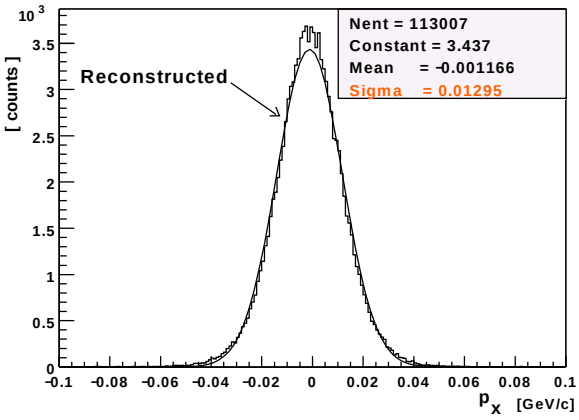

Fig. 9: p_X resolution.

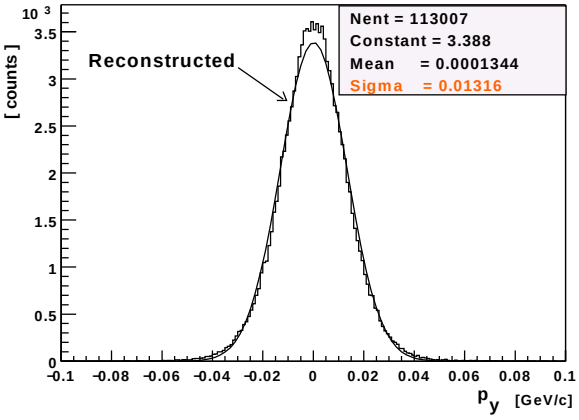

Fig. 10: p_Y resolution.

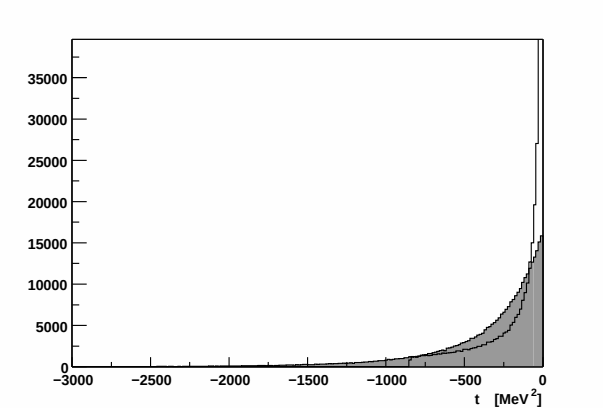

Fig. 11: Generated (white) and reconstructed (shaded) t distribution.

assuming $\sigma = 0.5$ mbarn and $N_T = 10^{-22}\mathrm{cm}^{-2}$, that gives $1.6 \cdot 10^6$ Primakoff polarizability events per day. Other input were tracking efficiency (92%), photon detection (58%), accelerator and COMPASS operation (60%), cuts to reduce background (75%), so a global efficiency of 24%. The result is that we expect to get $4 \cdot 10^5$ useful events per day, which is more then the total statistic, 7000 events, collected by the Serphukov experiment during the whole data taking. With such a statistical significance the measurement of the pion polarizabilities with the Primakoff reaction at COMPASS will allow to test:

1. the value of $\overline{\alpha_\pi}$ as compared with the existing data and with the theoretical prediction
2. the value of the sum $(\overline{\alpha_\pi} + \overline{\beta_\pi})$ with the existing data and the theoretical χPT prediction.

With the kaon beam we could also study the kaon polarizability, never measured until now. Since the cross section for kaon scales down as the inverse of the mass [Eq. (2)] at the first order approximation, this means that the cross section is three times smaller compared to the pion one. Also the values of the polarizability decrease by a factor 5.4 because of the ratio of the masses and the decay constant squared between the two mesons.

$$\overline{\alpha}_h = \frac{4\alpha_f}{m_h F_h^2}(L_r^9 + L_r^{10}) \rightarrow \overline{\alpha}_K = \frac{\overline{\alpha}_\pi}{5.4} \ . \tag{6}$$

Assuming such figure and the same conditions as in the pion case, but a flux of $3 \cdot 10^5$ kaons per second, we expect to collect $2 \cdot 10^4$ events per day. With such statistics an overall resolution of $0.6 \cdot 10^{-4}$ fm^3 is estimated. This resolution takes into account both the statistical and systematic error.

References

[1] U. Bürgi, Phys. Lett. B **377** (1996) 147.

[2] G. Backenstoss *et al.*, Phys. Lett. B **43** (1973) 431.

[3] J. Boyer *et al.*, Phys. Rev. D **42** (1990) 1350;
D. Babusci *et al.*, Phys. Lett. Bi **277** (1992) 158.

[4] T. A. Aibergenov *et al.*, Czech J. Phys. B **36** (1986) 948.

[5] Yu. M. Antipov *et al.*, Phys. Lett. B **121** (1983) 445.

[6] Yu. M. Antipov *et al.*, Z. Phys. C **26** (1985) 495.

[7] Antipov *et al.*, Prisma Zh. Eksp. Teor. Fiz **35**, No 7, (1982) 302.

[8] M. A. Moinester, Pion polarizabilities and Hybrid meson structure at COMPASS, hep-ex/0012063.

[9] A. Sadovski *et al.*, Test beam studies for a trigger for a Primakoff reaction measurement, COMPASS coll. meeting, Oct. 2000, Dubna Russia.

[10] M. Sans Merce, Ph.D thesis, Ludwig Maximilians University, Munich, 2001.

[11] R. Kuhn, Diploma thesis, Technical University Munich, 2001.

[12] A. Olchevski, M. Faessler, experimental requirements for COMPASS Initial Primakoff Physics program, COMPASS collaboration Meeting presentation, 2001.

[13] M. Buenerd, Nucl. Instrum. Meth. A **136** (1995) 128; V. Steiner, M. Moinester and M. Buenerd, POLARIS, A MonteCarlo event generator for polarizability experiment, private comunication.

[14] A. Vadim *et al.*, COMGEANT, http://valexakh.home.cern.ch/valexakh/wwwcomg/index.html.

[15] http://wwwinfo.cern.ch/asd/geant/index.html.

[16] B. Gobbo *et al.*, CORAL, http://coral.cern.ch/.

TRANSVERSITY AND Λ POLARIZATION

M. Anselmino
Dipartimento di Fisica Teorica, Università di Torino and
INFN, Sezione di Torino, Via P. Giuria 1, I-10125 Torino, Italy

Abstract
Two related issues are discussed, which might be easily explored by present and future COMPASS experiments. The first one deals with the new world of transversity, the fundamental polarized parton distribution so far totally unknown. The second issue concerns Λ production in polarized semi-inclusive processes, with a measurement of the Λ polarization, which might give novel information on distribution and fragmentation properties of polarized partons. In case of transverse polarization the detection of Λ's gives access to a new way of measuring transversities. Also the interesting case of Λ polarization in *unpolarized* processes is discussed.

1. TRANSVERSITY

The transverse polarization of quarks inside a transversely polarized nucleon, denoted by h_1, δq or $\Delta_T q$, is a fundamental twist-2 quantity, as important as the unpolarized distributions q and the helicity distributions Δq. It is given by

$$h_1(x,Q^2) = q^{\uparrow}_{\uparrow}(x,Q^2) - q^{\uparrow}_{\downarrow}(x,Q^2)\,, \tag{1}$$

that is the difference between the number density of quarks with transverse spin parallel and antiparallel to the nucleon spin [1]. Figure 1 shows the three fundamental quark distributions as seen in Deep Inelastic Scattering.

Transversity is the same as the helicity distribution only in a non relativistic approximation, but is expected to differ from it for a relativistic nucleon. Not much is known about it, apart from the fact that it should obey the Soffer's inequality [2]

$$2\,|h_1| \le (q + \Delta q)\,, \tag{2}$$

and that its integral is related to the tensor charge

$$a^t_q = \int_0^1 [h_{1q}(x,Q^2) - h_{1\bar{q}}(x,Q^2)]\,dx\,, \tag{3}$$

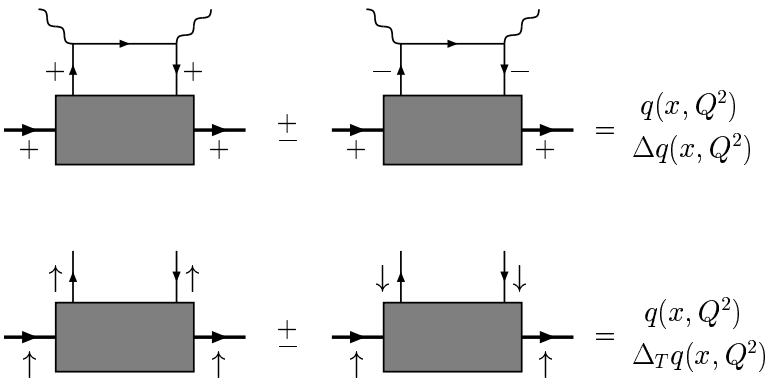

Fig. 1: The three leading twist quark distributions as seen in DIS.

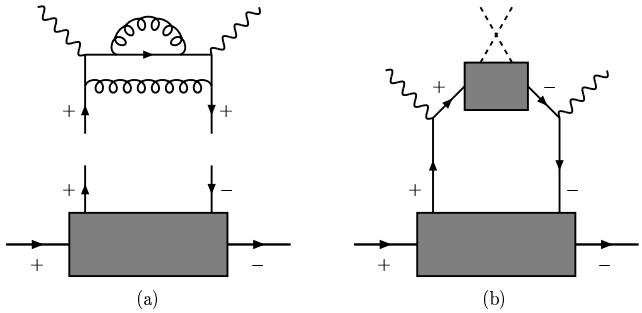

Fig. 2: The chiral-odd function h_1 (lower box) cannot couple to inclusive DIS dynamics, even with QCD corrections; it couples to semi-inclusive DIS, where chiral-odd non perturbative fragmentation functions may appear.

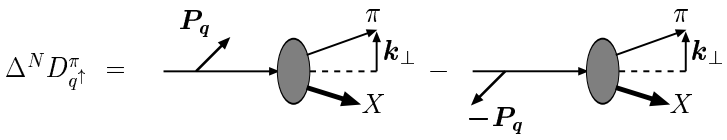

Fig. 3: Pictorial representation of Collins function; notice that a similar function is sometimes denoted by $H_1^\perp$ in the literature.

for which some estimates have been obtained using non perturbative QCD models [1].

When represented in the helicity basis (see Fig. 2) h_1 relates quarks with different helicities, revealing its chiral-odd nature. This is the reason why this important quantity has never been measured in DIS: the electromagnetic or QCD interactions are helicity conserving, there is no perturbative way of flipping helicities and h_1 decouples from inclusive DIS dynamics, as shown in Fig. 2a.

However, it can be accessed in semi-inclusive deep inelastic scatterings (SIDIS), where some non perturbative chiral-odd effects may take place in the non perturbative fragmentation process, Fig. 2b. Similarly, it could be accessed in Drell–Yan polarized processes, $p^\uparrow p^\uparrow \to \mu^+ \mu^- X$, where transverse spin asymmetries

$$A_{TT} = \frac{d\sigma^{\uparrow\uparrow} - d\sigma^{\uparrow\downarrow}}{d\sigma^{\uparrow\uparrow} + d\sigma^{\uparrow\downarrow}} \tag{4}$$

are related to the convolution of two transversity distributions. However, one expects very small numerical values for such asymmetries [3].

2. h_1 IN SIDIS

In order to measure the unknown transversity distribution in semi-inclusive DIS, one needs a chiral-odd partner to associate with h_1; these are usually new fragmentation functions and several suggestions have been made [4], which we shall briefly consider.

2.1 The Collins function

A chiral-odd function which might occur in the fragmentation of a transversely polarized quark into, say, a pion was first introduced by Collins [5] and is schematically represented in Fig. 3; it describes an azimuthal asymmetry in the hadronization process of a transversely polarized quark.

Such a function can give origin to a single spin asymmetry in $\ell\, p^\uparrow \to \ell\, \pi X$ processes, as indeed

observed by HERMES [6], and certainly observable by COMPASS experiments:

$$A_N = \frac{d\sigma^\uparrow - d\sigma^\downarrow}{d\sigma^\uparrow - d\sigma^\downarrow} \,. \tag{5}$$

At leading twist, this asymmetry, if attributed to the Collins function $\Delta^N D_{\pi/q^\uparrow}$, is given by:

$$A_N^\pi = \frac{\sum_q e_q^2 \, h_{1q}(x) \, \Delta^N D_{\pi/q^\uparrow}(z, k_\perp)}{2 \sum_q e_q^2 \, q(x) \, \hat{D}_{\pi/q}(z, k_\perp)} \, \frac{2(1-y)}{1+(1-y)^2} \, \sin\Phi_C \,, \tag{6}$$

where Φ_C is the azimuthal angle between the fragmenting quark polarization vector $\boldsymbol{P_q}$ and the pion transverse momentum $\boldsymbol{k}_\perp$. Thus, A_N clearly gives access to the transversity distributions h_{1q}, via the (unknown) Collins function: notice that a careful study of the dependence of A_N on the different DIS variables might help in obtaining separate information on h_1 and $\Delta^N D_{\pi/q^\uparrow}$; also, selection of particular kinematical ranges might help in the flavour decomposition [7].

2.2 The Sivers function

A mechanism similar to the Collins fragmentation was suggested for the proton distributions [8, 9], and the corresponding function denoted by $\Delta^N f_{q/p^\uparrow}$ or $f_{1T}^\perp$ [10]; it can again be described by Fig. 3 if one replaces the initial transversely polarized quark with a transversely polarized proton and the final pion with a quark [11]. The Sivers asymmetry was much debated, despite its phenomenological success [9, 12], because of some supposed problems with QCD time-reversal properties: however, very recently, a series of papers [13–15] have clarified the situation and fully promoted the rights of $\Delta^N f_{q/p^\uparrow}$.

When attributing the asymmetry (5) to the Sivers mechanism, at leading twist, one obtains:

$$A_N^\pi = \frac{\sum_q e_q^2 \, \Delta^N f_{q/p^\uparrow}(x, k_\perp) \, D_{\pi/q}(z)}{\sum_q e_q^2 \, q(x, k_\perp) \, D_{\pi/q}(z)} \, \sin\Phi_S \,, \tag{7}$$

to be compared with Eq. (6). The Sivers asymmetry does not allow access to transversity – it is a chiral-even function – but might contribute to A_N; such a contribution should be separated from that of the Collins asymmetry, if we want to use data on A_N to extract information on h_1. This is in principle possible if one notices that Eq. (7) does not depend on y and that the azimuthal angle dependence is different from the one in Eq. (6); Φ_S is now the angle between the proton polarization vector and the quark $\boldsymbol{k}_\perp$.

2.3 Other ways to approach transversity

Other approaches to elusive transversity have been proposed [4]. For example, within DIS, in Ref. [16] it was suggested to look at final states with two pions, originating from s and p wave states, whose interference might supply the necessary phase for a single spin asymmetry: these are the so-called interference fragmentation functions. They might avoid the danger that, in single inclusive production, the sum over many different channels averages the phases to zero.

Another possibility of measuring h_1 goes via the SIDIS production of spin 1 vector particles [17]; for example, one (measurable) non diagonal element of the helicity density matrix of a spin 1 meson, is related to h_1 and some unknown fragmentation amplitudes [18].

3. Λ POLARIZATION

Let us now turn to the second issue. Λ hyperons have the peculiar feature of revealing their polarization through the angular distribution of their weak decay, $\Lambda \to p\,\pi$; indeed such a feature has allowed many interesting measurements with unexpected and somewhat mysterious results [19].

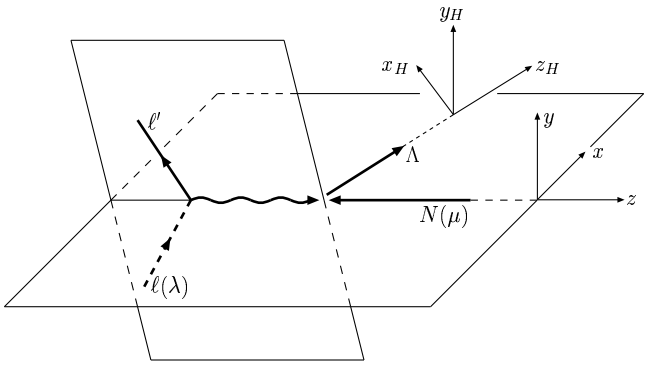

Fig. 4: Λ production in the $\gamma^* - p$ c.m. frame; the angular decay of the hyperon is measured for the particle at rest in the helicity frame, denoted by the pedices H; λ, μ and h denote, respectively, the initial lepton, nucleon and Λ helicities.

Let us consider the SIDIS processes, $\ell(\lambda)\, p(\mu) \to \ell\, \Lambda(h)\, X$, within the QCD factorization theorem at leading order, with several spin configurations, described by the helicities λ, μ and h; the Λ's are required to be produced in the current quark fragmentation region. The kinematics and our choice of reference frames are explicitly shown in Fig. 4; the Λ decay is observed in the helicity rest frame (x_H, y_H, z_H).

We define

$$\frac{d\sigma^{\ell(\lambda)\, p(\mu) \to \Lambda(h)\, X}}{dx\, dy\, dz} \equiv d\sigma^{\Lambda_h}_{\lambda\mu} \,. \tag{8}$$

Neglecting weak interaction contributions there are four independent helicity observables, which can be chosen and written as:

the unpolarized cross-section

$$d\sigma^{\Lambda} = \frac{2\pi\alpha^2}{sx}\, \frac{1+(1-y)^2}{y^2} \sum_q e_q^2\, q(x)\, D_{\Lambda/q}(z) \,, \tag{9}$$

the double spin asymmetry

$$A_{\parallel} = \frac{d\sigma^{\Lambda}_{++} - d\sigma^{\Lambda}_{+-}}{2\, d\sigma^{\Lambda}} = \frac{y(2-y)}{1+(1-y)^2}\, \frac{\sum_q e_q^2\, \Delta q(x)\, D_{\Lambda/q}(z)}{\sum_q e_q^2\, q(x)\, D_{\Lambda/q}(z)} \,, \tag{10}$$

the spin transfer from ℓ to Λ (with an unpolarized nucleon)

$$P_{+0} = \frac{d\sigma^{\Lambda_+}_{+0} - d\sigma^{\Lambda_-}_{+0}}{d\sigma^{\Lambda}} = \frac{y(2-y)}{1+(1-y)^2}\, \frac{\sum_q e_q^2\, q(x)\, \Delta D_{\Lambda/q}(z)}{\sum_q e_q^2\, q(x)\, D_{\Lambda/q}(z)} \,, \tag{11}$$

and the spin transfer from N to Λ (with an unpolarized lepton)

$$P_{0+} = \frac{d\sigma^{\Lambda_+}_{0+} - d\sigma^{\Lambda_-}_{0+}}{d\sigma^{\Lambda}} = \frac{\sum_q e_q^2\, \Delta q(x)\, \Delta D_{\Lambda/q}(z)}{\sum_q e_q^2\, q(x)\, D_{\Lambda/q}(z)} \,. \tag{12}$$

The above quantities are all measurable; P_{+0} means the polarization of the hyperon Λ semi-inclusively produced in the DIS scattering of a longitudinally polarized lepton (+ helicity) off an unpolarized proton (helicity 0), and so on. These combined measurements allow one to obtain new information and/or to test available information on longitudinally polarized and unpolarized fragmentation and

distribution functions, q, Δq, D and ΔD. A detailed discussion with numerical estimates, as well as a complete list of references, can be found in Refs. [20–22].

In particular, the above measurements should give some new information on the Λ fragmentation functions; in fact, from e^+e^- data one can only extract information on [23]

$$\sum_q [D_q^\Lambda + D_{\bar{q}}^\Lambda] \qquad \text{and} \qquad \sum_q [\Delta D_q^\Lambda - \Delta D_{\bar{q}}^\Lambda] \,. \tag{13}$$

3.1 Transverse polarization, polarized protons

We consider the process $\ell\, p^\uparrow \to \ell\, \Lambda^\uparrow\, X$ with an unpolarized lepton, a transversely polarized proton (S_N) and the measurement of the Λ transverse polarization P_N; transverse means orthogonal to the $\gamma^* - \Lambda$ plane, see Fig. 4. One has:

$$P_N^{[0S_N]} = \frac{2(1-y)}{1+(1-y)^2} \, \frac{\sum_q e_q^2 \, h_{1q}(x) \, \Delta_T D_{\Lambda/q}(z)}{\sum_q e_q^2 \, q(x) \, D_{\Lambda/q}(z)} \,, \tag{14}$$

where the transversity distribution h_1 appears coupled to $\Delta_T D = D_\uparrow^\uparrow - D_\uparrow^\downarrow$, the chiral-odd transversity fragmentation function (so far unknown).

Equation (14) offers a direct access to the product of h_1 and $\Delta_T D$ and one might hope to obtain separate information by studying the x and z dependences of P_N. Notice that there is no dependence on any $k_\perp$ in this case. Notice also that neglecting contributions from sea quarks (which should be safe in the large x and z regions) Eq. (14) simplifies to:

$$P_N^{[0S_N]} \simeq \frac{2(1-y)}{1+(1-y)^2} \, \frac{4h_{1u} + h_{1d}}{4u + d} \, \frac{\Delta_T D_{\Lambda/u}}{D_{\Lambda/u}} \,. \tag{15}$$

Convolutions of the same unknown functions appear in the transverse polarization of Λ's produced in pp interactions with one transversely polarized proton, $p\, p^\uparrow \to \Lambda^\uparrow\, X$, for example at RHIC [24]:

$$P_N(\Lambda) \sim \sum_{abc} f_{a/p} \otimes h_{1b} \otimes \Delta \hat{d\sigma}^{ab\to c\cdots} \otimes \Delta_T D_{\Lambda/c} \,, \tag{16}$$

where $f_{a/p}$ is a parton (quark or gluon) distribution function and the $\Delta\hat{d\sigma}$ are differences of polarized elementary QCD interactions. A combined measurement of P_N in both processes might help to extract more information.

3.2 Transverse polarization, unpolarized protons

This case is particularly interesting, as it relates to the longstanding problem of understanding the transverse polarization of Λ's and other hyperons produced in the unpolarized collisions of nucleons. This polarization might originate from spin effects in the fragmentation of unpolarized quarks into polarized baryons, the so-called polarizing fragmentation functions [25, 26]. These functions $\Delta^N D_{\Lambda^\uparrow/q}$ can, again, be described by Fig. 3 if one takes an initial *unpolarized* quark and replaces the final pion with a transversely (up or down) polarized Λ baryon [11].

Indeed the polarizing fragmentation functions can contribute to the transverse Λ polarization in SIDIS [27];

$$\begin{aligned} P_N(\Lambda, x, y, z, p_T) &= \frac{\sum_q e_q^2 \, q(x) \, \Delta^N D_{\Lambda^\uparrow/q}(z, p_T)}{\sum_q e_q^2 \, q(x) \, \hat{D}_{\Lambda/q}(z, p_T)} \\ &\simeq \frac{(4u+d) \, \Delta^N D_{\Lambda^\uparrow/u} + s \, \Delta^N D_{\Lambda^\uparrow/s}}{(4u+d) \, \hat{D}_{\Lambda/u} + s \, \hat{D}_{\Lambda/s}} \,, \end{aligned} \tag{17}$$

where p_T is the Λ transverse momentum in the $\gamma^* - p$ c.m. frame.

Equation (17) holds for neutral current, parity conserving, SIDIS processes. Even more interesting is the same quantity for the charged current weak process $\nu\, p \to \ell\, \Lambda^\uparrow\, X$, investigated by the NOMAD Collaboration [28]; in such a case one has an almost direct measurement of the polarizing fragmentation function:

$$P_N^{[\nu\ell]} \simeq \frac{\Delta^N D_{\Lambda^\uparrow/u}}{\hat{D}_{\Lambda/u}}\,. \tag{18}$$

Details and estimates can be found in Ref. [27].

4. CONCLUSIONS

The transversity distribution, the last fundamental missing piece of the polarized nucleon structure, can be accessed in semi-inclusive DIS. At the moment this looks like the most promising approach to the elusive transversity and should be strongly pursued. Ongoing and future COMPASS experiments offer an almost unique opportunity.

The main difficulty with measuring transversity is the necessity of coupling it to another unknown chiral-odd function, which is often very interesting by itself; the actual data are always products or convolutions of these new functions. However, luckily, the unknown functions depend essentially on different kinematical variables and one can devise a strategy to obtain separate information, provided enough data are available.

Typically, transversity contributes to spin asymmetries; another problem is that of controlling other possible contributions—independent of transversity—to these asymmetries. This might arise in case of Sivers and Collins contributions to A_N; whereas the latter is coupled to h_1, the former is not and such a contribution must be understood before drawing conclusions on h_1 from data on A_N. Also in this case some strategies are possible.

The measurement of transverse Λ polarization in SIDIS processes initiated by transversely polarized protons is a little explored, so far, channel to access h_1; the chiral-odd partner in this case is the transversity fragmentation function, which, again, is unknown: however, contrary to the Collins function, it does not require any intrinsic quark motion and does not vanish when $k_\perp = 0$. Moreover, one can expect it to be similar to the analogous longitudinal fragmentation function, and easy to model. Also, information on $\Delta_T D$ can be obtained from other processes.

We will learn more about transversity only by combining information from as many processes as possible, in different reactions and different kinematical ranges; the QCD Q^2 evolution of h_1 is known and should also be tested. Once a first knowledge about transversity is available, its many phenomenological applications to the explanation of observed spin asymmetries will test and improve our knowledge.

References

[1] Excellent recent reviews on the nucleon spin structure in general and on quark transverse spin in hadrons can be found in: B.W. Filippone and X. Ji, Adv. Nucl. Phys. **26** (2001) 1; V. Barone, A. Drago and P.G. Ratcliffe, Phys. Rept. **359** (2002) 1.

[2] J. Soffer, Phys. Rev. Lett. **74** (1995) 1292.

[3] J. Soffer, M. Stratmann and W. Vogelsang, Phys. Rev. D **65** (2002) 114024.

[4] For a recent review on ways of mapping the proton transversity see D. Boer, Nucl. Phys. A **711** (2002) 21.

[5] J.C. Collins, Nucl. Phys. B **396**, (1993) 161.

[6] HERMES Collaboration, A. Airapetian *et al.*, Phys. Rev. Lett. **84** (2000) 4047; Phys. Rev. D **64** (2001) 097101.

[7] M. Anselmino and F. Murgia, Phys. Lett. B **483** (2000) 74.

[8] D. Sivers, Phys. Rev. D **41** (1990) 83; Phys. Rev. D **43** (1991) 261.

[9] M. Anselmino, M. Boglione and F. Murgia, Phys. Lett. B **362** (1995) 164; M. Anselmino and F. Murgia, Phys. Lett. B **442** (1998) 470.

[10] D. Boer and P. Mulders, Phys. Rev. D **57** (1998) 5780.

[11] For a phenomenological definition of these new functions see, *e.g.*, M. Anselmino, e-Print Archive: hep-ph/0201150.

[12] See the talk by G. Rakness at SPIN 2002, Brookhaven National Laboratory, September 9-14, 2002, to appear in the proceedings.

[13] S.J. Brodsky, D.S. Hwang and I. Schmidt, Phys. Lett. B **530** (2002) 99; Nucl. Phys. B **642** (2002) 344.

[14] J.C. Collins, Phys. Lett. B **536** (2002) 43.

[15] X. Ji and F. Yuan, Phys. Lett. B **543** (2002) 66.

[16] R.L. Jaffe, X. Jin and J. Tang, Phys. Rev. Lett. **80** (1998) 1166.

[17] A. Bacchetta and P.J. Mulders, Phys. Rev. D **62** (2000) 114004.

[18] M. Anselmino, M. Boglione, J. Hansson and F. Murgia, Phys. Rev. D **54** (1996) 828.

[19] For a review of data see, *e.g.*, K. Heller, in Proceedings of Spin 96, C.W. de Jager, T.J. Ketel and P. Mulders, Eds., World Scientific (1997); or A.D. Panagiotou, Int. J. Mod. Phys. **A5** (1990) 1197.

[20] M. Anselmino, M. Boglione and F. Murgia, Phys. Lett. B **481** (2000) 253.

[21] M. Anselmino, M. Boglione, U. D'Alesio and F. Murgia, Eur. hys. J. **C21** (2001) 501.

[22] M. Anselmino, M. Boglione, U. D'Alesio, E. Leader and F. Murgia, Phys. Lett. B **509** (2001) 246.

[23] D. de Florian, J. Soffer, M. Stratmann and W. Vogelsang, Phys. Rev. D **57** (1998) 5811.

[24] D. de Florian, J. Soffer, M. Stratmann and W. Vogelsang, Phys. Lett. B **439** (1998) 176.

[25] M. Anselmino, D. Boer, U. D'Alesio and F. Murgia, Phys. Rev. D **63** (2001) 054029.

[26] P.J. Mulders and R.D. Tangerman, Nucl. Phys. B **461** (1996) 197; Nucl. Phys. B **484** (1997) 538 (E).

[27] M. Anselmino, D. Boer, U. D'Alesio and F. Murgia, Phys. Rev. D **65** (2002) 114014.

[28] NOMAD Collaboration, P. Astier *et al.*, Nucl. Phys. B **588** (2000) 3; Nucl. Phys. B **605** (2001) 3.

Λ PRODUCTION IN COMPASS

Aram Kotzinian
Yerevan Physics Institute, Alikhanian Brothers St. 2, Yerevan AM-375036, Armenia
and JINR, Moscow region, RU-141980 Dubna, Russia

Abstract
First Λ's and $\bar{\Lambda}$'s have been reconstructed from the COMPASS 2002 data. We briefly recall the motivation for measurements of longitudinal polarization of these hyperons. The role of hadronization mechanism in polarization phenomena in DIS and a purity method for extraction of polarized distribution functions are discussed. A model for the longitudinal polarization of Λ baryons produced in deep-inelastic lepton scattering is presented. Within the context of our model, the NOMAD data imply that the intrinsic strangeness associated with a valence quark has anticorrelated polarization. Predictions of our model for the COMPASS experiment are also given and the importance of $\bar{\Lambda}$ polarization measurements is discussed.

1. INTRODUCTION

It is generally accepted that information from deep inelastic scattering (DIS) experiments is an excellent source for investigating the internal structure of the nucleon. Experimental progress in recent years allows one to investigate the semi inclusive DIS (SIDIS). There is hope that, for example, the measurement of different hadron production asymmetries on proton and neutron targets will allow a further flavour separation of polarized quark distributions.

The knowledge of the hadronization mechanism is playing a very important role in the interpretation of SIDIS data. Traditionally one distinguishes two regions for hadron production: the current fragmentation region: $x_F > 0$ and the target fragmentation region: $x_F < 0$. The common assumption is that when selecting hadrons in the current fragmentation region and imposing a cut $z > 0.2$ we are dealing with the quark fragmentation.[1]

The measurements of the longitudinal polarization of the Λ hyperon produced in SIDIS was believed to provide two types of information. In the target fragmentation region it will provide an access to the polarization of intrinsic strangeness of the nucleon [1]. And in the current fragmentation region it will measure the polarization transfer from the quark q to the Λ hyperon, see, for example, Refs. [2–4]: $C_q^\Lambda(z) \equiv \Delta D_q^\Lambda(z)/D_q^\Lambda(z)$, where $D_q^\Lambda(z)$ and $\Delta D_q^\Lambda(z)$ are unpolarized and polarized fragmentation functions. Several experimental measurements of Λ polarization have been made in neutrino and antineutrino DIS. Longitudinal polarization of Λ hyperons was first observed in the old bubble chamber (anti) neutrino experiments [5–7] and according to Ref. [1] support the negative polarized strangeness scenario. The NOMAD Collaboration has recently published new and interesting results on Λ and $\bar{\Lambda}$ polarization with much larger statistics [8]. There are also recent results on longitudinal polarization of Λ hyperons from polarized charged lepton nucleon DIS processes coming from the E665 [9] and HERMES [10] experiments.

Recently the new preliminary data from HERMES on quark flavour separation has been presented [11]. The LO analysis of semi-inclusive DIS has been done by using the purity method and suggests that "the strange sea appears to be positively polarized" in contrast to generally accepted negatively polarized strange sea scenario at LO.

The natural question arises: *Is the negatively polarized strangeness scenario wrong or are the polarized quark distributions extracted by the purity method not precise?* In our opinion the second

[1] In this paper we are using the standard SIDIS notations.

alternative is right. In Section 2 the stability of purity method for polarized distribution function extraction is discussed. A method of calculation of the longitudinal polarization of Λ hyperons produced in SIDIS [12] is presented in Section 3, and our model predictions are compared to the available data in Section 4. A Short discussion on $\bar{\Lambda}$ polarization measurement is presented in Section 5. In Section 6 the preliminary distributions for Λ and $\bar{\Lambda}$ from COMPASS are presented. Finally, in Section 7 some conclusions are presented.

2. REMARKS ON THE PURITY METHOD

To make flavour decomposition of polarized quark distributions, the purity method has been used in the HERMES analysis [11]. In the LO approximation the virtual photon asymmetry is given by

$$A_1^h \simeq \frac{\sum_q e_q^2 \Delta q(x,Q^2) \int_{z_{min}}^1 dz D_q^h(z,Q^2)}{\sum_q e_q^2 q(x,Q^2) \int_{z_{min}}^1 dz D_q^h(z,Q^2)}. \tag{1}$$

This equation can be rewritten in the form

$$A_1^h \simeq \sum_q P_q^h(x) \frac{\Delta q(x)}{q(x)}, \tag{2}$$

where the purity, $P_q^h(x)$, is defined as

$$P_q^h(x) = \frac{e_q^2 q(x) \int_{z_{min}}^1 dz D_q^h(z)}{\sum_{q'} e_{q'}^2 q'(x) \int_{z_{min}}^1 dz D_{q'}^h(z)}, \tag{3}$$

and calculated using an unpolarized Monte Carlo event generator LEPTO [13] – JETSET [14]. Then using measured asymmetries for different hadrons one can find $\Delta q(x)$ by solving Eq. (2). The main assumption of this method is that all hadrons in the current fragmentation region with $z > 0.2$ are produced from the quark fragmentation so there are no additional terms in both the numerator and the denominator of Eq. (1). However, this assumption fails for moderate energies in the LUND fragmentation model incorporated in the JETSET program. In this program there is a pointer which shows the origin of produced hadrons. They can originate from quark or diquark fragmentation or low mass cluster decay. In Fig. 1, the fraction of events with hadrons produced via quark fragmentation

$$F_q = \frac{N_{hadron}(from\ quark\ fragmentation)}{N_{hadron}(tot)}, \tag{4}$$

is presented for different hadrons as a function of x_F. As one can see this fraction is less than one even at large values of x_F. Thus the assumption that hadrons in the current fragmentation region are produced only via quark fragmentation is not valid in the LUND model and purities obtained with the LEPTO Monte Carlo generator include contributions from the target remnant fragmentation.

When one takes into account the contribution from the target remnant, Eq. (1) for virtual photon asymmetry is modified:

$$A_{1p}^h = \frac{\sum_q [\Delta q(x) D_q^h(z) + \Delta M_q^{h/p}(x,z)]}{\sum_q [q(x) D_q^h(z) + M_q^{h/p}(x,z)]}\ . \tag{5}$$

The additional contributions from diquark fragmentation and other sources arise in the numerator and the denominator. It is important to note that even after tuning the LEPTO generator to unpolarized data nothing is known about $\Delta M_q^{h/p}(x,z)$.

To investigate the stability of the purity method the following MC exercise has been done. Using the PEPSI polarized MC generator [15] we generate the sample of 10^8 SIDIS events at HERMES energy for each polarization state of the target. The GRSV2000 LO (standard scenario) polarized and

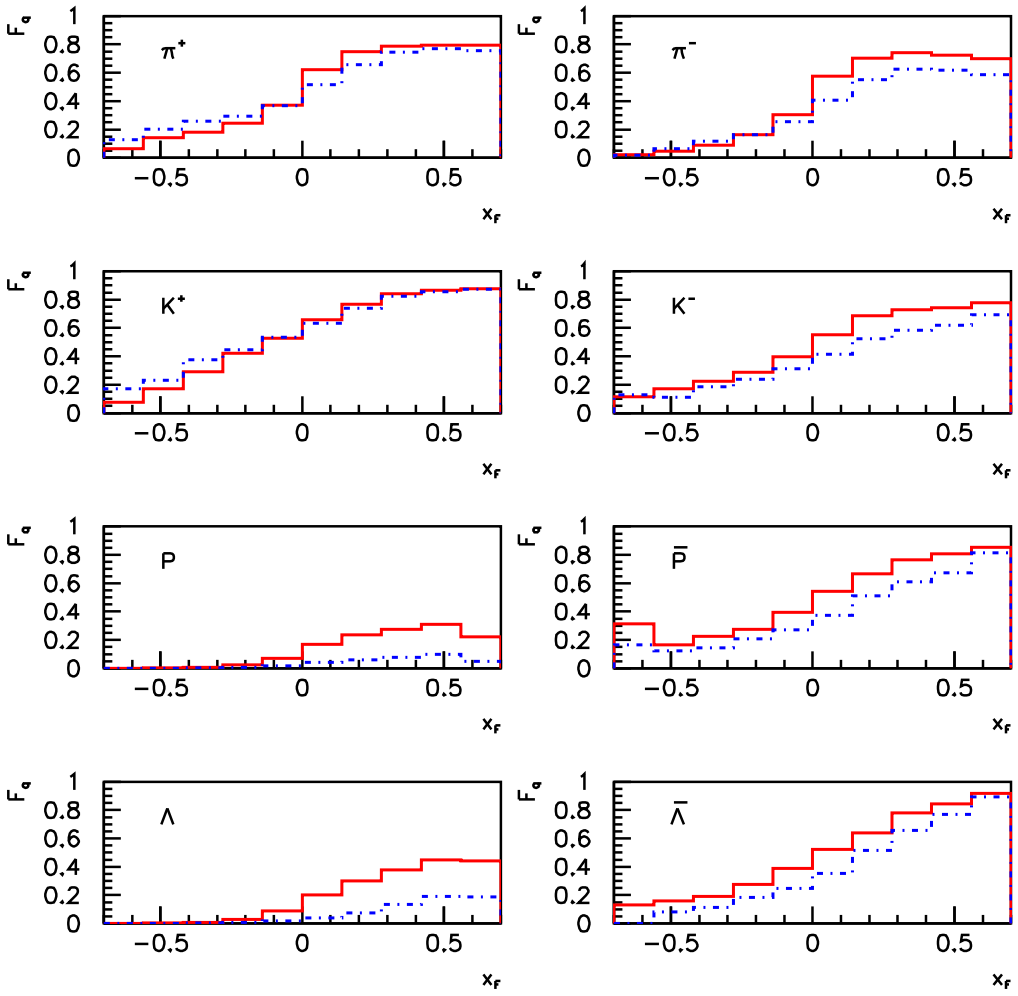

Fig. 1: Fraction of hadrons originating from quark fragmentation for COMPASS (solid line) and HERMES energies (dot-dashed line).

corresponding unpolarized GRV98 LO distribution functions have been chosen. To deal with current fragmentation we have selected $\pi^+, \pi^-, K^+, K^-, h^+$ and h^- with $x_F > 0$ and $z > 0.2$. To calculate asymmetries we considered two possibilities:

- **Model 1:** all hadrons give a contribution to the numerator of Eq. (5)
- **Model 2:** only hadrons from the quark fragmentation give a contribution to the numerator.

In both cases we assume that the purities are calculated from an unpolarized sample with non-zero $M_q^{h/p}(x,z)$. The polarized quark distributions are obtained by solving Eq. (2) and presented in the Fig. 2.

As one can see, the two models give rather different results. In particular, with *negative* input for the polarized strange sea distribution, **Model 2** leads to *positive* $\Delta s + \Delta\bar{s}$.

Up to now little is known about non-perturbative effects in hadronization. We see that at least in the LUND model Eq. (1) is incomplete and has to be replaced by Eq. (5). Even assuming that LEPTO is well tuned to unpolarized data we don't know anything about $\Delta M_q^{h/p}(x,z)$. The purity method is based on Eq. (1) and does not take into account non-perturbative effects of diquark or cluster hadronization in the polarized case. Without taking these effects into account it is hard to trust the polarized quark distribution obtained by the purity method.

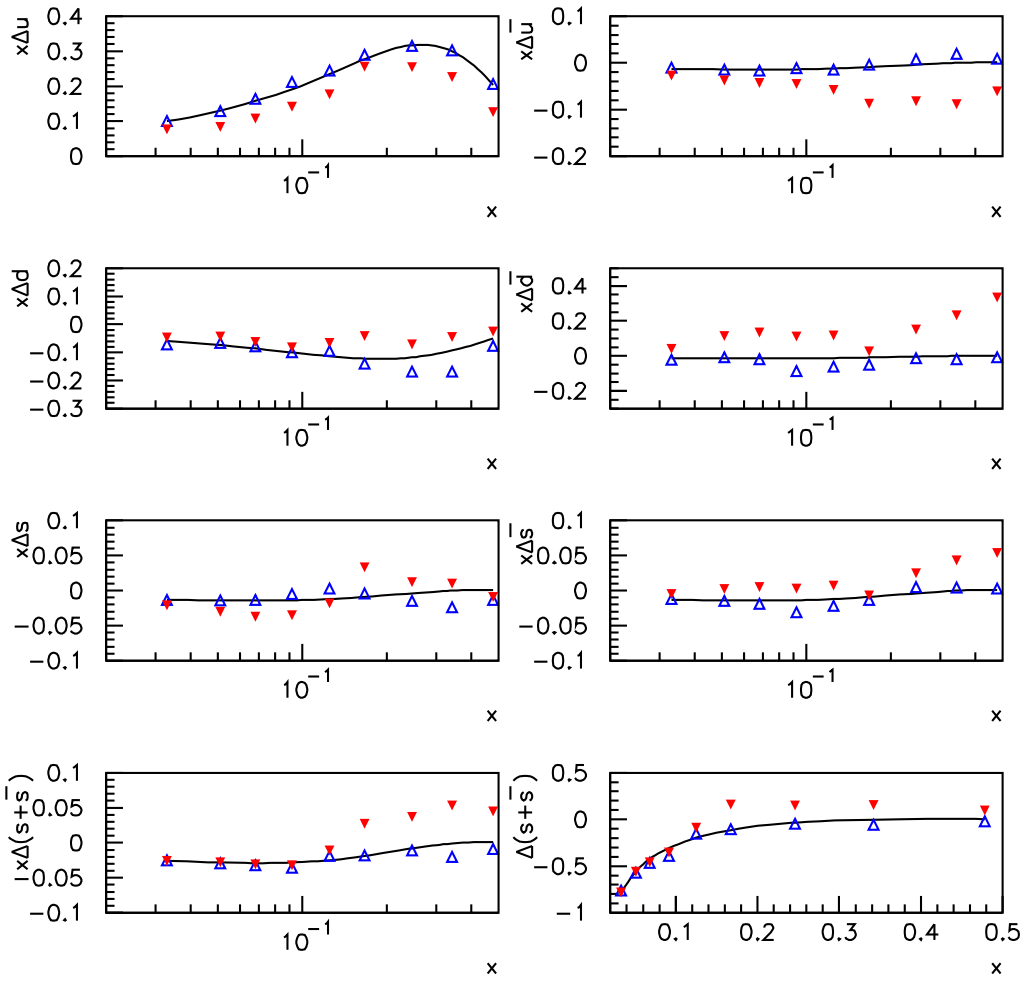

Fig. 2: Polarized quark distributions reconstructed by the purity method as a function of x_{Bj}: empty triangles – **Model 1**, full triangles – **Model 2**, solid line – the input distribution.

3. Λ PRODUCTION AND POLARIZATION IN DIS

Here a short description of the approach and results on Λ longitudinal polarization in DIS developed in the work [12] will be given.

Strange hadrons can be produced in SIDIS due to the struck quark or the nucleon remnant diquark fragmentation. The longitudinal polarization of the lepton can be transferred to strange hadrons during this fragmentation process. Λ hyperons can be produced *promptly* or as a decay product of heavier strange baryons (Σ^0, Ξ, $\Sigma^\star$). Therefore to predict a polarization for Λ hyperons in a given kinematic domain one needs to know the relative yields of Λ's produced in different channels and their polarization. We take into account all these effects by explicitly tracing the Λ origin predicted by the fragmentation model and assigning the polarization according to the polarized intrinsic strangeness model in the diquark fragmentation and by SU(6) and Burkardt–Jaffe models for the quark fragmentation.

3.1 Polarized intrinsic strangeness model

The main idea of the polarized intrinsic strangeness model applied to semi-inclusive DIS is that the polarization of s quarks and $\bar{s}$ antiquarks in the hidden strangeness component of the nucleon wave function should be (anti)correlated with that of the struck quark. This correlation is described by the spin correlation coefficients C_{sq}: $P_s = C_{sq} P_q$, where P_q and P_s are the polarizations of the initial struck (anti)quark and remnant s quark. In principle, C_{sq} can be different for the valence and sea quarks. We

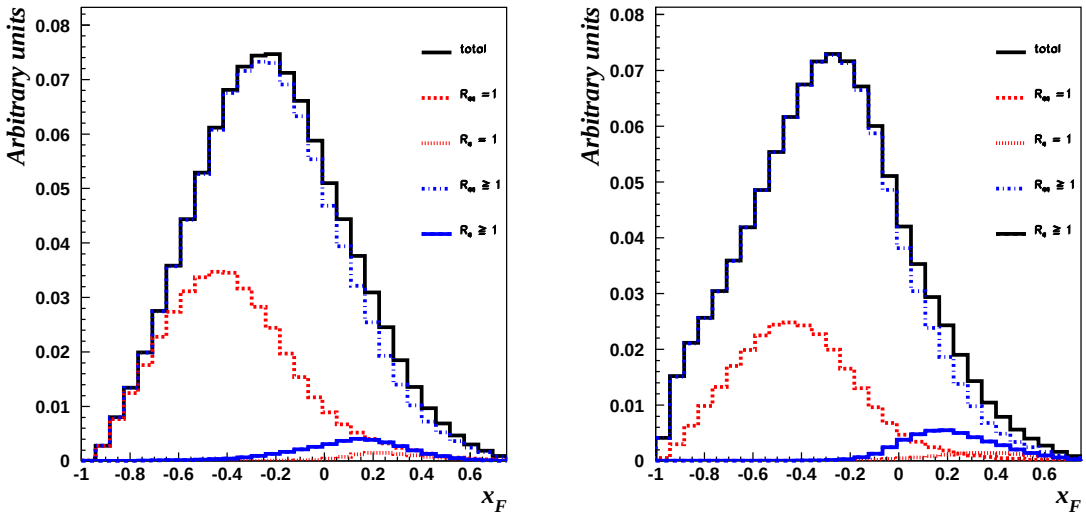

Fig. 3: Predictions for the x_F distributions of all Λ hyperons (solid line), of those originating from diquark fragmentation and of those originating from quark fragmentation, for the two model variants A and B, as explained in the legend on the plots. The left panel is for ν_μ CC DIS with $E_\nu = 43.8$ GeV, and the right panel for μ^+ DIS with $E_\mu = 160$ GeV.

leave $C_{sq_{val}}$ and $C_{sq_{sea}}$ as free parameters, that are fixed in a fit to the NOMAD data [8].

3.2 Polarization of strange hadrons in (di)quark fragmentation

We define the quantization axis along the three-momentum vector of the exchanged boson. To calculate the polarization of Λ hyperons produced in the diquark fragmentation we assume the combination of a non-relativistic $SU(6)$ quark–diquark wave function and the polarized intrinsic strangeness model described above. The polarization of Λ hyperons produced in the quark fragmentation via a strange baryon (Y) is calculated as: $P^q_\Lambda(Y) = -C^\Lambda_q(Y)P_q$, where $C^\Lambda_q(Y)$ is the corresponding spin transfer coefficient, P_q is the struck quark polarization which depends on the process. We use SU(6) and BJ models to compute $C^\Lambda_q(Y)$.

3.3 Fragmentation model

To describe Λ production and polarization in the full x_F interval, we use the LUND string fragmentation model, as incorporated into the JETSET7.4 program. We use the LEPTO6.5.1 Monte Carlo event generator to simulate charged-lepton and (anti)neutrino DIS processes. We introduce two rank counters: R_{qq} and R_q which correspond to the particle rank from the diquark and quark ends of the string, correspondingly. A hadron with $R_{qq} = 1$ or $R_q = 1$ would contain the diquark or the quark from one of the ends of the string. However, one should perhaps not rely too heavily on the tagging specified in the LUND model. Therefore, we consider the following two variants of nonzero spin transfer in fragmentation:

Model A: The hyperon contains the struck quark (the remnant diquark) only if $R_q = 1$ ($R_{qq} = 1$).

Model B: The hyperon contains the struck quark (the remnant diquark) if $R_q \geq 1$ and $R_{qq} \neq 1$ ($R_{qq} \geq 1$ and $R_q \neq 1$).

Clearly, **Model B** weakens the LUND tagging criterion by averaging over the string, while retaining information on the end of the string where the hadron originated.

In the framework of JETSET, it is possible to trace the particles' parentage. We use this information to check the origins of the strange hyperons produced in different kinematic domains, especially at various x_F. According to the LEPTO and JETSET event generators, the x_F distribution of the diquark

to Λ fragmentation is weighted towards large negative x_F.

However, its tail in the $x_F > 0$ region overwhelms the quark to Λ x_F distribution at these beam energies. In Fig. 3, we show the x_F distributions of Λ hyperons produced in diquark and quark fragmentation, as well as the final x_F distributions. These distributions are shown for ν_μ CC DIS at the NOMAD mean neutrino energy $E_\nu = 43.8$ GeV, and for μ^+ DIS at the COMPASS muon beam energy $E_\mu = 160$ GeV. The relatively small fraction of the Λ hyperons produced by quark fragmentation in the region $x_F > 0$ is related to the relatively small centre-of-mass energies — about 3.6 GeV for HERMES, about 4.5 GeV for NOMAD, about 8.7 GeV for COMPASS, and about 15 GeV for the E665 experiment — which correspond to low W.

We vary the two correlation coefficients $C_{sq_{val}}$ and $C_{sq_{sea}}$ in fitting Models A and B to the following four NOMAD points:

1) νp: $P_x^\Lambda = -0.26 \pm 0.05(stat)$,
2) νn: $P_x^\Lambda = -0.09 \pm 0.04(stat)$,
3) $W^2 < 15$ GeV^2: $P_x^\Lambda(W^2 < 15) = -0.34 \pm 0.06(stat)$,
4) $W^2 > 15$ GeV^2: $P_x^\Lambda(W^2 > 15) = -0.06 \pm 0.04(stat)$.

We find from these fits similar values for both the $SU(6)$ and BJ models: $C_{sq_{val}} = -0.35 \pm 0.05$, $C_{sq_{sea}} = -0.95 \pm 0.05$ (**Model A**) and $C_{sq_{val}} = -0.25 \pm 0.05$, $C_{sq_{sea}} = 0.15 \pm 0.05$ (**Model B**).

4. RESULTS ON Λ POLARIZATION

In Figs. 4 and 5 we show our model predictions compared to the available data from the NOMAD [8] and HERMES [10] experiments. One can conclude that our model quite well describes all the data. The NOMAD Collaboration has measured separately the polarization of Λ hyperons produced off proton

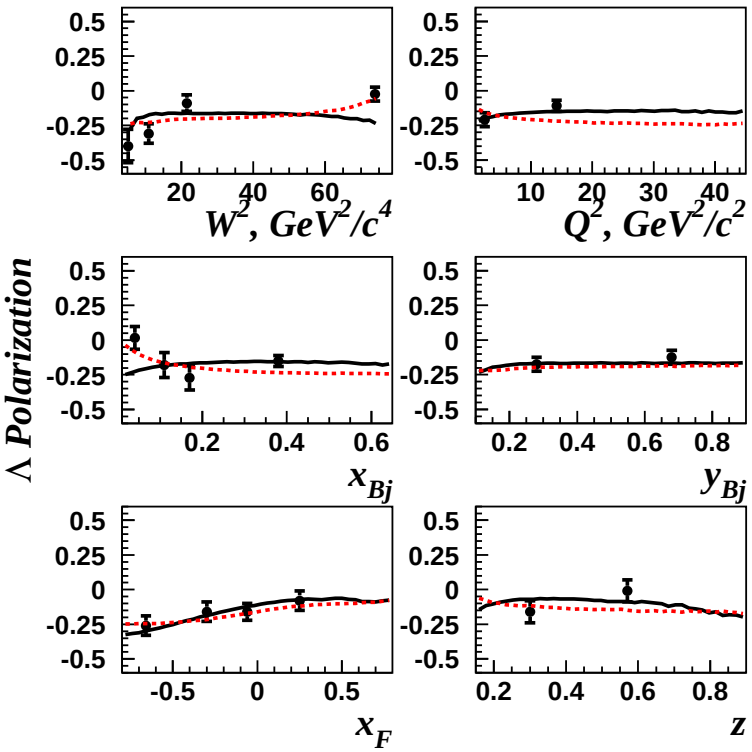

Fig. 4: The predictions of **Model A** – solid line and **Model B** – dashed line, for the polarization of Λ hyperons produced in ν_μ charged-current DIS interactions off nuclei as functions of W^2, Q^2, x_{Bj}, y, x_F and z (at $x_F > 0$). The points with error bars are from the NOMAD experiment.

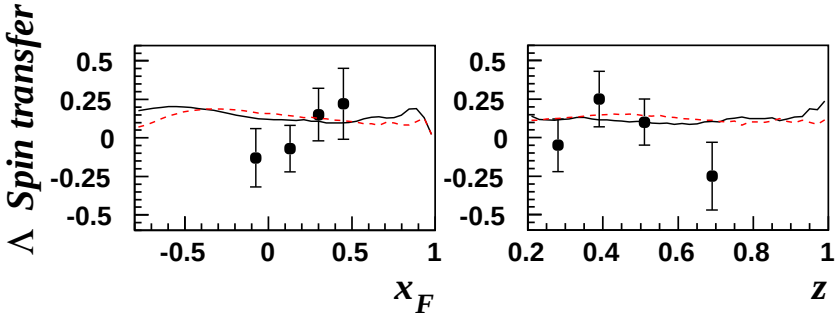

Fig. 5: The predictions of **Model A** – solid line, **Model B** – dashed line, for the spin transfer to Λ hyperons produced in e^+ DIS interactions off nuclei as functions of x_F and z (at $x_F > 0$). We assume $E_e = 27.5$ GeV, and the points with error bars are from HERMES experiment.

and neutron targets. We observe good agreement, within the statistical errors, between the **Model B** description and the NOMAD data while **Model A**, quite well reproducing the polarization of Λ hyperons produced from an isoscalar target, fails to describe target nucleon effects. We provide many possibilities for further checks of our approach for future data (see for details Ref. [12]).

The COMPASS Collaboration plans to investigate the polarization of Λ hyperons produced in the DIS of polarized μ^+ on a ^{6}LiD target. The beam energy and polarization are 160 GeV and -0.8, respectively. Thanks to the large statistics expected in this experiment, one can select kinematic regions where the predicted polarization is very sensitive to the value of the spin correlation coefficient for sea quarks, $C_{sq_{sea}}$. For example, in the region $x_F > -0.2$, which is experimentally accessible, and imposing the cut $0.5 < y < 0.9$, one ensures a large spin transfer from the incident lepton to the struck quark, and enhances the contribution from the sea quarks. The predicted Λ polarization is presented in Table 1.

Table 1: Predicted Λ polarization for COMPASS experiment

	Target nucleon		
P_Λ (%)	isoscalar	proton	neutron
Model A	-7.3	-7.3	-7.2
Model B	-0.4	-0.4	-0.4

As one can see the two models give quite different predictions and a new measurement of the Λ polarization can give preference to one of the models described.

5. $\bar{\Lambda}$ PRODUCTION AND POLARIZATION

As one can see in Fig. 1, $\bar{\Lambda}$'s in the current fragmentation region are mainly produced via quark fragmentation and the measurement of their polarization can provide information on spin transfer coefficients

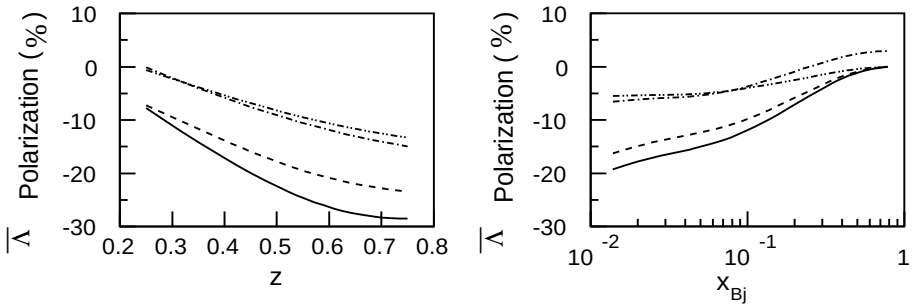

Fig. 6: Predictions for $\bar{\Lambda}$ polarization in COMPASS for different mechanisms of spin transfer: NQM, BGH (SU(6)+heavier hyperons) and BJ. For details see Ref. [3].

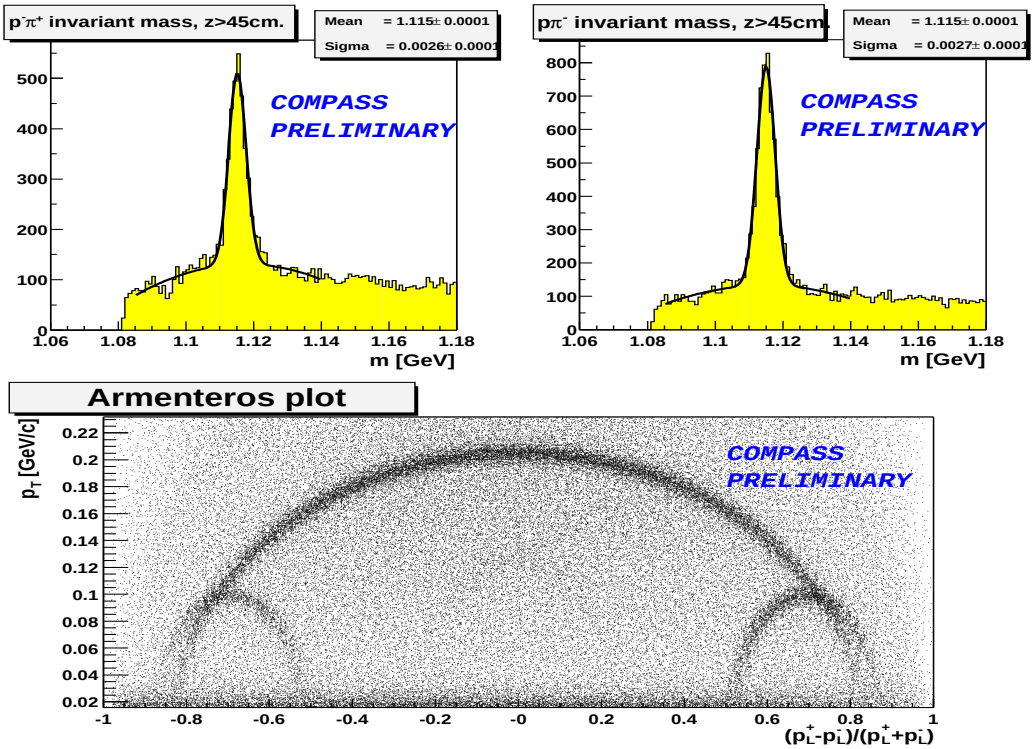

Fig. 7: Upper part: invariant mass distributions for $\bar{p}\pi^+$ and $p\pi^-$ pairs. Lower part: Armenteros plot with corresponding $\bar{\Lambda}$ (left) and Λ (right) ellipses

$C_q^{\Lambda}(z)$. In the literature one can find many models for $C_q^{\Lambda}(z)$. As an example in Fig. 6 the predictions of Ref. [3] for $\bar{\Lambda}$ polarization are presented for some of these models. These calculations have to be revised by taking into account the influence of the target remnant.

6. FIRST Λ's AND $\bar{\Lambda}$'s FROM COMPASS

The preliminary data analysis of the 2002 run demonstrated the COMPASS capability of Λ and $\bar{\Lambda}$ reconstruction. The selection criteria were the following:

- the V^0 vertex is 15 cm downstream of target,
- the transverse momentum of V^0's tracks with respect to its direction $p_T > 30$ MeV/c,
- the distance between V^0 momentum direction and primary vertex < 0.8 cm,
- with the $\pi^+\pi^-$ hypothesis, the V^0 mass is outside of the K_S^0 mass peak.

The invariant mass distribution of $\bar{p}\pi^+$ and $p\pi^-$ pairs and Armenteros plot are presented in Fig. 7. Estimations of the existing statistics show that COMPASS will have a sample of Λ and $\bar{\Lambda}$ larger than acquired in other experiments.

7. CONCLUSIONS

To treat the polarization phenomena in SIDIS it is very important to trace the origin of hadrons. The modern Monte Carlo event generators are very successful in the description of unpolarized SIDIS. We have learnt in Section 2 that according to the LUND model the essential part of hadrons are not produced by the quark fragmentation even in the current fragmentation region.

As we have demonstrated in Section 3 and Section 4 one can successfully describe the existing data on Λ longitudinal polarization in the combined SU(6) and intrinsic strangeness model when one take into account the origin of the strange hyperons predicted in the LUND model. Within the context

of our model, the NOMAD data imply that the intrinsic strangeness associated with a valence quark has anticorrelated polarization.

In contrast, the purity method, also based on the LEPTO event generator, assumes that all hadrons in the current fragmentation region are produced via quark fragmentation. As demonstrated in Section 2 this is not a good approximation and the results obtained by this method are highly questionable.

Finally, the measurement of $\bar{\Lambda}$ polarization is still actual and can allow one to distinguish between different spin transfer mechanisms.

Acknowledgements

I would like to thank A. Korzenev for providing the nice figures with preliminary Λ and $\bar{\Lambda}$ from COMPASS and M. G. Sapozhnikov and V. Alexakhin for useful discussions.

References

[1] J. Ellis, D. E. Kharzeev and A. Kotzinian, Z. Phys. **C69** (1996) 467 .

[2] The COMPASS Proposal, CERN/SPSLC 96-14, SPSC/P297, March 1996.

[3] A. Kotzinian, A. Bravar and D. von Harrach, Eur. Phys. J. C **2** (1998) 329.

[4] M. Burkardt and R. L. Jaffe, Phys. Rev. Lett. **70** (1993) 2537; R. L. Jaffe, Phys. Rev. D **54** (1996) R6581.

[5] J. T. Jones *et al.* [WA21 Collaboration], Z. Phys. C **28** (1987) 23.

[6] S. Willocq *et al.* [WA59 Collaboration], Z. Phys. C **53** (1992) 207.

[7] D. DeProspo *et al.* [E632 Collaboration], Phys. Rev. D **50** (1994) 6691.

[8] P. Astier *et al.* [NOMAD Collaboration], Nucl. Phys. B **588** (2000) 3;
D. V. Naumov [NOMAD Collaboration], AIP Conf. Proc. **570** (2001) 489, hep-ph/0101325;
P. Astier *et al.* [NOMAD Collaboration], Nucl. Phys. B **605** (2001) 3, hep-ex/0103047.

[9] M. R. Adams *et al.* [E665 Collaboration], Eur. Phys. J. C **17** (2000) 263, hep-ex/9911004.

[10] A. Airapetian *et al.* [HERMES Collaboration], Phys. Rev. B **64** (2001) 112005, hep-ex/9911017.

[11] H. E. Jackson, Int. J. Mod. Phys. A **17** (2002) 3551, hep-ex/0208015;
A. Miller, plenary talk at SPIN 2002, www.c-ad.bnl.gov/SPIN2002/presentations/miller.pdf.

[12] J. Ellis, A. Kotzinian and D. Naumov, hep-ph/0204206.

[13] G. Ingelman, A. Edin and J. Rathsman, Comput. Phys. Commun. **101** (1997) 108.

[14] T. Sjöstrand, *PYTHIA 5.7 and JETSET 7.4: physics and manual*, hep-ph/9508391;
T. Sjöstrand, Comput. Phys. Commun. **39** (1986) 347, **43** 367 (1987).

[15] L. Mankiewicz, A. Schäfer and M. Veltri, Comput. Phys. Comm. **71** (1992) 305,
http://www.thep.lu.se/ maul/pepsi.html.

INTRODUCTION TO GENERALIZED PARTON DISTRIBUTIONS

M. Diehl
Institut für Theoretische Physik E, RWTH Aachen, 52056 Aachen, Germany

Abstract
I give a brief introduction to generalized parton distributions, their physics, and opportunities for measuring them in μp collisions.

1. WHAT ARE GENERALIZED PARTON DISTRIBUTIONS?

Generalized parton distributions (GPDs) [1–4] have been recognized in the last few years as a tool to study hadron structure in new ways. Unifying the concepts of parton distributions and of hadronic form factors, GPDs contain a wealth of information about how quarks and gluons make up hadrons. Advances in experimental technology raise the hope of studying the exclusive processes where these functions appear.

The study of ordinary parton distributions provides us with detailed knowledge about the distribution of momentum and spin of quarks, antiquarks, and gluons. It is, however, important that the momentum probed in this way is the *longitudinal* momentum of the partons in a fast moving hadron. All information about the *transverse* structure is integrated over in the parton densities. One has in particular lost information about the role of the orbital angular momentum of partons in making a proton of total spin $\frac{1}{2}$. Clearly, orbital angular momentum should play a role at resolution scales where one can talk about partons: the simple splitting process $q \to qg$ of a light quark moving along the z-axis generates orbital angular momentum L_z, since this is the only way for it to conserve the total angular momentum J_z [5]. In order to access such information one needs quantities that involve transverse momenta, and this can be achieved in the exclusive scattering processes described by GPDs.

A good example to see the similarities and differences between usual parton densities and their generalization is the Compton amplitude. Via the optical theorem, the cross section for inclusive deep inelastic scattering (DIS) can be obtained from the imaginary part of the *forward* amplitude $\gamma^* p \to \gamma^* p$. In the Bjorken region of large photon virtuality Q^2 and collision energy, this amplitude factorizes into a parton distribution and a perturbatively calculable scattering process at the level of quarks and gluons. The simplest diagram for this is shown in Fig. 1a. The amplitude for deeply virtual Compton scattering (DVCS) $\gamma^* p \to \gamma p$, a completely exclusive process, factorizes in an analogous way if in addition to the Bjorken limit we require a small invariant momentum transfer t to the proton. Since the two proton momenta in the diagram of Fig. 1a are now different, the non-perturbative dynamics is not described by ordinary parton distributions, but by quantities which generalize them. In addition, the finite momentum transfer to the proton makes a second space–time structure of the process possible. Whereas in Fig. 1a the partonic subprocess is the scattering of a photon on a quark or antiquark, the virtual photon can also annihilate a quark–antiquark pair with transverse separation of order $1/Q$ in the proton target, as shown in Fig. 1b.

Like the usual parton densities, GPDs are defined through matrix elements of quark and gluon operators, for instance

$$\begin{aligned}(Pn) \int \frac{d\lambda}{2\pi}\, e^{i\lambda x (Pn)} \langle p', s' |\, \bar{q}(-\tfrac{1}{2}\lambda n)\, (n\gamma)\, q(\tfrac{1}{2}\lambda n)\, | p, s \rangle \\ = \quad \bar{u}(p', s')(n\gamma) u(p, s)\, H(x, \xi, t) + \bar{u}(p', s') \frac{i\sigma^{\alpha\beta} n_\alpha (p' - p)_\beta}{2m} u(p, s)\, E(x, \xi, t)\,. \end{aligned} \tag{1}$$

Here n is a light-like vector which determines the direction we call 'longitudinal'. These definitions provide the basis for deriving important properties of the distributions:

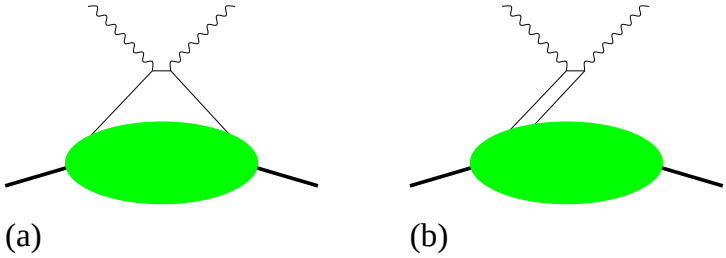

Fig. 1: Feynman diagrams for the Compton amplitude in the regime where it factorizes into a parton distribution and a hard partonic subprocess: (a) quark–photon scattering, (b) annihilation of a quark–antiquark pair.

- In the limit where the two states $|p, s\rangle$ and $p', s'\rangle$ become equal, one finds that H becomes the usual quark density, which thus provides boundary values for this function. On the other hand, the forward limit of the distribution E cannot be measured in the same way as usual parton distributions, since it appears multiplied by the momentum transfer $p' - p$. Evaluating the spinors in the right-hand side of Eq. (1) one finds in fact that E appears in the transition between a left- and a right-handed proton. Since the quark helicity remains the same, angular momentum balance requires orbital angular momentum, which is provided only if the proton momenta p and p' differ in their transverse components.
- Taking moments of these distributions in the momentum fraction x gives the matrix elements of *local* currents, for instance of the vector current in Eq. (1). The moments of GPDs are thus given by elastic form factors. The well-known electromagnetic Dirac and Pauli form factors, $F_1(t)$ and $F_2(t)$, are respectively obtained as lowest x-moments of the GPDs H and E. Of particular interest is the second moment $\frac{1}{2} \int dx\, x(H + E)$, whose value at $t = 0$ gives the *total* angular momentum of the quark species in question, including its spin and orbital angular momentum [2]. Note also that such moments are well suited to be calculated in lattice QCD.
- The quark–antiquark operator in Eq. (1) must be renormalized. The variation of the distributions with the renormalization scale μ is described by evolution equations that generalize the well-known DGLAP equations for parton densities, with evolution kernels known to two-loop accuracy [6]. Physically, μ^{-1} corresponds to the spatial resolution at which the partons are probed in the hard scattering process.

GPDs depend on three kinematical variables: x and ξ parametrize the independent longitudinal momentum fractions of the partons, whereas the dependence on $t = (p' - p)^2$ takes into account that there can also be a transverse momentum transfer. A very intuitive representation of the physics encoded in GPDs is obtained by a Fourier transform from $(p' - p)_\perp$ to transverse position $b_\perp$ [7–9]. The resulting picture is shown in Fig. 2. GPDs describe at the same time the longitudinal momentum of partons and their distance from the transverse 'centre' of the proton, and in this sense provide a fully three-dimensional

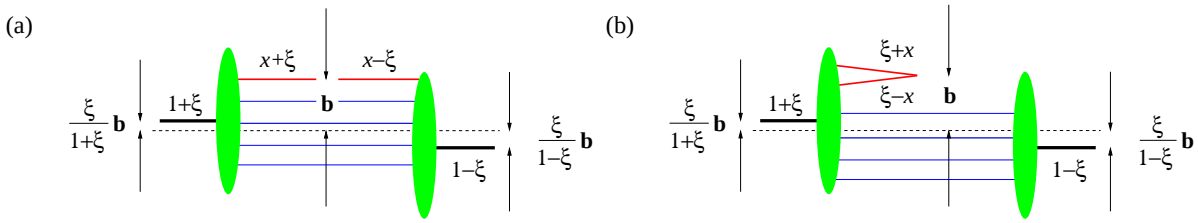

Fig. 2: Representation of a GPD in impact parameter space. Longitudinal momentum fractions refer to the average proton momentum $\frac{1}{2}(p + p')$ and are indicated above or below lines. The regions (a) and (b) correspond to those in Fig. 1.

image of partons in a hadron.

The usual parton densities are obtained in this picture by setting $\xi = 0$ and integrating over the transverse position $b_\perp$. Further analysis shows that the 'blobs' in Fig. 2 represent the light-cone wave functions of the incoming or the outgoing proton [10]. This highlights another difference between GPDs and their forward limit. Usual parton densities are given by squared wave functions and therefore represent probabilities. In contrast, GPDs correlate wave functions for different parton configurations and thus are genuinely quantum-mechanical interference terms. In region (b) they coherently probe $q\bar{q}$ pairs within the target.

There is an increasing amount of effort to better understand the dynamics of GPDs by various strategies of modelling them, a recent overview is given in Ref. [11]. Among many interesting features is the possibility to treat these quantities with methods of chiral perturbation theory and thus to investigate the role of chiral symmetry and its breaking in nucleon structure. Much remains to be done in this area: the rich physics content of GPDs is mirrored in a considerable complexity of their behaviour on x, ξ and t. Theoretical ideas will have to be tested against the constraints from data.

2. HOW TO MEASURE GENERALIZED PARTON DISTRIBUTIONS?

The appearance of GPDs in exclusive scattering processes is established by factorization theorems [12], which are very similar to those for inclusive processes such as DIS or Drell–Yan pair production. The foremost example is DVCS shown in Fig. 1. It is the process whose theory is most advanced, and the one which is probably the cleanest for extracting information on the unknown distributions. A large class of other reactions is provided by meson production, see Fig. 3. It provides a wealth of different channels and thus a handle to disentangle GPDs for different quark flavours and for gluons and to test the universality of the extracted functions. The comparatively large cross sections of some channels (for instance the production of ρ^0 mesons) will allow detailed studies in several kinematical variables. On the other hand the complexity of these processes, containing nonperturbative information on both the target and the produced meson, makes them more difficult to analyse. Also, there is reason to believe that the values of Q^2 where the simple factorized description of Fig. 3 is adequate, are larger than for DVCS, maybe 10 GeV^2 and more.

Fortunately there are predictions of factorization which can be tested directly in the data, without previous knowledge of the nonperturbative functions one aims to extract. In the limit of large Q^2 at fixed Bjorken variable x_B and fixed t, the amplitude for $\gamma^* p \to \gamma p$ should become independent of Q^2 up to logarithmic corrections; this is the precise analog of Bjorken scaling for DIS. The analogous scaling predicted for the meson production amplitude is like $1/Q$. In practice such tests require a sufficiently large lever arm in Q^2 at fixed x_B: for this the rather high beam energy of COMPASS presents an important advantage. A further prediction concerns the helicity structure of the process: at large Q^2 the dominant amplitudes for DVCS are for a transverse γ^*, whereas for meson production longitudinal γ^* and longitudinal meson polarization should dominate. Other polarizations are suppressed by further

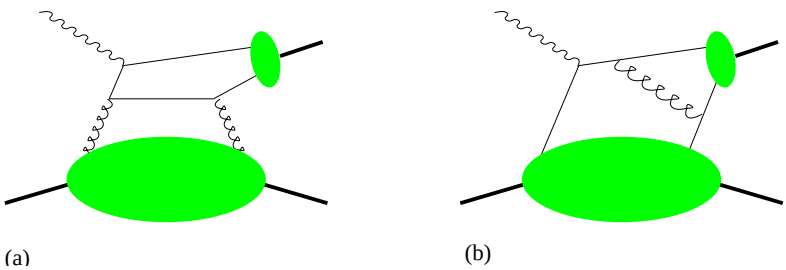

Fig. 3: Diagrams for meson leptoproduction with (a) gluon and (b) quark exchange with the target.

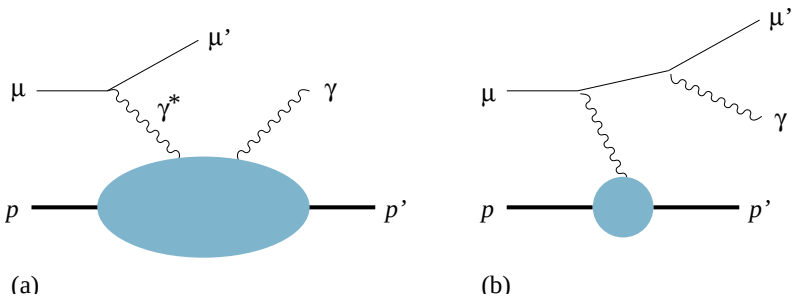

Fig. 4: Diagrams for the (a) Compton and (b) the Bethe–Heitler processes, contributing to leptoproduction $\mu p \to \mu p \gamma$.

powers of $1/Q$. The meson polarization is experimentally accessible from the decay angular distribution if the meson decays (for instance $\rho^0 \to \pi^+\pi^-$). Information on the polarization of the virtual photon is contained in the azimuthal angle φ between the hadron and the lepton planes in the leptoproduction process $\mu p \to \mu p \rho$, $\mu p \to \mu p \gamma$, etc. This angle corresponds in fact to a rotation around the momentum of the exchanged γ^* and is hence intricately related with the angular momentum along this direction.

The cleanest and most detailed access to the exclusive dynamics at amplitude level is possible in DVCS. In this case not only Compton scattering (Fig. 4a) but also the Bethe–Heitler process (Fig. 4b) contribute to the leptoproduction amplitude. Which mechanism dominates at given Q^2 and x_B depends mainly on the lepton beam energy E_ℓ. Large values of $1/y = 2m_p E_\ell \, x_B/Q^2$ favour DVCS and small values of $1/y$ favour Bethe–Heitler. The Bethe–Heitler process is completely calculable in QED, together with our knowledge of the elastic proton form factors at small t.

In kinematics where the Bethe–Heitler amplitude is sizeable, one can use the interference of the two processes to gain information about the Compton amplitude, including its phase. This is highly valuable since GPDs enter the $\gamma^* p$ amplitude through integrals of the type

$$\int dx \, \frac{H(x,\xi,t)}{x - \xi + i\epsilon}. \tag{2}$$

Since GPDs are real-valued due to time reversal invariance, the real and imaginary parts of this expression contain very distinct information on H. This information can be accessed in suitable observables, which can be identified by using the structure of the Bethe–Heitler and Compton processes at large Q^2 and small t, but without knowledge of the unknown Compton amplitudes [13]. To see how this works let us consider an unpolarized target and discuss the dependence of the cross section on the angle φ, and on the charge e_ℓ and longitudinal polarization P_ℓ of the muon beam. We schematically have

$$\begin{aligned}
&\frac{d\sigma(\mu p \to \mu p \gamma)}{d\varphi} \\
&= A_{\rm BH}(\cos(\varphi), \cos(2\varphi), \cos(3\varphi), \cos(4\varphi)) \\
&+ A_{\rm INT}(\cos(\varphi), \cos(2\varphi)) \Big(e_\ell \Big[c_1 \cos(\varphi) \, {\rm Re}\mathcal{A}(\gamma_T^*) + c_2 \cos(2\varphi) \, {\rm Re}\mathcal{A}(\gamma_L^*) + \ldots \Big] \\
&\qquad\qquad + e_\ell P_\ell \Big[s_1 \sin(\varphi) \, {\rm Im}\mathcal{A}(\gamma_T^*) + s_2 \sin(2\varphi) \, {\rm Im}\mathcal{A}(\gamma_L^*) \Big] \Big) \\
&+ A_{\rm VCS}(\cos(\varphi), \cos(2\varphi), P_\ell \sin(\varphi)),
\end{aligned} \tag{3}$$

where $A_{\rm BH}$, $A_{\rm INT}$, c_i, s_i are known expressions and $\mathcal{A}$ represents $\gamma^* p \to \gamma p$ amplitudes for different γ^* polarization. The $\ldots$ in brackets stand for a φ-independent term and a term with $\cos(3\varphi)$. Both are expected to be small in the kinematics under study but can readily be included in a full analysis. With muon beams one naturally reverses both charge and helicity at once, but we see how all four expressions in the interference can be separated: in the cross section difference $\sigma(\mu^+) - \sigma(\mu^-)$ the Bethe–Heitler

contribution $A_{\rm BH}$ drops out and one has access to the real parts of $\mathcal{A}(\gamma^*_{T,L})$. With angular analysis one can separate these two and test, for instance, the scaling predictions $\mathcal{A}(\gamma^*_T) \sim Q^0$ and $\mathcal{A}(\gamma^*_L) \sim Q^{-1}$ of the factorization theorem. In the sum of cross sections $\sigma(\mu^+) + \sigma(\mu^-)$ the imaginary parts of $\mathcal{A}(\gamma^*_{T,L})$ can be separated from the Bethe–Heitler and VCS contributions by their angular dependence, since their coefficients change sign under $\varphi \to -\varphi$ whereas the other contributions do not.

In the region of moderate to large x_B DVCS can be analysed along similar lines to meson production, if necessary after subtraction of the Bethe–Heitler term and integration over φ. Part of this kinematics overlaps with the x_B and Q^2 values where HERMES can access Compton amplitudes through the Bethe–Heitler interference due to its lower beam energy [14]. Comparison of data in this region will provide valuable cross checks, with the analysis in the interference region giving more detailed access to the Compton process and the analysis in the VCS dominated regime being less involved and hence more robust.

3. CONCLUSIONS

Generalized parton distributions permit one to study qualitatively new aspects of hadron structure, including detailed information on the longitudinal and transverse distribution of quarks and gluons, their orbital angular momentum, quantum mechanical interference effects, and $q\bar{q}$ pairs in the target wave function. The theory of how to measure these quantities in exclusive processes rests on solid foundations. Valuable data on Compton scattering and meson production can be obtained at COMPASS in a wide kinematical region, and with specific advantages from having polarized lepton beams of both charges.

Acknowledgements

I thank the organizers for their kind invitation to this workshop, and Nicole d'Hose and Dietrich von Harrach for valuable discussions.

References

[1] D. Müller, D. Robaschik, B. Geyer, F. M. Dittes, and J. Hořejši, Fortsch. Phys. **42** (1994) 101 [hep-ph/9812448].

[2] X. Ji, Phys. Rev. Lett. **78** (1997) 610 [hep-ph/9603249].

[3] A. V. Radyushkin, Phys. Rev. D **56** (1997) 5524 [hep-ph/9704207].

[4] J. Blümlein, B. Geyer, and D. Robaschik, Phys. Lett. B **406** (1997) 161 [hep-ph/9705264].

[5] P. G. Ratcliffe, Phys. Lett. B **192** (1987) 180.

[6] A. V. Belitsky, A. Freund, and D. Müller, Nucl. Phys. B **574** (2000) 347 [hep-ph/9912379].

[7] M. Burkardt, Phys. Rev. D **62** (2000) 071503 [hep-ph/0005108]; hep-ph/0207047.

[8] J. P. Ralston and B. Pire, hep-ph/0110075.

[9] M. Diehl, Eur. Phys. J. C **25** (2002) 223 [hep-ph/0205208].

[10] S. J. Brodsky, M. Diehl, and D. S. Hwang, Nucl. Phys. B **596** (2001) 99 [hep-ph/0009254]; M. Diehl, T. Feldmann, R. Jakob, and P. Kroll, Nucl. Phys. B **596** (2001) 33 [hep-ph/0009255].

[11] K. Goeke, M. V. Polyakov, and M. Vanderhaeghen, Prog. Part. Nucl. Phys. **47** (2001) 401 [hep-ph/0106012].

[12] J. C. Collins, L. Frankfurt and M. Strikman, Phys. Rev. D **56** (1997) 2982 [hep-ph/9611433]; J. C. Collins and A. Freund, Phys. Rev. D **59** (1999) 074009 [hep-ph/9801262].

[13] M. Diehl, T. Gousset, B. Pire, and J. P. Ralston, Phys. Lett. B **411** (1997) 193 [hep-ph/9706344]; A. V. Belitsky, D. Müller, and A. Kirchner, Nucl. Phys. B **629** (2002) 323 [hep-ph/0112108].

[14] HERMES, A. Airapetian et al., Phys. Rev. Lett. **87** (2001) 182001 [hep-ex/0106068]; V. A. Korotkov and W. D. Nowak, Eur. Phys. J. C **23** (2002) 455 [arXiv:hep-ph/0108077].

POSSIBLE MEASUREMENTS OF GPDs AT COMPASS

N. d'Hose[1], *E. Burtin*[1], *P.A.M. Guichon*[1], *J. Marroncle*[1], *M. Moinester*[2], *J. Pochodzalla*[3], *A. Sandacz*[4]
[1] CEA-Saclay, SPhN-DAPNIA-DSM, F-91191 Gif-sur-Yvette, Cedex, France
[2] School of Physics and Astronomy, Tel Aviv University, 69978 Ramat Aviv, Israel
[3] Johannes Gutenberg-Universität Mainz, Becherweg 45, D-55099 Mainz, Germany
[4] Soltan Institute for Nuclear Studies, ul. Hoza 69, PL-0681 Warsaw, Poland

Abstract
This paper presents the reactions which can be performed at COMPASS to study the Generalized Parton Distributions (GPDs). The high-energy muon beam at CERN allows one to measure Hard Exclusive Meson Production or Deeply Virtual Compton Scattering (DVCS) in the Bjorken regime in a large range of Q^2 and x_{Bj} ($1.5 \leq Q^2 \leq 7.5$ GeV^2 and $0.03 \leq x_{Bj} \leq 0.25$). Exploratory measurements dedicated to ρ^0 or π^0 production can be investigated with the present setup. DVCS measurement requires an upgrade of the COMPASS setup.

1. GOAL OF AN EXPERIMENT WITH THE HIGH ENERGY MUON BEAM

The Generalized Parton Distributions (GPDs) provide a unified description of the nucleon. As explained by M. Diehl [1], they interpolate between the parton distributions and the hadronic form factors. Experimentally the GPDs can be accessed in exclusive measurements such as Hard Exclusive Meson (ρ, π...) Production (HEMP) and Deeply Virtual Compton Scattering (DVCS). The latter reaction is the simplest from the theoretical point of view but also the most difficult experimentally because one has to select perfectly the final state (one lepton, one proton and one photon) among all the possible reactions. In practice we can now start the investigation of Meson Production and we foresee an upgrade of the COMPASS setup for DVCS measurement.

Experiments have already been undertaken at very high energy with the HERA collider to study mainly the gluon GPDs at very small x_{Bj} ($\leq 10^{-2}$). Larger values of x_{Bj} have been investigated in fixed target experiments at JLab (6 GeV, with plans for an upgrade at 11 GeV) and HERMES (at 27 GeV). The experimental program using COMPASS at CERN (at 100 and/or 190 GeV) will enlarge the kinematical domain to a large range of Q^2 and x_{Bj} ($1.5 \leq Q^2 \leq 7$ GeV^2 and $0.03 \leq x_{Bj} \leq 0.25$) (see Fig. 1). A large range in Q^2 is required to control the factorization in a hard, perturbatively calculable amplitude and a soft amplitude which is parametrized by the generalized parton distributions $H, E, \tilde{H}, \tilde{E}$. The GPDs depend on three kinematical variables: x and ξ parametrize the longitudinal momentum fractions of the partons, while t relates to the transverse momentum transfer.

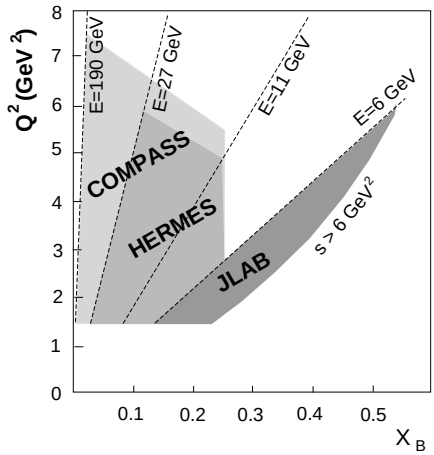

Fig. 1: Kinematical coverage for various planned or proposed experiments. The limit $s \geq 6$ GeV^2 assures to be above the resonance domain, and $Q^2 > 1.5$ GeV^2 allows one to reach the Deep Inelastic regime.

Since the theoretical proof of factorization assumes that the transfer t is finite (that is $t/Q^2 \to 0$) [1, 2], we consider in the following $|t|$ smaller than 1 GeV^2. Another condition of factorization concerns the helicity of the virtual photon. In case of Hard Exclusive Meson Production it is mandatory

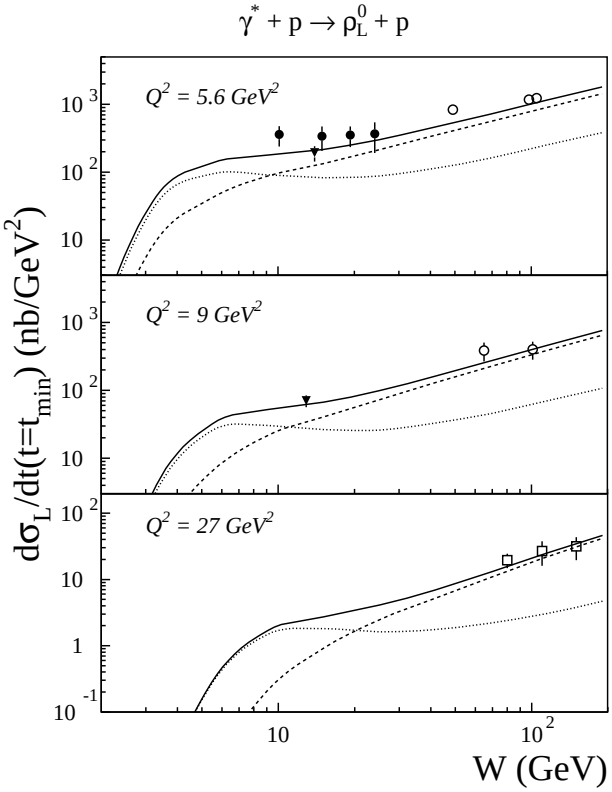

Fig. 2: Longitudinal forward differential cross section for ρ_L^0 production (Fig. from Ref. [3]). Predictions reproduce quark contributions (dotted lines), gluon contributions (dashed lines) and the sum of both (full lines). The data are from NMC (triangles) [4], E665 (solid circles) [5], ZEUS 93 (open circles) [6] and ZEUS 95 (open squares) [7].

to impose that the virtual photon be longitudinal in order to select the perturbative gluon exchange. Experimentally we should consider Rosenbluth separation for π^0 production, while for ρ^0 production we can select longitudinal ρ^0's through the angular distribution of the decay products and assume the s-channel helicity conservation. Hard Exclusive Meson Productions seem more complex to analyse as they contain non-perturbative information on both the target and the produced meson. Nevertheless they offer the possibility to disentangle different GPDs (vector meson production depends on H and E only; pseudo-scalar production depends on $\tilde{H}$ and $\tilde{E}$ only) and to separate contributions from different flavours. Forward differential longitudinal ρ_L^0 electroproduction cross section measurements which provide the largest counting rates, have already been undertaken and are presented in Fig. 2 as a function of c.m. energy W for three values of Q^2 (5.6, 9 and 27 GeV^2). The theoretical curve is an incoherent sum of the quark and gluon contributions [3]. No measurement has been done at x_{Bj} larger than 0.05. Thanks to the expertise of the NMC Collaboration for these absolute measurements we will explore a larger domain in x_{Bj}, Q^2 and t with the muon beam available at CERN.

Deeply virtual Compton scattering is accessed by photon lepto-production: $lp \to l'p'\gamma$. In this reaction, the final photon can be emitted either by the leptons (Bethe–Heitler process) or by the proton (genuine DVCS process). If the lepton energy is large enough (see Fig. 3 with $E_\mu = 190$ GeV, $Q^2 = 4\,\mathrm{GeV}^2$, $x_{Bj} = 0.1$), the DVCS contribution dominates over the BH contribution so that the cross section is essentially the square of the DVCS amplitude which, at leading order, has the form:

$$T^{DVCS} \sim \int_{-1}^{+1} \frac{H(x,\xi,t)}{x-\xi+i\epsilon} dx \ldots \sim \mathcal{P}\int_{-1}^{+1} \frac{H(x,\xi,t)}{x-\xi} dx \ldots - i\pi H(\xi,\xi,t)\ldots$$

(where $\xi \sim x_{Bj}/2$ and t are fixed by the experiment). At smaller lepton energy (see Fig. 3 with E_μ = 100 GeV and same values of Q^2 and x_{Bj} as above), the interference between BH and DVCS becomes

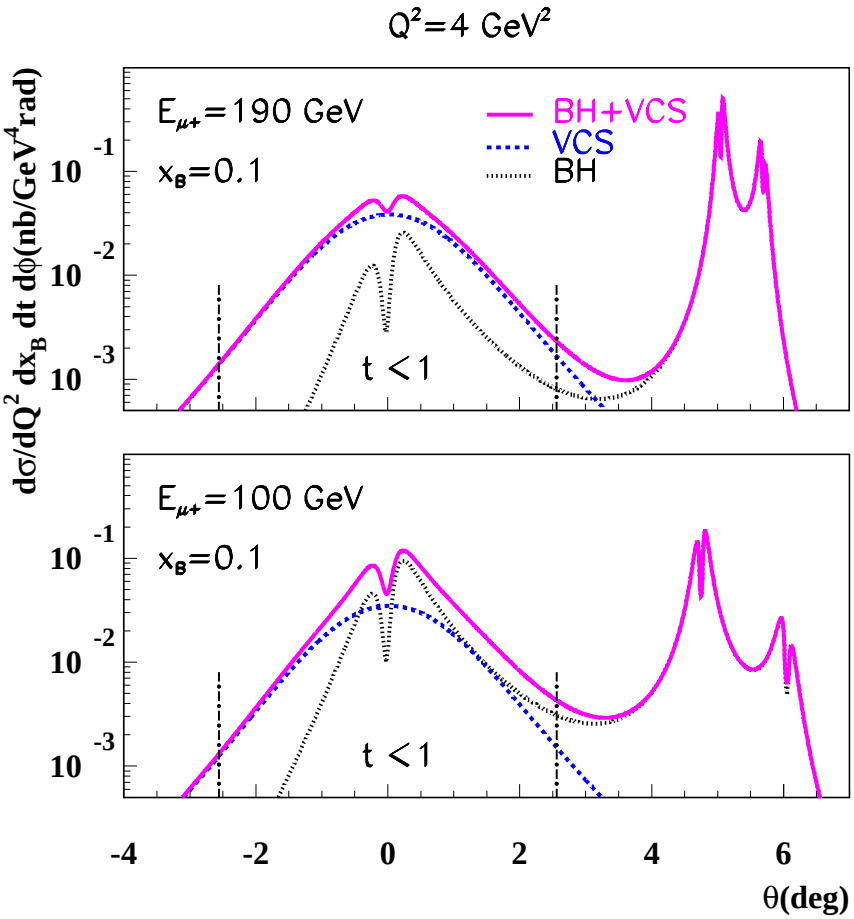

Fig. 3: Cross sections for the photon leptoproduction $\mu p \to \mu p \gamma$ as a function of the outgoing real photon angle (relative to the virtual photon direction). Comparison between BH (dotted lines), DVCS (dashed lines) and the total cross sections (full lines) for two energies of the muon beam available at CERN: 190 and 100 GeV. The interesting domain is limited by a transfer $|t|$ smaller than 1 GeV^2, i.e. θ investigating a small region around 0 degree.

large and offers a unique opportunity to study Compton scattering amplitude including its phase. A careful analysis of the dependence of the cross section on the azimuthal angle ϕ between the leptonic and hadronic planes and on Q^2 allows one to disentangle higher-twist effects and to select the real or imaginary parts of the DVCS amplitude (see the details in the previous text of M. Diehl [1]). If a longitudinally polarized lepton beam and an unpolarized target are used, the angular analysis and the Q^2 dependence of the cross section difference $\sigma(e^{\uparrow}) - \sigma(e^{\downarrow})$ allow one to select the imaginary part of the DVCS amplitude and thus the GPDs at the specific values $x = \xi$. This study is being investigated at HERMES [8] and JLab [9]. If two muon beams of opposite charge and polarization are used, the angular analysis and the Q^2 dependence of the sum of cross sections $\sigma(\mu^{+\downarrow}) + \sigma(\mu^{-\uparrow})$ allow also one to select the imaginary part of the DVCS amplitude. Moreover the same method applied to the difference of cross sections $\sigma(\mu^{+\downarrow}) - \sigma(\mu^{-\uparrow})$ allows one to select the real part of the DVCS amplitude which, for a given ξ, is sensitive to the complete dependence on x of the GPDs. The deconvolution (over x) of this formula to extract the GPDs is not yet clearly solved, but comparison to model predictions can easily be made. It is clear that the muon beam of high energy at CERN can offer many possibilities in order to investigate the many-faceted problem of the GPDs knowledge.

Figure 4 shows the azimuthal distribution of the charge asymmetry which can be measured at COMPASS and the strong sensitivity to two different models [10]. The first one is based on a simple parametrization of the GPDs: $H^f(x,\xi,t) = H^f(x,\xi,0)F_1^f(t)/2$ where $F_1^f(t)$ represents the elastic

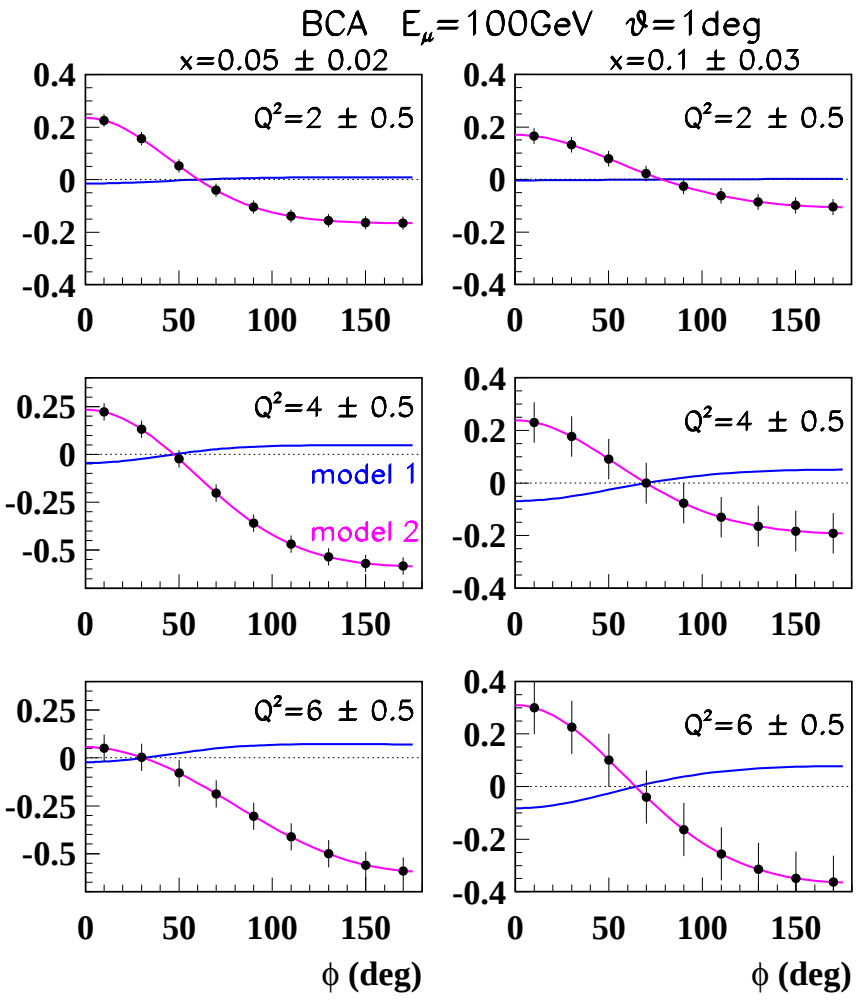

Fig. 4: Azimuthal distribution of the beam charge asymmetry measured at COMPASS at E_μ= 100 GeV and $|t| \leq 0.6$ GeV^2 for two domains of x_{Bj} ($x_{Bj} = 0.05 \pm 0.02$ and $x_{Bj} = 0.10 \pm 0.03$) and three domains of Q^2 ($Q^2 = 2 \pm 0.5$ GeV^2, $Q^2 = 4 \pm 0.5$ GeV^2 and $Q^2 = 6 \pm 0.5$ GeV^2) obtained in six months of data taking with a global efficiency of 25% and with $2 \cdot 10^8$ μ per SPS spill ($P_{\mu^+} = -0.8$ and $P_{\mu^-} = +0.8$).

Dirac form factor for the quark flavour f in the nucleon. The second one [11–14] relies on the fact that the GPDs measure the contribution of quarks with longitudinal momentum fraction x to the corresponding form factor as is suggested by the sum rule:

$$\int_{-1}^{+1} H^f(x,\xi,t)dx = F_1^f(t).$$

As one can associate the Fourier transform of form factors with charge distributions in position space, one can expect that the GPDs contain information about the distribution of partons in transverse position space. In fact it has been demonstrated that, when t is purely transverse which amounts to $\xi = 0$, then $H(x,0,t)$ is the Fourier transform of the probability density to find a quark with momentum fraction x at a given distance from the centre of momentum in the transverse plane. Qualitatively one expects that quarks with a large x come essentially from the small valence 'core' of the nucleon, while the small x region should receive contributions from the much wider meson 'cloud'. Therefore one expects a gradual increase of the t-dependence of $H(x,0,t)$ as one goes from larger to smaller values of x. This suggests the parametrization: $H(x,0,t) = q(x)e^{t\langle b_\perp^2\rangle} = q(x)/x^{\alpha t}$ where $\langle b_\perp^2\rangle = \alpha \cdot \ln\frac{1}{x}$ represents the increase of the nucleon transverse size with energy. The domain of small x_{Bj} reached at COMPASS is related to

the observation of see quarks or meson 'cloud' or also gluons and it provides a large sensitivity to this three-dimensional picture of partons inside a hadron.

2. GENERAL REQUIREMENTS FOR COMPASS

The highest luminosity reachable at COMPASS is required to investigate these exclusive measurements. The experiment will use 100–190 GeV/c muons from the M2 beam line. Limits on radio-protection in the experimental hall imply that the maximum flux of muon to be expected is of $2 \cdot 10^8$ muons per SPS spill (5.2 s spill duration, repetition each 16.8 s). Under these circumstances, we can reach a luminosity of $\mathcal{L} = 5 \cdot 10^{32}$ cm^{-2}s^{-1} with the present polarized ^{6}LiD or NH_3 target of 1.2 m long, and only a luminosity of $\mathcal{L} = 1.3 \cdot 10^{32}$ cm^{-2}s^{-1} with a future liquid hydrogen target of 2.5 m length.

In order to get useful cross sections with positive and negative muon beams, it is necessary to perform a precise absolute luminosity measurement. This has already been achieved by the NMC Collaboration within a 1% accuracy [15]. The integrated muon flux was measured continuously by two methods: either by sampling the beam with a random trigger (provided by the α emitter ^{241}Am) or by sampling the counts recorded in two scintillator hodoscope planes used to determine incident beam tracks. The beam tracks were recorded off-line, in the same way as the scattered muon tracks, to determine exactly the integrated usable muon flux.

Moreover μ^+ and μ^- beams of 100 GeV energy, with the same and as large as possible intensity as well as exactly opposite polarization (to a few %) are required. The muons are provided by pion and kaon decay and are naturally polarized. The pions and kaons come from the collision of the SPS 400 GeV proton beam on a Be primary target. A solution was proposed by Lau Gatignon [16]. It consists in: 1) selecting 110 GeV pion beams from the collision and 100 GeV muon beams after the decay section in order to maximize the muon flux; 2) keeping constant the collimator settings which define the pion and muon momentum spreads (both the collimator settings in the hadron decay section and the scrapper settings in the muon cleaning section) in order to fix the μ^+ and μ^- polarizations at exactly the opposite value ($P_{\mu^+} = -0.8$ and $P_{\mu^-} = +0.8$); 3) fixing N_{μ^-} to $2 \cdot 10^8$ μ per SPS spill with the longest 500 mm Be primary target; 4) using a shorter target to find N_{μ^+} close to $2 \cdot 10^8$ μ per SPS spill.

This paragraph presents the experimental procedure to select the exclusive HEMP or DVCS channel and the difference equipments that are required. They are mostly part of the existing high-resolution COMPASS spectrometer: muon detection which insures a good resolution in x_{Bj} and Q^2, meson detection and identification in RICH or photon detection in calorimeters of good energy and position resolutions to allow two-photon separation. The COMPASS spectrometer intercepts only forward outgoing particles (until 10 degrees) and the photon or meson detection limits the experiment to small x_{Bj} values ($x_{Bj} \leq 0.15$). At these high energies the complete final state, including the low-energy recoiling proton, needs to be detected because missing-mass techniques are not efficient due to the experimental resolutions (the resolution in missing mass which is required is $(m_p + m_\pi)^2 - m_p^2 = 0.25$ GeV^2 and the experimental resolution which can be achieved is larger than 1 GeV^2). Consequently the high-resolution COMPASS spectrometer needs to be completed by a recoil detector to measure precisely the proton momentum and exclude other reactions under high-luminosity conditions. In the next section we shall try to by-pass the necessity of a recoil detector to investigate the cleanest channel: $\mu p \rightarrow \mu p \rho^0$ where ρ^0's are identified through their decay to two charged pions accurately measured in the forward COMPASS spectrometer.

3. A PRAGMATIC SOLUTION WITH THE PRESENT SETUP

With the present COMPASS setup we can undertake Hard Exclusive ρ^0 Production (with the largest cross section) as we can benefit from the good expertise for this measurement in the previous NMC and SMC experiments and so produce data in this field as soon as possible. At the same time we can also investigate Hard Exclusive π^0 Production to see the limit of this setup.

In this context the constraints and limits of these experiments are the following:
1) With the present polarized ^{6}LiD or NH_3 target the production occurs on quasi-free nucleons in the nucleus or in the coherent scattering on the nucleus.
2) Luminosity determination is needed, but can be realized indirectly by measuring at the same time unpolarized Deep Inelastic Scattering and using known or calculated structure functions F_2 and R (the 'EMC' nuclear effects have to be taken into account).
3) The selection of longitudinal ρ^0 will be made by the angular distribution of the decay product. No Rosenbluth separation is envisagable for π^0 production.
4) The absence of a recoil detector prevents the complete exclusivity of the channel.

Precise simulations of exclusive ρ^0 and π^0 production have been performed [17, 18] and were already presented at the COMPASS meeting in Munich in 2000. The selection of exclusive events can be summarized as follows:
1) Deep inelastic events are selected by cuts on variables depending on the scattered muon kinematics:

$$2 \leq Q^2 \leq Q^2_{max} \text{ and } 35(20) \leq \nu \leq 170(90) \text{ GeV for } \rho^0$$
$$1 \leq Q^2 \leq Q^2_{max} \text{ and } 15(10) \leq \nu \leq 170(85) \text{ GeV for } \pi^0$$

The values outside(inside) the brackets correspond to the beam energy of 190(100) GeV.
2) ρ^0 and π^0 are identified through decays: $\rho^0 \to \pi^+\pi^-$ and $\pi^0 \to \gamma\gamma$. Only two hadrons of opposite charge associated with the vertex defined by the incident and scattered muons are required for ρ^0 production and only two photons with the incident and scattered muons are demanded for π^0 production. For ρ^0, hadrons have to be identified as pions. It is then required that each pion decay is emitted in the laboratory at an angle smaller than 180 mrad (the acceptance limit of the forward spectrometer) and its momentum is above 2 GeV. For π^0 it is demanded that each decay photon has energy above 2 GeV and enters either electromagnetic calorimeter ECAL1 or ECAL2. In addition, the separation of two photons at the entrance of a calorimeter should be larger than 4 cm.
3) To isolate at best the exclusive ρ^0 events, a cut on the inelasticity I [1] is used. In Fig. 5 the inelasticity distribution is shown for the SMC ρ^0 sample [19] for the events with the invariant mass in the central part of the ρ^0 invariant mass peak. For the inelasticity distribution the peak at $I = 0$ is the signal of exclusive ρ^0 production. Non-exclusive events, where in addition to detected fast hadrons, slow undetected hadrons are produced, appear at $I \geq 0$. However, due to the finite resolution, they are not resolved from the exclusive ρ^0 peak. For the cut $-0.05 \leq I \leq 0.05$ defining the exclusive sample, the amount of the residual non-exclusive background for the SMC experiment was up to about 10% at large Q^2.
4) Finally for the ρ^0 channel a cut on the invariant mass of the two pions can be applied in order to reduce the non-resonant background. For the SMC sample the invariant mass distribution after selections, including the cut on inelasticity, is shown in Fig. 5. Although the shape of the mass spectrum varies with Q^2, a mass cut, i.e. $0.62 \leq m_{\pi^+\pi^-} \leq 0.92$ GeV^2, allows a selection of ρ^0 events with the relatively low amount of non-resonant background.
It is clear that the good resolution on charged particles associated to ρ^0 decay allows the criteria 3 and 4 and thus provides a good signature of the exclusive ρ^0 channel. The selection of the π^0 channel depends strongly on the quality of the electromagnetic calorimeters, but constraints cannot be so nicely determined.

The simulation uses event generators based on a traditional parametrization on NMC data for ρ^0 production and on two models of GPDs for π^0 production. Secondary interactions of the decay charged pions, absorption of the decay photons in the target, kinematical smearing based on the experimental resolution, trigger acceptance, acceptance for pions and photons and track reconstruction efficiency are considered. A global ρ^0 selection efficiency which takes into account secondary interactions, three-track efficiency, two-pion acceptance, a cut on I and $M_{\pi^+\pi^-}$ and muon trigger acceptance is evaluated to

[1] $I = \frac{M_X^2 - M_p^2}{W^2}$ where $W^2 = (p+q)^2$ is the total energy squared in the virtual photon–proton system and $M_{X^2} = (p+q-v)^2$ is the missing mass squared of the undetected recoiling system (p, q, v are the four-momenta of the target proton, virtual photon and meson respectively.)

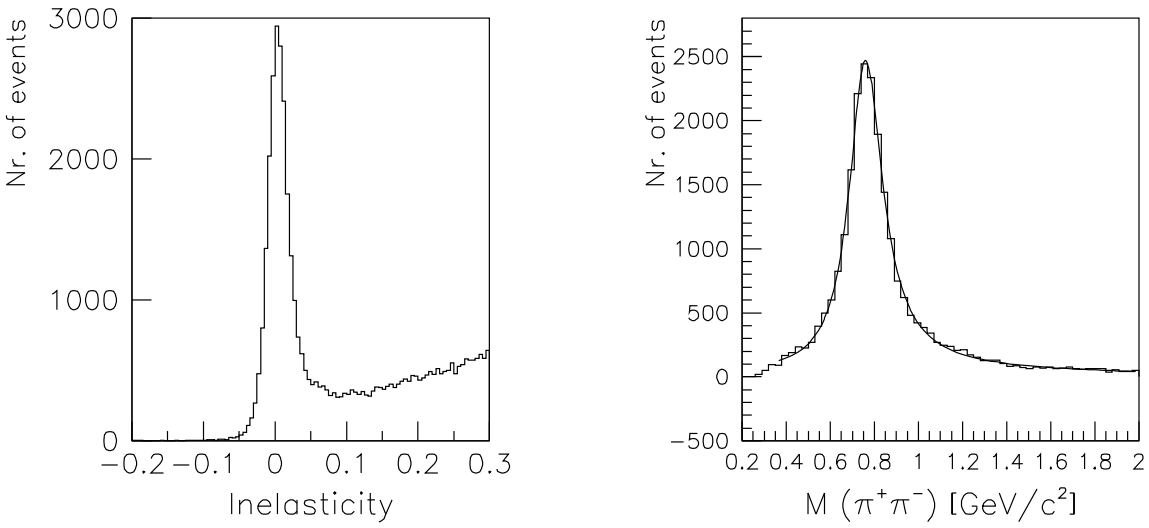

Fig. 5: The SMC results [19] for $\mu N \to \mu\rho^0 N$. (left) Inelasticity distribution after selections; (right) mass spectrum after selection including the cut $-0.05 \leq I \leq 0.05$. The full line represents a prediction according to the Söding model.

Table 1: Total cross sections and counting rates.

	190 GeV	100 GeV	
$\sigma^{tot}_{\mu N \to \mu X}$	48 nb	38 nb	
$\sigma^{tot}_{\mu N \to \mu\rho^0 N}$	286 pb	250 pb	$\langle Q^2 \rangle \sim 2.9$
$N^{cuts}_{\mu N \to \mu\rho^0 N}/year$	97 kevents	15 kevents	$\langle x_{Bj} \rangle \sim 0.034$
$\sigma^{tot}_{\mu N \to \mu\pi^0 N}$	1.3 to 5.2 pb	5.8 to 23 pb	$\langle Q^2 \rangle \sim 1.6$
$N^{cuts}_{\mu N \to \mu\rho^0 N}/year$	625 to 2500 events	1860 to 7440 events	$\langle x_{Bj} \rangle \sim 0.040$

0.21(0.04) with the medium Q^2 trigger (which consists of the 'middle trigger' and the 'ladder trigger' of the muon trigger hodoscopes) and to 0.36(0.30) with the full Q^2 range trigger (which includes, in addition, the newly implemented 'outer trigger'). The values outside(inside) the brackets correspond to the beam energy of 190(100) GeV. A global π^0 selection efficiency which takes into account secondary interaction, two-photon acceptance and muon-trigger acceptance is found close to 0.30.

Total cross sections integrated over the Q^2 and ν acceptance and expected counting rates (with the medium Q^2 trigger) for a period of 150 days (1 year) assuming an overall SPS and COMPASS efficiency of 25% are presented in Table 1. The two limits for π^0 production correspond to the two models. About two-thirds of the produced ρ^0 are longitudinally polarized.

The background to the reaction $\mu N \to \mu\rho^0 N$ has been studied. It is due to the events with at least two slow undetected particles which are outside the acceptance of the spectrometer or for which tracks are not reconstructed due to inefficiency and which pass all selections for exclusive ρ^0 events. A first possible source of this background is ρ^0 production with diffractive dissociation of the target $\mu N \to \mu\rho^0 N^*$ with the subsequent decay of the excited state N^* in $N + k\pi$. In the lower part of Fig. 6 a schematic drawing of the inelasticity distribution for these events is presented. Although the smearing effects are not taken into account it is clear that the events from diffractive dissociation of the target into the lowest masses excitations of the nucleon will contribute to the exclusive ρ^0 sample in the inelasticity cut. An estimation has been found close to 20%.
A second source of background will originate from the large number of inclusive deep inelastic events. Simulation with a sample of 5000 events only, using the generators LEPTO and JETSET, has given an

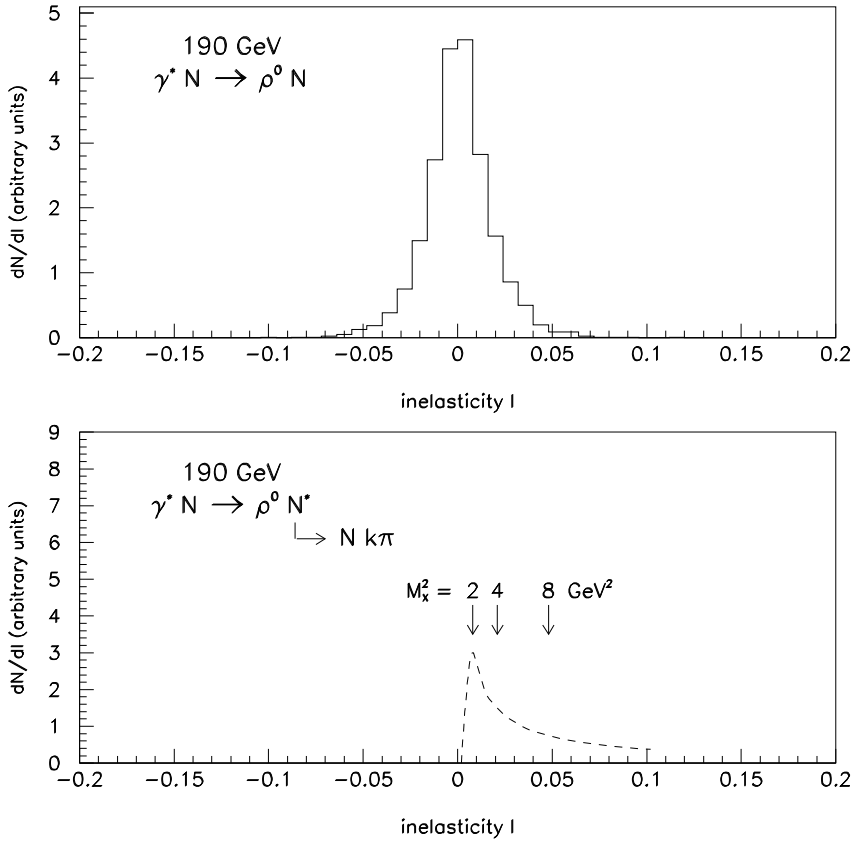

Fig. 6: Inelasticity distribution for the simulated $\mu N \rightarrow \mu\rho^0 N$ events at 190 GeV; (bottom) calculated distribution of the inelasticity for $\mu N \rightarrow \mu\rho^0 N^*$ for a continuum distribution of N^* masses.

upper limit of contamination of 20% also.

4. AN IDEAL SOLUTION WITH A COMPLETED SETUP

As mentioned in the previous section it is clear that only a recoil detector which allows low-energy recoiling proton detection will help to select exclusive channels such as HEMP or DVCS. The latter reaction is surely the most delicate because one has to select a final state with one muon, one photon and one low-energy proton among many competing reactions listed below:
1) Hard Exclusive π^0 Production $\mu p \rightarrow \mu p \pi^0$ where π^0 decays in two photons, for which the photon with higher energy imitates a DVCS photon, and the photon with smaller energy is emitted at large angle outside of the acceptance or its energy is below the photon detection threshold.
2) Diffractive dissociation of the proton $\mu p \rightarrow \mu \gamma N^*$ with the subsequent decay of the excited state N^* in $N + k\pi$. (The low-energy pions are emitted rather isotropically.)
3) Inclusive Deep Inelastic Scattering with, in addition to the reconstructed photon, other particles produced outside the acceptance or for which tracks are not reconstructed due to inefficiency.
Moreover one has to take into account a background which includes beam halo tracks with hadronic contamination, beam pile-up, particles from the secondary interactions, and external bremsstrahlung.

A simulation has been realized in order to define the proper geometry of the detector complementing the present COMPASS setup and to analyse the operational conditions. The goal was to maximize the ratio of DVCS events over DIS events for a sample of events with one muon and one photon in the COMPASS spectrometer acceptance plus only one proton of momentum smaller than 750 MeV/c and angle larger than 40 degrees (it is the typical kinematics of a DVCS event at small t). The simulation relies on the event generator program PYTHIA 6.1 [20] which includes most of the known processes [21]

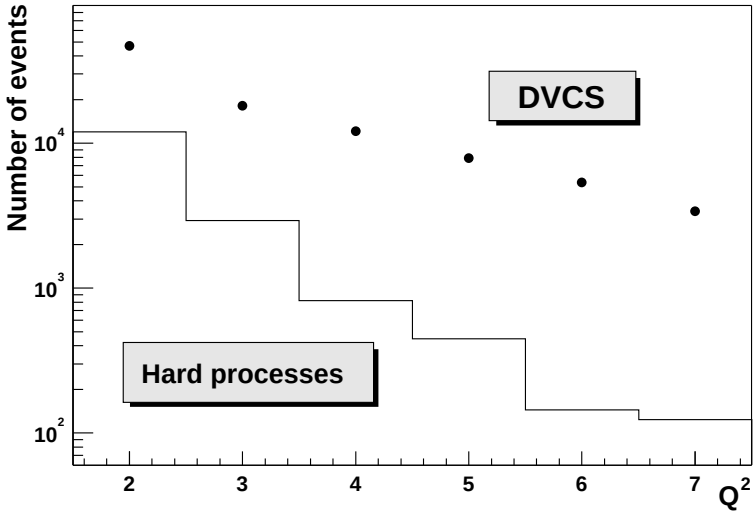

Fig. 7: Number of events for DVCS (dots) and DIS (histogram) processes as a function of Q^2 for selection of events with only one muon, one photon and one recoiling proton and condition for charged particle detection up to 40 degrees and for photon detection up to an angle of 24 degrees and above a threshold of 50 MeV.

such as Deeply Inelastic Scattering and Deeply Meson Production. The experimental parameters such as maximum angle and energy threshold for photon detection and maximum angle for charged particle detection could then be tuned. With photon detection extended up to 24 degrees and above an energy threshold of 50 MeV and with charged particle detection up to 40 degrees, one observes that the number of DVCS events as estimated with models is more than an order of magnitude larger than the number of DIS events over the whole useful Q^2 range (see Fig. 7).

The COMPASS setup will be instrumented with two electromagnetic calorimeters ECAL1 and ECAL2 [22, 23]. They are mainly constituted of lead-glass blocks called GAMS. They are cells of 38.4 $\times$ 38.4 $\times$ 450 mm^3. Typical characteristics of such calorimeter are:

- energy resolution: $\sigma P_\gamma/P_\gamma = 0.055/\sqrt{P_\gamma}$ + 0.015,
- position resolution: $\sigma_x = 6.0/\sqrt{P_\gamma} + 0.5$ in mm,
- high rate capability: 90% of signal within 50 ns gate with no dead time,
- effective light yield: about 1 photoelectron per MeV; hence low-energy photons of down 20 MeV can be reconstructed.

The separation of the overlapping electromagnetic showers in the cellular GAMS calorimeter is carefully studied in Ref. [24]. The result of the study shows that at 10 GeV one can reach a 100% level of the separation efficiency for a minimum distance between two photon tracks at the entrance of the calorimeter of $D = 4$ cm. The last value is slightly shifted to $D = 5$ cm at 40 GeV.
This excellent performance of the calorimeters will provide a key role in the perfect separation between DVCS events and hard π^0 events.

One possible solution to complement the present COMPASS setup is presented in Fig. 8. It consists of one recoil detector described below, an extended calorimetry from 10 to 24 degrees, and a veto for charged forward particles until 40 degrees. This calorimeter has to work in a crowded environment and in a magnetic fringe field of SM1 and therefore it has to be studied further.

At the present time our studies have focused on the possibility to design and successfully operate a dedicated recoil detector. One goal is to identify and measure the protons' momenta between a minimum value and 750 MeV/c. A solution consists in a large time-of-flight setup between a thin segmented cylindrical layer of scintillator counters, about 3m long and surrounding the 2.5 m long target, and a

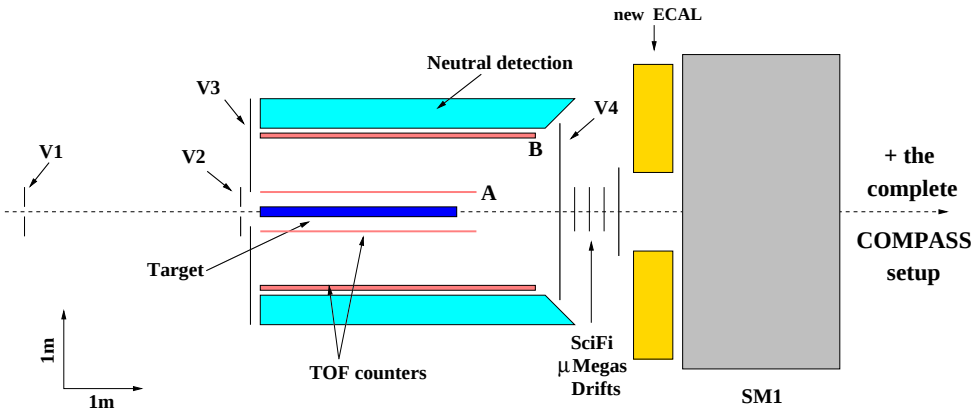

Fig. 8: Proposal for a detector complementing the COMPASS setup. A recoil detector, an extended calorimetry from 10 to 24 degrees, and a veto (V4) for charged forward particles until 40 degrees have been added.

thick layer at about 1 m distance from the first layer. The thickness of the first layer has to be as small as possible in order to detect protons of minimum momentum. With an hydrogen target of 3 cm diameter, target wall thickness of about 3 mm of equivalent scintillator and a first layer of 4 mm, a minimum momentum of 270 MeV/c is reached. All the counters are read at both sides by photomultiplier counters to determine time and position with very accurate resolutions (300 ps and 1.8 cm). The consequent resolution in momentum varies from 3 to 10%. The resolution in t is twice this value, thus it is very desirable to further study all the parameters which can be improved. Moreover, the exclusion of extra particles has to be studied with kinematical fits depending on the experimental resolution and/or with low-energy π^0 detection. This detector has to work in a high-rate environment. It has to be as large and hermetic as possible within a reasonable cost. The actual realisation of such performances is under active investigation.

Counting rates, given in Table 2, have been estimated assuming six months of data taking (1 year) assuming an overall efficiency of 25% and considering the present COMPASS setup where the photon detection is limited to 10 degrees plus a proton detection from 250 to 750 MeV/c ($|t| \leq 0.64$ GeV^2). This statistics allows for the ϕ distribution presented in Fig. 4 for $Q^2 = 2$, 4 and 6 GeV^2 and $x_{Bj} = 0.05$ and 0.10. Studies devoted to the t dependence of the cross section can be investigated but for that it is quite worth while to try to improve the t resolution.

We have tested the concept of this detector using the already existing muon beam and a simplified setup (one sector of scintillators with reduced length). The muon beam was scattered off a 10 cm long polyethylene target, mostly equivalent in radiation length to the foreseen long liquid hydrogen target. We used three scintillators read out at both sides, a 4 mm thick one close to the target (A), a 5 cm thick one 80 cm away from the target (B) and an extra scintillator (C) to know if particles go through B or are stopped in B. The rates observed in the scintillator close to the target, using the nominal intensity of $2 \cdot 10^8$ muons per spill, is of the order of 1 MHz (mainly due to Möller electrons). It demonstrates that the background environment is acceptable for the time-of-flight system.

The result of the time of flight operation [see Fig. 9(a)] shows a clear proton signal. With the knowledge of the β velocity and the energy lost in B for stopped particles, one can reconstruct their masses. It is done in Fig. 9(b) where one can see pions, protons and deuterons for raw data, corrected data and the target out contribution which is about two orders of magnitude smaller.

The position resolution obtained on A and B and the time-of-flight resolution are better than 2 cm and 300 ps respectively. Extension to long (3 m) and thin scintillators have to be studied carefully and technology has to be improved to achieve still better resolution. An efficiency study of such a recoil detector is being performed.

Table 2: Number of events for bins in x_{Bj} and Q^2.

E_μ = 190 GeV			
	$x_{Bj} = 0.05 \pm 0.02$	$x_{Bj} = 0.10 \pm 0.03$	$x_{Bj} = 0.20 \pm 0.07$
$Q^2 = 2 \pm 0.5$	10058	8897	2000
$Q^2 = 3 \pm 0.5$	3860	2540	1300
$Q^2 = 4 \pm 0.5$	2058	1136	600
$Q^2 = 5 \pm 0.5$	1472	677	520
$Q^2 = 6 \pm 0.5$	875	459	357
$Q^2 = 7 \pm 0.5$	642	299	242
E_μ = 100 GeV			
	$x_{Bj} = 0.05 \pm 0.02$	$x_{Bj} = 0.10 \pm 0.03$	$x_{Bj} = 0.20 \pm 0.07$
$Q^2 = 2 \pm 0.5$	13670	9921	4300
$Q^2 = 3 \pm 0.5$	5933	3200	2000
$Q^2 = 4 \pm 0.5$	4532	1537	770
$Q^2 = 5 \pm 0.5$	3000	995	600
$Q^2 = 6 \pm 0.5$	1806	885	499
$Q^2 = 7 \pm 0.5$	810	870	352

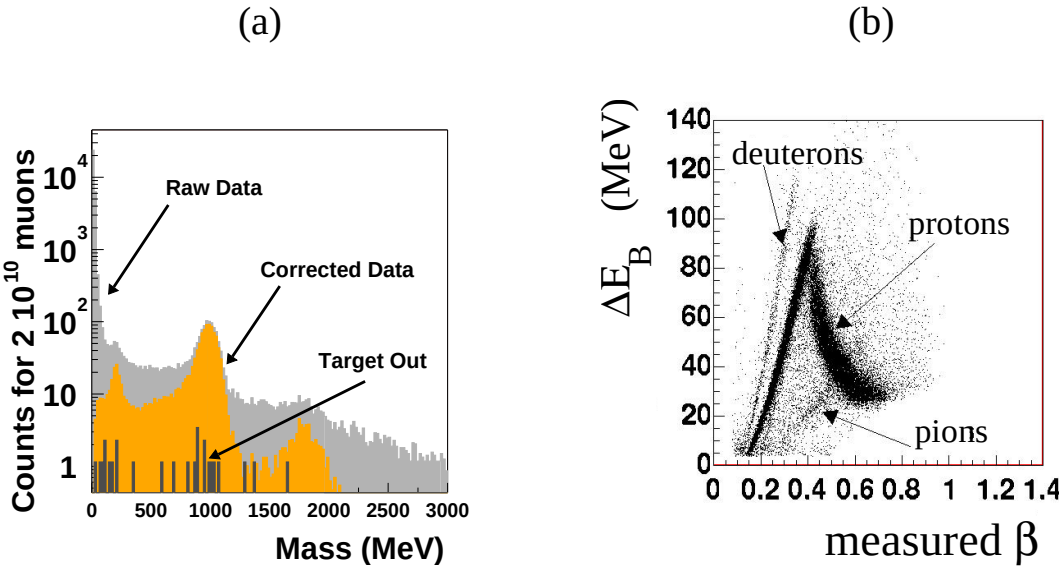

Fig. 9: (a): Energy lost in the B scintillator as a function of the measured β. (b): Mass distribution of particles stopped in B. The three peaks are pions, protons and deuterons respectively.

5. CONCLUSIONS

This study takes advantage of the high energy of the muon beam available at CERN which provides a large Q^2 and x_{Bj} range and encourages us for the following roadmap. Hard Exclusive Meson Production has to be undertaken as soon as possible with the present setup. A large number of ρ^0 events (a few 10K) can be produced in one year. The ρ^0 channel which decays in $\pi^+\pi^-$ is the easiest channel to isolate, the π^0 channel is more difficult but very important to test the calorimetry performances. A complete experiment with both Hard Exclusive Meson Production with a large set of mesons and Deeply Virtual Compton Scattering has to be envisaged in a next step with a completed COMPASS setup. For this purpose one needs a 'long' hydrogen target, a recoil detector, and an extension of the calorimetry at larger angles.

COMPASS is the unique place which provides μ^+ and μ^- of 100 GeV in order to study carefully two scales of observation $x_{Bj} = 0.05 \pm 0.02$ and $x_{Bj} = 0.10 \pm 0.03$ on a large domain of Q^2 from 2 to 7 GeV^2 and to measure the azimuthal distribution of the Beam Charge Asymmetry which seems very promising to test the geometrical interpretation of GPDs.

Acknowledgements

We acknowledge useful discussions with Dietrich von Harrach, Fritz Klein, Alain Magnon and all members of the Saclay COMPASS group.

References

[1] M. Diehl, Introduction to Generalized Parton Distributions, Contribution to these Proceedings.

[2] J.C. Collins, L. Frankfurt and M. Strikman, Phys. Rev. D **56** (1997) 2982.

[3] M. Vanderhaeghen, P.A.M. Guichon and M. Guidal, Phys. Rev. **D 60** (1999) 094017.

[4] NMC Collaboration, M. Arneodo *et al.*, Nucl. Phys. B **429** (1994) 503.

[5] E665 Collaboration, M.R. Adams *et al.*, Z. Phys. C **C74** (1997) 237.

[6] ZEUS Collaboration, M. Derrick *et al.*, Phys. Lett. B **356** (1995) 601.

[7] ZEUS Collaboration, J. Breitweg *et al.*, Eur. Phys. J. C **6** (1999) 603.

[8] HERMES Collaboration, A. Airapetian *et al.*, Phys. Rev. Lett. **88** (2001) 182001.

[9] CLAS Collaboration, S. Stepanyan *et al.*, Phys. Rev. Lett. **87** (2001) 182002.

[10] L. Mossé, P.A.M. Guichon and M. Vanderhaeghen, private communication.

[11] M. Burkardt, Phys. Rev. D **62** (2000) 07503; hep-ph/0207047.

[12] J.P. Ralston and B. Pire, hep-hp/0110075.

[13] M. Diehl, Eur. Phys. J. C **25** (2002) 233; ibid. C **31** (2003) 277 (E).

[14] A.V. Belitsky and D. Müller, Nucl. Phys. A **711** (2002) 118; hep-hp/0206306.

[15] NMC Collaboration, P. Amaudruz *et al.*, Phys. Lett. B **295** (1992) 159; R.P. Mount, Nucl. Instrum. Meth. **187** (1981) 401.

[16] L. Gatignon, private communication.

[17] J. Pochodzalla, L. Mankiewicz, M. Moinester, G. Piller, A. Sandacz and M. Vanderhaeghen, hep-ex/9909534.

[18] A. Sandacz, COMPASS Note 2000-1 (2000).

[19] A. Tripet, presented at the 7th International Workshop on DIS and QCD, Nucl. Phys. B , Proc. Suppl. **79** (1999).

[20] PYTHIA 6.1, User's manual, T. Sjöstrand *et al.*, High Energy Physics Event Generation with PYTHIA 6.1, Comput. Phys. Commun. **135** (2001) 238; hep-ph/0010017.

[21] C. Friberg and T. Sjöstrand, hep-ph/0007314.

[22] A Proposal for a Common Muon and Proton apparatus for Structure and Spectroscopy, CERN/SPSLC 96-14 and wwwcompass.cern.ch.

[23] V. Poliakov, Presentation of ECAL1 and ECAL2, January 25, 2001.

[24] A.A. Lednev, Separation of the overlapping electromagnetic showers in the cellular GAMs-type calorimeters, Preprint IHEP 93-153 (1993), Protvino, Russia.

List of Participants

Antonio Amoroso	Univ. Turin
Vladimir Anosov	JINR, Dubna
Mauro Anselmino	Univ. Turin
Yuri Arestov	IHEP, Protvino
Barbara Badelek	CERN
Günter Baum	Univ. Bielefeld
Yann Bedfer	CEA Saclay
Peter Berglund	Helsinki Univ. Technology
Colin Bernet	CEA Saclay
Paula Bordalo	LIP Lisbon
Franco Bradamante	INFN Trieste
Andrea Bressan	Univ. Trieste
Etienne Burtin	CEA Saclay
Augusto Ceccucci	CERN
Suh-Urk Chung	BNL
Marialaura Colantoni	Univ. Turin and INFN
Peter S. Cooper	FNAL
Silvia Dalla Torre	INFN Trieste
Sudebsankar Dasgupta	Calcutta, India
Nikolas Dedek	LMU München
Oleg Denisov	INFN Turin
Claude Détraz	CERN
Lova Dhara	Calcutta, India
Markus Diehl	RWTH Aachen
Sergei Donskov	IHEP, Protvino
Valery Dorofeev	IHEP, Protvino
Norihiro Doshita	Nagoya Univ.
Umberto Dosselli	INFN Padua
Wolfgang Dünnweber	LMU München
Anatoli Efremov	JINR, Dubna
Wolfgang Eyrich	Univ. Erlangen
Martin Faessler	LMU München
Peter Fauland	Univ. Bielefeld
Michael Finger	JINR, Dubna
Miroslav Finger	Charles Univ., Prague and JINR
Horst Fischer	Univ. Freiburg
Jan Friedrich	TU München
Rafaello Garfagnini	INFN Turin
Jürg Gasser	Univ. Bern
Lau Gatignon	CERN
Sergei Gerassimov	TU München
Marcello Giorgi	Univ. Trieste
Stephen Godfrey	Carleton Univ. and DESY
Stefan Goertz	Ruhr Univ. Bochum
Boris Grube	TU München
Andreas Grünemaier	Univ. Freiburg
Kenneth Gustafsson	Helsinki Inst. of Physics
Dietrich von Harrach	Univ. Mainz

Sonia Hedicke	Univ. Freiburg
Fritz-Herbert Heinsius	Univ. Freiburg and Bonn
Martin von Hodenberg	Univ. Freiburg
Nicole d'Hose	CEA Saclay
Christoph Ilgner	LMU München
Antonin Janata	JINR, Dubna
Eva-Maria Kabuss	Univ. Mainz
Chung-Wen Kao	Univ. Manchester
Wolfgang Kastaun	Univ. Freiburg
Andrei Kataev	Inst. for Nuclear Research, Moscow
Bernhard Ketzer	TU München and CERN
Guennadi Khaoustov	IHEP, Protvino
Kay Königsmann	Univ. Freiburg
Jaakko Koivuniemi	Helsinki Univ. of Technology
Vladimir Kolossov	IHEP, Protvino
Evgueni Komissarov	JINR, Dubna
Kaori Kondo	Nagoya Univ.
Alexander Korzenev	Univ. Mainz
Aram Kötzinian	JINR, Dubna
Daniel Kramer	Technical Univ. Liberec
Roland Kuhn	TU München
Fabienne Kunne	CEA Saclay
Ronald Kunne	IPN Orsay
Krysztof Kurek	Soltan Inst., Warsaw
Massimo Lamanna	CERN
Jean-Marc Le Goff	CEA Saclay
Elliot Leader	Imperial College, London
Mario Leberig	Univ. Mainz
Angelo Maggiora	INFN
Alain Magnon	CEA Saclay
Gerhard Mallot	CERN
Claude Marchand	CEA Saclay
Dominique Marchand	IPN Orsay
Anna Martin	Univ. Trieste and INFN Trieste
Rita de Masi	TU München
Craig McNeile	Univ. Liverpool
Werner Meyer	Ruhr Univ., Bochum
Murray Moinester	Tel Aviv Univ.
Dieter Mueller	Univ. Wuppertal
Claudio Mulatero	Univ. Turin
Jan Nassalski	Soltan Inst., Warsaw
Stepan Neliba	Czech Technical Univ., Prague
Damien Neyret	CEA Saclay DAPNIA/SPhN
Rudolf Novak	Czech Technical Univ., Prague
Luca Oberto	Univ. Turin
Daniele Panzieri	INFN Turin
Stephan Paul	TU München
Dmitri Pechekhonov	JINR, Dubna
Stephane Platchkov	CEA Saclay
Josef Pochodzalla	Univ. Mainz

Vladimir Poliakov	IHEP, Protvino
Catarina Quintans	LIP Lisbon
Sergio Ramos	LIP Lisbon
Jean-Marc Richard	ISN Grenoble
Klaus Rith	Univ. Erlangen-Nurnberg
Vladimir Romanovski	IHEP, Protvino
Mikhail Sapozhnikov	JINR, Dubna
Igor Savin	JINR, Dubna
Paolo Schiavon	Univ. and INFN Trieste
Lars Schmitt	TU München
Hans Schmitt	Univ. Freiburg
Hans-Wolfgang Siebert	Univ. Heidelberg
Lily Sinha	Calcutta, India
Miloslav Slunecka	Charles Univ., Prague and JINR
Valentine Sougoniaev	IHEP, Protvino
Hasko Stenzel	JLU Giessen
Oleg Tchikilev	IHEP, Protvino
Fulvio Tessarotto	INFN Trieste
Andreas Teufel	Univ. Erlangen
Leonid Tkachev	JINR, Dubna
Marco Traini	Univ. Trento
Richard Webb	Univ. Erlangen
Eric Weise	ISKP Univ. Bonn
Michael Wiesmann	TU München
Wojciech Wislicki	Soltan Inst., Warsaw
Jiawei Zhao	Univ. Mainz